Roles of WIP and WICH/WIRE proteins in formation and maturation of invasive protrusions in human breast cancer cells

by
Esther García González

A thesis submitted in fulfilment of the requirements for the degree of Doctor of Philosophy

Supervised by Dr Inés M. Antón Gutiérrez

Centro Nacional de Biotecnología (CNB-CSIC)
Molecular Biology Department
Faculty of Sciences
Universidad Autónoma de Madrid

January 2014

UNIVERSIDAD AUTONOMA DE MADRID

CNB
CENTRO NACIONAL DE BIOTECNOLOGIA

This work was performed in the laboratories of Dr Inés M. Antón (Centro Nacional de Biotecnología (CNB-CSIC)) and Prof Laura Machesky (The Beatson Institute for Cancer Research). This study was supported by grants from the Spanish Ministry of Science and Innovation (BFU2010-21374/BMC) and Cancer Research UK. The author held contracts from the Comunidad Autónoma de Madrid (CAM, March 2009 to March 2013), the Fundación Severo Ochoa (March 2013 to September 2013), and short-term fellowships from EMBO and the CSIC.

INDEX

FIGURES INDEX

INTRODUCTION

MATERIALS AND METHODS

RESULTS

TABLES INDEX

1. ABSTRACT

Metastasis is a multistep process wherein cancer cells separate from the primary tumour, cross the surrounding extracellular matrix (ECM), and disperse throughout the body to reach distant tissues where they proliferate and establish themselves as a secondary tumour. Metastasis involves several intracellular processes including signal cascades, some of which reorganize the actin cytoskeleton. Matrix-cell interaction is thus essential in the first steps of cancer progression, as it adapts internal signalling pathways in response to external stimuli from the ECM, modulating cell invasiveness and motility.

Cancer cells develop specialised invasive membrane protrusions to migrate across the ECM. WIP (WASP-interacting protein) is located at these protrusions and its mRNA levels correlate to poor prognosis in diverse cancer types. WIP and the closely related WICH/WIRE interact with N-WASP, to form complexes that might participate in cancer invasion. In this study, we aimed to elucidate the contribution of WIP and WICH/WIRE to this invasive behaviour by examining 2D and 3D invasion by cancer cells that lack WIP or WICH/WIRE. WIP, but not WICH/WIRE, is highly expressed in basal B breast cancer cells in contrast to luminal cells. Although both proteins play supporting roles in cancer invasion by recruiting N-WASP and Nck, WIP might replace WICH/WIRE in this process. We demonstrate here that WIP and WICH/WIRE are implicated in efficient invasion of MDA-MB-231 breast cancer cells, by regulating adhesion and ECM remodelling through FAK and Src kinases. Furthermore, we suggest that WIP constitutes a therapeutic target in metastasis-directed treatment and a prognosis marker for breast cancer patients.

RESUMEN

El proceso de metástasis se compone de varios pasos a través de los cuales las células tumorales se separan del tumor inicial o primario, invaden a través de la matriz extracelular que rodea al tumor, y se dispersan hacia tejidos distantes, donde proliferan y establecen un tumor secundario. Hay muchos procesos intracelulares que regulan la metástasis, incluyendo cascadas de señalización, algunas de las cuales están implicadas en la reorganización del citoesqueleto de actina. Por tanto, la interacción de la célula con la matriz extracelular es esencial en los primeros pasos de la progresión tumoral, ya que esta interacción contribuye a la adaptación de vías de señalización intracelulares en respuesta a estímulos externos procedentes de la matriz, contribuyendo así a modular la invasividad y motilidad celulares.

Las células tumorales desarrollan protrusiones de la membrana especializadas para invadir y migrar a través de la matriz extracelular. WIP (del inglés "*WASP-interacting protein"*) se localiza en estas protrusiones, y los niveles de expresión de su ARN mensajero se correlacionan con una mala prognosis en varios tipos de cáncer. WIP y WICH/WIRE (otro miembro de la familia WIP) interaccionan con N-WASP, formando un complejo que podría participar en el proceso de invasión tumoral. En este estudio, nos propusimos elucidar la contribución de WIP y WICH/WIRE en el comportamiento invasivo de células tumorales deficientes en WIP o WICH/WIRE. Sólo WIP se expresa de forma abundante en células de cáncer de mama de fenotipo basal B, a diferencia de aquellas de fenotipo luminal. Aunque ambas proteínas contribuyen al reclutamiento de N-WASP y Nck contribuyendo así a la invasión, WIP es capaz de reemplazar a WICH/WIRE en este proceso. En este estudio demostramos además que WIP y WICH/WIRE son necesarias para que las células MDA-MB-231 invadan de forma eficiente, ya que a través de las kinasas FAK y Src regulan la adhesión celular y la degradación de la matriz extracelular. Además, proponemos que WIP podría utilizarse como marcador pronóstico y diana terapéutica en pacientes de cáncer de mama metastásico.

Introduction

2. INTRODUCTION

2.1 CANCER PROGRESSION

Epithelial cells may undergo malignant transformation due to DNA damage (e.g., in cell cycle suppressors, oncogenes or telomeres (Gupta and Massague, 2006)). This provokes abnormal cell proliferation that leads to hyperplasia and loss of tissue architecture, originating a carcinoma *in situ* (Beckmann et al., 1997). Carcinoma cells later lose cell-cell contacts and acquire migratory and invasive characteristics, and detach from the epithelium, which allows them to reach the blood or lymph vessels. Some tumour cells succeed in dispersing throughout different organs or tissues, where they are able to establish and grow to form a secondary tumour (Fidler, 2003) (Fig. I1). It is necessary that part of the cell population conserve the ability to initiate a tumour, maintaining properties of cancer stem cells (Gupta and Massague, 2006).

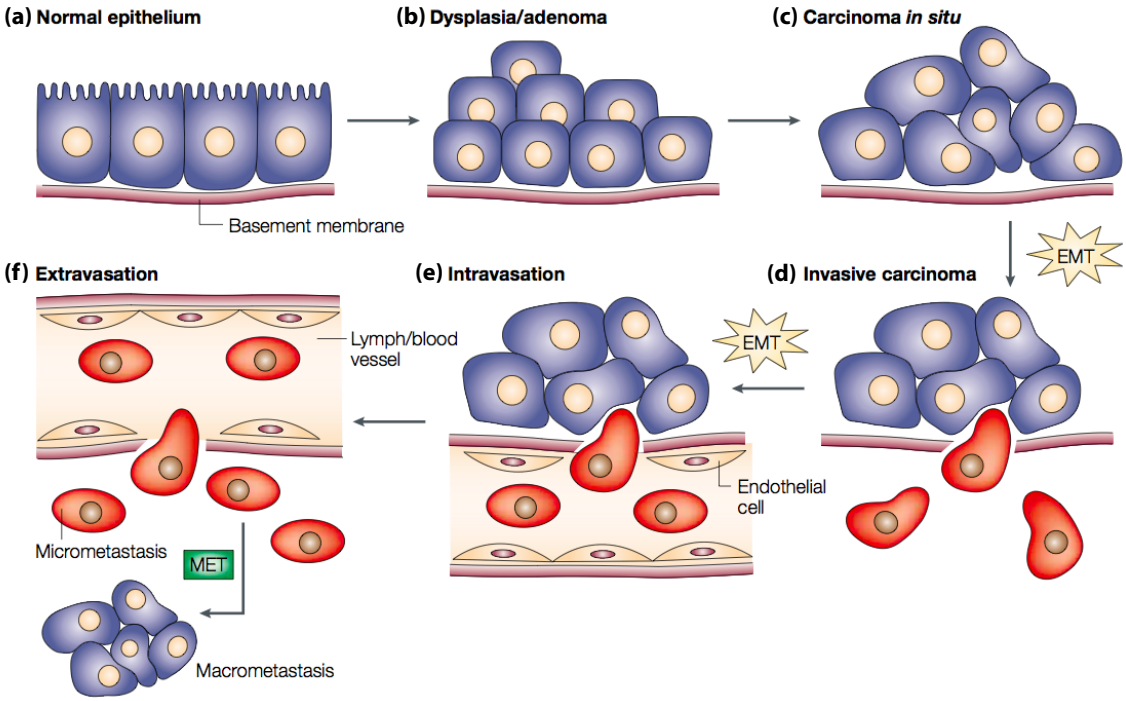

Figure I1: Sequential steps during cancer progression. During carcinoma progression, normal epithelium (a) proliferates abnormally, leading to dysplasia (b), and is transformed, originating a carcinoma in situ (c). Tumour cells lose cell-cell and cell-extracellular matrix (ECM) contacts in a process termed epithelial to mesenchymal transition (EMT), detaching from one another and the ECM (d), which allows them to escape from the primary tumour and migrate to nearby vessels (e). Some cells spread to distant tissues, where they recover epithelial characteristics by mesenchymal to epithelial transition (MET), establishing a secondary tumour (f) in a process known as metastasis (Thiery, 2002).

The malignant behaviour of carcinoma cells responds to several pressures, some intrinsic (genotoxic stress from hyperactivated oncogenes, growth, apoptotic and senescence signals) and some extrinsic (such as hypoxia, pH, oxidative stress or components and mechanical forces from the ECM) (Gupta and Massague, 2006). Constituents of intracellular junctions and ECM adhesion such as integrins, membrane receptors or focal contacts, are therefore essential in the first steps of metastasis (Cavallaro and Christofori, 2004; Friedl and Wolf, 2003). Through interaction with the ECM, carcinoma cells migrate and cross the matrix towards the vessels in response to chemotactic signals. For effective locomotion, cells must emit pseudopods and contract to promote net cell movement, as well as to remodel the surrounding ECM (Friedl and Wolf, 2009).

2.1.1 Breast cancer

Mammary carcinoma is the most common cancer in women worldwide (World Health Organisation, 2013). Metastasis due to dispersion of the primary tumour to other organs constitutes the main cause of death in breast cancer patients. The most common metastases develop in lung, lymph nodes and bone (Minn et al., 2005) (Fig. I2). Breast cancers are broadly heterogeneous, although the most common types are ductal and lobular, depending on the localisation of the primary tumour.

Breast carcinomas are clinically classified in three main groups: 1) oestrogen receptor (ER)-positive, 2) human epidermal receptor 2 (HER2 or ERBB2)-positive and 3) triple-negative tumours, which lack expression of ER, PR (progesterone receptor) and HER2 (Perou et al., 2000). Primary tumours expressing any of these receptors were traditionally grouped as luminal-like, whereas triple-negative carcinomas were termed basal-like. Established breast cancer cell (BCC) lines are organised similarly, following the same criteria and terminology (Neve et al., 2006). Of all breast cancers, basal-like have the poorest prognosis, as lack of ER, PR and HER2 limits their clinical treatment, which generally focuses on targeting these receptors. A controversy remains concerning basal-like BCC classification, as they are frequently divided into two subgroups: basal A, some of which express HER2 (and could therefore also be catalogued as luminal-like),

and basal B, strictly triple-negative cells that are characterised by a stem-like expression profile (e.g., $CD44_{high}/CD24_{low}$) that leads to a highly invasive phenotype. Luminal cells preserve a differentiated phenotype and maintain tight cell-cell junctions (Neve et al., 2006; Perou et al., 2000).

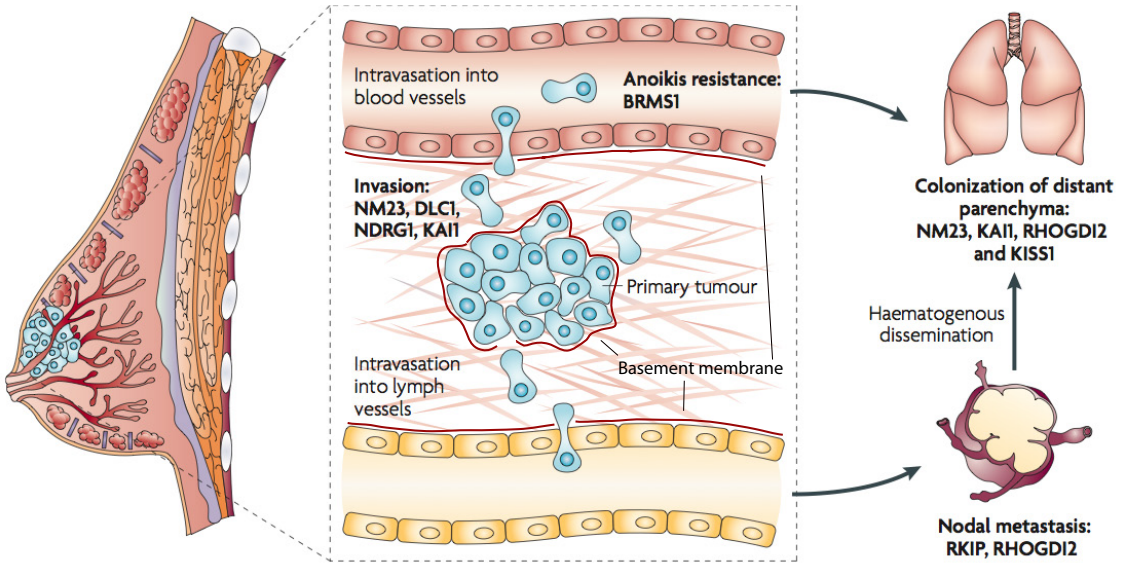

Figure I2: Breast cancer metastasis. Genetic deregulation of normal mammary cells leads to neoplasia. After invasion of the basement membrane (BM) and stroma, surviving cells travel through the blood or lymph vessels and metastasise predominantly in lung and lymph nodes. Adapted from (Smith and Theodorescu, 2009).

Wyckoff et al., 2007). EMT is necessary for cancer cells to dedifferentiate and acquire invasive properties that facilitate cell dispersion, whereas MET becomes essential during secondary tumour formation (Fig. I1).

Several signalling pathways regulate EMT. Members of the transforming growth factor β (TGFβ) family activate SMAD transcription factors, leading to loss of apical-basal cell polarity. The Notch pathway regulates EMT by activating the nuclear factor-κB (NF-κB) or TGFβ. The Wnt signalling pathway regulates levels of β-catenin and its redistribution between cytoplasm and the nucleus, modulating expression of several EMT transcription factors. Receptor tyrosine kinases and other membrane proteins are also able to regulate EMT, as is the case of E-cadherin. The union of the E-cadherin cytoplasmic tail to β-catenin normally sequesters β-catenin. When E-cadherin expression is lost (a frequent event in some carcinomas), β-catenin is released to the cytoplasm and

is able to enter the nucleus (Polyak and Weinberg, 2009).

Not only epithelial markers are altered during EMT; expression of mesenchymal markers such as vimentin is also modified during this process. After lost of adherent junctions, vimentin-containing filaments replace intermediate cytokeratin filaments in mesenchymal-like cells, promoting migration and invasion (Thiery, 2002). Vimentin is overexpressed in several types of cancer, especially in basal-like breast carcinomas; in addition, its expression correlates with poor prognosis in triple-negative breast cancer patients (Satelli and Li, 2011; Yamashita et al., 2013).

2.1.3 External components surrounding carcinomas determine the modes of cancer invasion

The tumour environment is essential for determining invasiveness and inducing EMT. Tumour cells in contact with the stroma interface show increased expression of EMT markers (Franci et al., 2006). Stromal cells are also important in promoting cancer invasion, as observed in tumour-associated macrophages (TAM), which contribute to cancer cell intravasation and therefore metastasis (Ishihara et al., 2013; Robinson et al., 2009); or cancer-associated fibroblasts (CAFs) that play a supporting role in mechanosensing and ECM remodelling (Angelucci et al., 2012; Calvo et al., 2013).

Mammary gland is formed by a bi-layered epithelium laid on basement membrane (BM) and surrounded by collagen-rich connective tissue, blood and lymph vessels, and adipose tissue (Fig. I3). Interstitial tissue (constituted by ECM and stromal cells such as fibroblasts or immune cells) in the gland contains type I collagen and interconnected glycoproteins forming a dense and heterogeneous fibrillar tissue. However, adipose tissue is rich in type IV collagen, laminin and perlecan that constitute a BM surrounding adipocytes (Bissell and Radisky, 2001; Gritsenko et al., 2012). Cells from the normal mammary gland express a variety of integrins, hemidesmosomal junction proteins and E-cadherin, maintaining a strong adhesion between them and to the ECM.

Cancer cells can migrate individually or collectively through the stroma and the vessels. Both types of migration have been visualised *in vivo*, but to date how this is regulated remains unclear. While individual migration appears faster than collective

migration and involves mostly blood vessels (Condeelis and Segall, 2003; Giampieri et al., 2009), collective migration has been observed preferentially in lymph vessels (Giampieri et al., 2009). In breast cancer, ductal carcinoma cells remain connected invading collectively in strands that progress through the ECM aggressively (Brennan et al., 2010; Jeschke et al., 2007); whereas in lobular carcinoma cells most cell junction proteins are down regulated (Yoder et al., 2007). Still, invasive lobular carcinomas invade mostly collectively as thin multicellular sheets and strands following collagen fibres/ structures (Gritsenko et al., 2012).

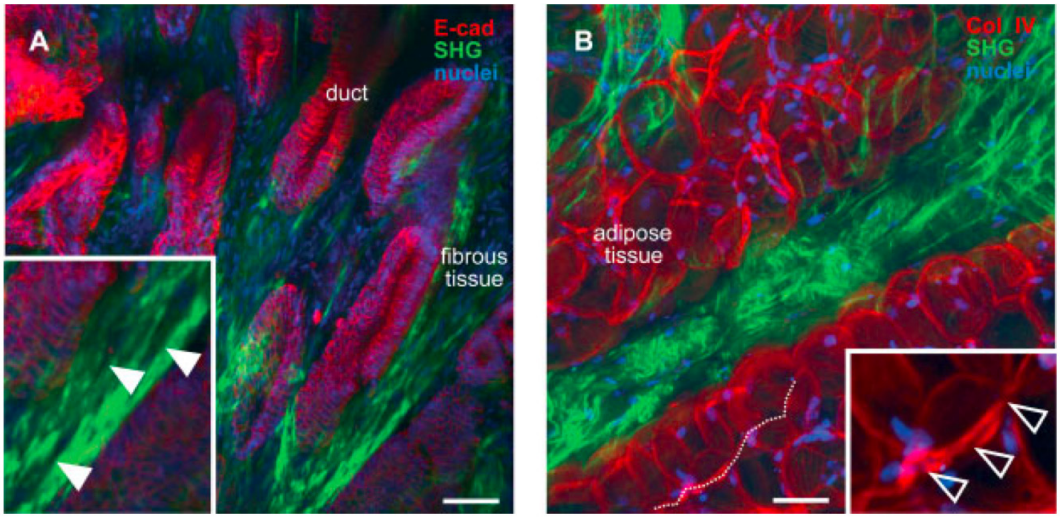

Figure I3: 3D reconstruction of human mammary gland tissue. Images show 3D-projections from 200µm-thick sections. (A) Ducts were stained for E-cadherin (red) and nuclei (DAPI, blue). Fibrillar collagen was visualised using Second-Harmonic Generation (SHG, green). (B) Adipose tissue visualised using anti-type IV collagen (red), fibrillar collagen (SHG, green) and DAPI (blue). Bars: 100µm. From (Gritsenko et al., 2012).

During cancer invasion, ECM remodelling —by individual or collective invasion— can occur via cell contraction (amoeboid invasion) or proteolytic cell invasion (mesenchymal invasion). This depends on tissue structure and cell morphology. The influence of tissue structure is defined by chemical composition, fibre crosslinking grade (which determines tissue geometry), fibre alignment, and density (directly related to pore size). Adaptation of cell morphology in response to tissue structure depends on volume and deformability of nucleus and cytoplasm, which are greatly influenced by the actomyosin cytoskeleton (Wolf and Friedl, 2011).

2.2 The actin cytoskeleton

Actin filaments, microtubules and intermediate filaments constitute the cytoskeleton. Microtubules are composed of α/β tubulin heterodimers and are involved mainly in cell division, vesicle trafficking and stabilisation of membrane protrusions (Alberts, 2008). Intermediate filaments (e.g., keratin, vimentin or lamin) play different roles in the cell: mechanical force, disassembly of the lamina and nuclear envelope, organelle anchorage, or cell-cell and cell-ECM adhesion (Alberts, 2008). Due to the interests of our laboratory, we focused on the role of actin-binding proteins and regulators of the actin cytoskeleton in cancer cell invasion.

Actin filaments (F-actin) are constituted of asymmetric polymerised globular actin monomers (G-actin, 42 kDa). This asymmetry is preserved in actin filaments, which have a (-)-end (slow growth) and a (+)-end (fast growth). F-actin formation is mediated by hydrolysis of adenine nucleotide triphosphate (ATP) to adenine nucleotide diphosphate (ADP). When free G-actin is bound to ATP, its binding to the (+)-end of the filament is favoured, whereas when ATP-G-actin is joined to the filament, ATP is hydrolysed, promoting detachment of the ADP-G-actin monomer (Wanger et al., 1985).

The actin cytoskeleton is involved in proliferation, cell shape, cell locomotion and invasion, phagocytosis and endocytosis, and cell growth (Dominguez and Holmes, 2011). These processes require contractile forces to drive changes in morphology or to generate the necessary force to protrude and retract the cell rear, allowing locomotion (Friedl and Wolf, 2009).

2.2.1 Actin-binding proteins

Many cell proteins are able to bind G-actin and/or F-actin, thus regulating actin polymerisation and its cell distribution. According to their function, actin-binding proteins can be classified as follows (Winder and Ayscough, 2005):

- Actin-nucleating: actin polymerisation is energetically unfavourable until there is a nucleus of at least three monomers. Nucleating factors promote this event and

increase the polymerisation rate. These proteins can form new filaments from the side of pre-existing filaments or by severing other filaments. The **Arp2/3** complex (actin-related proteins 2 and 3) acts as an actin-nucleating factor, creating branched filaments.

- Regulators of filament growth:
  - Capping proteins such as **tensin** block addition of new monomers, which reduces the overall length of the filament, favouring actin dynamics.
  - Severing proteins weaken non-covalent unions between actin molecules to break the filament. This is the case of **gelsolin** that, in addition to severing filaments, also acts as a capping protein.
  - Dissociating proteins include **ADF/cofilin**, which binds to ADP-F-actin and promotes dissociation of ADP-actin and depolymerisation.
  - Stabilizing proteins like **tropomyosin**, which protects actin from severing and regulates filament interaction with myosin.
- Monomer-binding proteins bind to ADP-G-actin once it is released from the filament, facilitating nucleotide exchange from ADP to ATP (such as **profilin**), and deliver the monomer to barbed ends or nucleating factors to support polymerisation (e.g., profilin, **WASP** (Wiskott-Aldrich syndrome protein) or **WIP** (WASP-interacting protein)).
- Actin-bundling proteins contribute to the alignment of actin filaments (tight or loose), as is the case of **fascin**, **fimbrin** or **F-actinin**.
- Actin-crosslinking proteins allow perpendicular organisation of F-actin. Among these proteins are **filamin** and **spectrin**.

Other actin-binding proteins use actin as a scaffold or tracking support instead of regulating actin dynamics (Winder and Ayscough, 2005):

- Myosins are molecular motors involved in contractility and generation of tension; they track on actin and are also regulated by ATP hydrolysis.
- Membrane anchors such as **talin** and **vinculin** that connect the actin cytoskeleton to cell adhesion receptors (e.g., integrins).
- Cytoskeletal linkers bind actin cytoskeletal components to microtubules, intermediate filaments or both, as is the case of **plectin**.

2.2.2 WASP-interacting protein family

WASP family members are key regulators of actin polymerisation. Through activation by members of the Rho-GTPase family (Cdc42, Rac and Rho), they interact directly with the Arp2/3 complex, and promote actin polymerisation (Machesky and Insall, 1998). WASP and its close homologue N-WASP (neural-WASP) are activated and/or localised by direct interaction with Cdc42 (Rohatgi et al., 1999), whilst the three members of the SCAR-WAVE (suppressor of cAMP receptor/WASP-family verprolin homology protein) subgroup are indirectly activated and/or localised by Rac (Eden et al., 2002; Etienne-Manneville and Hall, 2002). Other members of this family are WASH, WHAMM and JMY (Campellone and Welch, 2010; Rottner et al., 2010).

The mammalian family of WASP-interacting proteins (WIP) consists of three known members, CR16 (corticosteroids and regional expression 16), WICH/WIRE (WIP-CR16 homologous/WIP-related) and WIP itself (Fig. I4). These proteins bind to G-actin at their N-terminal verprolin (V) homology domain and stabilise F-actin. WIP family proteins bind N-WASP (and also WASP in the case of WIP) through a domain situated at their C-terminal region (Aspenstrom, 2002; Ho et al., 2001; Kato et al., 2002; Sasahara et al., 2002).

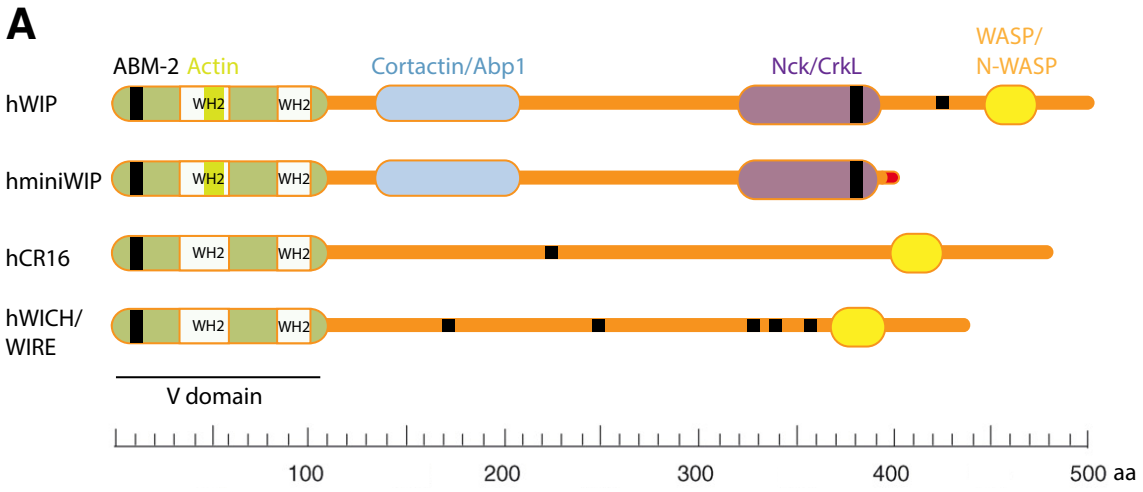

Figure I4: Human WIP family proteins. The WIP family includes WIP, CR16 and WICH/WIRE. All members share a similar structure composed of a verprolin homology domain (V domain) that includes two WASP-homology 2 (WH2) domains for actin binding. The V domain is followed by multiple proline-rich motifs, shown in WIP to bind cortactin and the actin-binding protein (Abp-1) or the adaptors Nck or CrkL, and finally, an (N-)WASP-binding site. Mini-WIP is a WIP isoform that lacks the (N-)WASP-binding site. WIP family proteins have between two and six actin-based motility 2 domains (ABM-2) for profilin binding (Garcia et al., 2012).

2.2.2.1 CR16

Human CR16 was first described as a glucocorticoid-regulated brain protein (Nichols et al., 1990). Its sequence —483 amino acids (a.a.) long— is similar to that described for WIP (25% identity) (Anton et al., 2007). CR16 functions remain mostly unknown. It is expressed mainly in brain and testis, but no deficiency-related effect was found in the central nervous system; in contrast, knock-out mice show male-specific sterility due to abnormal spermatogenesis by Sertoli cells (Suetsugu and Takenawa, 2003).

2.2.2.2 WICH/WIRE

Human WICH/WIRE protein, whose name derives from its simultaneous discovery by two groups (Aspenstrom, 2002; Kato et al., 2002), is 440 a.a. long and shares 30% similarity with WIP (Anton et al., 2007). It plays different roles in the cell, dependent or independent of N-WASP activity. In association with N-WASP, WICH/WIRE mediates actin cytoskeleton reorganisation to promote formation of stress fibres, filopodia and ruffle-like protrusions in porcine aortic endothelial cells (PAE) (Aspenstrom, 2004), and drives actin filament crosslinking (Kato and Takenawa, 2005). WICH/WIRE also participates in endocytosis of the platelet-derived growth factor receptor beta (PDGFRβ) in transfected PAE cells (Aspenstrom, 2004) and in integrity of the zonula adherens junctions in Caco-2 cells, forming a complex with N-WASP and E-cadherin, and linking cadherin junctions to the actin cytoskeleton (Kovacs et al., 2011).

Independently of N-WASP interaction, WICH/WIRE induces filopodia in mouse embryonic fibroblasts through the insulin receptor substrate p53 (IRSp53) and is dependent on Cdc42 activation (Misra et al., 2010a).

2.2.2.3 WIP

Human WIP is a proline-rich, 503 a.a. protein that is ubiquitously expressed, but it is found in higher levels in haematopoietic cells (de la Fuente et al., 2007; Ramesh et al., 1997). Two other WIP forms have been described to date, Prlp2 and mini-WIP (Koduru et al., 2007). Prlp2 expression originates from alternative splicing of one of

the last exons of the *WIPF1* gene, but this seems to be an infrequent event and little is known of the possible functions of this isoform in the cell (Anton et al., 2007). Mini-WIP results from truncated transcription of *WIPF1*, resulting in a 403 a.a.-long protein that lacks the C-terminal WASP-binding domain (WBD). Mini-WIP is expressed mainly in peripheral blood cells (Koduru et al., 2007).

WIP controls actin cytoskeleton dynamics by direct interaction with G- and F-actin (Martinez-Quiles et al., 2001), and via other regulatory proteins such as cortactin (or the blood cell variant HS-1), Nck (non-catalytic region of tyrosine kinase adaptor protein), CrkL and profilin (Anton et al., 2007). The best-characterised roles of WIP are linked to its interaction with WASP and N-WASP (we will refer to both proteins as (N-)WASP hereafter). WIP recruits (N-)WASP to specific subcellular locations (Chou et al., 2006; Sasahara et al., 2002), regulates their activity, and promotes WASP stability, protecting it from degradation by calpain and proteasome in immune system cells (Chou et al., 2006; de la Fuente et al., 2007). Most WIP and (N-)WASP remain in complex (80%) (de la Fuente et al., 2007; Sasahara et al., 2002), in which WIP preserves (N-)WASP in an auto-inhibited conformation (Kim et al., 2000; Miki et al., 1998). By promoting the (N-)WASP inactive form, WIP regulates its activation by Cdc42 and PIP_2 (phosphatidylinositol 4,5-bisphosphate) (Martinez-Quiles et al., 2001; Prehoda et al., 2000).

WIP has diverse roles in many different cell types. Based on its expression in lymphoid cells, WIP is critical for immune cell function, as its absence affects proliferation and correct activation and migration of T, B and dendritic cells (Anton et al., 2002; Banon-Rodriguez et al., 2013; Gallego et al., 2006; Le Bras et al., 2009). WIP is also involved in immune synapse formation in T cells, and correct polarisation and transport of lytic granules to the synapse in NK cells (Anton et al., 2002; Krzewski et al., 2008) as well as phagocytic cup formation in macrophages (Tsuboi and Meerloo, 2007). In non-immune cells, WIP also has numerous functions. It is important for cell adhesion, spreading and migration of primary and NIH3T3 fibroblasts (Banon-Rodriguez et al., 2013; Lanzardo et al., 2007), and it negatively regulates murine neuritogenesis *in vitro* and *in vivo* (Franco et al., 2012). In addition, the WIP homologue verprolin is responsible for endocytosis and actin reorganisation in yeast (Thanabalu et al., 2007) and WIP plays a critical role during pathogen infection by contributing to actin tail generation by vaccinia virus and

some bacteria (Lommel et al., 2004; Moreau et al., 2000).

WIP is also a central factor in development and disease. As observed in patients with Wiskott-Aldrich syndrome (WAS) (in which WASP is mutated), a mutation in the *WIPF1* gene originates an immune deficiency whose symptoms resemble those of WAS. In this single patient, WASP levels were reduced due to diminished WIP (Lanzi et al., 2012). Eight patients with micro-deletions in 2q31.1 —where the smallest overlapping region correlates with the *WIPF1* gene— showed symptoms of developmental delay, growth retardation or microcephaly in at least half of the cases (Mitter et al., 2010). The way these non-immune symptoms are caused by a WIP expression defect, as well as their potential link to WIP function in neuron development, are topics under research.

2.2.3 WIP-binding proteins

2.2.3.1 N-WASP

While WASP is highly expressed in haematopoietic cells, N-WASP is expressed ubiquitously, and localises mostly in cytoplasm, lamellipodia and nucleus (Nakagawa et al., 2001; Suetsugu and Takenawa, 2003). Like the other family members, N-WASP has a WCA domain formed by the V domain (see section 2.2.2) that binds actin, and a cofilin and acidic (CA) region that binds the Arp2/3 complex (Miki et al., 1996). In addition to its interaction with the Arp2/3 complex, N-WASP operates as a scaffold to synchronise signals from small GTPases, tyrosine kinase receptors, and cytoskeletal proteins (Miki et al., 1998). N-WASP is implicated in clathrin-dependent and -independent endocytosis (Lommel et al., 2001; Yarar et al., 2007), dorsal ruffle formation in primary fibroblasts (Legg et al., 2007), generation of lamellipodia (Nakagawa et al., 2001) and cell invasion (Calle et al., 2008; Yamaguchi et al., 2005).

2.2.3.2 Cortactin

Cortactin is a widely expressed protein; through its C-terminal SH3 (Src-homology 3) domain (Kirkbride et al., 2011), it interacts with the Arp2/3 complex, F-actin and other proteins such as Src family kinases, Abl, p21-activated kinase 1 (PAK1) and Nck. WIP

also binds to cortactin through its SH3 domain, and both proteins coincide at the cell periphery (Kinley et al., 2003). Cortactin has important functions in cell motility; it acts as a marker of lamellipodia and affects their persistence and stability (Bryce et al., 2005; van Rossum et al., 2006), as well as cell spreading and assembly of focal complexes (Bryce et al., 2005). Cortactin also regulates dynamics of invasive protrusions such as invadopodia and podosomes, as well as trafficking of metalloproteinases in these structures and dendritic spines (reviewed in (Kirkbride et al., 2011)). Cortactin is highly expressed in breast carcinomas (Clark et al., 2009; Schuuring et al., 1992), underlining its importance in cancer progression.

2.2.3.3 Nck

The widely-expressed adaptor Nck proteins (Nck1 and Nck2) are mostly cytosolic. They bear one SH2 domain and three SH3 domains, through which they interact with several proteins including Abl, FAK, PAK1 and (N-)WASP (Buday et al., 2002). Nck contributes to Arp2/3 complex-dependent actin polymerisation by interacting with (N-) WASP and WIP (see section below). Nck participates in cell migration, since it contributes to chemotaxis in response to PDGF and ruffle formation (Banon-Rodriguez et al., 2013; Ruusala et al., 2008), in cell adhesion (Chaki et al., 2013; Ruusala et al., 2008), invasion (Stylli et al., 2009) and cell infection by vaccinia virus (Donnelly et al., 2013), many of the functions identified for WIP.

2.2.4 Arp2/3-mediated actin polymerisation

Although the Arp2/3 complex itself can nucleate actin, this reaction is unfavourable and needs Arp2/3 complex interaction with nucleation-promoting factors (NPF) such as (N-)WASP to facilitate this process (Higgs and Pollard, 1999; Rohatgi et al., 1999). (N-)WASP activation promotes a conformational change that activates the Arp2/3 complex (Prehoda et al., 2000), and presents ATP-G-actin to the Arp2/3 complex, allowing nucleation of a newly-branched filament (Goley and Welch, 2006). WIP, which in resting cells is bound to (N-)WASP, is phosphorylated after cell activation, enabling (N-) WASP activation by Cdc42 and PIP_2 that leads to activation of the Arp2/3 complex (Higgs and Pollard, 1999; Prehoda et al., 2000; Sasahara et al., 2002). Recruitment of Nck to

both (N-)WASP and WIP is necessary to activate the Arp2/3 complex efficiently (Ditlev et al., 2012).

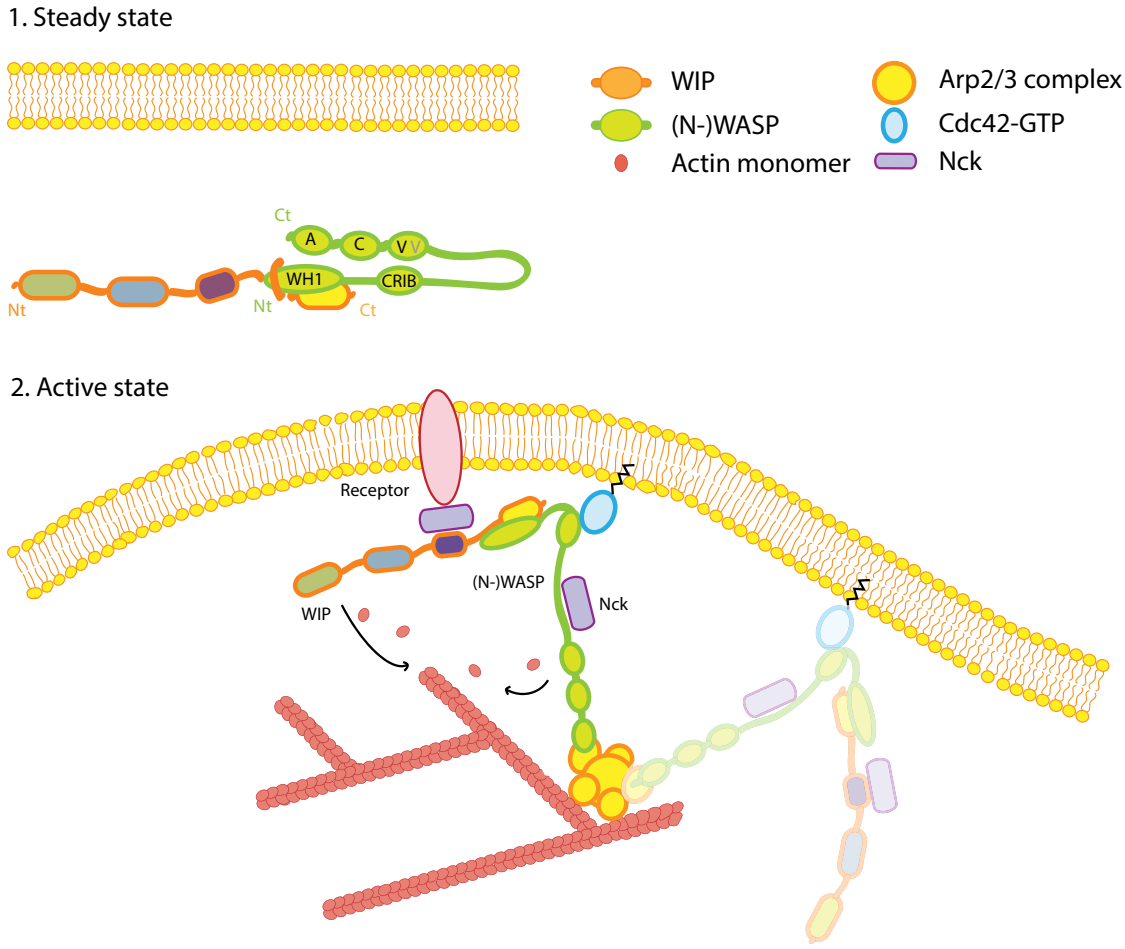

Figure I5: Model of WIP/(N-)WASP complex activation. (1) In resting cells, WIP and (N-)WASP form a cytoplasmic complex. WIP wraps around the WH1 (WASP-homology 1) domain of (N)WASP to promote the inactive conformation. (2) Following cell stimulation, WIP binding to adaptor molecules (CrkL or Nck) recruits the complex to the membrane. The combination of WIP and (N-)WASP phosphorylation with Nck and Cdc42-GTP binding to (N-)WASP releases intramolecular interactions and exposes the VCA (verprolin-cofilin-acidic region) domain. Once (N-)WASP is activated, the VCA domain interacts with actin monomers and activates the Arp2/3 complex, leading to branched actin filament formation. A recent model suggests a 4:2:1 stoichiometry for Nck/N-WASP/Arp2/3 (Ditlev et al., 2012). Nt: N terminus; Ct: carboxyl terminus (Garcia et al., 2012).

2.3 Actin-rich protrusions drive invasion

Subject to the nature and composition of the surrounding ECM, cells develop diverse protrusions during invasion that depend on actin nucleation. During amoeboid migration, cells thus develop filopodia, lamellipodia and blebs to allow migration through

the surrounding tissue, “squeezing” across the fibres that form the ECM (Charras and Paluch, 2008; Friedl and Wolf, 2003; Nurnberg et al., 2011). To overcome barriers such as the ECM or BM, however, mesenchymal cells usually require specialised structures with proteolytic activity, e.g., podosomes and invadopodia (together termed invadosomes (Linder, 2009)). These pseudopods consist of modified adhesion structures that protrude from areas of the cell in contact with the matrix. Whereas podosomes are dynamic and develop during physiological processes such as inflammation, invadopodia are exclusive to cancer cells, and tend to be larger and have more stable dynamics (Linder et al., 2011; Murphy and Courtneidge, 2011). An actin core surrounded by adhesion and scaffolding proteins, metalloproteinases and kinases constitutes both forms of pseudopods (Gimona et al., 2008; Linder et al., 2011), although organisation varies between these structures. Proteins such as the Arp2/3 complex, N-WASP or cortactin are essential for podosome and invadopodium function (Calle et al., 2008; Clark et al., 2007; Yamaguchi et al., 2005) and together with F-actin, serve as markers to identify these structures.

Invadosomes share components with focal adhesions (FA); although these latter structures are traditionally associated with cell adhesion, contractility and migration, they have been distinguished only recently as proteolytic structures (Wang and McNiven, 2012). The latest studies and new advances in cell imaging in 3D systems have raised new questions as to whether the origin of invadosomes and FA differs *in vivo.* Recent publications support the hypothesis that FA are in fact precursors of invadopodia, where proteins such as Src and focal adhesion kinase (FAK) would facilitate recruitment and activation of invadopodial components such as N-WASP or cortactin (Oikawa et al., 2008).

Development of actin-rich structures is greatly influenced by ECM composition, especially in the case of FA, which require force and tension to develop; this depends directly on matrix stiffness and physical organisation as well as on intracellular contractility (reviewed in (Harunaga and Yamada, 2011) and (Wolf and Friedl, 2011)). This fact indicates that the methods used to study these structures can have considerable impact on their visualisation. Invadosomes and FA have been widely characterised in rigid 2D systems in which the matrix is situated on only one side of the cell, but analyses performed in 3D systems show marked differences in the way cells protrude and migrate (reviewed in (Jayo and Parsons, 2012)) (Fig. I6). Some studies have corroborated the existence

of FA in different 3D systems (reviewed in (Harunaga and Yamada, 2011)), although no clear evidence confirms their presence *in vivo*. In contrast, a publication supports the development of invadopodia *in vivo* (Gligorijevic et al., 2012).

	2D	3D		
ECM features	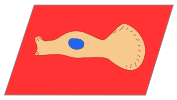 ECM-coated surface	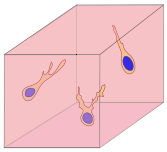 Matrigel/Collagen gels	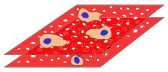 Mesenteric native basement membrane	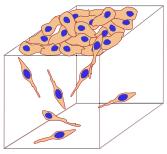 Organotypic culture
Structure	Non-fibrillar	Non-fibrillar/fibrillar	Fibrillar	Fibrillar modified
Stiffness	Very high	Medium (concentration-dependent)	High	High
Pore size	No pores	Small pores	Large pores	Large pores plus stromal cell-made tracks
Composition	Controllable	Type IV collagen, laminin, proteoglycans, etc/type I collagen	Type IV collagen, laminin, proteoglycans, etc	Type I collagen and stromal cell deposition
FA composition	β_1, β_3 integrins, talin, paxillin, vinculin, pFAK, VASP	β_1 integrin/β_1, paxillin, vinculin	β_1 integrin, talin, paxillin, vinculin (?)	Unknown
References	Reviwed in (Scales and Parsons, 2011)	(Poincloux, Collin et al. 2011; Hakkinen, Harunaga et al. 2011; Kubow and Horwitz 2011)		(Sabeh, Ota et al. 2004; Timpson, McGhee et al. 2011a; Timpson, McGhee et al. 2011b

Figure I6: In vitro models for the study of cell invasion: composition and structure

2.4 Regulation of invasion and cell motility in cancer cells

Invadopodia and FA share common components, some of which are signal transducers and actin dynamics regulators, as described above. This is the case of integrin receptors, which interact directly with the ECM and allow communication between the matrix and the cell. Expression of integrin β1 that localises at FA and invadopodia is necessary for invadopodium formation, while its downregulation fosters development of FA (Destaing et al., 2010). Integrin activation initiates a signalling cascade that promotes activation of FAK and Src kinases; this complex is involved in regulation of FA and invadopodium dynamics by controlling FA disassembly and invadopodium assembly (Chan et al., 2009; Oikawa et al., 2008). At FA, autophosphorylation of FAK in its tyrosine (Tyr)397 residue promotes FAK binding to Src (and activation of Src Tyr416; Fig. I7 A) and other signalling molecules that mediate cellular events such as survival, proliferation,

migration and invasion (Guan, 2010). Absence of FAK induces invadopodium formation due to release of active Src, which allows activation of invadopodial components (Chan et al., 2009). FAK is nonetheless necessary to recruit Src to FA and promotes their disassembly, as well as activating Src-dependent proteins such as Tks5 and cortactin, which are involved in developing invadopodia and podosomes (Burger et al., 2014; Oikawa et al., 2008; Oser et al., 2009; Stylli et al., 2009).

Tks5 and cortactin interact with major regulators of the actin cytoskeleton such as Nck, N-WASP, WIP and the Arp2/3 complex (Kinley et al., 2003; Oikawa et al., 2008; Stylli et al., 2009; Yamaguchi et al., 2005). Tks5 and cortactin recruit Nck to invadopodia, which is essential for invadopodium development (Oser et al., 2010; Stylli et al., 2009) (Fig. I7 B). Cortactin is also able to recruit the Arp2/3 complex to invadopodia, inducing actin polymerisation (Oser et al., 2009; Tehrani et al., 2007); with N-WASP, it is essential for ECM degradation, as it recruits MT1-metalloproteinase (MT1-MMP) to the mature invadopodium (Clark et al., 2007; Yu et al., 2012) (Fig. I7 C). WIP interacts not only with Nck and cortactin, but also with Tks5 (Oikawa et al., 2008), suggesting that it has an important role during invadopodium formation.

WIP is located at the podosomes of immune cells, osteoclasts and endothelial cells (Chabadel et al., 2007; Chou et al., 2006; Moreau et al., 2003) and has a central role in correct podosome organisation and function (Banon-Rodriguez et al., 2011; Tsuboi, 2006). Exogenous WIP is located at invadopodia of WIP-GFP-expressing MTLn3 cells (Yamaguchi et al., 2005), but when our study was initiated, there was no evidence for the existence of endogenous WIP in these structures or for a specific function. N-WASP nonetheless contributes to invadopodium formation and degradation by invasive protrusions, thus regulating MT1-MMP secretion to invasive pseudopods (Gligorijevic et al., 2012; Yamaguchi et al., 2005; Yu et al., 2012). Whether N-WASP modulates ECM remodelling through WIP activation is still unknown, but WIP binding to N-WASP seems to be essential for invadopodium generation (Yamaguchi et al., 2005).

Recent publications show direct and indirect connexions between WIP and cancer cell invasiveness. As for other cytoskeletal proteins, *WIPF1* gene expression appears to be directly related to poor prognosis in colorectal cancer, breast cancer and glioma patients; it is co-expressed with a group of oncogenes that include c-myc and p53 (Staub

et al., 2009). WIP is upregulated after EMT induction of prostate cancer cells, as well as other genes involved in cell adhesion or integrin signalling, increasing cell migration and invasiveness (Gu et al., 2007). Although little is known concerning WIP association with invasive protrusions, its interaction with key contributors to the development and maturation of invadopodia indicates a role for WIP as a potential regulator of cancer cell invasion.

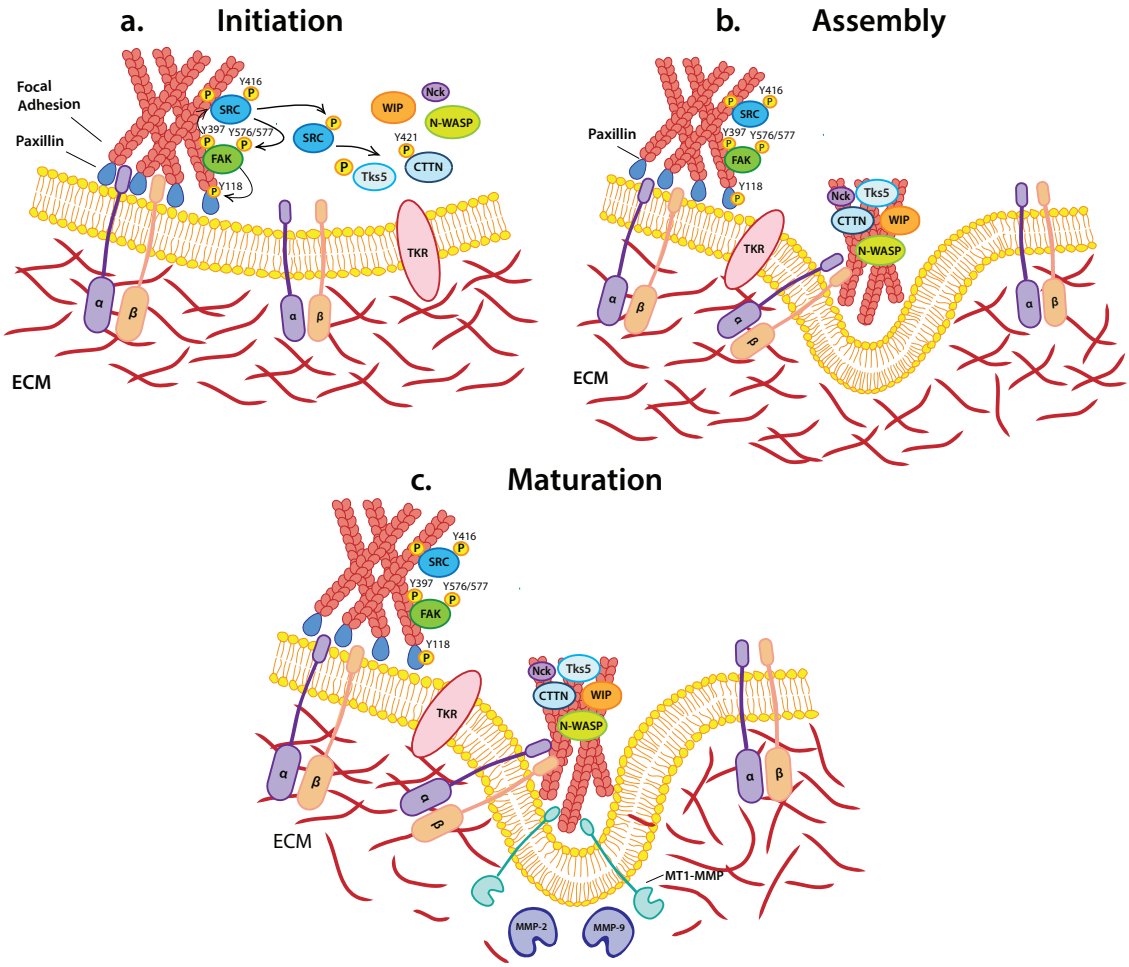

Figure I7: Sequential signals that drive invadopodium-mediated ECM degradation. (a) In response to ECM signals, pTyr397-FAK binds to and activates Src by phosphorylation of its Tyr416. Src activation allows phosphorylation of the FAK catalytic domain (Tyr576/577-FAK), which later activates paxillin and associated signalling pathways such as ERK. Free active Src also activates other substrates such as cortactin and Tks5. Active pTyr421-cortactin and Tks5 recruit Nck, WIP and N-WASP to initiate invadopodium formation. (b) A complex formed by cortactin, WIP and N-WASP localises at invadopodia and facilitates actin polymerisation. (c) Once the invadopodium has protruded towards the ECM, MT1-metalloproteinase (MT1-MMP) accumulates at the plasma membrane to activate other MMP (mainly MMP-2 and MMP-9) and degrade matrix fibres. Cortactin and N-WASP are implicated in MT1-MMP trafficking to the membrane of invasive protrusions. Adapted from (Murphy and Courtneidge, 2011).

Aims

3. AIMS

Previous publications and preliminary results from our laboratory supported a role for WIP in migration and development of invasive protrusions and its association with poor prognosis in some carcinomas. The main purpose at the outset of this study was thus to elucidate whether WIP contributes to cancer cell invasion and dispersion of tumour cells during metastasis, and therefore whether WIP might be used as a diagnostic marker or therapeutic target molecule.

To achieve this goal, we established the following objectives:

1. **To determine whether WIP expression in established human breast cancer cell lines correlates with their invasive capacity**

2. **To define the localisation of endogenous WIP at invadopodia and other invasive protrusions**

3. **To determine the WIP contribution to the invasive behaviour of BCC by:**
    a. Overexpressing WIP in poorly invasive BCC
    b. Silencing WIP expression in invasive BCC

4. **To examine the molecular mechanisms that regulate the interaction between WIP and associated proteins** (WICH/WIRE, N-WASP, cortactin and Nck) **and their contribution to invasive structures during cancer progression**

5. **To study the association between WIP and EMT by analysing epithelial and mesenchymal markers in BCC that overexpress or are silenced for WIP**

Materials and Methods

4. MATERIALS AND METHODS

4.1. CELL CULTURE

4.1.1 Breast cancer cell lines

In this study, we used the following breast cancer cell lines (BCC): MDA-MB-231 (American Type Culture Collection), MDA-MB-157 and Hs578T (provided by Dr Santos Mañes, CNB-CSIC, Madrid, Spain); MDA-MB-468 (provided by Dr Francisco Wandosell, CBM, Madrid, Spain); MCF-7 (provided by Dr Ana Cuenda, CNB-CSIC); T47D, BT474 and MCF10A (provided by Dr Isabel Mérida, CNB-CSIC). This collection gathers a wide range of cell lines of diverse tumour origin, gene expression and invasive behaviour. Some clinical and pathological features as well as culture conditions of these cell lines are detailed in Table M1 (Neve et al., 2006). Cells were cultured at 37°C and 5% CO_2. All culture media were supplemented with 2 mM L-glutamine and antibiotics (1,000 U/ml penicillin and 0.1 mg/ml streptomycin) (all from Sigma).

4.1.2 Generation of lentiviral particles

Lentiviral particle stocks were produced in human 293T cells by co-transfecting the envelope plasmid pMD.2G, the packaging plasmid pCMVR8.91, and one of the following transfer vectors: pLKO.1-puro, pLKO.1-Neo-CMV-tGFP or pLNT/Sffv-eGFP, (Table M2) (Zufferey et al., 1997). The 293T cells were cultured in complete DMEM and, after reaching 80% confluence, transfected with polyethylenimine (PEI, Sigma). For each vector, OptiMEM (serum-free medium, Gibco) was used to dilute PEI (25 µg/ml) and DNA, and the mixtures were incubated (5 min, room temperature (RT)). Final concentrations of DNA plasmids were 7.5 µg/ml of pCMVR8.91, 2.5 µg/ml pMD2G and 10 µg/ml transfer vector. PEI and DNA were mixed and incubated (15 min, RT). After gently washing cells in OptiMEM, growth medium was removed and dd the PEI-DNA mixture added to the cells (4 h, 37°C). The transfection mixture was replaced with fresh culture medium and incubated (48-72 h, 37°C), after which the supernatant containing lentiviral particles was collected and centrifuged (1,000 g, 5 min) to remove remaining cells, filtered (0.45 µm), aliquoted and stored at -80°C.

Cell line	Gene cluster	ER/PR/HER2 expression	Tumour type	Culture medium
BT474	luminal	+/+/+	IDC	RPMI, FBS, In, $NaHCO_3$
HS578T	basal B	-/-/-	IDC	DMEM, FBS, In
MCF10A	basal B	-/-/-	F	DMEM/F12, HS, EGF, HC, In
MCF7	luminal	+/+/-	IDC	DMEM, FBS
MDA-MB-157	basal B	-/-/-	MC	DMEM, FBS
MDA-MB-231	basal B	-/-/-	AC	DMEM, FBS
MDA-MB-468	basal A	-/-/-	AC	DMEM, FBS
T47D	luminal	+/+/-	IDC	RPMI, FBS, SP, $NaHCO_3$

Table M1: Clinical and pathological features of BCC used in this study. Tumour type: IDC, invasive ductal carcinoma; F, fibrocystic disease; MC, metaplastic carcinoma; AC, adenocarcinoma. Specific culture conditions: RPMI, Roswell Park Memorial Institute medium; DMEM, Dulbecco's Modified Eagle's Medium (both from Sigma); F-12, Ham's F12 nutrient mixture (Gibco); FBS, foetal bovine serum 10%; HS, horse serum 5% (both from Sigma); HC, hydrocortisone 0.5 mg/ml (Calbiochem); EGF, epidermal growth factor 20 ng/ml (Peprotech); In, insulin (10 µg/ml, Gibco); NaHCO3 0.075% (Sigma); SP, sodium pyruvate (1 mM, Sigma).

4.1.3 Generation of stable WIP and WIRE "knock-down" cells

For loss of function analysis, the expression of *WIPF1* (WIP, NCBI Reference Sequence NM_003387) or *WIPF2* (WICH/WIRE, NM_133264) genes was silenced via RNA interference expression. MDA-MB-231 cells were infected with lentiviral particles containing shRNA (small hairpin RNA)-encoding plasmids pLKO.1-puro (Sigma MISSION®) against various target sequences of WIP and WICH/WIRE genes (Table M2).

Gene target	ID	Sequence (5'-3')
WIP	#151	CCGGCAATACAGAGAAGCCTACCTTCTCGAGAAGGTAGGCTTCTCTGTATTGTTTTT
	#1388	CCGGCCTCCACCATCAACATCTATTCTCGAGAATAGATGTTGATGGTGGAGGTTTTT
	#676	CCGGCATTCAATCAAGTCCGCACAACTCGAGTTGTGCGGACTTGATTGAATGTTTTT
	#266	CCGGCCAATACTGGACAAACCTAAACTCGAGTTTAGGTTTGTCCAGTATTGGTTTTT
	#1430	CCGGCCATGTGAAGATGAGTGGGAACTCGAGTTCCCACTCATCTTCACATGGTTTTT
WICH/ WIRE	#29	CCGGCCGGTCTTTCTTGGATGATTTCTCGAGAAATCATCCAAGAAAGACCGGTTTTT
	#30	CCGGCCCGCCTACAACAGAGAGAAACTCGAGTTTCTCTCTGTTGTAGGCGGGTTTTT
	#31	CCGGGCGCCCTCTTACAGGACATTTCTCGAGAAATGTCCTGTAAGAGGGCGCTTTTT
	#32	CCGGCAGAGGATATATCCCAGCAAACTCGAGTTTGCTGGGATATATCCTCTGTTTTT
	#33	CCGGGCCACAGAGACACAATTCTTTCTCGAGAAAGAATTGTGTCTCTGTGGCTTTTT

Table M2: Sequences of shRNA-encoding plasmids used in this study

MDA-MB-231 cells at 50% confluence were infected using pLKO.1-puro-control (empty vector), pLKO.1-puro-shWIP or pLKO.1-puro-shWIRE lentiviral stocks in the presence of 5 µg/ml polybrene (Sigma) to increase viral infection efficiency (24 h, 37°C); the virus-containing medium was then replaced with fresh medium. At 48 h post-infection, 1 µg/ml puromycin (Sigma) was added to select efficiently infected cells. Cells were stably maintained in 1 µg/ml puromycin, with serial passages every 2-3 days.

For experiments in which WIP and WICH/WIRE were silenced, we performed sequential infections. Cells were first infected with pLKO.1-puro-control or pLKO.1-puro-shWIRE, which was less efficient in reducing protein expression, and stably maintained after antibiotic selection. Once cells grew stably, they were re-infected with pLKO.1-puro-control or pLKO.1-puro-shWIP. To avoid overcompensation due to reduction in protein expression, we performed experiments 48 h after the second infection.

4.1.4 Plasmid DNA amplification and transfection

4.1.4.1 XL2-Blue bacterial transformation

For bacterial transformation, 20 µl of XL2-Blue ultracompetent cells were thawed on ice and mixed with 50 ng DNA (20 min, 4°C), then heat-shocked (2 min, 37°C), followed by 1 min incubation on ice. Luria broth medium (LB, 50 µl) was added to the mixture and incubated (30 min, 37°C). Cells were seeded onto LB-agar containing plates with the appropriate selective antibiotic.

4.1.4.2 Plasmid DNA purification

The bacterial culture (200 ml) was grown in LB containing the selective antibiotic and processed for DNA purification using the PureLink HiPure Plasmid Filter Maxiprep Kit (Invitrogen) according to manufacture's instructions.

4.1.4.3 Protein expression in mammalian cells by nucleofection

DNA plasmids (Table M3) were transfected using the Amaxa Nucleofector system programmes X-013 (MDA-MB-231), X-005 (MDA-MB-468) and P-020 (MCF-7) according to manufacturer's instructions. Briefly, 80% confluent cells were harvested by trypsinisation, counted, and aliquots (1-2 x 10^6 cells) prepared for each plasmid. Cells were then pelleted and suspended in 100 µl solution V (Amaxa, Lonza) and 2 µg of the desired DNA for each aliquot. This mixture was transferred to nucleofection cuvettes and electroporated. Cells were rapidly diluted in culture medium, seeded into 6-well plates and incubated (37°C). Once the cells had attached to the plate, the medium was replaced by fresh medium and cultured (37°C). Cells were used for invasion experiments 24 h after transfection.

Protein	Vector	Bacterial resistance	Mammalian resistance	Origin
Src	pcDNA3	Ampicillin	G418	Dr J Martín-Pérez IIB-Alberto Sols, Madrid
DN-Src	pCI	Ampicillin	G418	Dr J Martín-Pérez IIB-Alberto Sols, Madrid
mCherry-WIP	pLNT/Sffv-mCherry	Ampicillin	-	Dr G Jones King's College London
eGFP-WIP	pLNT/Sffv-eGFP	Ampicillin	-	Dr G Jones King's College London
eGFP-WIP-ΔCBD (Δ110-170)	pLNT/Sffv-eGFP	Ampicillin	-	Dr G Jones King's College London
eGFP-WIP-ΔNBD (Δ321-415)	pLNT/Sffv-eGFP	Ampicillin	-	Dr G Jones King's College London
eGFP-WIP-ΔWBD (Δ450-503)	pLNT/Sffv-eGFP	Ampicillin	-	Dr G Jones King's College London
Flag-WIP	pCMV-Tag2A	Kanamycin	G418	Dr S Tsuboi Oyokyo Kidney Resh Inst
Flag-WIRE	pCMV-Tag2A	Kanamycin	G418	Dr S Tsuboi Oyokyo Kidney Res Inst
eGFP-mWIP	pEGFP-C3	Kanamycin	G418	Dr K Rottner University of Bonn

Table M3: Collection of DNA constructs used in this study

4.2 Invasion assays

4.2.1 Inverse invasion assay

Inverted invasion assays were performed as described (Hennigan et al., 1994). Briefly, 4-5 mg/ml Matrigel (BD BioScience) was allowed to polymerise in transwell inserts (Corning) for at least 1 h (37°C). Inserts were then inverted, and 5 x 10^5 cells seeded directly onto the outer filter surface and allowed to adhere (5 h) (Fig. M1). After serial washing by dipping inserts in serum-free DMEM to remove unattached cells, inserts were placed in 500 µl serum-free medium and, to create a chemotactic gradient, 100 µl

of 10% FBS-supplemented medium were added to the Matrigel-containing chamber (Fig. M1). Some experiments were performed with DMSO or the MMP inhibitor GM6001 (25 µM, Santa Cruz). At 72 to 96 h after seeding, cells were stained with the Calcein-AM viability marker (4 µM, Invitrogen) in DMEM (1 h, 37°C). Cells that did not cross the transfilter were removed with a tissue and the invading cells were visualised by confocal microscopy (Bio-Rad) using a 40x objective. Serial optical sections were captured at 10-µm intervals.

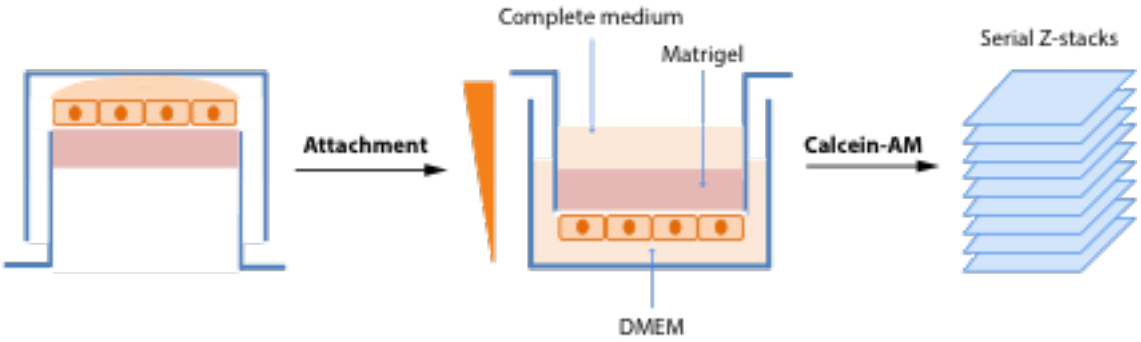

Figure M1: Inverse invasion assay. In a modification of traditional transwell-Matrigel inserts, cells were plated onto the outer side of the transfilter and inverted after cell attachment. Migration was promoted by adding complete medium onto a thick Matrigel layer. After several days invasion, live cells were stained with Calcein-AM and visualised by confocal microscopy.

The area covered by cells was measured in each section using the ImageJ software (US National Institutes of Health) plugin "Area Calculator" in 8-bit images (threshold 30-50/255). Relative invasion was calculated as the area covered by cells that invaded 20 µm or higher relative to total cell area of the Z-stack. At least three independent experiments in duplicate were performed for each sample.

4.2.2 Circular invasion assay

The circular invasion assay (CIA) was performed as described (Yu and Machesky, 2012). Cells were plated onto 35 mm micro-dishes using biocompatible silicon inserts (both from Ibidi) to generate a cell-free space (Fig. M2). After overnight incubation and removal of the insert, 250 µl 4.5-5.5 mg/ml Matrigel diluted in DMEM was overlaid onto the cell monolayer and allowed to polymerise (2 h, 37°C). After addition of growth medium to stimulate cell motility, cells were allowed to invade the polymerised Matrigel and imaged with a time-lapse microscope. Some experiments were performed in the

presence of DMSO or 25 µM GM6001. Cells were incubated in a humidified atmosphere with 5% CO_2 (24 h, 37°C) before fixation in 4% paraformaldehyde (PFA, MERCK) and immunofluorescence (IF) analysis.

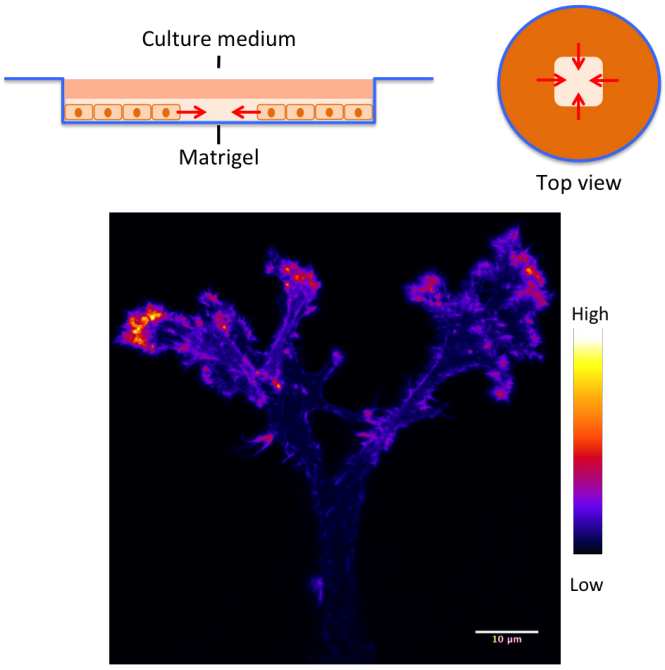

Figure M2: Circular invasion assay. Cells were cultured using a silicon insert that acts as a barrier, leaving an empty gap in the centre of the dish (top). After reaching confluence, the cell monolayer was covered by a thin layer of Matrigel. Once Matrigel polymerised, culture medium was added to promote migration. After the time-lapse imaging, cells were fixed and stained for F-actin (intensity of fluorescence, bottom) and other proteins. F-actin concentrated at the distal part of the protrusions, where active polymerisation is needed.

The cell-free area was measured at 6 h intervals using the ImageJ Freehand Selection tool. A minimum of four time-lapse positions were measured for each sample in at least three independent experiments. The increment of the area covered by cells was calculated for each time point and normalised to control cells at 18 h. To quantify elongation of invading cells, length/width ratio was calculated in 10-20 cells for each condition. Using the ImageJ Straight Line selection tool, we quantified length as distance from most distal protruding tip of the cell to the opposite base of the nucleus. Width was measured as the widest distance of the cell crossing the nucleus. Paxillin distribution was analysed as described in section 4.5.2.

4.2.3 Basement membrane invasion assay

Basement membranes (BM) were prepared as described (Hotary et al., 2006; Witz et al., 2001) by isolation from mouse peritoneum and mounted on 6.5-mm diameter transwells (Corning, Fig. M3), where they were sealed with a 50:50 wax:paraffin mixture.

After stripping the overlying mesothelial cells from the membrane using 1 N ammonium hydroxide (30 min) and washing with PBS (3.8 mM NaH_2PO_4, 16.2 mM Na_2HPO_4, 150 mM NaCl), BM were sterilised using 70% ethanol. On top of the BM, we seeded 2 x 10^5 (for quantification of degradation experiments) or 5 x 10^4 cells (to examine invadopodium formation) in 100 µl growth medium; 500 µl of the same medium were added to the bottom chamber. After 3-4 days invasion, samples were fixed and processed for IF. BM and cells were stained for type IV collagen, F-actin and DAPI and visualized by confocal microscopy (Fig. M3). Serial optical sections were captured along the BM at 2-µm intervals.

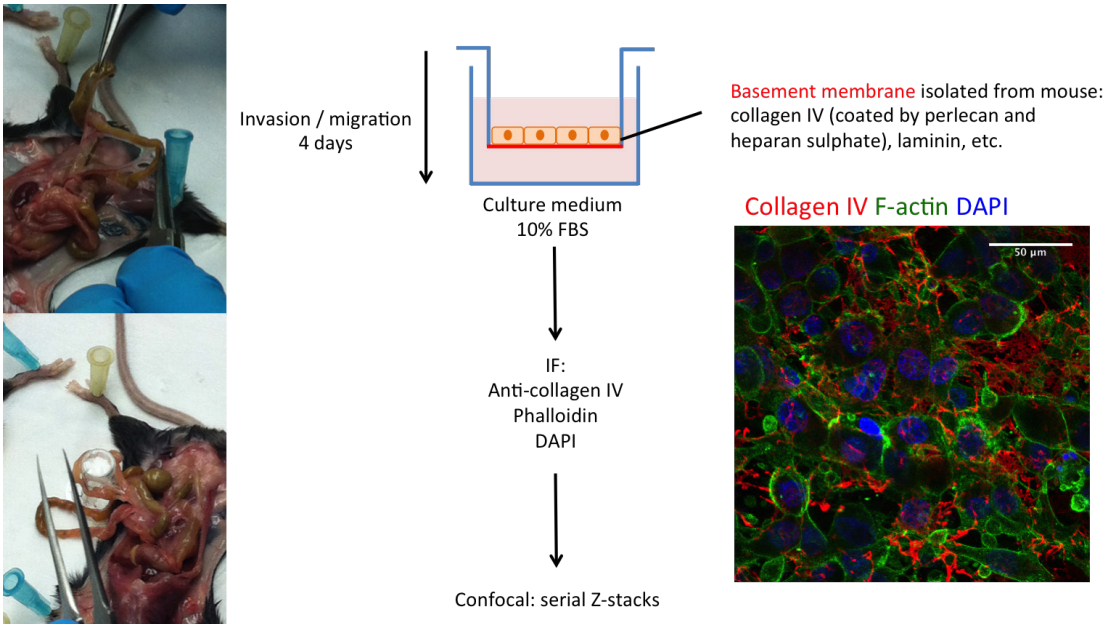

Figure M3: Isolation of murine basement membrane and assay for the study of cell invasion. BM were isolated from mouse mesothelium and mounted onto transwell inserts (left), replacing the original transfilter. After cell clearance of the BM, cancer cells were plated on top of the BM for several days and allowed to invade and cross the membrane. BM were then fixed and stained to visualise type IV collagen fibres (red) and cells (F-actin in green, nuclei in blue; right).

To characterise invasion in this system, we analysed two parameters: remaining type IV collagen in the BM and cell distribution along the BM. The amount of remaining collagen in the membrane was measured in 8-bit Z-projections using the ImageJ plugin Area Calculator (threshold: 30-50/255) and normalised to native membrane values. Cell distribution was analysed by manual counting of DAPI-positive nuclei using the ImageJ plugin Cell Counter at three sections of the BM: top (above the membrane), medium

(sunken cells surrounded by type IV collagen) and bottom (beneath the membrane). The percentage of cells in each section was calculated for each BM. Each parameter was quantified in duplicate samples from 3 to 5 images per experiment; at least three independent experiments were performed.

4.2.4 Fluorescent gelatin invasion assay

The ability of cells to form invadopodia and degrade the matrix was analysed using fluorescent matrix-coated dishes prepared as described (Bowden et al., 2001). Gelatin type A from porcine skin (2 mg/ml, Sigma) was diluted at 37°C in a buffer containing 50 mM $Na_2B_4O_7$ and 61 mM NaCl, pH 9.3, and subsequently labelled with rhodamine B isothiocyanate (final concentration 36 μg/ml; Sigma) by mixing (2 h, in the dark). Unbound dye was removed by extensive dialysis against PBS in the dark (2-3 days, RT). Acid-washed coverslips (1 M HCl) were coated with 80 μl pre-warmed rhodamine-gelatin and crosslinked with 0.5% glutaraldehyde (TAAB) in PBS (15 min). After washing with PBS, coverslips were quenched with 5 mg/ml sodium borohydride (3 min), followed by extensive washing with PBS. The coverslips were then sterilised with 70% ethanol (5 min) and incubated in serum-free medium (1-24 h) before use. Cells (2.5×10^4) were cultured on gelatin for 5-48h (depending on the cell line used), fixed and processed by IF (Fig. M4).

The number of **invadopodium-forming cells, degrading cells** and cells forming active invadopodia were calculated by examining 25 random fields imaged with a wide field microscope and a 63x objective. Invadopodium-forming cells were considered those that showed F-actin- and cortactin-positive dots ≤0.25 μm^2 at the ventral area of the cells. In the case of WIRE-deficient cells, this quantification was confirmed in confocal images to verify potential misreading in discriminating invadopodium-like structures from vesicles or other intracellular structures. Only cells completely or partially above the dark areas of gelatin degradation were considered degrading cells in this analysis.

Degraded area for each degrading cell was measured in images acquired as described above. Calculations were performed after subtracting a light background of 50 units and manually establishing a threshold to define degradation for each gelatin

image file. Percentage of degraded area was calculated relative to the cell area using the ImageJ plugin Synchronise Measure and normalised to controls. These measurements were made in at least 20 cells/condition of at least three independent experiments.

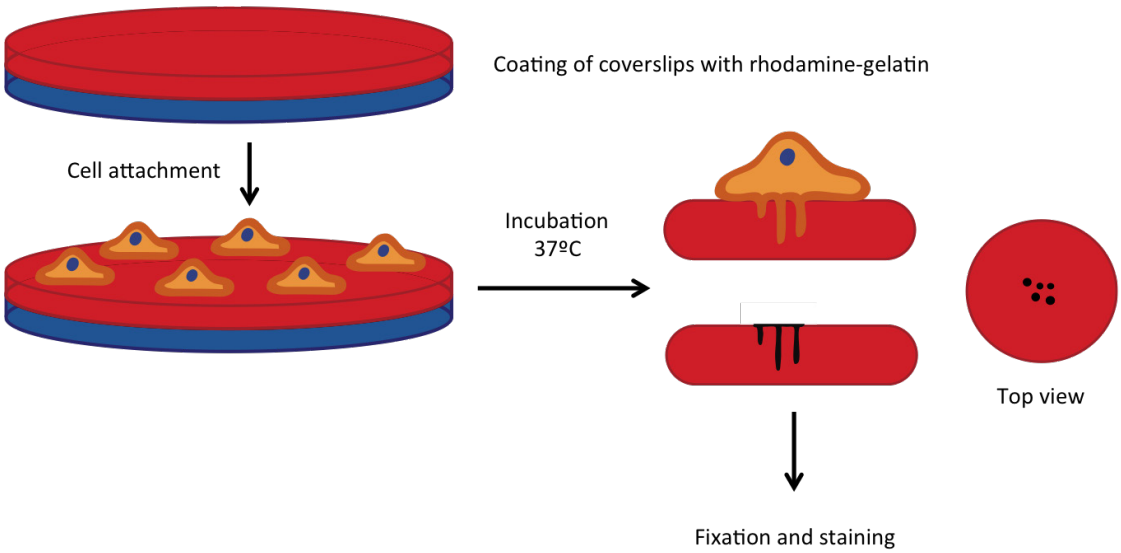

Figure M4: Fluorescent gelatin invasion assay. Gelatin was coupled to rhodamine B, after which glass coverslips were coated with fluorescent gelatin. The cells were cultured on gelatin and processed for IF using antibodies against invadopodium markers. The areas where cells emitted invadopodia through the matrix and successfully degraded it appear as dark spots in the gelatin.

4.2.4.1 Inhibition of invadopodium formation/maturation using different drug treatments

For experiments in which cells were plated onto fluorescent gelatin and treated with chemical inhibitors (Table M4), 2.5 x 10^4 cells were seeded in growth medium supplemented with 10 µM GM6001 to synchronise invadopodium formation, plus appropriate drug treatment or DMSO as vehicle if needed (protocol adapted from (Ayala et al., 2008) and Methods section from Invadosome Consortium website: http://www.invadosomes.org). After incubation with both inhibitors (1 h, 37°C), cells were washed extensively with growth medium to inactivate GM6001, and re-incubated with the desired inhibitor-supplemented medium.

Reagent	Target	Concentration/IC50	Origin
Cytarabine (AraC)	DNA synthesis	2 µM (DMSO)	Calbiochem 251010
Dasatinib	Src and Bcr-Abl kinases	5-20 nM (DMSO)	Dr J Martín-Pérez IIB-Alberto Sols, Madrid
GM6001	MMP family	10-25 µM (DMSO)	Santa Cruz Biotechnology sc-203979
Imatinib	Bcr-Abl, c-kit, PDGF-R, and Src	2µM (DMSO)	Selleckchem S2475
Okadaic acid	Protein phosphatases 1 and 2A	10 µM (DMSO)	Calbiochem 459618
PP2	Src kinases	5-20 µM (DMSO)	Dr J Martín-Pérez IIB-Alberto Sols, Madrid
Sodium fluoride	Protein phosphoseryl and phosphothreonyl phosphatases (PSP)	5 mM (H_2Od)	Sigma
Sodium orthovanadate	Tyrosine phosphatases	1-2 µM (H_2Od)	Calbiochem 567540
Wiskostatin	N-WASP	3 µM (DMSO)	BIOMOL International 253449-04-6
187-1	N-WASP	2 µM (H_2Od)	TOCRIS Bioscience 2067

Table M4: Enzyme inhibitors used in this study

4.3. Migration Assays

4.3.1 Random migration assay

For random migration experiments, 35 mm glass-bottom dishes or 6-well plates (MatTek) were coated with 10 mg/ml bovine fibronectin (in PBS; Calbiochem)(1 h, RT). After washing with PBS, 7 x 10^4 cells were seeded and cultured overnight, then imaged by time-lapse phase-contrast microscopy using a 20x objective for 5 h with 2-3 min time-steps before fixation in 4% PFA. To examine cell movement, velocity and persistence, we tracked 25 single cells for each condition using the ImageJ plugin Manual Tracking and analysed their trajectories using the plugin Chemotaxis (both developed by Ibidi).

To observe WIP localization in migrating cells, we used time-lapse fluorescence microscopy. Cells were first infected with pLNT-eGFP or pLNT-eGFP-WIP, and after 24 h, nucleofected with Red-LifeAct plasmid (Riedl et al., 2008) to visualise F-actin. At 24 h post-transfection (48 h post-infection), cells were trypsinised and plated on fibronectin-coated glass-bottom dishes and images acquired for 1h using a 2-3 min time-step.

4.3.2 Wound healing assay

In wound healing migration experiments, silicon inserts (Ibidi) were attached to 6-well plastic plates and 4.2 x 10^4 cells were seeded in each chamber in 70 µl growth medium (overnight, 37°C). Inserts were removed and fresh medium containing 2 µM AraC (Table M4) was added to inhibit proliferation. Time-lapse imaging was performed for 24 h using a phase-contrast microscope with a 20x objective, by image acquisition with a 10 min time-step. As described for CIA (section 4.2.2), the area covered by cells was measured at 5 h intervals using ImageJ Freehand Selection. The increase in cell-covered area was calculated for each time point and normalised to control cells at 15 h. Duplicates were analysed for each sample and 3 time-lapse positions were measured for each "wound"/replica in at least three independent experiments.

4.4 Immunoassays

4.4.1 Immunofluorescence

For IF analysis, fixed cells from glass coverslips, glass-bottom dishes or BM were permeabilised using 0.05% Triton X-100 (Panreac) in PBS. After washing in PBS, cells were incubated with Antibody Diluent blocking solution (DAKO) for at least 30 min, followed by primary antibody (overnight, 4°C) (Table M5), except anti-collagen IV antibody, which was incubated for 2-3 h at RT. After extensive washing in PBS, cells were incubated with secondary antibodies or fluorescent phalloidin (in DAKO Antibody Diluent; 45 min, RT) (Table M6). In some cases, cell nuclei were stained with DAPI or TO-PRO, which were diluted in PBS (10 min, RT). Coverslips, plates and BM inserts were mounted using Fluoromount-G (Southern Biotech).

4.4.2 Immunoblot (Western blot)

For Western blot (WB) analysis, cells were scraped into ice-cold lysis buffer (150 mM NaCl, 50 mM Tris-HCl pH 7.4, 1 mM EDTA, 1 mM EGTA, 0.1% Triton X-100), complete protease inhibitor cocktail and PhosSTOP phosphatase inhibitor cocktail (both from Roche). After 15 min incubation on ice, lysates were clarified by centrifugation (13600 g, 5 min, 4°C). Protein concentration was determined using a Bradford protein-assay (Bio-Rad) according to manufacturer's instructions.

Soluble lysates were diluted in 5X loading buffer (325 mM Tris-HCl pH 6.8, 10% SDS, 25% glycerol, 5% β-mercaptoethanol, 0.5% bromophenol blue) and boiled (5 min). Proteins were resolved by 8-10% SDS-PAGE (sodium dodecyl sulphate-polyacrylamide gel electrophoresis) in electrophoresis buffer (25 mM Tris pH 8.3, 192 mM glycine, 0.1% SDS) using Precision Plus Dual Color Standards molecular weight markers (Bio-Rad). Proteins were transferred to a 0.2 µm nitrocellulose membrane (Bio-Rad), previously equilibrated in transfer buffer (25 mM Tris pH 8.3, 192 mM glycine, 20% methanol), using a humid system (Mini Trans-Blot, Bio-Rad) at 120-140V (constant) for 90 min.

To avoid non-specific signal, membranes were incubated in blocking solution (5% dehydrated skim milk in PBS-T (PBS-0.05% Tween 20) or TBS-T (10 mM Tris-HCl pH 8, 150 mM NaCl, 0.05% Tween 20)). For analysis of phosphorylated proteins, 5 mM NaF and/or 2 mM Na_3VO_4 (Table M4) were added to the blocking solution. After overnight incubation with primary antibodies (in blocking solution, Table M5), membranes were washed in PBS-T or TBS-T and incubated with HRP (horseradish peroxidase)-conjugated secondary antibodies (1 h, RT) (Table M6). After extensive washing, the membrane was developed by a chemiluminiscence reaction using as substrates Western Lightning-ECL (Perkin Elmer) or Luminata Crescendo Western HRP Substrate (Millipore). Densitometry analyses were performed using ImageJ. Data were normalised to GAPDH and to control sample or the sample that gave maximum signal.

Antigen	Specificity	Isotype	MW (kDa)	Concentration	Origin
Arp2/3 complex	p34-Arc/ARPC2	Rb Pc IgG	34	WB: 10 µg/ml	Millipore #07-227
β-catenin	C-t β-catenin (a.a. 680-781)	Mo Mc IgG_1	92	WB: 1/1000 IF: 1/100	Santa Cruz Biotechnology sc-7963 (E-5)
Active β-catenin	β-catenin (a.a. 36-44)	Mo Mc IgG_{1k}	92	WB: 1/500 IF: 1/100	Millipore (clone 8E7) #05-665
CD44	CD44 (156-3C11)	Mo Mc IgG_{2a}	80	WB: 1/1000 IF: 1/100	Cell Signalling #3570
Collagen IV	Mo collagen IV	Rb Pc IgG	160	IF: 1/200	abcam ab19808
Cortactin	Hu Mo cortactin	Mo Mc IgG_1	80/85	WB: 1.2 µg/ml IF: 12 µg/ml	Millipore (clone 4F11) #05-180
pY421-Cortactin	Hu pY421-cortactin	Rb Pc IgG	80/85	WB: 1.2 µg/ml IF: 10-20 µg/ml	Sigma SAB4504372
CR16	Hu CR16	Go Pc	43	WB: 0.4 µg/ml	Santa Cruz Biotechnology (P-14) sc-167543
E-cadherin	Extracelular domain (a.a. 600-707)	Rb Pc	120/ 135	WB: 0.2 µg/ml IF: 2 µg/ml	Santa Cruz Biotechnology (H-108) sc-7870
FAK	Hu, Mo FAK	Rb Pc	125	WB: 1/1000 IF: 1/100	Invitrogen AH00502
pY397-FAK	Hu, Mo pY397-FAK	Rb Pc	125	WB: 1/1000 IF: 1/100	Invitrogen 44624-6
pY576/577-FAK	Hu pY576/577-FAK	Rb Pc	125	WB: 1/750 IF: 1/200	Cell signaling #3281
Fascin	Hu fascin	Mo Mc IgG_1	55	WB: 1 µg/ml IF: 10 µg/ml	abcam ab78487 Clone 55K2
GAPDH	Hu GAPDH	Mo Mc IgG_1	36	WB: 10-20 ng/ml	AbD Serotech MCA4740 Clone 4G5
MMP-14 (MT1-MMP)	Catalytic domain	Mo Mc IgG_1	63/65	WB: 1 µg/ml IF: 10 µg/ml	Millipore MAB3328
Nck	Hu a.a. 279-377	Mo Mc IgG_{2b}	47	WB: 2 µg/ml IF: 2.5 µg/ml	BD Biosciences 610100

N-WASP	Hu N-WASP	Rb Pc	65	WB: 0.2 µg/ml IF: 2 µg/ml	SIGMA HPA005750
N-WASP	Hu, Mo a.a. 111-210	Rb Pc	65	WB: 0.2 µg/ml IP: 2 µg	Santa Cruz Sc-20770 H-100
Paxillin	Hu N terminus paxillin	Rb Mc IgG	68	WB: 1/1000 IF: 1/200	abcam Ab32084 Y113
Src	Hu Src	Mo Mc	60	WB: 1/1000	Cell Signaling #2110
pY416-Src	Hu pY416-Src	Rb Pc	60	WB: 1/1000 IF: 1/100	Cell Signaling #2101
pY527-Src	Hu pY527-Src	Rb Pc	60	WB: 1/1000 IF: 1/100	Cell Signaling #2105
Tyr-tubulin	Tyr-tubulin	Mo Mc IgG_3	55	IF: 1/400	Sigma T9028 Clone TUB-1A2
Vimentin	Hu vimentin	Mo Mc IgG_{1K}	57	IF: 1/50	DAKO M0725 Clone V9
WICH/WIRE	Hu WICH/WIRE	Rb Pc	55	WB: 0.1 µg/ml IP: 2 µg	Sigma HPA024467
WIP	Hu aa. 11-16 Mo aa. 11-18	Mo Mc	62	WB: 1/1000 IF: 1/100	Protein Tools CNB-CSIC PT94/3 2H3 1G5
	Hu aa. 33-42 Mo aa. 31-42	Mo Mc	62	WB: 1/1000 IF: 1/100	Protein Tools CNB-CSIC PT94/3 2H3 G8
	Hu Mo aa. 484-497	Rb Pc	62	WB: 1/1000 IF: 1/100	Dr R Geha Children's Hospital Boston C14
	Hu Mo aa. 483-497	Rb Pc	62	WB: 1/1000 IF: 1/100	Protein Tools CNB-CSIC C19
	Hu aa. 186-177 and 293-300	Rb Pc	62	WB: 1/1000 IF: 1/100 IP: 2 µg	Santa Cruz Sc-25533 H-224
	Hu Mo aa. 13-18	Mo Mc IgG_{1k}	62	WB: 1/1000 IF: 1/100 IP: 2 µg	Dr R Geha, Children's Hospital Boston Clone 3D10

Table M5: Primary antibodies. MW: molecular weight. Species: Hu, human; Mo, mouse; Rb, rabbit; Go, goat. Type: Mc, monoclonal; Pc, polyclonal. Application: WB, Western blot; IF, immunofluorescence; IP, immunoprecipitation

Reagent	Type	Concentration	Origin
Anti-mouse IgG HRP	Goat Pc	WB: 1/5000	Santa Cruz Sc-2005
Anti-rabbit IgG HRP	Goat Pc	WB: 1/5000	Santa Cruz Sc-2004
Anti-goat IgG HRP	Donkey Pc	WB: 1/2000	DAKO P 0449
Alexa Fluor 405 anti-mouse IgG	Goat Pc	IF: 1/500	Invitrogen A-31553
Alexa Fluor 488 anti-mouse IgG	Donkey Pc	IF: 1/500	Invitrogen A-11029
Alexa Fluor 488 anti-rabbit IgG	Donkey Pc	IF: 1/500	Invitrogen A-11034
Alexa Fluor 488 phalloidin	-	IF: 1/500	Sigma- Aldrich P5282
Alexa Fluor 594 anti-rabbit IgG	Donkey Pc	IF: 1/500	Invitrogen A-11037
Alexa Fluor 647 anti-rabbit IgG	Donkey Pc	IF: 1/500	Invitrogen A-21245
Alexa Fluor 660 phalloidin	-	IF: 1/250	Invitrogen A-22285
TRITC phalloidin	-	IF: 1/500	Sigma-Aldrich P1951
DAPI	-	IF: 1µg/ml	Sigma 32670
TO-PRO-3 Iodide (642/661)	-	IF: 1/200	Invitrogen T3605

Table M6: Cell markers and secondary antibodies. Type: Pc, polyclonal. Application: WB, Western blot; IF, immunofluorescence

4.4.3 Epitope mapping: PEPSCAN

A peptide array was designed to determine the epitopes recognised by distinct anti-WIP antibodies. WIP arrays (human and murine) were made by SPOT synthesis, as described (Frank and Overwin, 1996). Twelve a.a.-length partially overlapping peptides

that covered the entire length of WIP were spotted on a filter membrane.

Non-specific binding was blocked using 1% gelatin in TBS (at least 4 h, RT). After overnight incubation with a WIP-specific primary antibody (Table M5), the membrane was washed in TBS-T and incubated with an HRP-labelled secondary antibody (Table M6) for 1-2 h in blocking solution. The membrane was washed extensively and developed as for WB.

The membrane was incubated sequentially with antibodies after stripping, which was performed in two steps, first by triple sonication in stripping buffer A (8 M urea, 1% SDS in PBS; 5 min, 40°C), and second by three-time incubation with stripping buffer B (acetic acid:ethanol:H_2O_d 10:50:40). Before incubation with a new primary antibody, the membrane was incubated with secondary antibody to confirm stripping efficiency.

4.4.4 Immunoprecipitation

For immunoprecipitation (IP) experiments, cells were lysed in ice-cold lysis buffer (150 mM NaCl, 50 mM Tris-HCl pH 7.4, 1 mM EDTA, 1 mM EGTA, 1% Triton X-100 and complete protease inhibitor cocktail). Clarified lysates (500 μg, 13600 g, 5 min, 4°C) were incubated with A/G agarose beads (4 h, 4°C) (Protein A/G PLUS-Agarose Immunoprecipitation Reagent; Santa Cruz) previously blocked with 2% BSA and coupled to 2 μg anti-WIP, -WICH/WIRE or -N-WASP rabbit polyclonal antibodies or 2 μg rabbit IgG as control. Beads were then washed thrice with washing buffer (150 mM NaCl, 50 mM Tris-HCl pH 7.4, 1 mM EDTA, 1 mM EGTA, 0.1% Triton X-100), suspended in 2X loading buffer and boiled (10 min). IP, input and output lysates were examined by WB.

4.5 Microscopy

4.5.1 Time-lapse microscopy/Live cell imaging

For all time-lapse experiments, cells were incubated in a humidified 5% CO_2 atmosphere at 37°C. Time-lapse phase contrast imaging was performed using a Nikon inverted fluorescence microscope TE 200 Wide Field fitted with a Nikon Plan-Fluor

10x/0.3NA objective or a Leica inverted fluorescence microscope DMI6000B with a Leica HC PL 10x0.3NA objective lens and 1.6x magnification. Nikon microscope imaging was performed using a CoolSnap HQ2 charge-coupled device camera (Photometrics) equipped with a Perfect Focus System device. The Leica microscope was fitted with a monochrome digital camera Orca R2, 12bit/16bit (Hamamatsu). Images were collected and processed with Metamorph v.7.7.7 (Molecular Devices) or LAS AF v. 2.6.0 (Leica).

For confocal live imaging, cells expressing eGFP/eGFP-WIP and Red-LifeAct were imaged with a Leica SP5 TCS inverted confocal system equipped with a Leica HCX PL Apo CS lambda blue 63x/1.4NA oil objective lens. Images were collected and processed with LAS AF v. 2.6.0 software.

4.5.2 Confocal microscopy and image processing

Confocal images were collected using the following inverted confocal microscopes:

- Bio-Rad Radiance 2100 confocal system in a Zeiss Axiovert 200 microscope equipped with a Zeiss PlanNeoFluar 20x/0.5NA and Zeiss Plan-Apochromat 63x/1.4NA oil objective lens. Images were collected with LaserSharp 2000 v. 5.2 acquisition software.
- Leica SP5 TCS confocal system equipped with a Leica HCX PL Apo CS 40x/1.25NA oil objective lens and a Leica HCX PL Apo CS lambda blue 63x/1.4NA oil objective lens. Images were collected and processed with LAS AF v. 2.6.0 software.
- Fluoview FV1000 confocal microscope (Olympus) equipped with a uPlan-SApochromat 60x/1.35NA oil objective lens. Images were collected with FV10-ASW1.7 acquisition software.

Images were subsequently processed using the free-source imaging package ImageJ (http://rsbweb.nih.gov/ij/). Orthogonal projections were generated from 10-40 µm Z-series with a 0.13 to 0.2 µm step size. Z-projections were generated from 2.0-6.0 µm Z-series with a 0.5 µm step size for cells cultured on gelatin and 10-20 µm Z-series with a 0.5-0.75 µm step size for cells in Matrigel. Cell fluorescence intensity was quantified using the ImageJ Freehand Selection tool and measuring the parameters “Area”, “Mean Grey Value” (the sum of grey values of all pixels in the selection divided by the number

of pixels) and “Integrated Density” (defined as the product of “Area” and “Mean Grey Value”) for at least 15 cells per condition. Corrected total cell fluorescence (CTCF) was calculated as:

> CTCF = integrated density – (area of selected cell X mean fluorescence of background readings)

CTCF was measured in whole cells and the cell periphery for each cell analysed. To analyse paxillin distribution in invading cells, the area of anti-paxillin staining at FA and total cell paxillin were measured in 8-bit Z-projections from 2-3 stack images from the ventral area of the cell, using the ImageJ Threshold tool (80-100/255 for protein at FA; 30-40/255 for total protein) in 10-20 cells per condition. The percentage of paxillin accumulated at FA was then calculated.

4.6 Statistical analysis

Statistical analysis was performed using Prism 5.0b for Mac OS X software (GraphPad Software, Inc.). Data were represented as mean ± standard deviation (SD). Student’s t-test was used to compare mean values, one-way ANOVA to compare measures of multiple observations, two-way ANOVA to compare two nominal variables, and the Chi square test to compare distribution of nominal variables.

Results

5. RESULTS

5.1 Characterisation of WIP antibodies by WB and epitope mapping (PEPSCAN)

Our initial approach to identify and localise WIP in cancer cells was to obtain and characterise the tools necessary for analysis. Using several anti-WIP antibodies (Table M5), we used WB to analyse the isoforms expressed in MDA-MB-157 (not shown) and Hs578T cells (Fig. R1 A). Although all the antibodies had been tested for specificity, we found that they detected additional bands in WB. Except for 3D10, all antibodies recognised a ~60 kDa band (near the theoretical molecular weight of WIP, ≈62 kDa). Antibody, 3D10 preferentially recognised a smaller isoform, mini-WIP (≈34-38 kDa) (Koduru et al., 2007), whose expression was undocumented to date in cancer cells. H-224 antibody also recognised mini-WIP as well as WIP (antibody PT94/3 2H3 E5 G8 appears to detect mini-WIP (Fig. R1 A), but data for the mini-WIP signal was inconsistent in these experiments). Later experiments showed that 3D10 also recognised the full-length WIP isoform, although its affinity for mini-WIP in human cells appeared stronger, as separate incubation was needed to detect both isoforms.

We analysed WIP expression in several transformed cell lines using PT94/3 2H3 E5 G8 and H-224 antibodies, which yielded the strongest signal for full-length WIP in MDA-MB-157 and Hs578T cells. These antibodies detected different protein levels in the same lysates (Fig. R1 B). To verify antibody specificity, we tested WIP expression in $WIP^{+/+}$ and $WIP^{-/-}$ murine fibroblasts and spleen cells (Fig. R1 B, C). Although H-224 mainly recognised human WIP, we observed a weak signal only in WT fibroblasts. Likewise, PT94/3 2H3 E5 G8 and other clones derived from the same hybridoma fusion distinguished a band only in $WIP^{+/+}$ spleen samples (where WIP expression is higher than in fibroblasts). The diverse recognition pattern shown by each antibody suggests that these cells probably express different isoforms and/or post-translational modifications. Tests using C19 (not shown), 3D10 and C14 antibodies showed dissimilarities in WIP levels in BCC (Fig. R1 D), but H-224, 3D10 and C14 tended to show higher signal intensity in basal B cells.

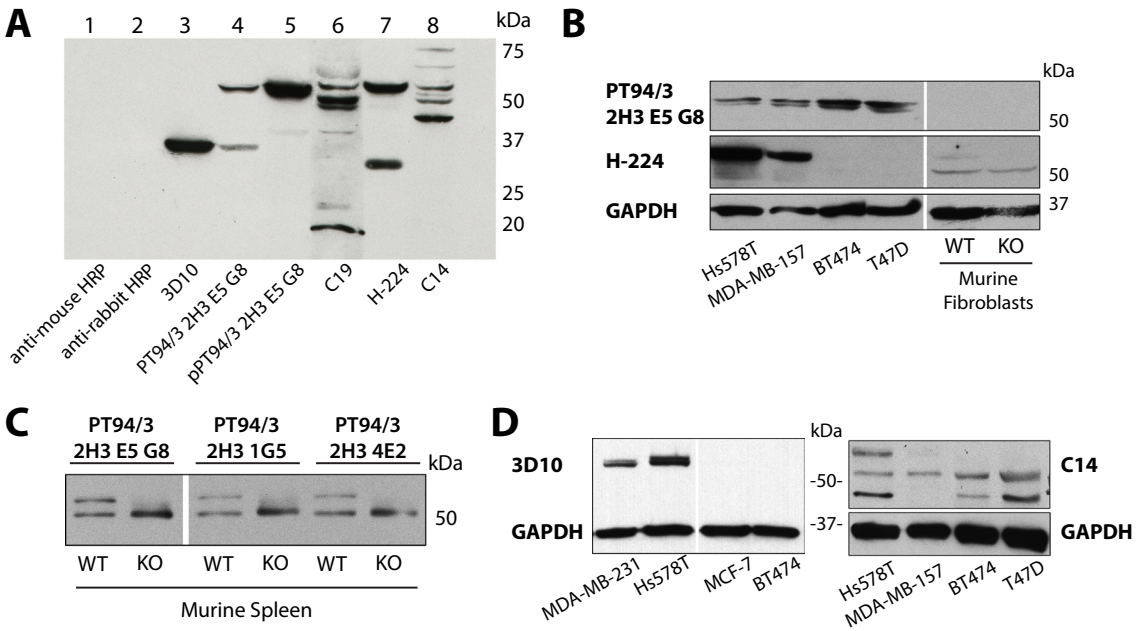

Figure R1: WIP expression pattern screened using various WIP antibodies. Soluble lysates from Hs578T cells (30 µg/lane) were analysed by WB using various anti-WIP antibodies. (A) Lane 1, anti-mouse-HRP control; lane 2, anti-rabbit-HRP control; lane 3, 3D10 (mouse); lane 4, PT94/3 2H3 E5 G8 (mouse); lane 5, purified PT94/3 2H3 E5 G8; lane 6, C19 (rabbit); lane 7, H 224 (rabbit), lane 8, C14 (rabbit). (B) PT94/3 2H3 E5 G8 and H-224 recognise different forms of WIP in BCC. (C) PT94/3 2H3 E5 G8 recognises WIP specifically in mouse immune cells. (D) 3D10 and C14 antibodies detect different WIP levels in diverse BCC.

To identify the epitopes recognised by these antibodies, we used PEPSCAN analyses (Geysen et al., 1984) on the human and murine WIP sequences. Positive dots obtained by WB were contrasted with the overlapping peptide sequences of each protein to infer the consensus peptide that corresponds to or contains each epitope (Fig. R2); Figure R3 shows the localisation of epitopes identified in our experiments or previous studies (Koduru et al., 2007; Sasahara et al., 2002). PT94/3 2H3 1G5 antibody recognises part of the same region as 3D10 (PTFALA), which belongs to a well-conserved part of the sequence, the N-terminal domain. Although PT94/3 2H3 E5 G8 also identifies its epitope in this area, its affinity is weaker than that of 3D10 (Fig. R1). Although we found a very specific, conserved H-224 antibody epitope in human and murine sequences (the sequence is repeated twice in the protein), the WB signal in mouse samples was poor. Information from the manufacturer confirmed that the antibody recognises the murine protein weakly.

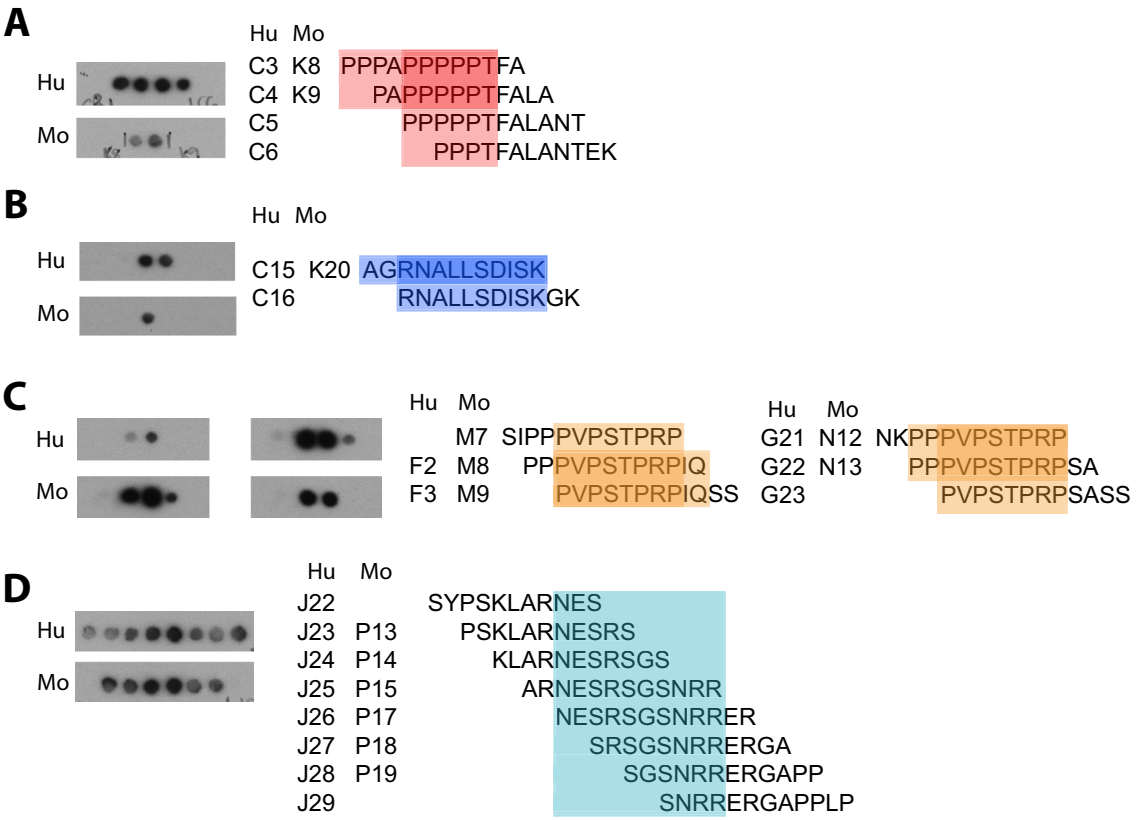

Figure R2: PEPSCAN epitope mapping of anti-WIP antibodies. Consensus peptide sequences from human WIP. Images show WB experiments performed on PEPSCAN membrane using human (top panels) and murine (bottom) WIP sequences. WIP recognised by (A) PT94/3 2H3 1G5, (B) PT94/3 2H3 E5 G8, (C) H-224 and (D) C19 antibodies (Table M5).

Of the antibodies tested, H-224 was the most robust tool for this study, as it recognises human WIP and mini-WIP with high affinity; it was also suitable for WB, IF and IP experiments. Except where indicated, we used H-224 to measure WIP expression in this study.

5.2 Expression and localisation of WIP family proteins in Breast Cancer Cells

Based on studies that linked high WIP levels with poor prognosis in some cancer types (Staub et al., 2009) and identified its expression pattern in BCC (Charafe-Jauffret et al., 2006), we used a breast cancer model to study WIP implication in the invasive behaviour of cancer cells. Our initial approach consisted of examining WIP expression and localisation in a collection of BCC. Charafe-Jauffret's meta-analysis indicated that

WIP mRNA expression was significantly higher in basal B cells compared to basal A or luminal cells (Fig. R4).

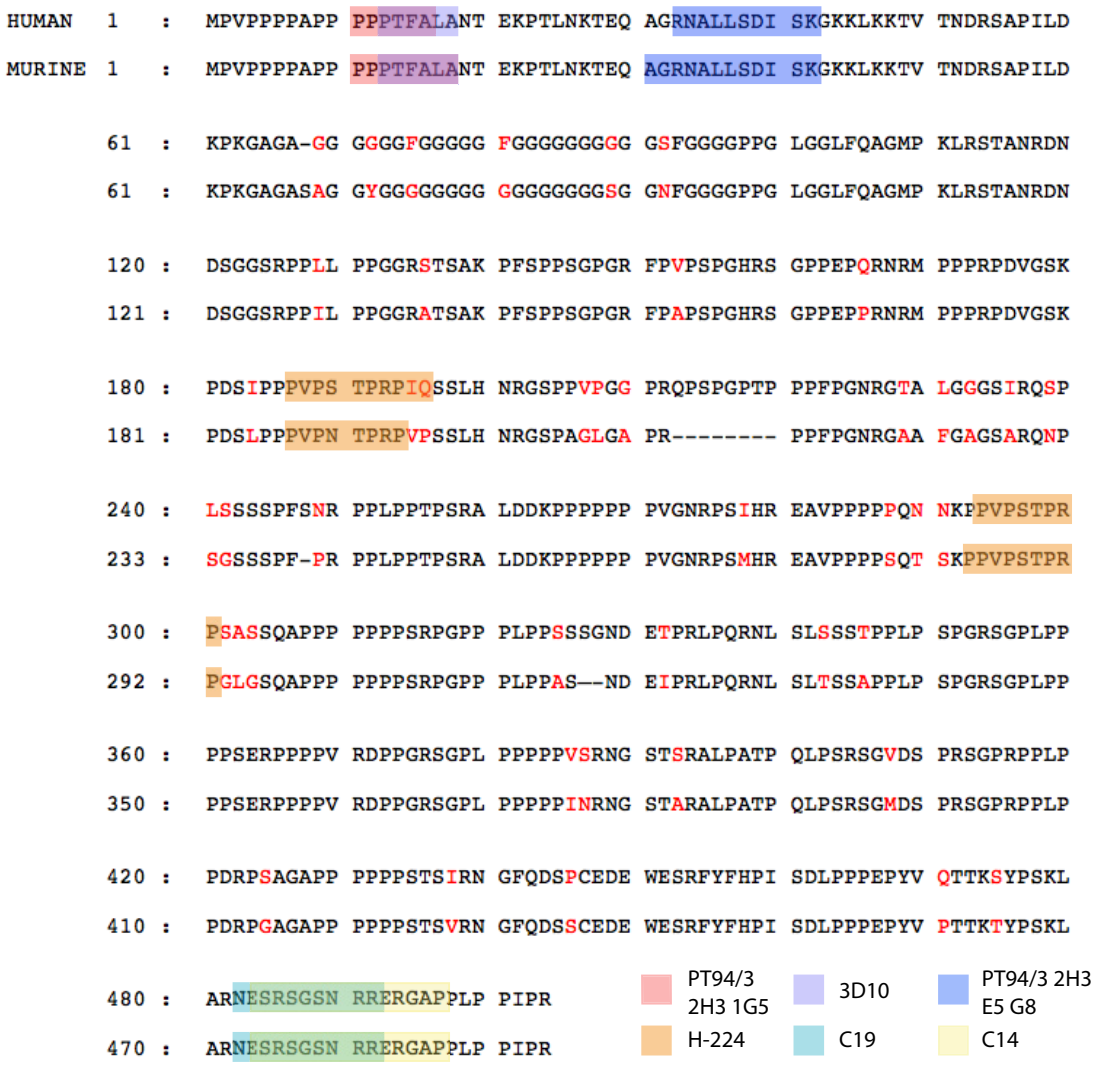

Figure R3: Epitope localisation in human and murine WIP amino acid sequences. Epitopes recognised by PT94/3 2H3 1G5, 3D10 (Koduru et al., 2007), PT94/3 2H3 E5 G8, H-224, C19 and C14 (Sasahara et al., 2002) antibodies (Table M5).

To corroborate whether WIP is expressed differentially between BCC groups (Fig. R4), we performed WB analysis of a collection of basal B and luminal cell lines (Table M1). As observed for mRNA levels, basal B cells expressed higher levels of WIP, and frequently also of mini-WIP; however, luminal cells barely expressed either isoform (Fig. R5). We also examined the expression of the other two WIP family members, WICH/WIRE and CR16, but detected no differences in their expression between groups (Fig. R5). In addition, we analysed the expression of other proteins associated with the

formation or maturation of invadopodia and other cancer invasion models, N-WASP (Gligorijevic et al., 2012; Yamaguchi et al., 2005; Yu et al., 2012), cortactin (Artym et al., 2006; Clark et al., 2007) and fascin (Li et al., 2010) (Fig. R5).

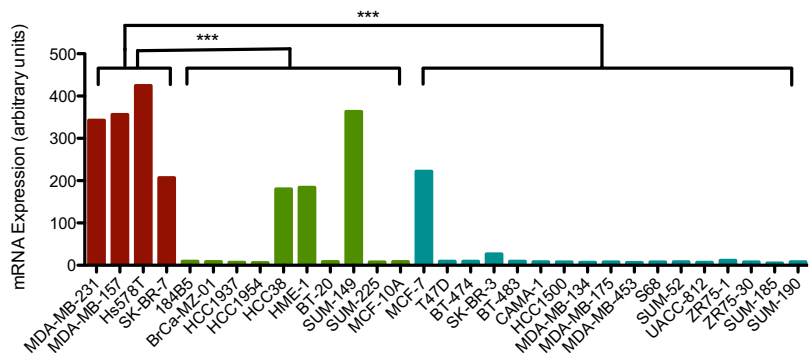

Figure R4: WIP mRNA expression in BCC. Data extracted from an array (Charafe-Jauffret et al., 2006), represented individually and analysed by 1-way ANOVA as replicates of basal B, basal A and luminal groups.

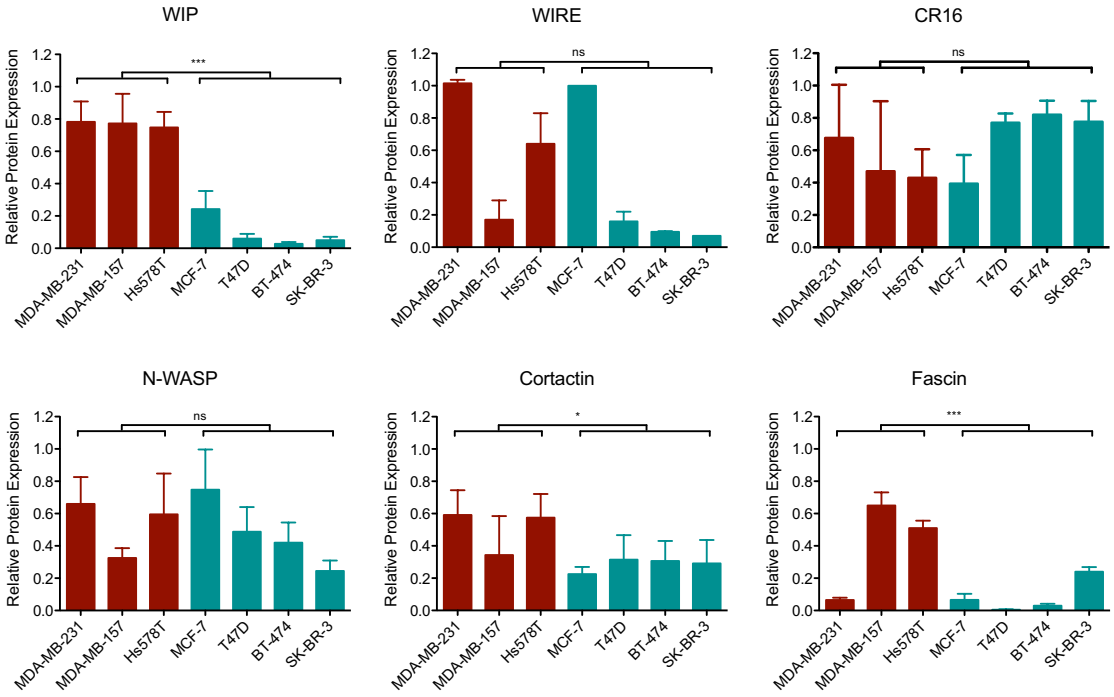

Figure R5: WIP is differentially expressed in basal B compared to luminal BCC. (A) Lysates of basal B and luminal cells were analysed by WB using antibodies to WIP, WIRE, CR16, N-WASP, cortactin, fascin and GAPDH (not shown). Protein expression values were normalised to the highest value in each graph. Data show mean ± SD of at least three independent experiments. *, p <0.05; ***, p <0.001 by 2-way ANOVA.

Our data indicate that cortactin and fascin are more highly expressed in basal B than luminal cells, confirming previous studies (Cai et al., 2010; Rezaul et al., 2010; Rodriguez-Pinilla et al., 2006; Sarrio et al., 2008). Despite these differences, none of these proteins showed a differential expression pattern as striking as found for WIP,

which presented not only significant differences between basal B and luminal groups, but also for each basal B cell line tested (individual significance not shown). In contrast, there was no expression difference for N-WASP, WICH/WIRE or CR16.

Several groups have reported that basal B cells show a strong invasive phenotype *in vitro* and/or *in vivo*, at difference from that observed for luminal cells, which are poorly invasive (Blick et al., 2008; Charafe-Jauffret et al., 2006; Kenny et al., 2007). To confirm the invasive behaviour of these cell lines, we plated basal B (MDA-MB-231, MDA-MB-157 and Hs578T) and luminal cells (MCF-7, T47D and BT474) on fluorescent gelatin, allowed them to invade for 16, 24 or 48 h, and analysed invadopodium formation (Fig. M4). After IF staining for the invadopodium markers F-actin and cortactin, we observed that only basal B cells were able to invade the gelatin after invadopodium-mediated degradation (Fig. R6). In contrast, luminal cells were neither able to form invadopodia nor to degrade the matrix at any incubation time. Results were similar when MDA-MB-231 and MCF-7 cells were plated on BM (Fig. R7). After 4 days incubation, MDA-MB-231 had partially degraded the membrane, as less type IV collagen remained in the BM. In contrast, MCF-7 cells showed no alteration in BM structure.

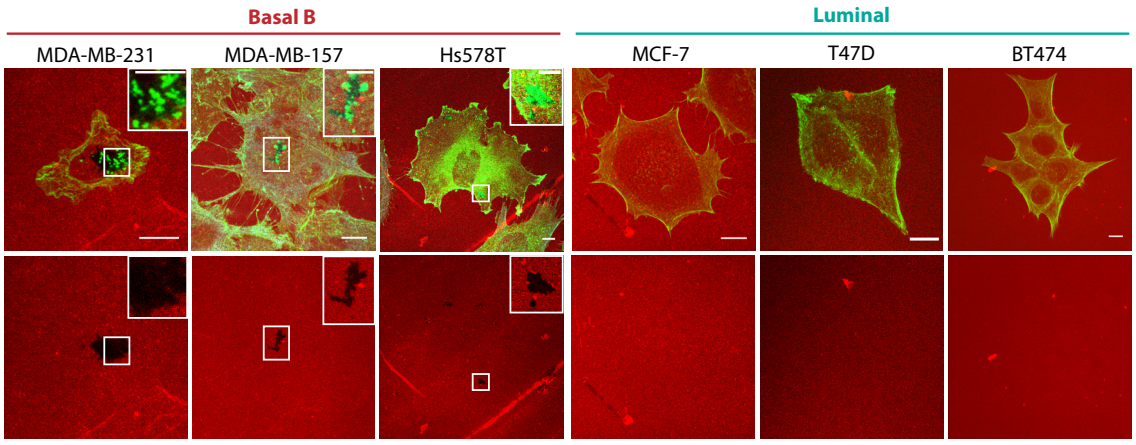

Figure R6: WIP expression correlates with BCC invasiveness on gelatin. Basal B (MDA-MB-231, MDA-MB-157 and Hs578T) and luminal cell lines (MCF-7, T47D and BT474) were plated on rhodamine-gelatin (red) and incubated (16 h). After fixation in 4% PFA and IF staining with the invadopodium markers F-actin (green) and cortactin (not shown), cells were visualised by confocal microscopy. The images show representative Z-projections in which invadopodia localise at areas of active degradation (dark areas in the gelatin). Bars: 10 µm (insets, 5 µm).

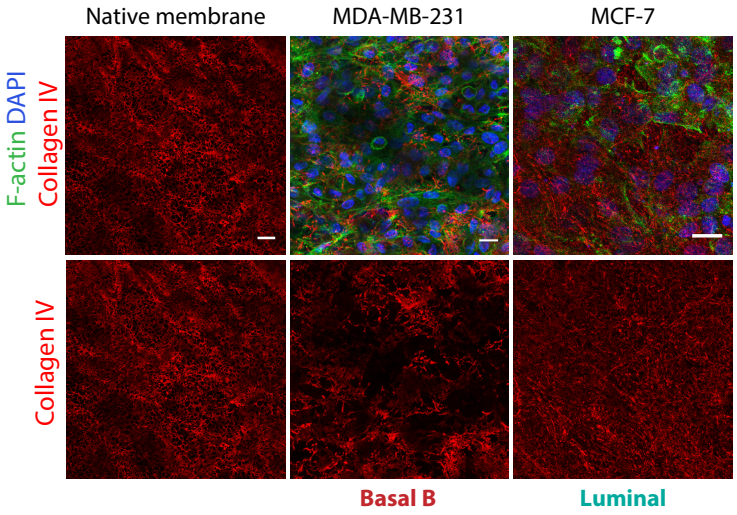

Figure R7: MDA-MB231 and MCF-7 invasiveness on BM. MDA-MB-231 and MCF-7 cells were cultured on mouse peritoneal BM (4 days). After fixation in 4% PFA, samples were stained by IF for mouse type IV collagen (red), F-actin (green) and DNA (blue, DAPI) and visualised by confocal microscopy. Bars: 20 µm.

These results not only validate these assays as a useful means to discriminate the invasiveness of basal B and luminal cells, but also confirm a correlation between the invasive behaviour and WIP levels in BCC.

5.2.1 WIP family protein localisation in BCC

After verifying that all WIP family members were expressed in BCC (at higher or lower levels, Fig. 5), we examined their localisation in the cell. For this purpose, we analysed endogenous expression of WIP and CR16 by IF —WICH/WIRE analysis was not feasible, as no available antibody was suitable for IF. As observed by WB, WIP is expressed much more strongly in basal B cells, where it localises mainly to the leading edge of lamellipodia in the vicinity of F-actin (Fig. R8) and cortactin (not shown). WIP also concentrated at the perinuclear area, where the Golgi apparatus is situated. To examine whether WIP co-localises at Golgi, we stained Hs578T cells for the cis-Golgi network marker GM130 (Nakamura et al., 1995). Although both proteins shared a common location in the cell, we observed no specific co-localisation in Hs578T cells (Fig. R9 A); WIP distribution in these cells instead resembled microtubule localisation. We therefore used a specific stain for tyrosinated tubulin (Tyr-tubulin) to detect dynamic microtubules, and observed that WIP overlapped with the Tyr-tubulin signal (Fig. R9 B). IF detection of CR16 was difficult with the antibodies used, but some differences in expression were observed between BCC (Fig. R8). In contrast to WIP, CR16 was excluded from the perinuclear area, and its cytoplasmic localisation was variable among cell types.

WIP localisation at the leading edge of the cell suggests that it is present in lamellipodia during 2D migration, as described (Kinley et al., 2003). To support these observations in invasive cells, we performed time-lapse microscopy using MDA-MB-231 cells expressing GFP-WIP and the F-actin marker LifeAct (Lemieux et al., 2013; Riedl et al., 2008), plated on fibronectin to promote migration. As observed in fixed cells, WIP reaches areas of active migration in bursts with F-actin; WIP appears earlier than actin at lamellipodia (Fig. R10, Movie R1).

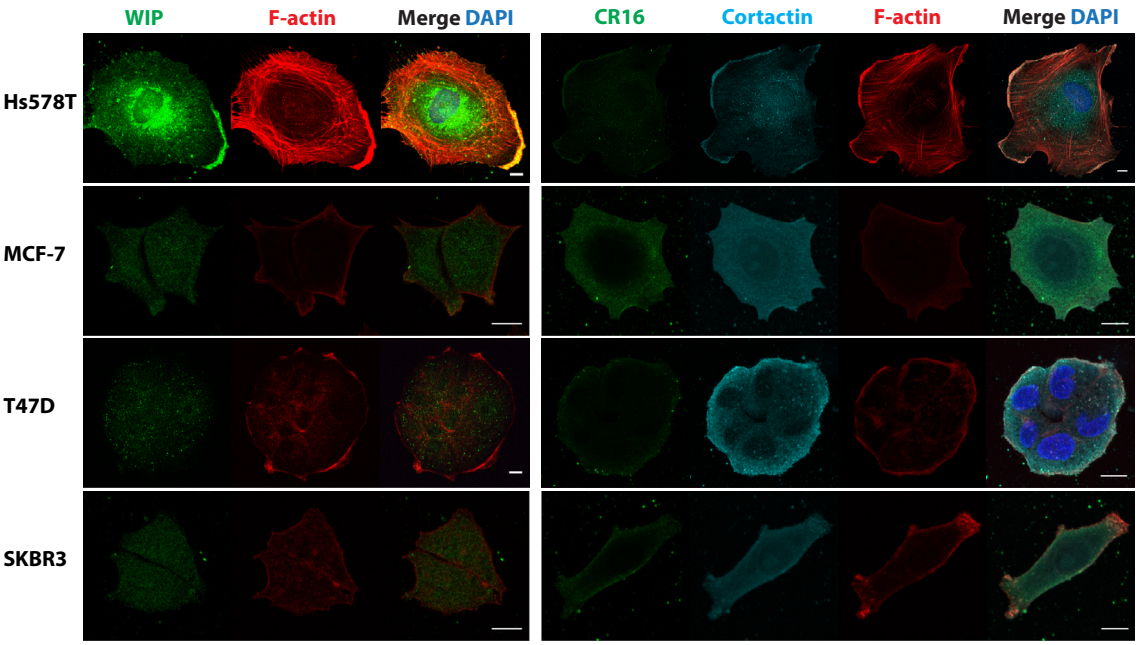

Figure R8: WIP and CR16 localisation in BCC. Cells were grown on glass coverslips (24 h), fixed in 4% PFA and stained by IF for WIP (green, left) or CR16 (green, right), F-actin (red), cortactin (cyan) and nuclei (blue, DAPI) and visualised by confocal microscopy. Bars: 10 µm.

Exogenous expression of WIP suggests that is located at invadopodia of MTLn3 cells (Yamaguchi et al., 2005). To verify whether WIP localises at invadopodia in BCC, we induced basal B cells invasion of fluorescent gelatin and stained the cells for WIP and invadopodial markers. Endogenous WIP indeed localised with F-actin and cortactin at sites of gelatin degradation in MDA-MB-231 (Fig. 11 A, (Garcia et al., 2012)), MDA-MB-157 and Hs578T cells (not shown). To determine whether WIP also localised at other invasive protrusions, we performed circular invasion assays (CIA, (Yu and Machesky, 2012)). CIA consists of a 2D-3D invasion system in which a cell monolayer is attached to a glass-bottom dish, but is also surrounded by matrix (in this case, Matrigel). To move

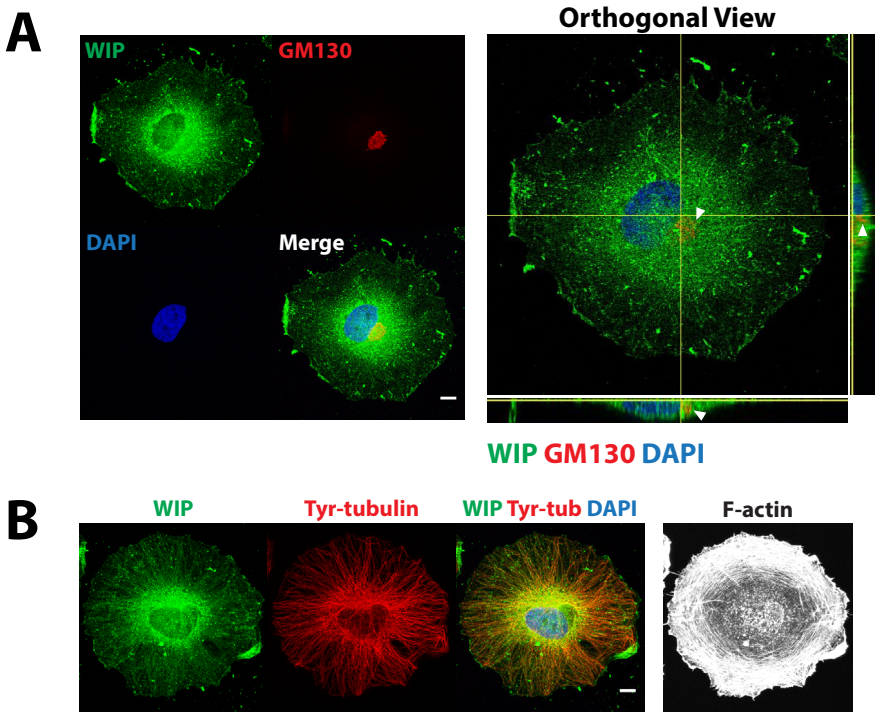

Figure R9: Endogenous localisation of WIP in Hs578T. Cells were cultured on glass coverslips (24 h), fixed in 4% PFA and stained by IF for WIP (green), F-actin (grey), nucleus (blue, DAPI) and cis-Golgi (A, red) or microtubules (B, red) and visualised by confocal microscopy. (A) Representative images of WIP and GM130 localisation are shown as Z-projections (left) and orthogonal views (right). (B) WIP and Tyr-tubulin show similar localisation in the cells (Z projections). Bars: 10 µm.

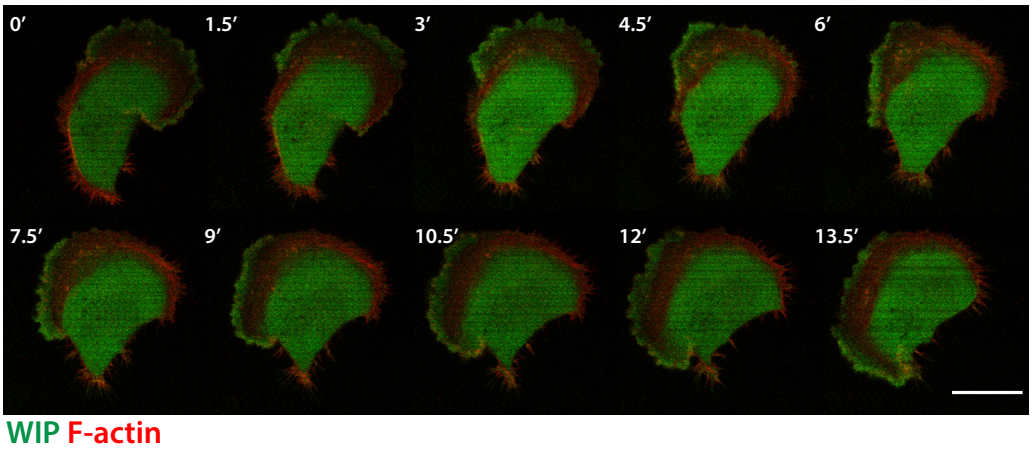

Figure R10: WIP localisation in migrating MDA-MB-231 cells. Cells were infected with pLNT-GFP-WIP lentivirus and then nucleofected with Red-LifeAct. At 24 h post-transfection, cells were plated on fibronectin-coated dishes and imaged by time-lapse confocal microscopy. GFP WIP (green), F-actin (red). Bar: 20 µm.

forward, cells are forced to remodel the matrix, driving invasion in a way similar to that observed in 3D gels (Yu and Machesky, 2012). This assay also facilitates IF compared to conventional 3D systems. Using CIA, we found that WIP localised with F-actin and cortactin at the distal tip of invasive protrusions that formed in Matrigel (Fig. 11 B, (Garcia et al., 2012)). WIP was generally detected inside the nucleus (see Fig. 11 B), but whereas in CIA the cell population showed uniform nuclear expression in invading cells, nuclear WIP levels were highly variable in cells cultured on gelatin.

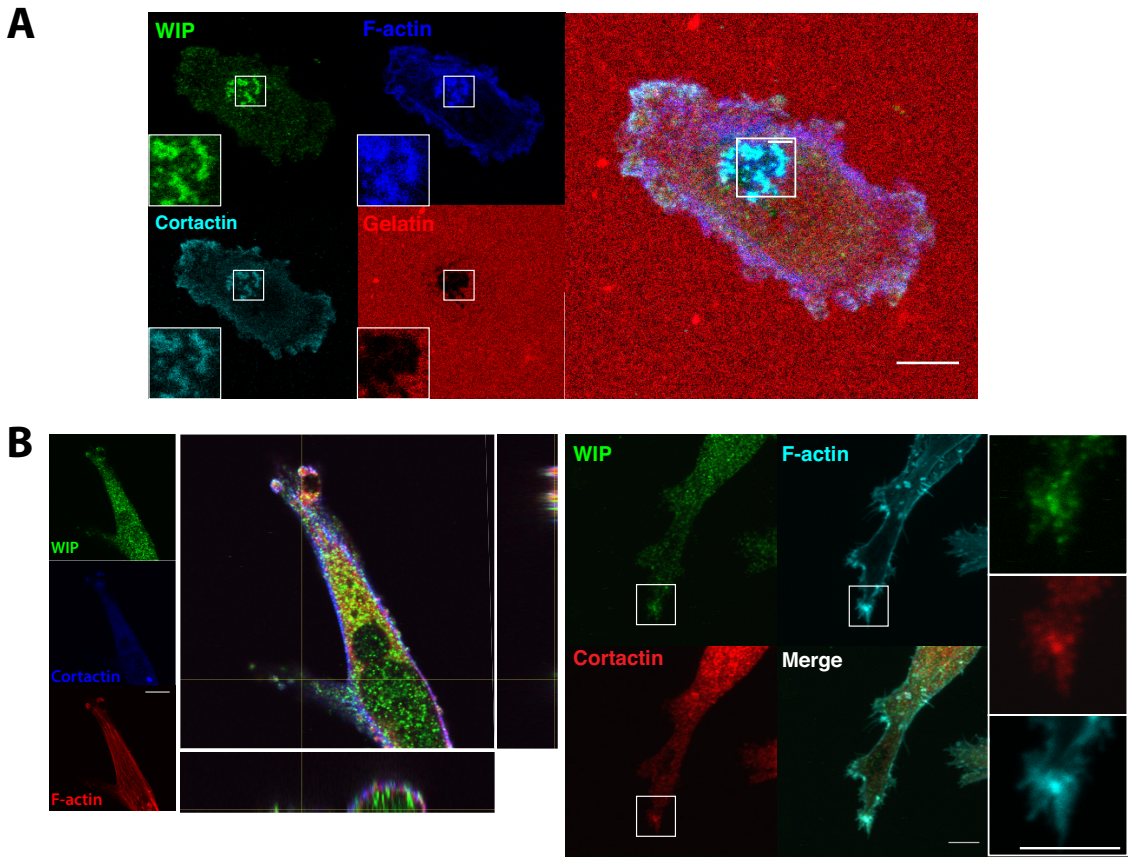

Figure R11: WIP is localised at invadopodia and invasive protrusions in MDA-MB-231 cells. Endogenous WIP localises at invasive protrusions that develop in 2D and 3D matrices. IF of MDA-MB-231 plated on: (A) rhodamine-gelatin coated coverslips were incubated for 6 h before fixation with 4% PFA, and stained for WIP (green) and invadopodial markers: F-actin (blue) and cortactin (cyan). The degraded matrix appears as dark areas in the gelatin. Magnifications of the boxed area show the distribution of WIP, F-actin, cortactin and gelatin separately and merged. (B) CIA: after 24 h invading into Matrigel cells were fixed and stained for F-actin (red, left; cyan, right), cortactin (blue, left; red,) and WIP (green). Magnifications of the boxed area show the distribution of WIP, F-actin and cortactin separately. Bars: 10 µm (insets, 4 µm).

In summary, these results indicate that although WIP family proteins are widely expressed in basal B and luminal BCC, their levels vary between cell lines. Significant

differences in expression were found between cell types only in the case of WIP, which is expressed strongly in basal B cell lines but weakly in luminal cells. CR16, which is expressed mainly in brain and testis, was found at low levels in BCC compared to WIP and WICH/WIRE, and was weakly expressed in migrating structures; we therefore focussed our study on WIP and WICH/WIRE. We showed endogenous WIP in invasive protrusions that develop in gelatin and Matrigel, and previous studies suggest that WIP has a role in cancer cell invasion (Yamaguchi et al., 2005), although the way this occurs is not known. There are no previous data regarding WICH/WIRE functions in invasion, or its location at invasive structures, making this protein an interesting target for in-depth exploration of its function and its potential relationship with WIP. To study these questions, we used gain- and/or loss-of-function experiments to characterise the potential roles of WIP and WICH/WIRE in the invasive behaviour of cancer cells.

5.3 Effect of exogenous WIP expression in luminal BCC

Basal B cells, which express high levels of WIP, are able to invade gelatin and type IV collagen; we therefore tested whether an increase in WIP expression in luminal cells was sufficient to induce invasive behaviour in these cells. We overexpressed GFP-WIP or mCherry-WIP by transducing cells with lentiviral particles, which yielded high expression levels without cell damage. We first examined the localisation of exogenous WIP by IF, and whether its overexpression induced morphological change in the cells. Although WIP levels were variable, we found that exogenous WIP induced formation of actin-rich protrusions in MCF-7 cells, which formed larger lamellipodia than controls; in T47D cells, we observed the formation of different types of structures (Fig. R12). When these cells were plated on rhodamine-gelatin, however, we observed no changes in their invasive ability, with no invadopodium formation or matrix degradation (Fig. R13). To determine whether cell changes were associated to EMT, we used WB to analyse E-cadherin levels in infected cells, but found no alterations in WIP-overexpressing cells (Fig. R13 A). Exogenous WIP expression thus induced actin-rich protrusions, but did not promote invadopodium formation in luminal BCC.

Overexpression of WIP in luminal cells was thus insufficient to induce invadopodium-mediated invasion and had no effect on expression of the epithelial

marker E-cadherin in any cell line tested.

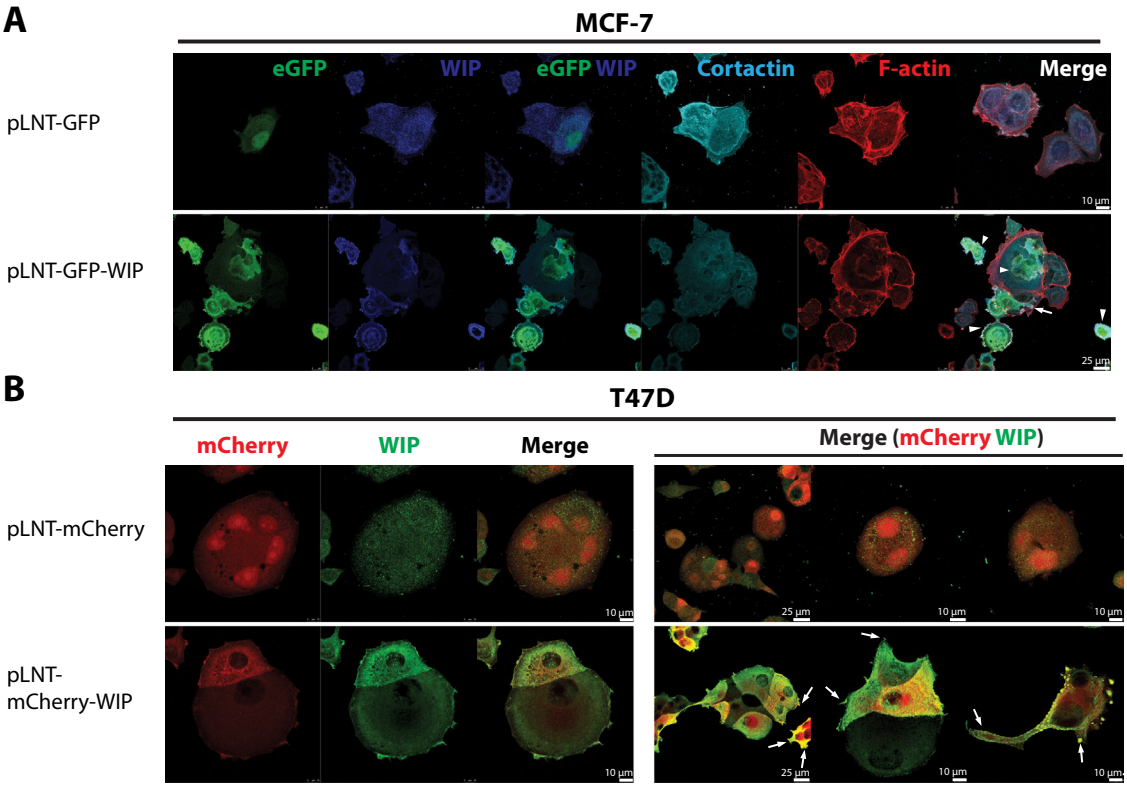

Figure R12: Exogenous WIP expression in luminal BCC. MCF-7 and T47D cells were plated on glass coverslips 24 h after lentiviral infection (pLNT-control or pLNT-WIP) and cultured (24 h). After fixation in 4% PFA, (A) MCF-7 cells were stained by IF for F-actin (red), cortactin (cyan) and WIP (blue) and (B) T47D cells were stained for WIP (green) and visualised by confocal microscopy. Bars: 25 (A) and 10 µm (B). Arrows indicate cell protrusions; arrowheads indicate large lamellipodia.

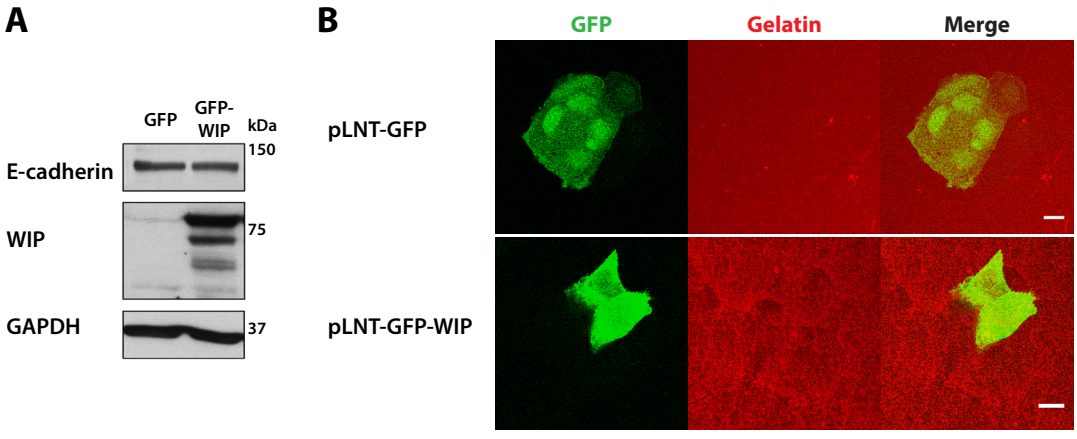

Figure R13: WIP overexpression in T47D cells is not sufficient to induce invadopodium formation. Cells were infected with lentiviral particles pLNT-eGFP and pLNT-eGFP-WIP (green). At 24 h post-infection, cells were plated on (A) plastic for subsequent WB analysis or (B) rhodamine-gelatin (red) for analysis of invadopodium formation and gelatin degradation (24h). Bar = 10 µm.

5.4 Effect of WIP or WICH/WIRE depletion on breast cancer invasion

5.4.1 Impact of WIP or WICH/WIRE depletion on 3D invasion by MDA-MB-231 cells

The MDA-MB-231 cell line is an established model for the study of tumour cell invasion (Lacroix and Leclercq, 2004; Neve et al., 2006). As WIP and WICH/WIRE are strongly expressed in this cell line (Fig. R5), we generated stable MDA-MB-231 WIP- or WIRE-deficient cells by expressing shRNA via lentiviral infection. After testing up to five independent shRNA, we selected two each that targeted these proteins for subsequent experiments. We found that these shRNAs depleted WIP by 85%, mini-WIP by up to 97%, and WICH/WIRE between 50-80% (Fig. R14). Whilst targeting WIP had no effect on the expression of WICH/WIRE or WIP-binding partners such as N-WASP (Fig. R15) or cortactin (not shown); reduction of WICH/WIRE increased WIP levels, whereas it decreased N-WASP and MT1-MMP levels (Fig. R15).

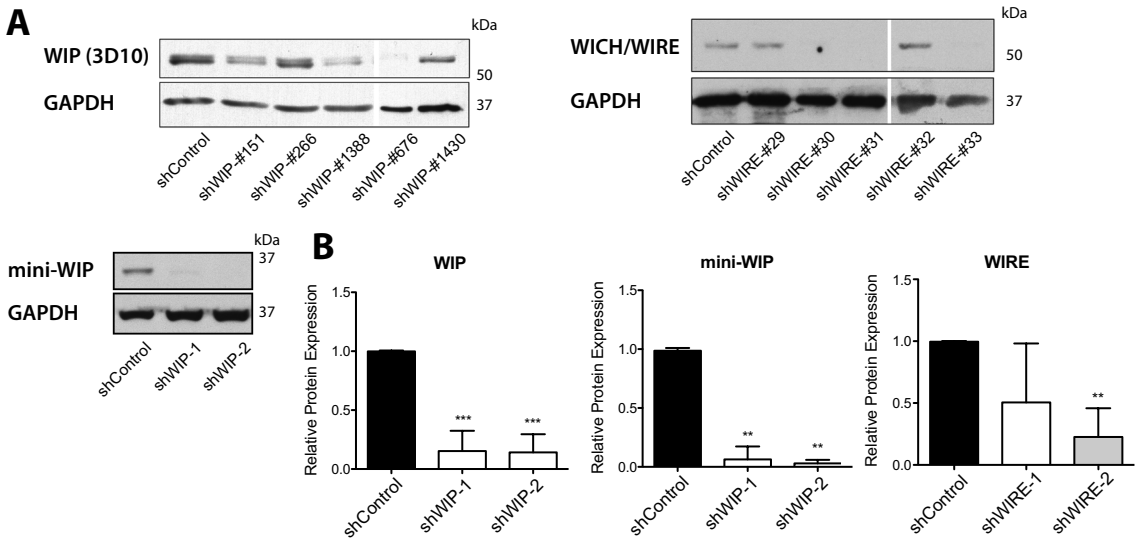

Figure R14: Selection of shRNAs to silence WIP and WICH/WIRE protein expression. Cells were infected with lentiviral particles bearing pLKO.1-puro that encode shRNAs against WIP or WICH/WIRE. Soluble lysates from stable puromycin-resistant cells were analysed by WB. (A) Expression of WIP, mini-WIP, WICH/WIRE in WIP- or WIRE-deficient cells. The two most efficient shRNAs for each protein were selected for experiments. (B) Densitometric quantification of proteins showed in (A). Protein expression was normalised to control samples. Data show mean ± SD of at least three independent experiments. **, p <0.01, ***, p <0.001 by 1-way ANOVA and Tukey's post-hoc-test.

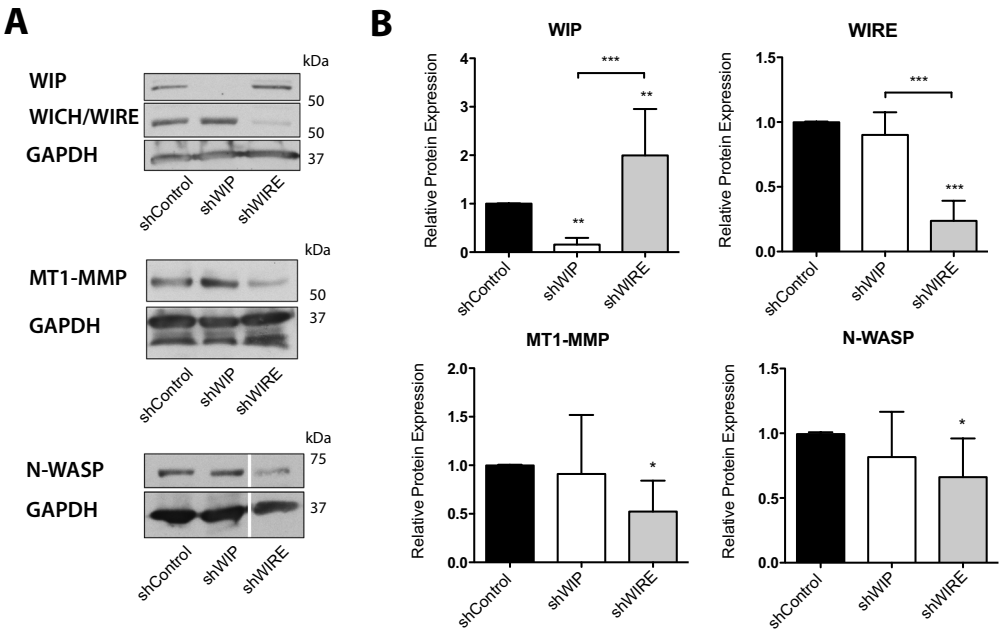

Figure R15: Effect of WIP or WICH/WIRE silencing on the expression of related proteins. Cells were infected with lentiviral particles bearing pLKO.1-puro encoding shRNAs against WIP or WICH/WIRE. Soluble lysates from stable control (shControl), WIP- (shWIP) or WIRE-silenced cells (shWIRE) were analysed by WB. (A) Expression of WIP, WICH/WIRE, N-WASP and MT1-MMP in WIP- or WIRE-silenced cells. (B) Densitometric quantification of proteins in (A). Protein expression was normalised to control samples. Data show mean ± SD of at least three independent experiments. *, $p < 0.05$; **, $p < 0.01$; ***, $p < 0.001$ by 1-way ANOVA and Tukey's post-hoc-test.

The localisation of WIP at invadopodia and podosomes (Chabadel et al., 2007; Chou et al., 2006; Moreau et al., 2003; Yamaguchi et al., 2005), together with the roles of WIP and WICH/WIRE in podosomes organisation and function (Banon-Rodriguez et al., 2011; Calle et al., 2008; Tsuboi, 2006), led us to study the role of these proteins during cancer invasion. For this purpose, we tested the ability of WIP- and WIRE-depleted cells to invade 3D matrices, using two different shRNAs for each protein, with similar results. For clarity, data for only one specific shRNA are presented (Fig. R16). When MDA-MB-231 cells were allowed to invade thick Matrigel plugs in an inverse invasion assay (Hennigan et al., 1994), we found that absence of WIP or WICH/WIRE significantly impaired invasion to an equivalent degree (Fig. R16). Whereas control cells were able to cross the filter barrier and invade deep into the matrix, WIP-depleted cells invaded ~30% of control values; WIRE-deficient cell invasion decreased similarly to 27-30% (Fig. R16 B). Although the morphology of invading WIP-deficient cells remained unaltered, WIRE-depleted cells showed a more rounded shape and aggregated to form acinar-like

structures (Fig. R16 A). To clarify whether these effects were due to a decrease in the MMP activity needed for Matrigel degradation, we allowed the cells to invade in the presence of the MMP-inhibitor GM6001. This treatment of control and WIP-depleted cells reduced invasion compared to vehicle treatment, with no further effects in WIRE-deficient cells (Fig. R16 A and B).

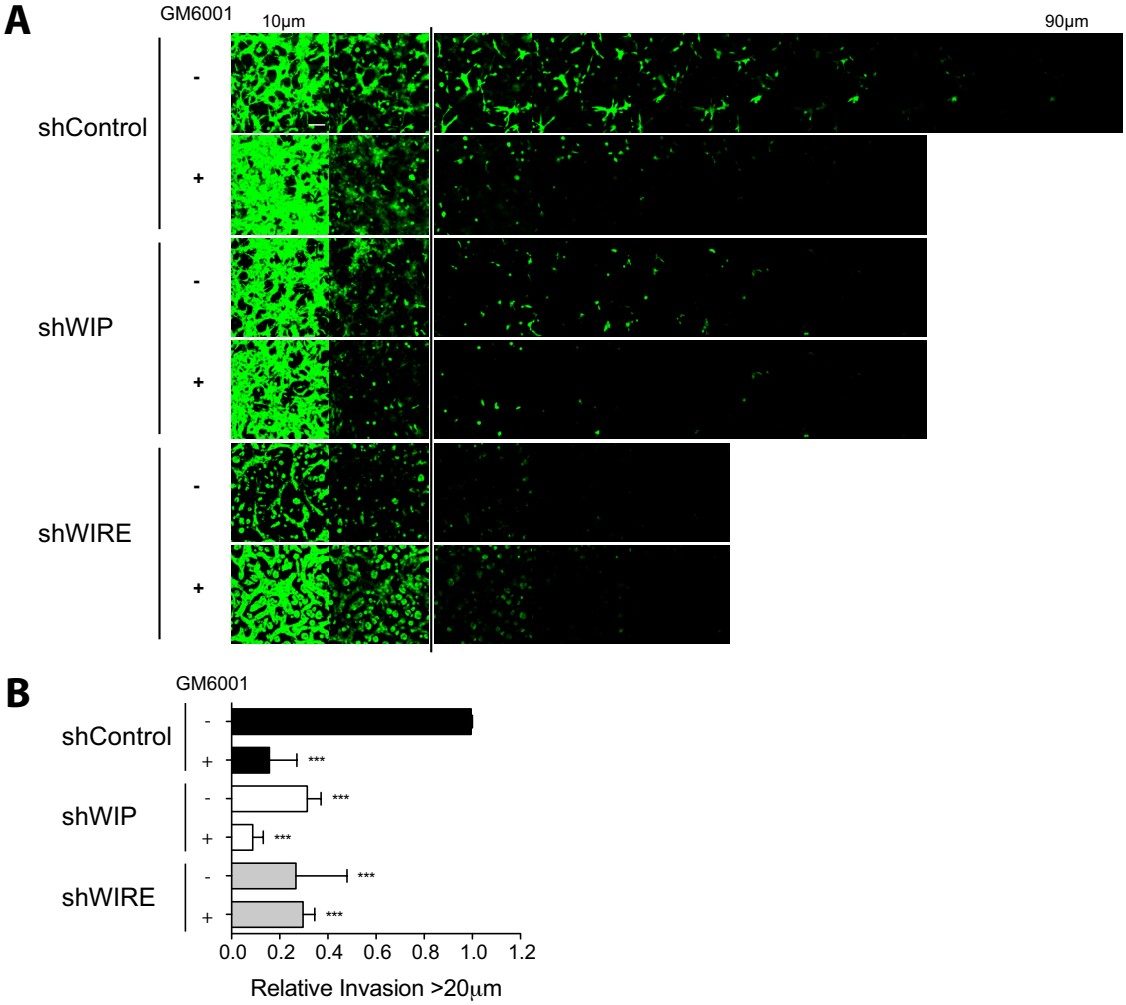

Figure R16: WIP and WICH/WIRE mediate invasion of 3D Matrigel plugs. (A) Matrigel invasion by MDA-MB-231 cells stably infected with control shRNA (shControl), WIP shRNA (shWIP) or WIRE shRNA (shWIRE) in an inverted invasion assay. Cells were incubated with DMSO (vehicle) or 25 µM GM6001. After calcein-AM staining (green), live cells were visualised by confocal microscopy. Serial optical sections were acquired at 10 µm intervals and are shown sequentially, with depth increasing from left to right. Bar: 100 µm. (B) Quantification of invasion is expressed as relative invasion above a 20 µm threshold, normalised to control samples. Invasion was determined by measuring the area covered by cells (µm2) for each section. Data show mean ± SD of at least three independent experiments. ***, p <0.001 by 1 way ANOVA and Tukey's multiple comparison test.

The ability of WIP- and WIRE-deficient cells to invade Matrigel was also reduced in CIA (Fig. R17 A, Movie 2). After 18 h, invasion by WIP- and WIRE-deficient cells reduced to 70% and 60-65% of the control value, respectively (Fig. R17 B). In CIA, invasion is dependent on ECM remodelling (Yu and Machesky, 2012; Yu et al., 2012); we therefore examined the effect of inhibiting MMP activity in this system. As observed in inverse invasion assays, GM6001 treatment reduced control cell invasion to WIP- and WIRE-deficient cell levels. Treatment of WIP- and WIRE-depleted cells provoked a further reduction in their invasive capacity (40% of the maximum in both cases; Fig. R17 B). To determine the contribution of each protein to invasion, we generated double WIP/WIRE-depleted cells by sequential interference. Absence of WIP and WICH/WIRE reduced invasion in a similar way to individual depletion, indicating that inhibiting both proteins did not have an additive effect (Fig. R17 B).

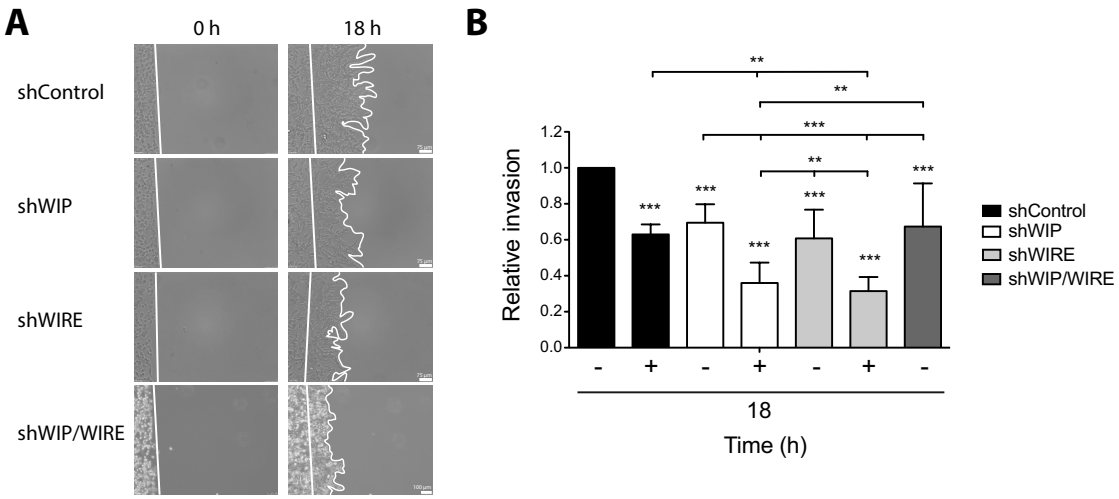

Figure R17: WIP and WICH/WIRE are necessary for efficient invasion in CIA. Stably infected MDA-MB-231 cells (shControl, shWIP, shWIRE or shWIP/WIRE double knock-down) were cultured on 35 mm-diameter dishes around a silicon insert, until they reached confluence. After insert removal, Matrigel was added and allowed to polymerise before addition of growth medium to stimulate invasion. (A) Representative images acquired by time-lapse microscopy. White lines indicate the cell front at t = 0 h and t = 18 h. (B) Relative invasion was normalised to invaded area in control samples at 18 h. Data show mean ± SD of at least three independent experiments. **, p <0.01, ***, p <0.001 by 2-way ANOVA and Bonferroni's post-hoc-test.

When we focused on single cell events, we also detected differences in leading cell invasion of Matrigel. Whereas in CIA, control cells migrated and formed large, persistent protrusions, WIP depletion promoted formation of unstable structures that protruded

and retracted repeatedly, impairing efficient forward cell migration (Fig. R18, Movie 3). WICH/WIRE deficiency had no specific effect on perseverance of invading cells, which still formed invasive protrusions towards the matrix, but these appeared more complex and branched (Fig. R18 and R19 A). These cells nonetheless formed shorter protrusions, with a more rounded shape as indicated by a decrease in length/width ratio (Fig. R19). The Matrigel-invasive capacity of WIP- and WIRE-deficient cells, which was lower than that of controls, was similar although it occurred in different manners.

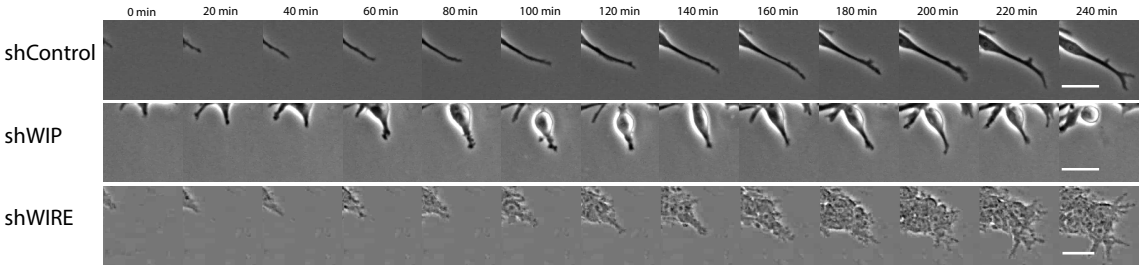

Figure R18: WIP is necessary for advance of cell protrusions in Matrigel. CIA time-lapse images were magnified to examine behaviour of single cell protrusions. The montage shows representative protrusions from control, WIP- and WIRE-deficient cells invading Matrigel. Bar: 50 µm.

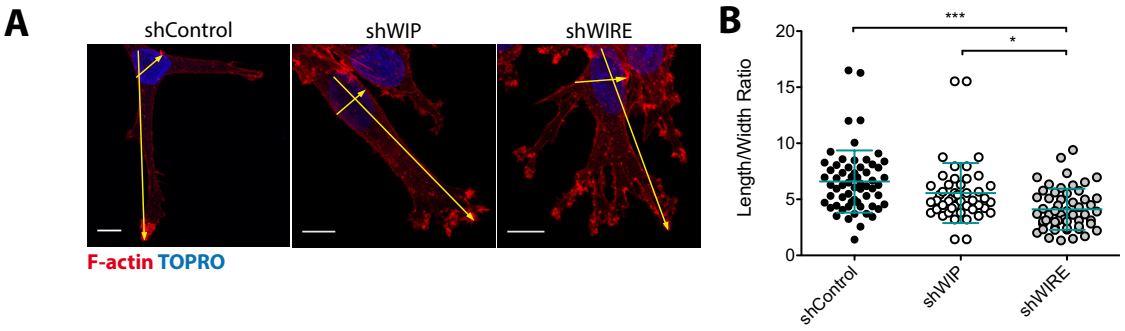

Figure R19: Absence of WICH/WIRE reduces elongation of protrusions in CIA. (A) IF images of control, WIP- and WIRE-deficient cells invading Matrigel stained for F-actin (red) and DNA (TO-PRO, blue). Bars: 10 µm. (B) Quantification of length/width ratio of leading cells invading Matrigel. Each dot represents a single cell. Data show mean ± SD of at least three independent experiments. *, P<0.05; ***, P<0.001 by 1-way ANOVA and Tukey's multiple comparison test.

CIA results from WIP-deficient cells correlated to those obtained in other migration experiments. In standard wound-healing experiments (without matrix), WIP-depleted cells migrated significantly more slowly than controls (Fig. R20, Movie 4). When these cells were allowed to migrate randomly on fibronectin, WIP-depleted cells showed

significantly less velocity, covered smaller distances and were less persistent in their movement (Fig. R21, Movie 5). These results suggested a defect in cell adhesion, leading us to analyse proteins potentially involved in this process such as FA components. In WIP-deficient cells, CIA analysis of proteins located at FA showed altered paxillin distribution at the cell base in contact with the glass surface (Fig. R22).

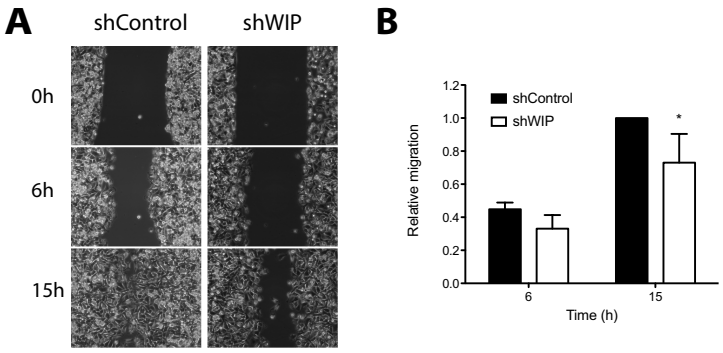

Figure R20: Absence of WIP slows wound closure by MDA-MB-231 cells. Stably infected shControl and shWIP cells were cultured as a monolayer and induced to migrate by addition of 10% FBS-containing medium. (A) Representative images of wound-healing assay at 0, 6 and 15 h. (B) Relative migration was normalised to the increase in cell-covered area in control samples at 15 h. Data show mean ± SD of at least three independent experiments. *, p <0.05, by 2-way ANOVA and Bonferroni's post-hoc-test.

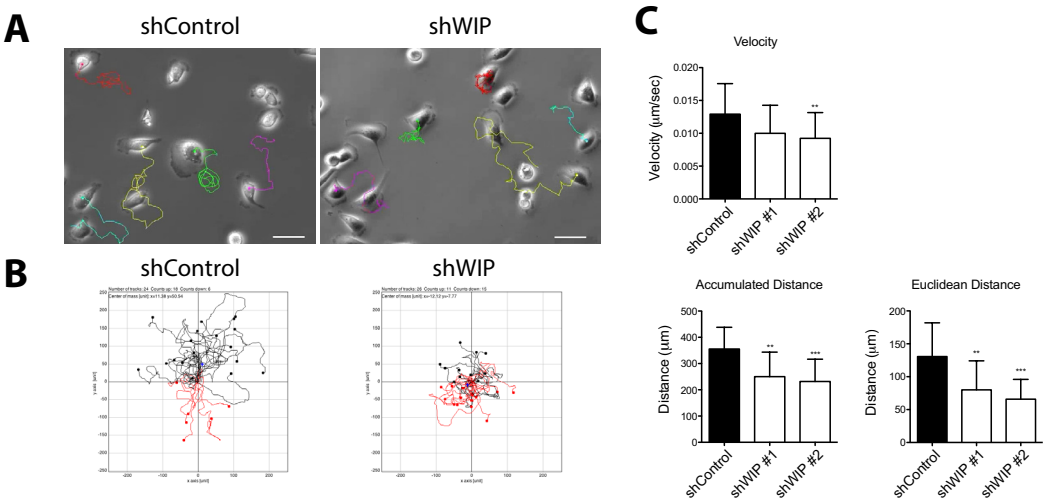

Figure R21: WIP depletion reduces cell velocity and persistence during random migration. Stably infected shControl and shWIP cells were grown on fibronectin at low confluence and time-lapse microscopy was performed (5 h). (A) Representative images show trajectories of shControl and shWIP in the presence of 10% FBS-containing medium after 5 h of time-lapse acquisition. Bars: 50 µm. Images were quantified and analysed using the ImageJ Chemotaxis plugin. (B) Analysis shows tracking of shControl and shWIP cells. Trajectories in black show net cell movement towards the upper areas from the origin at t = 0 h, while trajectories in red show net cell movement to lower areas. (C) Quantification of velocity, accumulated and Euclidean distances. Data show mean ± SD of two independent experiments. **, p <0.01; ***, p <0.001 by 1-way ANOVA and Tukey's post-hoc-test.

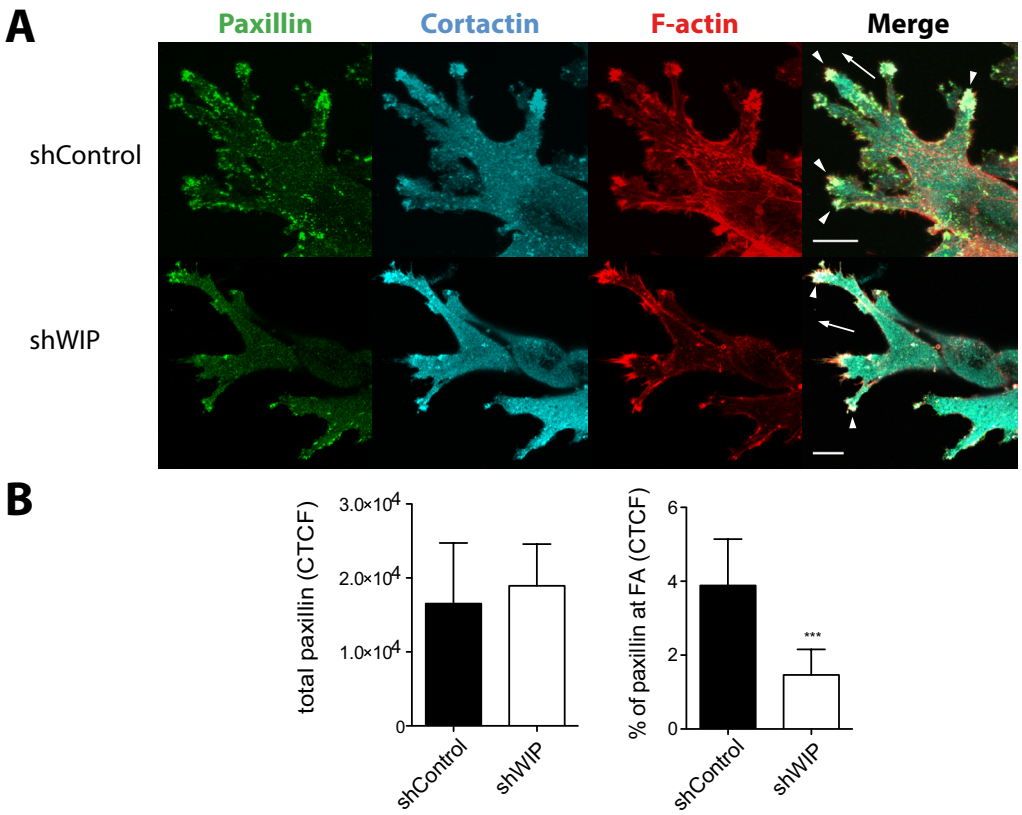

Figure R22: WIP depletion alters paxillin distribution at FA in CIA. (A) IF images of control and WIP-deficient cells stained for paxillin (green), cortactin (cyan) and F-actin (red). Arrows indicate the direction of invading cells towards Matrigel; arrowheads show invasive protrusions where F-actin, cortactin and paxillin localise. Bars: 10 µm. (B) Quantification of CTCF and percentage of paxillin recruited at FA (see Methods). Data show mean ± SD of at least three independent experiments. ***, p <0.001 by Student's t test.

WIP and WICH/WIRE therefore contribute to invasion of Matrigel, but this occurs in different ways. Whereas WIP silencing alters paxillin recruitment at FA and affects the stability of protrusions alone or with a matrix, lack of WICH/WIRE reduces cell elongation on Matrigel.

5.4.2 Contribution of WIP and WICH/WIRE to invadopodium mediated-invasion

To better understand how these proteins are involved in invasion by MDA-MB-231 cells, we used mouse peritoneal BM to explore their ability to remodel the ECM (Fig. R7). MDA-MB-231 cells were allowed to invade BM for up to four days remodelled and degraded most type IV collagen fibres, making it difficult to distinguish

the native structure of the BM in some cases. In contrast, WIP- or WIRE-depleted cells barely degraded collagen fibres and the BM structure remained mostly intact (Fig. R23 A and B). Control cells were thus able to penetrate and cross the BM, whereas WIP- and WIRE-deficient cells were unable to cross completely (Fig. R23 C). Distribution of WIP- and WIRE-deficient cells nonetheless differed significantly, as WIRE-depleted cells better penetrated the BM, but were unable to migrate further, whilst WIP-depleted cells remained mainly on top of the BM (Fig. R23C). As described for CIA, we plated WIP/WIRE-silenced cells on BM; no differences were detected compared to single knock-down cells (Fig. R23).

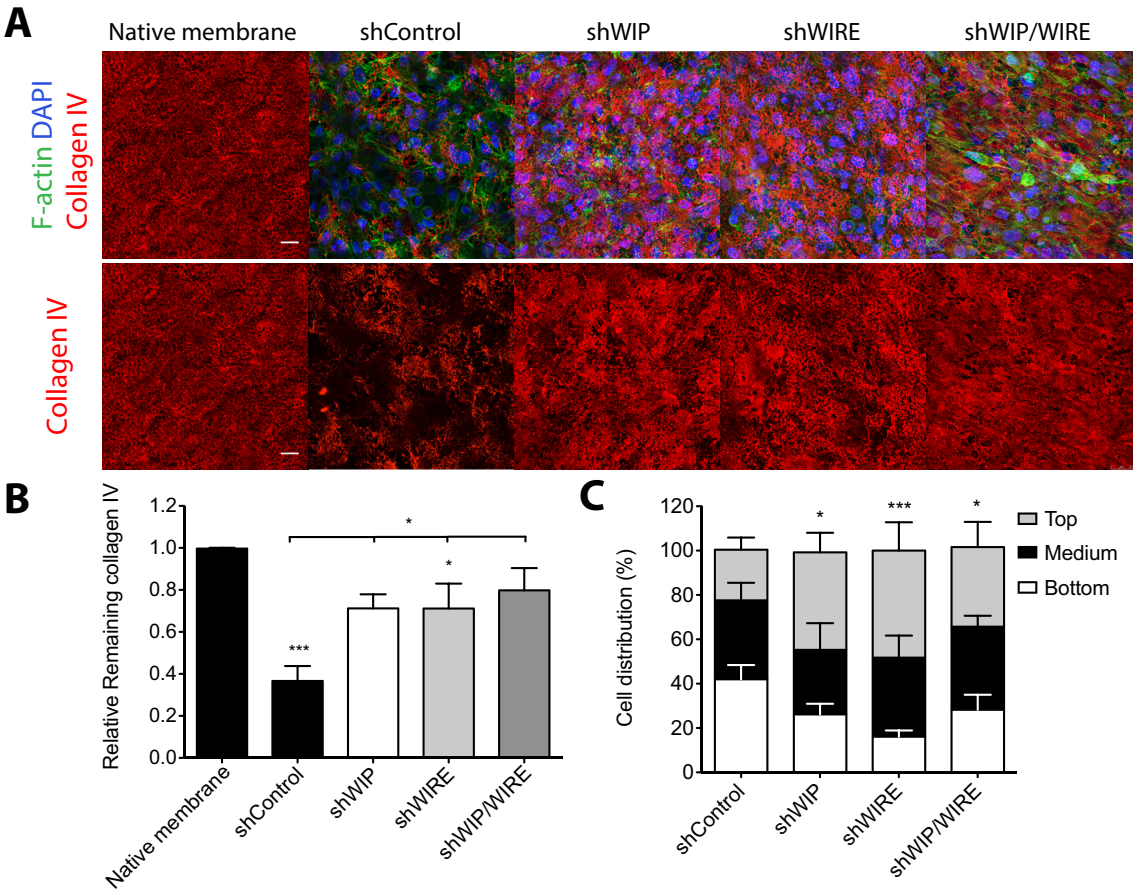

Figure R23: WIP and WICH/WIRE are needed for efficient degradation and migration through BM. (A) Stably infected MDA-MB-231 cells (shControl, shWIP, shWIRE or shWIP/WIRE) were cultured on mouse BM (4 days), fixed and stained for collagen IV (red), F-actin (green) and DNA (DAPI, blue). Bar: 20 µm. (B) Remaining type IV collagen in BM was measured after membrane remodelling and degradation and normalised to native membrane levels. Data show mean ± SD of at least three independent experiments. *, $p < 0.05$; ***, $p < 0.001$ by 1-way ANOVA and Tukey's multiple comparison test. (C) Cell distribution across the membrane was calculated as the percentage of cells located at three different sectors of the stack: on top of the BM (grey), embedded in the BM (black) and beneath the BM (white). Data show mean ± SD of three independent experiments. *, $p < 0.05$; *** $p < 0.001$ by the Chi square test.

At a shorter incubation time (24 h), MDA-MB-231 cells emitted invadopodia, observed as F-actin-positive dots in contact with the BM, that protruded towards the BM, while non-invasive MCF-7 showed smaller areas of contact between F-actin and type IV collagen that remained mostly on top of the BM (Fig. R24).

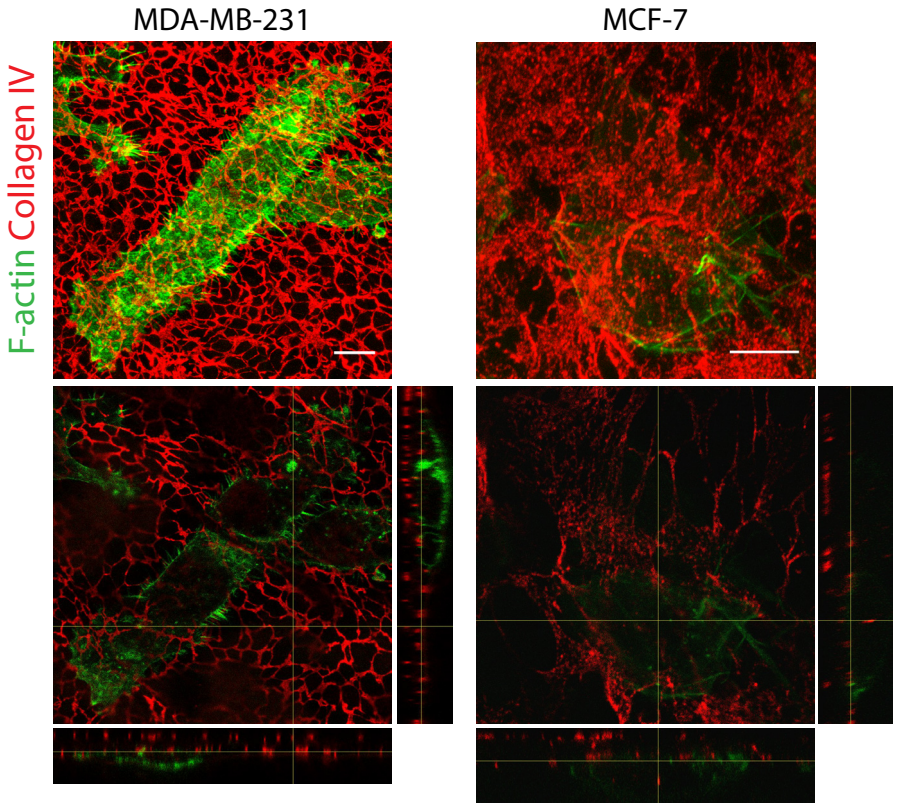

Figure R24: MDA-MB-231 invade BM by developing invadopodia. MDA-MB-231 and MCF-7 cells were cultured on mouse peritoneal BM (24 h), fixed and stained for type IV collagen (red) and F-actin (green). Bars: 10 µm.

Inefficient invasion of BM by MCF-7 cells led us to test the capacity of WIP- and WIRE-deficient cells to form invadopodia; we thus plated these cells on fluorescent gelatin-coated glass coverslips. As predicted, control cells were able to form invadopodia (F-actin- and cortactin-positive dots) and generated dark areas in the gelatin that indicated matrix degradation (Fig. R25 A). In contrast, WIP-deficient cells had reduced ability to form invadopodia and consequently, to degrade gelatin (Fig. R25 A and B). The remaining cells able to form invadopodia degraded less gelatin than controls (Fig. R25 B). WIRE-deficient cells formed ventral protrusions that we identified as invadopodia, since they concentrated F-actin and cortactin at these sites, but as in BM experiments, matrix

degradation was impaired (Fig. R25 A and B). These results suggest that WIP participates in invadopodium formation, whereas WICH/WIRE contributes to their degradative activity.

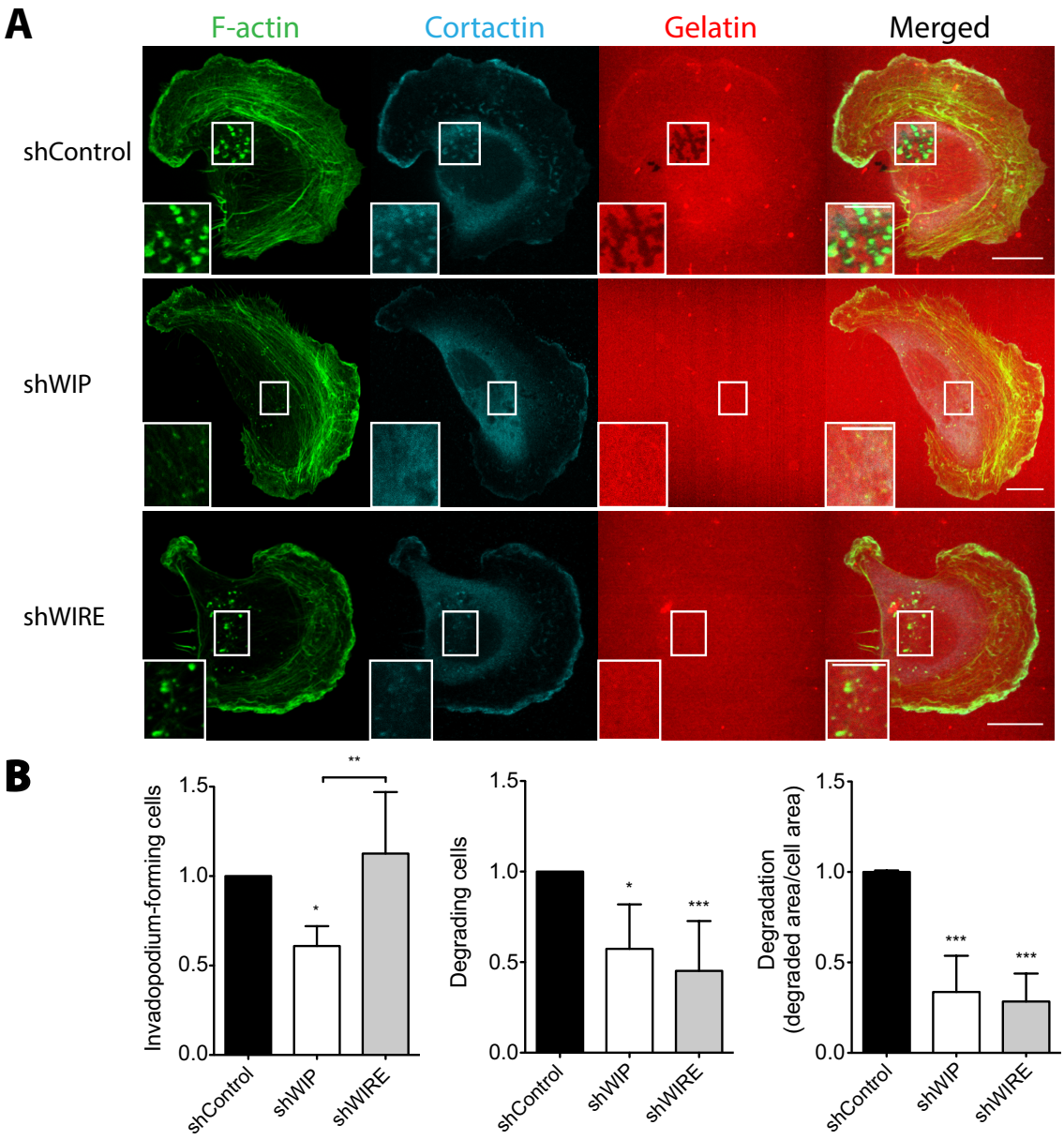

Figure R25: WIP and WICH/WIRE are necessary for invadopodium-mediated degradation. (A) Stably infected MDA-MB-231 cells (shControl, shWIP or shWIRE) were plated on rhodamine-gelatin-coated glass coverslips (red, 5 h), fixed and stained for F-actin (green) and cortactin (cyan). Bars: 10 µm (insets, 5 µm). (B) Quantification of invadopodium-forming cells, degrading cells and degraded area (calculated as degraded area/cell area) were normalised to control values. Data show mean ± SD of at least three independent experiments. *, p <0.05; **, p <0.01; ***, p <0.001 by the Chi square test for invadopodium-forming and degrading cells, and Student's t test for degraded area measurements.

5.4.3 Mechanisms involved in WIP- and WICH/WIRE-mediated invasion

5.4.3.1 WIP and WICH/WIRE modulate FAK/Src activity

FA and invadopodium dynamics are regulated by FAK and Src kinases (Schlaepfer et al., 2004). The two proteins form a complex that allows precise mutual regulation (Mitra et al., 2005), connecting the signalling pathways that control the formation of these two actin structures. We used IF analysis of phosphorylated epitopes to examine the activity of both kinases in the absence of WIP or WICH/WIRE. WIP-deficient cells tended to show increased activation of FAK autophosphorylation residue Tyr397 (Fig. R26 A and B). In control and WIP- or WICH/WIRE-depleted cells, pTyr397-FAK was observed in the cytoplasm and more intensely at FA. Subcellular distribution of pTyr397-FAK-positive FA differed in WIP-deficient cells, with a significant increase in pTyr397-FAK-positive central FA (Fig. R26 C). pTyr397-FAK frequently accumulated close to areas of invadopodium formation, where it commonly localises near cortactin foci of newly-formed (non-degrading) or mature invadopodia (situated in areas of degradation, Fig. R27).

FAK autophosphorylation on Tyr397 regulates Src phosphorylation on Tyr416 (Mitra et al., 2005). We examined Src activity by quantifying pTyr416-Src and subsequent Src-dependent FAK phosphorylation on Tyr576/577 at the FAK catalytic domain. WIRE-depleted cells tended to show a decrease in pTyr416-Src and thus, a similar reduction in pTyr576/577-FAK (Fig. R28 A and B). To determine whether the subcellular distribution of phosphorylated proteins would provide further details, we used IF to examine fluorescence distribution from pTyr416-Src. Active Src in WIRE-deficient cells decreased significantly, whereas it showed a slight but non-significant increase in WIP-depleted cells (Fig. R28 C and D). Whilst in control cells pTyr416-Src was found mainly at the cell periphery and areas close to invadopodia, in WIP-deficient cells it was seen mostly at the periphery. As a control of reduced Src activity, we measured pTyr416-Src fluorescence levels in cells treated with the Src inhibitor PP2 (Table M4), and confirmed reduced Src activation. Cells lacking WICH/WIRE showed significantly lower levels of active Src than PP2-treated cells. (Fig. R28 C and D).

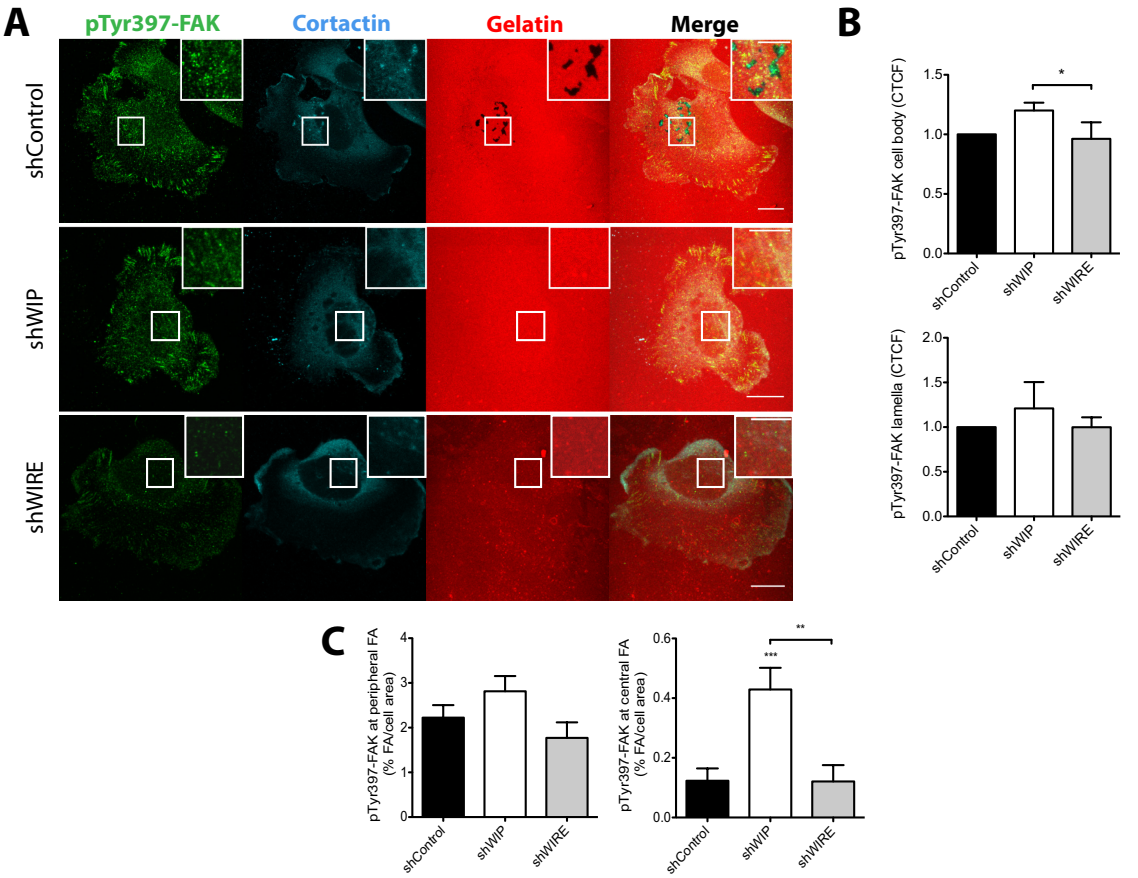

Figure R26: Absence of WIP promotes pTyr397-FAK-positive central FA. shControl-, shWIP- or shWIRE-infected cells were allowed to invade gelatin, fixed and stained for several proteins. Cell total corrected fluorescence (CTCF) was quantified on Z-projections from stacks of 2-3 images acquired with a 0.5 µm step size from the ventral area of the cell. (A) Representative images of cells plated on rhodamine-gelatin (5 h, red), stained for pTyr397-FAK (green) and cortactin (cyan). Bars: 10 µm (insets, 5 µm). (B) Distribution of pTyr397-FAK-related fluorescence in stained cells. (C) Distribution of pTyr397-FAK at peripheral and central FA. Data were normalised to control and shown as mean ± SEM of two independent experiments. *, p <0.05; **, p <0.01; ***, p <0.001 by 1-way ANOVA and Tukey's multiple comparison test.

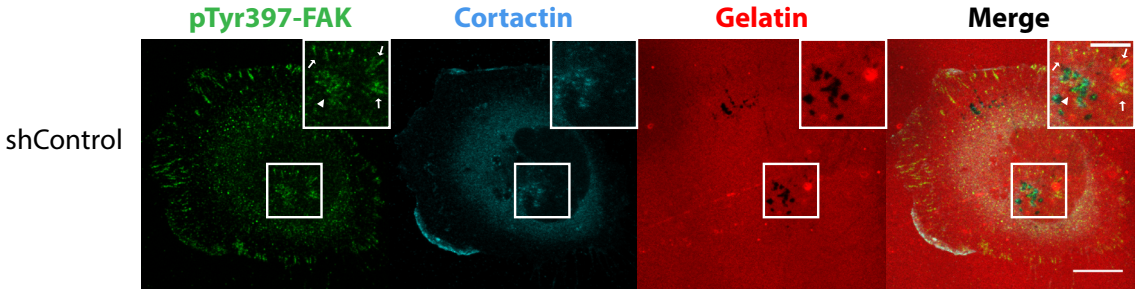

Figure R27: pY397-FAK localise close to areas of invadopodium formation. Control cells invading rhodamine-gelatin (5 h). (A) Images show pTyr397-FAK staining, which localises at peripheral FA, central FA (arrows) and surrounding cortactin-positive areas of active invadopodia (arrowheads). Bars: 10 µm (insets, 5 µm).

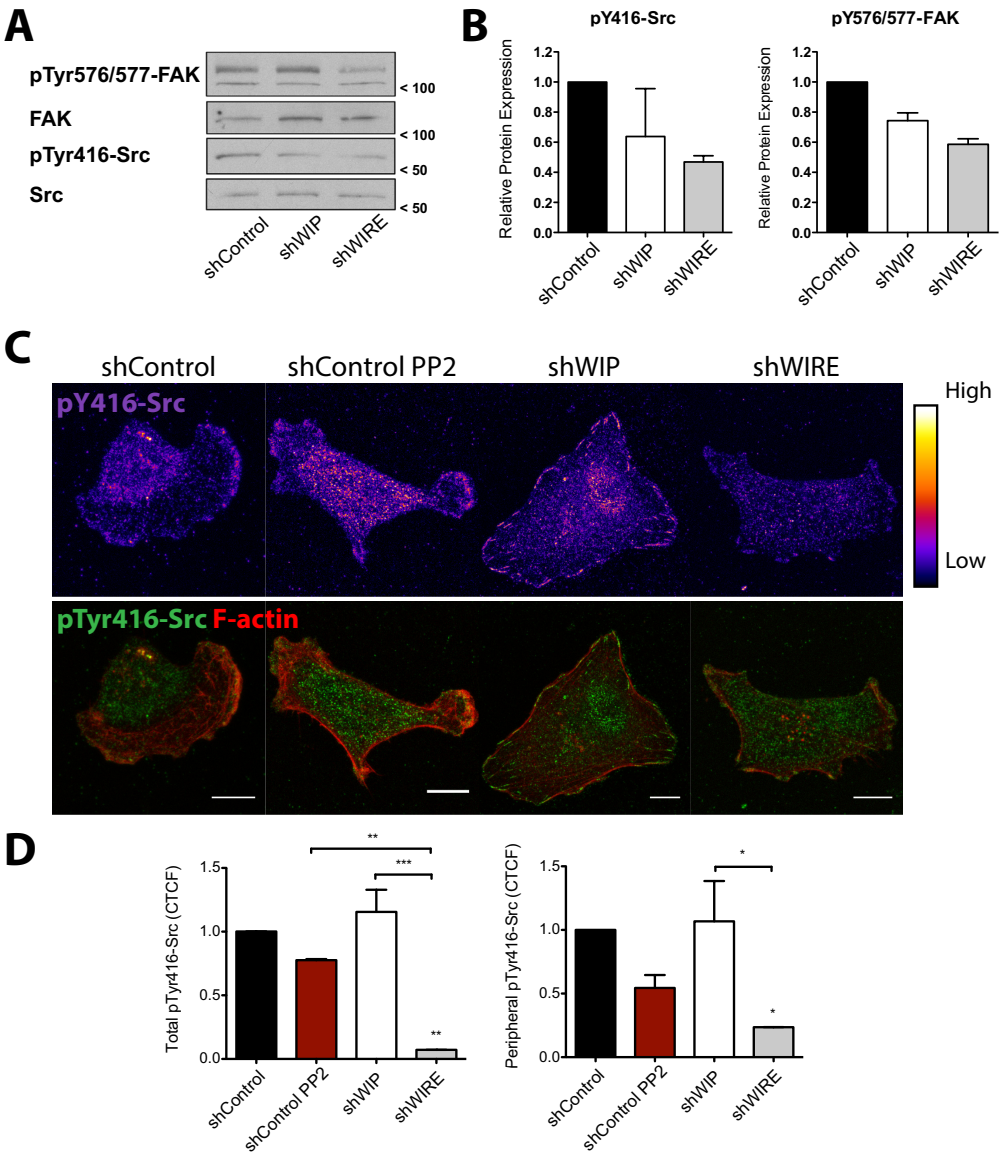

Figure R28: WIP and WICH/WIRE control Src localisation and activity. shControl-, shWIP- or shWIRE-infected cells were allowed to invade gelatin (3 h) and scraped into iced-cold lysis buffer to prepare soluble lysates (A, B), or fixed and processed by IF (C, D). (A) Representative WB image shows pTyr576/577-FAK, FAK, pTyr416-Src and Src expression. (B) Quantification of pTyr416-Src and pTyr576/577-FAK levels. (C) Representative images of cells invading gelatin in the presence or the absence of 10 µM PP2, stained by IF for pTyr416-Src (pseudocolour, top; green, bottom) and F-actin (red). Bars: 10 µm. (D) Fluorescence distribution in pTyr416-Src-stained cells. CTCF of total and peripheral pTyr416-Src levels was quantified on Z-projections from stacks of 2-3 images acquired with 0.5 µm step size from the ventral area of the cell. Data were normalised to control and shown as mean ± SD of three independent experiments. *, p <0.05; *, p <0.01; ***, p <0.001 by 1-way ANOVA and Tukey's multiple comparison test.

Proteins other than the FAK-Src complex contribute to cell migration and FA turnover, including Nck (Chaki et al., 2013). Nck interacts directly with WIP, N-WASP, and presumably WICH/WIRE (Aspenstrom, 2004), constituting a key factor in this pathway.

We examined Nck expression and localisation in WIP- and WIRE-deficient cells by IF; total Nck levels were vaguely reduced in both cell types (Fig. R29). Subcellular distribution also differed; Nck accumulated mostly at the periphery in WIP-deficient cells (with levels similar to those of controls in these areas), whereas in WIRE-deficient cells, remaining Nck was polarised to central areas.

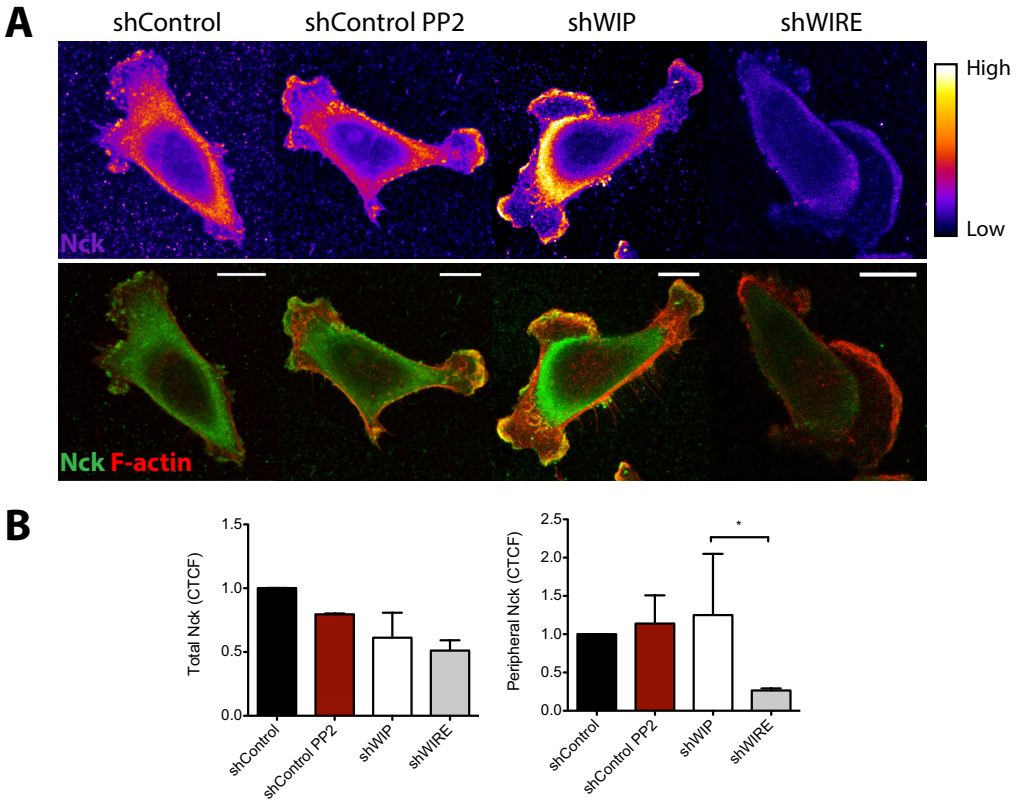

Figure R29: Lack of WIP or WICH/WIRE alters Nck localisation. shControl cells or shControl cells treated with 10 µM PP2, shWIP or shWIRE were plated on gelatin, incubated (3 h), fixed in 4% PFA and stained by IF for Nck (pseudocolour, top; green, bottom) and F-actin (red). (A) Representative images of cells grown on gelatin. Bars: 10 µm. (B) Quantification of total and peripheral Nck levels. Data were normalised to control and shown as mean ± SD of three independent experiments. *, $p < 0.05$ by 1-way ANOVA and Tukey's multiple comparison test

To verify that the effects observed in invading cells after WIRE reduction were due to altered Src activity, we tested several molecules that inhibit this kinase with different specificities, using control cells invading gelatin to calibrate the concentration that gave the maximum effect (Fig. R30). With all drugs tested, Src inhibition reduced cell ability to form invadopodia and degrade the matrix, similar to observations in WIP- but not in WIRE-depleted cells (Fig. R31 A and B). Nck distribution in control cells after Src inhibition with PP2 was also comparable to that in WIP-depleted cells (Fig. R29).

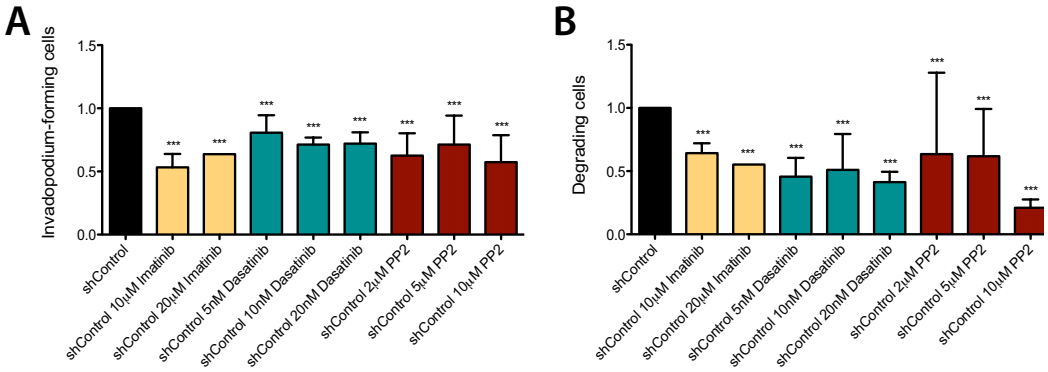

Figure R30: Titration of Src inhibitors for invadopodium formation and degradation. shControl cells were allowed to invade rhodamine-gelatin in the presence of various concentrations of the Src inhibitors imatinib, dasatinib and PP2 (3 h). Quantification of relative invadopodium-forming (A) and gelatin-degrading cells (B) were normalised to shControl values. Data show mean ± SD of at least three independent experiments (except 20 µM Imatinib, for which only one experiment was performed). ***, p <0.001, Chi square test.

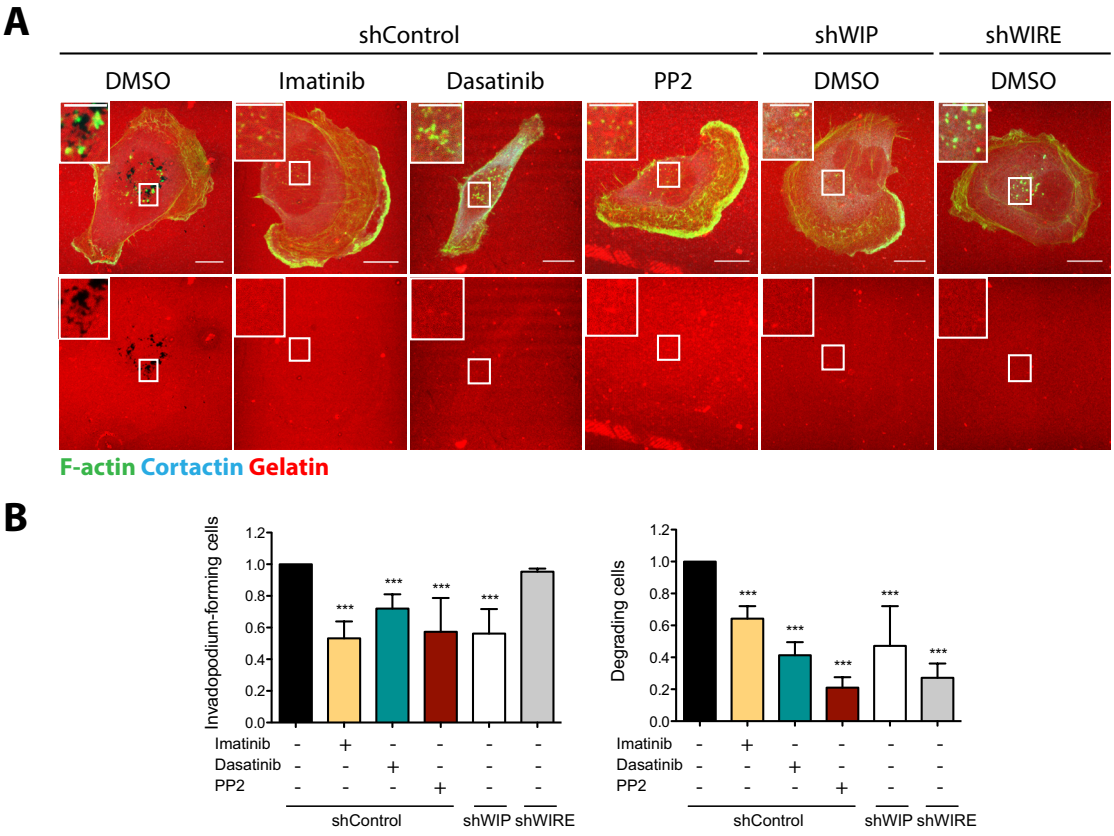

Figure R31: Src inhibition mimics the effect of silencing WIP in invadopodium formation and degradation. shControl-, shWIP- and shWIRE-infected cells were allowed to invade rhodamine-gelatin-coated glass coverslips (red) in the presence of vehicle or the Src inhibitors imatinib (10 µM), dasatinib (20 nM) and PP2 (10 µM) (5 h); (A) representative images of shControl cells incubated in DMSO or Src inhibitors and shWIP and shWIRE show F-actin (green) and cortactin (cyan) markers. Bars: 10 µm (insets, 5 µm). (B) Quantification of relative invadopodium-forming cells and degrading cells were normalised to shControl values. Data show mean ± SD of at least three independent experiments. ***, p <0.001 by the Chi square test.

To test whether recovery of Src activation would be sufficient to overcome the lack of WIP and/or WICH/WIRE, we expressed a wild type (WT-Src) and an inactive form of Src (DN-Src) in control and depleted cells. WIP-deficient cells expressing WT-Src recovered not only the ability to form invadopodia at levels similar to control cells (Fig. R32), but also function, since they were able to degrade gelatin. In contrast, no effect was observed when this construct was expressed in control or WIRE-deficient cells. DN-Src expression in control cells mimicked the defects observed in the absence of WIP and had no additive effect in WIP-depleted cells.

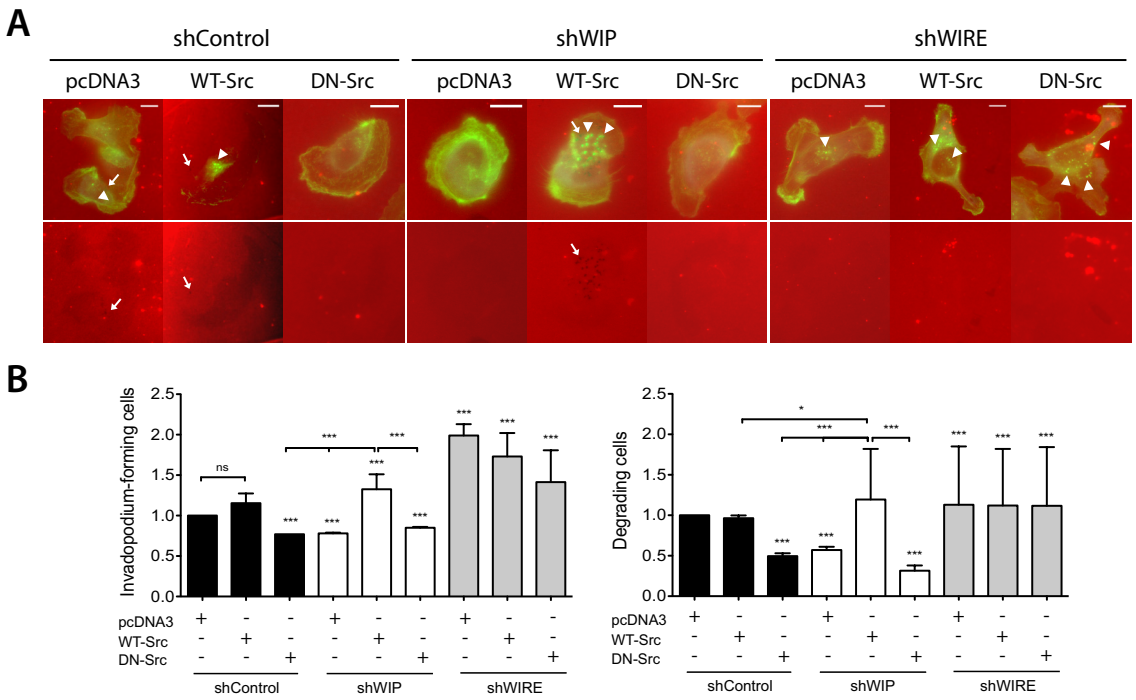

Figure R32: Src overexpression overcomes the defects due to lack of WIP. Exogenous expression of WT-Src and DN-Src in shControl, shWIP and shWIRE cells. (A) Representative images of cells invading on rhodamine-gelatin (red) show F-actin staining (green). Arrowheads indicate invadopodia, arrows indicate areas of gelatin degradation. Bars: 10 µm. (B) Values for invadopodium-forming and degrading cells were normalised to those for controls. Data show mean ± SD of at least three independent experiments. *, p <0.05; ***, p <0.001, Chi square test.

These results suggest that WIP, but not WICH/WIRE, acts upstream of Src during invadopodium formation and maturation.

5.4.3.2 N-WASP activation is necessary for efficient invadopodium-mediated invasion

N-WASP makes an important contribution to tumour invasion by regulating MMP and remodelling the ECM (Gligorijevic et al., 2012; Yu et al., 2012). Loss of WIP nonetheless renders a distinct phenotype from loss of N-WASP. Nck and N-WASP regulate the actin-binding activity of WIP and WICH/WIRE (these proteins share a common actin-binding domain) (Aspenstrom, 2002; Kato et al., 2002; Ramesh et al., 1997). We therefore studied the association between these proteins during invasion. We immunoprecipitated N-WASP, WIP and WICH/WIRE. By WB analysis, we examined the proteins that co-immunoprecipitated in each case and found that, in MDA-MB-231 cells, N-WASP interacted with both WIP and WICH/WIRE (Fig. R33).

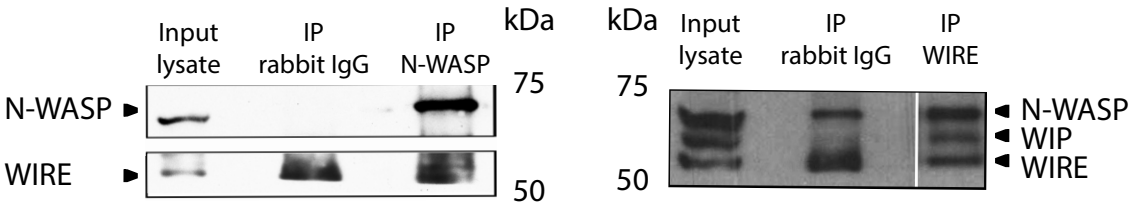

Figure R33: N-WASP interacts with WIP and WICH/WIRE in MDA-MB-231 cells. Co-immunoprecipitation of N-WASP-WIP and N-WASP-WICH/WIRE-WIP in MDA-MB-231 cell lysates. Nitrocellulose membranes were incubated with anti-N-WASP, -WICH/WIRE and -WIP antibodies. The image shows a representative WB in which N-WASP (left) or WICH/WIRE (right) proteins were immunoprecipitated.

Subsequently, we tested whether WIP or WICH/WIRE overexpression was sufficient to rescue invasion in cells lacking expression of one of these proteins. WIP overexpression in control MDA-MB-231 and MDA-MB-468 cells (basal A) reduced endogenous WICH/WIRE levels (Fig. R34), suggesting an intricate regulation between WIP and WIRE expression and function in BCC. Related to WIRE reduction, preliminary data also showed a decrease in N-WASP expression after WIP overexpression (Fig. R34), which correlated with our primary characterisation of the effects of WIRE depletion (Fig. R15). WIRE overexpression did not rescue any of the effects of WIP depletion (Fig. R35). In contrast, WIP overexpression in WIRE-deficient cells rescued the ability to degrade gelatin (Fig. R35). This suggests that WICH/WIRE binding to N-WASP is important for its role in invasion.

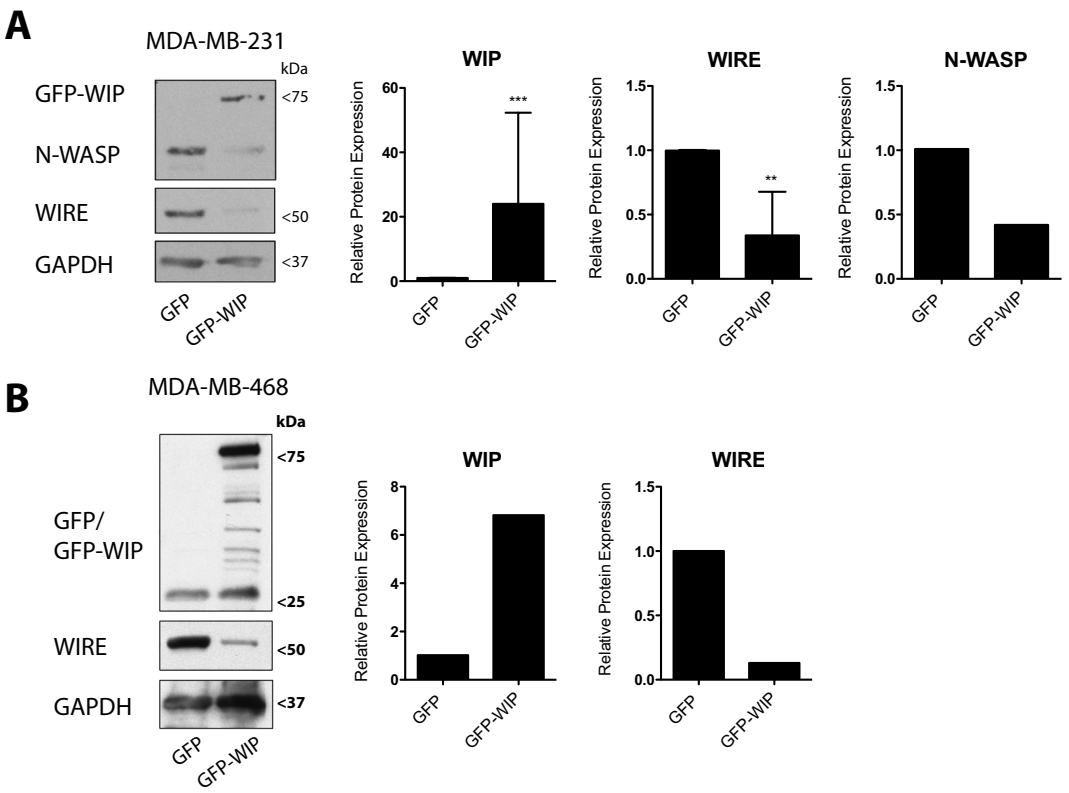

Figure R34: WIP overexpression downregulates WICH/WIRE levels. Soluble lysates from MDA-MB-231 (A, n = 3 for WIP and WIRE; n = 1 for N-WASP) or MDA-MB-468 cells (B, n = 1) transiently overexpressing GFP or GFP-WIP (by infection or nucleofection) were analysed by WB (left). Quantification of WB experiments is shown (right). Data show mean ± SD. **, p <0.01; ***, p <0.001 by Student's t-test.

Treatment of control cells with the N-WASP inhibitor wiskostatin supports these results, as treated cells mimic the defects observed in cells that lack WIRE but not those that lack WIP, where wiskostatin treatment had an additive effect on invadopodium activity (Fig. R36). Wiskostatin treatment not only mimicked the non-invasive behaviour of WIRE-depleted cells, but also increased the number and size of vesicles surrounded by F-actin and cortactin-positive dots, as observed in WIRE-depleted cells (Fig. R37). In addition, analyses of MT1-MMP fluorescence distribution showed that in the absence of WICH/WIRE or in cells cultured in the presence of wiskostatin, we found a non-significant increase of MT1-MMP at the cell periphery, suggesting an abnormal traffic of this MMP when WIRE is lost or N-WASP is inactive. These results suggest that during invasion, N-WASP and WICH/WIRE cooperation is necessary for correct maturation of invadopodia.

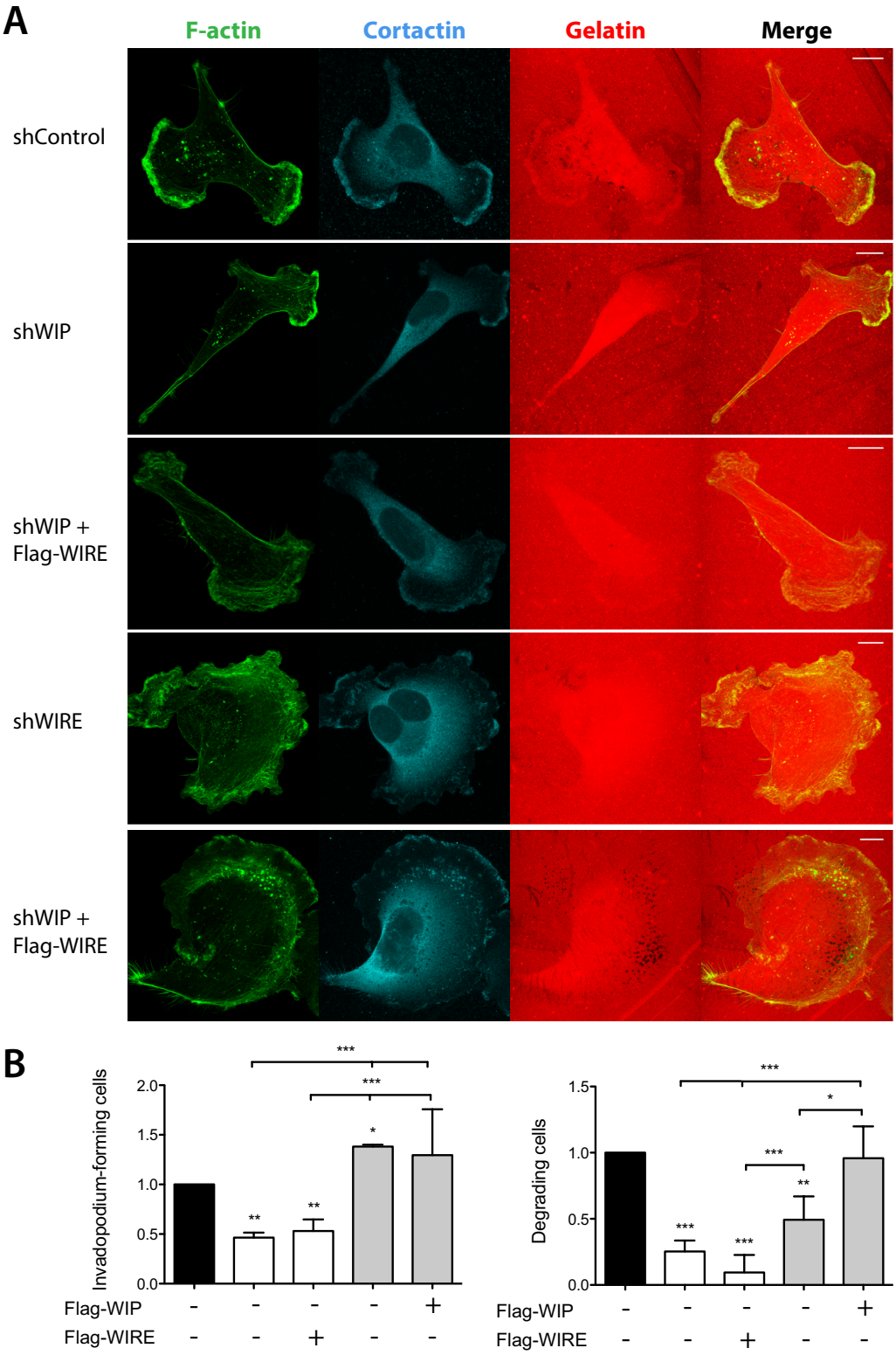

Figure R35: Exogenous WIP expression rescues efficient invasion by WIRE-deficient cells. Overexpression of Flag-WIP or Flag-WIRE in WIP- and WIRE-deficient cells. (A) Representative images of cells invading on rhodamine-gelatin (red) show F-actin (green) and cortactin (cyan) staining. Arrowheads indicate invadopodia, arrows indicate areas of gelatin degradation. Bars: 10 µm. (B) Values for relative invadopodium formation and degradation were normalised to control values. Data show mean ± SD of at least three independent experiments. *, p <0.05; **, p <0.01; ***, p <0.001, Chi square test.

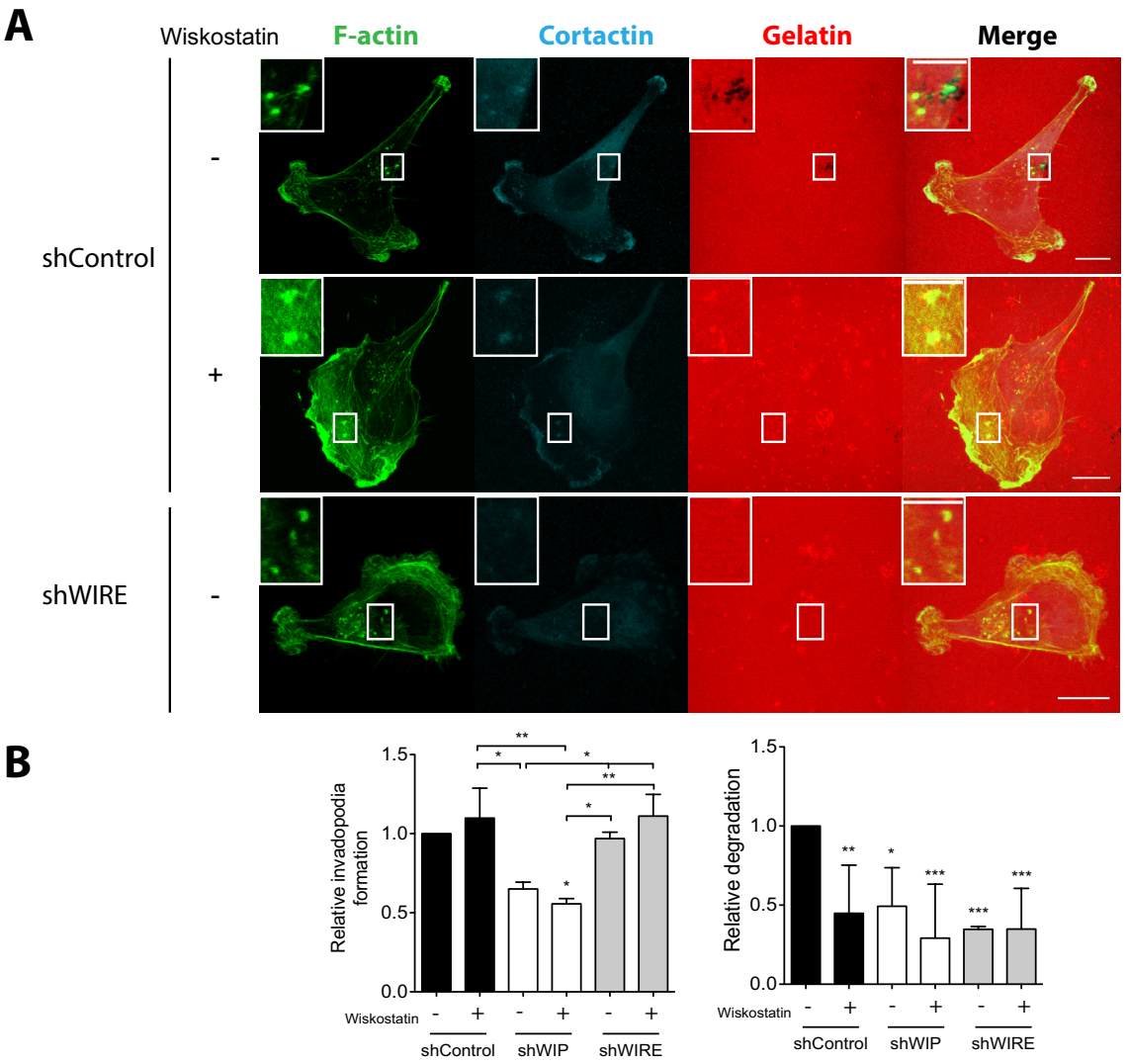

Figure R36: Wiskostatin treatment of control cells mimics WIRE deficiency. shControl, shWIP and shWIRE MDA-MB-231 cells were allowed to invade rhodamine-gelatin (red) in the presence of vehicle or 3 µM wiskostatin (3 h). (A) Cells were fixed and stained for F-actin (green) and cortactin (cyan). Bars: 10 µm (insets, 5 µm). (B) Quantification of invadopodium formation and activity of cells in A. Data show mean ± SD of at least three independent experiments. *, p <0.05; **, p <0.01; ***, p <0.001 by the Chi square test.

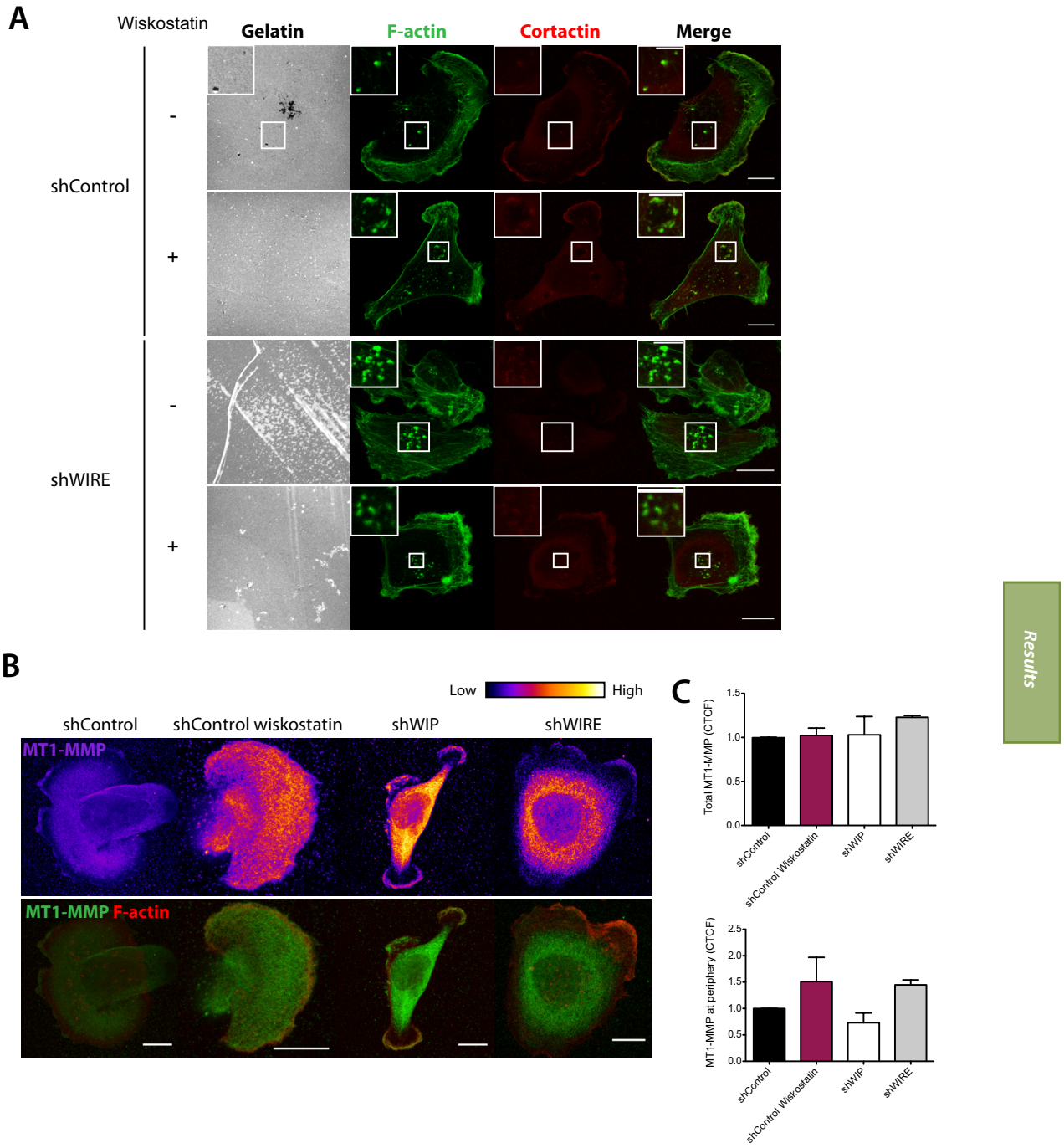

Figure R37: Wiskostatin treatment and WIRE deficiency promote formation of vesicles surrounded by F-actin and cortactin. shControl, shWIP and shWIRE MDA-MB-231 cells were allowed to invade rhodamine-gelatin (gray) in the presence of vehicle or 3 µM wiskostatin (3 h). (A) Cells were fixed and stained for F-actin (green) and cortactin (red) or (B) MT1-MMP (pseudocolour, top; green, bottom) or F-actin (red). Bars: 10 µm (insets, 5 µm). (C) Fluorescence distribution (CTCF) of total and peripheral MT1-MMP levels was quantified on Z-projections from stacks of 2-3 images acquired with 0.5 µm step size from the ventral area of the cell. Data were normalised to control and shown as mean ± SD of two independent experiments.

5.4.3.3 Nck binding to WIP contributes to invadopodium maturation

Recruitment of the adaptor protein Nck by cortactin is necessary for successful invadopodium maturation (Oser et al., 2009; Yamaguchi et al., 2005). Nck interaction with WIP and N-WASP promotes actin polymerisation (Ditlev et al., 2012), but how these interactions contribute to invadopodium-mediated invasion remains unclear. As WIP also associates with cortactin, we studied the contribution of these interactions to invadopodium activity. We used MDA-MB-231 cells to express different forms of WIP lacking its binding domains to cortactin (ΔCBD-WIP), Nck (ΔNBD-WIP) or N-WASP (ΔWBD-WIP, Fig. R38 A). Overexpression of full-length WIP enhanced invadopodium formation, while gelatin degradation remained unaffected (Fig. R38). Cells expressing ΔCBD-WIP and ΔWBD-WIP did not promote invadopodium formation and remained at control levels. ΔNBD-WIP-expressing cells not only showed an increase in invadopodium formation, but also in the number of degrading structures (Fig. R38).

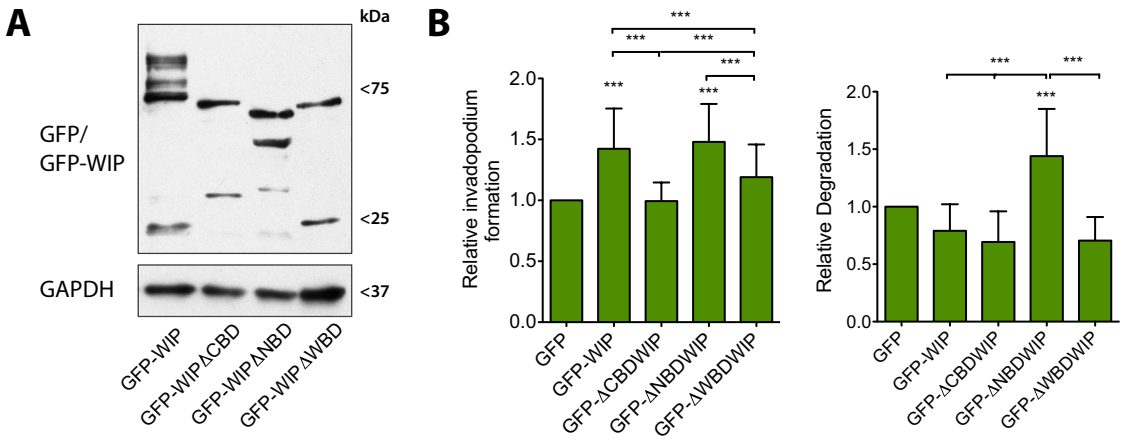

Figure R38: WIP binding to cortactin and N-WASP are needed to induce invadopodium formation. MDA-MB-231 cells overexpressing WIP or WIP mutants that lacked the binding domains to cortactin, Nck or N-WASP were plated on rhodamine-gelatin (5 h). (A) Representative WB shows GFP and GAPDH expression. (B) Quantification of invadopodium formation and degradation were normalised to GFP-expressing cell control values. Data show mean ± SD of at least three independent experiments. ***, p <0.001 by the Chi square test.

Since WIP overexpression overcomes the defects during invasion derived from WIRE depletion (Fig. R33), we examined whether any of the previously studied WIP-binding domains mediated this process. After overexpression of full-length WIP or WIP mutants, we found no alterations in invadopodium formation in WIRE-deficient cells

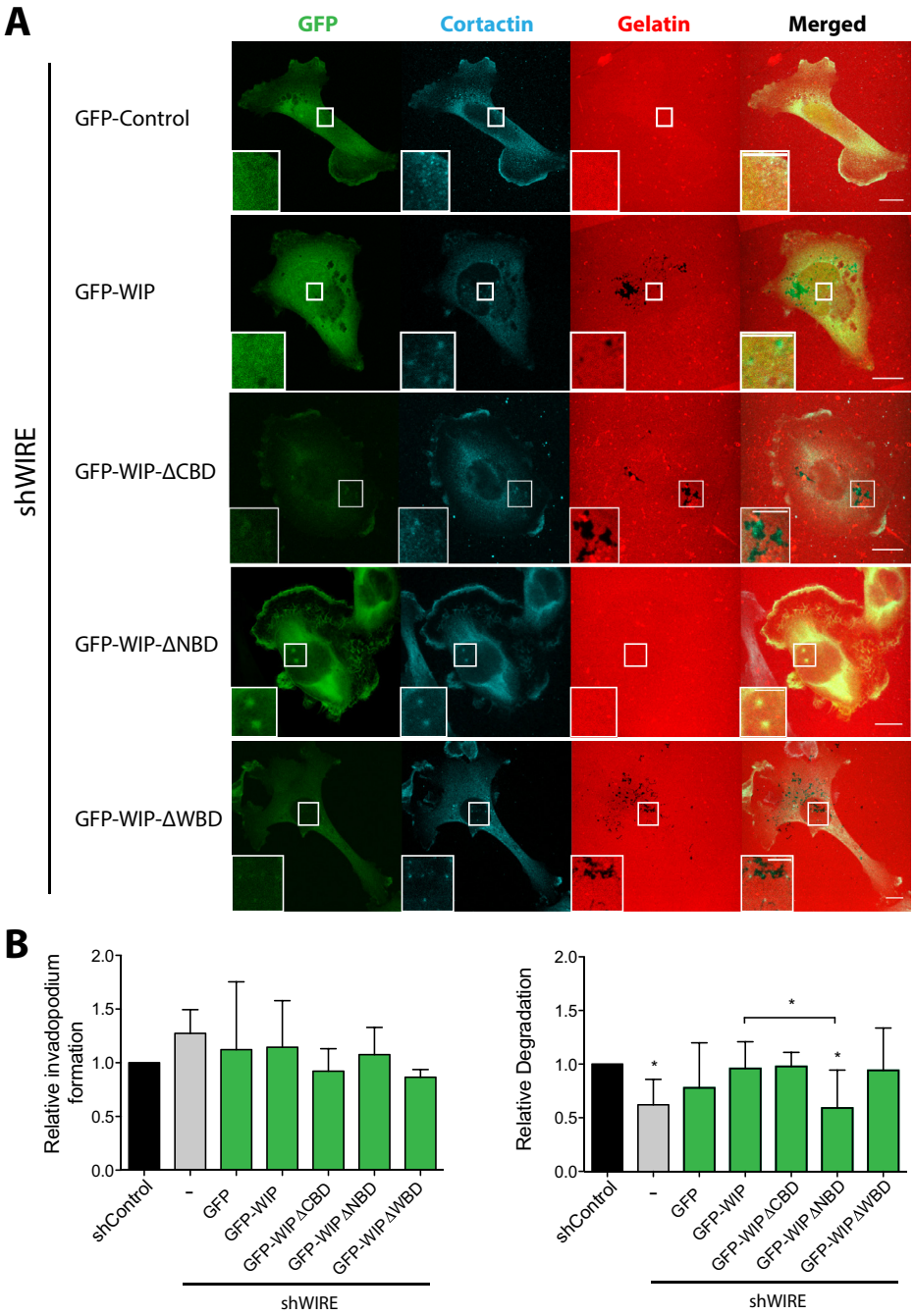

Figure R39: The WIP Nck-binding domain is essential in rescuing lack of WIRE. MDA-MB-231 shWIRE cells were nucleofected with plasmids encoding GFP-WIP, GFP-ΔCBD-WIP, GFP-ΔNBD-WIP or GFP-ΔWBD-WIP and plated on fluorescent gelatin (red). (A) Representative images of shWIRE GFP-expressing cells (green) co-stained by IF for cortactin (cyan). Bars: 10 µm (insets, 5 µm). (B) Values for relative invadopodium formation and degradation were normalised to control values. Data show mean ± SD of at least three independent experiments. *, p <0.05 by the Chi square test.

(Fig. R39). As anticipated, the ability of invadopodia to degrade gelatin was regained after WIP expression, except in ΔNBD-WIP-expressing cells, whose degradation levels were similar to those of WIRE-deficient cells (Fig. R39). Although contrasting, the effects of control and WIRE-deficient cells that lack the Nck-binding domain differed significantly from those of other cells bearing WIP or WIP mutants (Fig. R40).

In summary, WIP binding to Nck produces opposite effects in the presence or absence of WICH/WIRE; this suggests the need for a balance in the Nck bound to these proteins when both WIP and WICH/WIRE are expressed. When WIP is overexpressed but unable to bind Nck, the ability of invadopodia to degrade gelatin increases compared to controls, whereas when this mutant is overexpressed in the absence of WICH/WIRE, gelatin degradation is significantly reduced. These events indicate that WICH/WIRE is necessary for invadopodium maturation.

5.5 WIP IS NECESSARY FOR THE MESENCHYMAL PHENOTYPE OF BASAL B CELLS

Although we demonstrated that WIP and WICH/WIRE contribute to matrix degradation and invasion by MDA-MB-231 cancer cells, only WIP is differentially expressed in BCC. We hypothesised that in addition to controlling cell invasion, WIP might regulate other components that contribute to the invasive behaviour of these cells. Since WIP is overexpressed in prostate cancer cells after EMT induction (Gu et al., 2007), we tested whether WIP is involved in EMT regulation. Using WB, we analysed epithelial marker levels after WIP overexpression in luminal cells, but found no alteration in their expression (Fig. R13). MDA-MB-231 (mesenchymal-like) WIP-deficient cells showed notable changes in cell morphology only after at least one month in culture, when they acquire epithelial-like characteristics (Fig. R41 A). Analysis of epithelial and mesenchymal marker expression indicated a tendency toward increased E-cadherin and β-catenin in MDA-MB-231 and Hs578T WIP-depleted cells (Fig. R41 B and C), whereas the mesenchymal marker vimentin was significantly reduced in WIP-depleted MDA-MB-231 cells (Fig. R42).

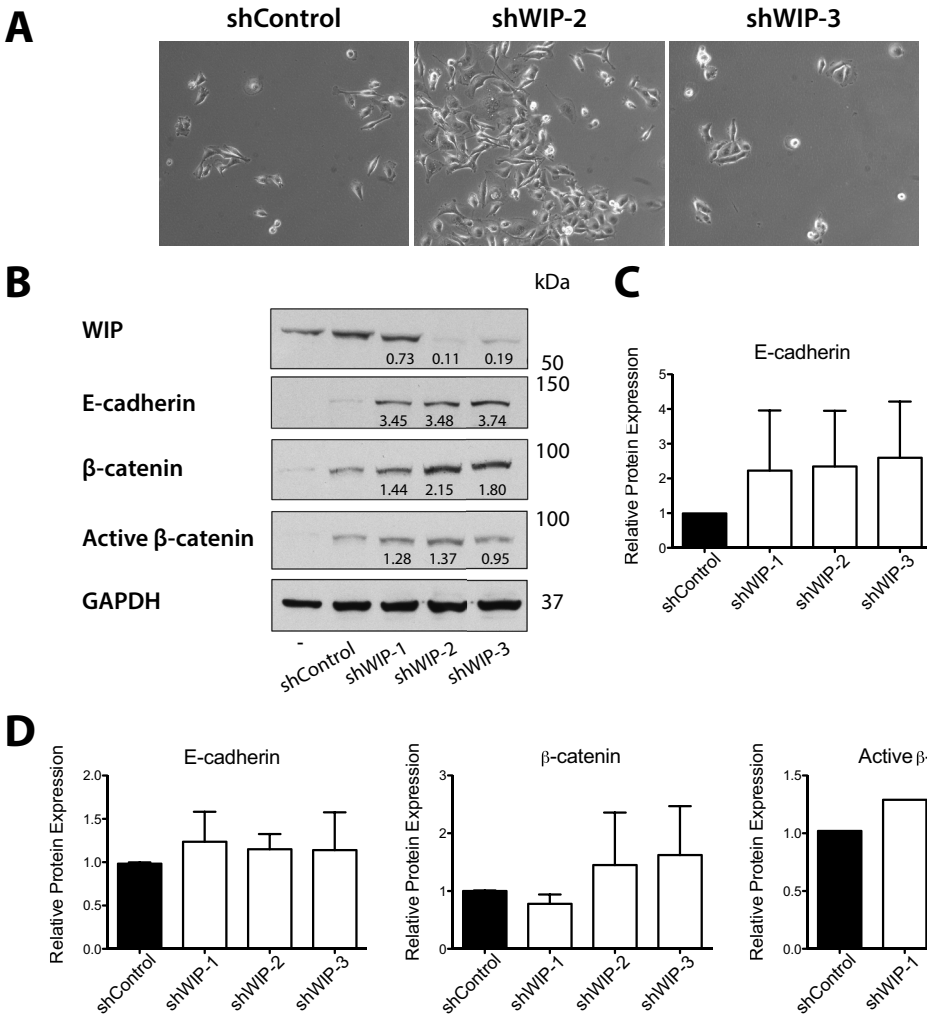

Figure R40: WIP induces an increase in epithelial markers. (A) Representative images of cultured MDA-MB-231 cells stably infected with shControl or various shWIP. (B) Representative WB of MDA-MB-231 shows E-cadherin, β-catenin, active β-catenin and GAPDH levels in shControl and shWIP total cell lysates (30 µg/lane). (C) Densitometric analysis of E cadherin in shControl and shWIP MDA-MB-231 cells (n = 2). (D) Densitometric analyses of E cadherin (n = 3), β-catenin (n = 3) and active β-catenin (n = 1) in Hs578T shControl and shWIP cells. Data show mean ± SD. Values were normalised to controls.

WIP depletion clearly altered the mesenchymal phenotype in MDA-MB-231 cells and, although with variable intensity, induced an increase in epithelial markers in the basal B cell lines tested. Because tumour growth is another central process in cancer progression, we measured cell proliferation in WIP-deficient MDA-MB-231 cells. Lack of WIP significantly reduced proliferation, to an extent similar to chemical treatment with the proliferation inhibitor AraC (Table M4, Figure R42).

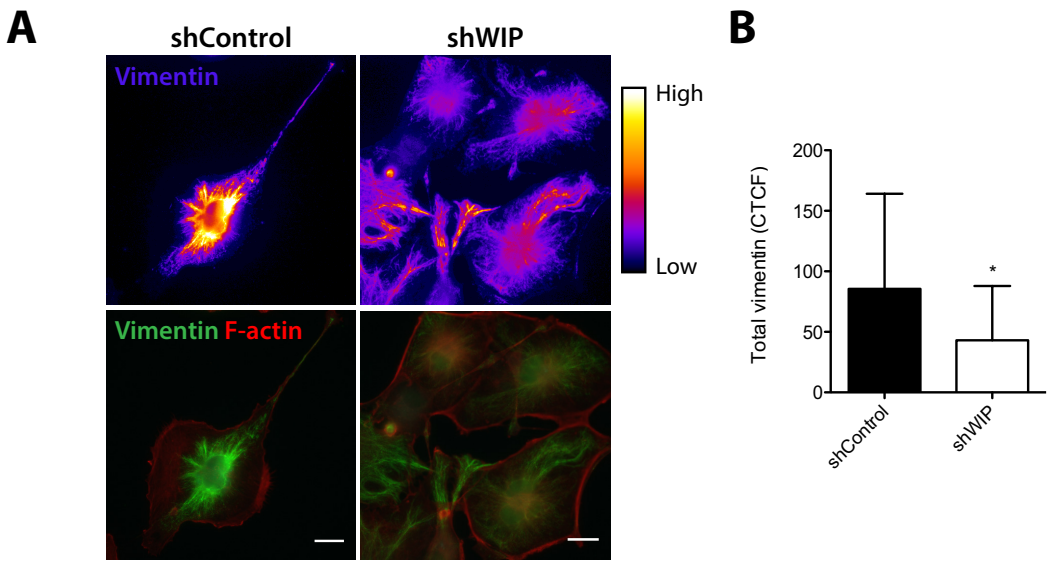

Figure R41: Lack of WIP provokes a decrease in the mesenchymal marker vimentin. MDA-MB-231 cells were stably infected with shControl or shWIP. (A) Cells were cultured on glass coverslips (24 h), fixed in 4% PFA and stained by IF for vimentin (pseudocolour, green) and F actin (red). (B) Quantification of vimentin fluorescence intensity (CTCF) is shown. Data were normalised to controls and are shown as mean ± SD (n = 1 experiment, where 15-20 cells were analysed per condition). *, p <0.05 by t-Student's test.

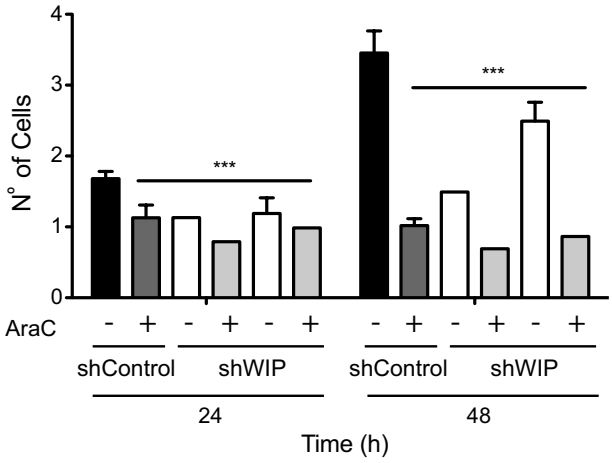

Figure R42: Proliferation is impaired in WIP-deficient cells. MDA-MB-231 cells stably infected with shControl or shWIP were plated and cultured (48 h). Cell number was calculated every 24 h after trypsinisation and cell collection. Data were normalised to the number of cells seeded at t = 0, and are shown as mean ± SD of three independent experiments. ***, p <0.001 by 1-way ANOVA and Tukey's multiple comparison test.

Although further experiments should be performed to confirm these data, preliminary results suggest that WIP has an important role in controlling not only the invasive behaviour of BCC, but also other alterations in the phenotype of these cells that are necessary for different stages of tumour progression.

Discussion

6. DISCUSSION

In this study, we provide insights into the way WIP and WICH/WIRE contribute to BCC invasiveness, using diverse biochemical and advanced cellular approaches that mimic conditions of *in vivo* invasion. We describe a previously unidentified role for WICH/WIRE in cancer invasion, and characterise the means by which WIP and WICH/WIRE regulate the activity and localisation of the FAK/Src complex and of the adaptor protein Nck. Our results lead to a model in which WIP plays an essential role in the generation of invasive protrusions and FA stability, which would regulate invadopodium initiation and/or persistence. Once the invadopodium is established, WICH/WIRE contributes to the degradative activity of invadopodia and possibly to that of other invasive protrusions. We found that both proteins are well expressed in BCC, that their expression in the cell is precisely regulated, and that WIP can replace WICH/WIRE functions. Closely related to its role in invasiveness, WIP has an unpredicted function in the regulation of proliferation and mesenchymal properties, as WIP levels are strong in basal B cells and weak in luminal cells. The data presented here highlight WIP as a key element in cell invasion and cancer progression.

6.1 Characterisation of WIP expression in human BCC

Using PEPSCAN and WB techniques, we characterised various anti-WIP antibodies and selected the commercial antibody H-224 as the most appropriate for examining WIP expression in human tumour cells. Although H-224 recognises a highly conserved sequence in the human and murine proteins, we barely detected WIP in murine samples using this antibody in WB (Fig. R1 A). This could be due to differences in the amino acid sequences immediately before and after the epitope regions (Fig R3), leading to conformational changes in the protein, which could alter antibody access to the epitope.

Most antibodies tested recognised bands of diverse sizes (Fig. R1). These bands might represent degradation sub-products or various WIP isoforms; additional analyses are therefore needed to confirm these hypotheses. We found that basal B BCC expressed a ≈34 kDa product that correlates with the size of the mini-WIP isoform (Koduru et al., 2007). This band was recognised by H-224 and 3D10 antibodies; the latter recognises

specifically mini-WIP in diverse immune cells (Koduru et al., 2007). Added to the fact that WIP-shRNAs specifically reduce the levels of this product (Fig. R14), our results strongly suggest that basal B BCC express mini-WIP, although at variable levels. Mini-WIP lacks the WIP N-WASP-binding domain (Koduru et al., 2007), which suggests that this isoform competes with WIP binding to other proteins such as actin, cortactin or Nck. Further analyses are necessary to determine whether this isoform is indeed mini-WIP, and its relative affinity to WIP-binding partners.

WIP is ubiquitously expressed in mammalian cells, and particularly in immune cells where it is needed for correct immune response, as it is involved in migration, invasion and formation of the immune synapse (Anton et al., 2002; Calle et al., 2008; Krzewski et al., 2008; Tsuboi and Meerloo, 2007). Similarly, the very high WIP levels in basal B BCC imply a role in mesenchymal cell migration and invasion (Fig. R5). WIP localisation at the cell leading edge together with F-actin and cortactin emphasises its importance in lamellipodium dynamics (Figs. R8 and R10), and its presence at the distal tip of invasive protrusions (Fig. R11) might indicate its relevance in invasion. WIP localises near microtubules in Hs578T cells (Fig. R9), but we found no evidences to support its involvement in cell trafficking or other microtubule-related functions. WAFL (WASP and FKBP-like) interacts with WIP, is located on microtubules, and has a role in early endocytic traffic (Viklund et al., 2009); these findings indicate a probable link between WIP and microtubules.

6.2 WIP AND WICH/WIRE REGULATE INVASION IN DIFFERENT WAYS

In this study, we used diverse matrices to analyse cancer cell-driven invasion. The results of these experiments indicate that WIP and WICH/WIRE contribute to invasion in 2D and 3D systems, but participate in different manners.

6.2.1 WIP regulates FA localisation and invadopodium formation

Although the WIP contribution to invadopodium-mediated invasion was described a few years ago (Yamaguchi et al., 2005), our study provides the first evidence of endogenous WIP in invadopodia and invasive protrusions that develop in Matrigel

(Fig. R11) (Garcia et al., 2012). Apart from the importance of WIP binding to N-WASP in invadopodium formation, little was initially known regarding the mechanisms through which WIP mediates this process. In this study, we confirm the importance of WIP in invadopodium formation and describe its contribution to 3D invasion and BM degradation, which are thought to better mimic *in vivo* invasion than gelatin invasion assays (Friedl and Wolf, 2008). Ongoing *in vivo* experiments will further clarify the importance of WIP in cancer invasion and metastasis.

As mentioned above, the absence of WIP provoked no changes in cell morphology or protrusion elongation in Matrigel, but significantly reduced cell invasiveness (Figs. R16 and R17). In migration experiments, we observed that WIP controls persistence of movement and velocity (Fig. R20). When matrix was added, behaviour was comparable, as protrusion duration in CIA was shorter than in controls (Fig. R18). In addition, altered paxillin recruitment to FA in these cells (Fig. R21) confirms a cell adhesion defect, and could explain why MMP inhibition in WIP-deficient cells induced a further reduction of invasion in Matrigel plugs (Fig. R16).

Results for cells invading gelatin initially appeared different from the findings above, since lack of WIP impaired invadopodium formation and degradation. The fact that these cells protrude more efficiently in Matrigel than in gelatin suggests that polarisation and interaction with the ECM are essential factors in invasion. In Matrigel experiments, cells were completely or mostly surrounded by the matrix, in contrast to gelatin assays in which the matrix was only situated ventrally. Depending on the system used, these differences determine the development of a range of cell morphologies and protrusion diversity (Fig. D1). There have been many studies to clarify how cancer cells invade *in vivo*. Mesenchymal cells tend to invade (Fig. D1 A), forming strands of cells independently of whether they invade collectively or as single cells. In 3D matrices, cancer cells elongate and protrude towards the edge of the tumour, forming branched protrusions that provide proteolytic activity and motility (Friedl and Wolf, 2008; Kubow and Horwitz, 2011). In 2D conditions, migratory and invasive activities are separate, as cells form lamellipodia and invadopodia that collaborate to facilitate net movement (Fig. D1 B). There is little evidence to support the existence of invadopodia or FA in 3D or *in vivo* (Gligorijevic et al., 2012; Harunaga and Yamada, 2011; Kubow and Horwitz, 2011);

this makes understanding the relationship between the actin structures visualised in 2D and 3D matrices one of the most challenging topics of study in cell biology at the moment.

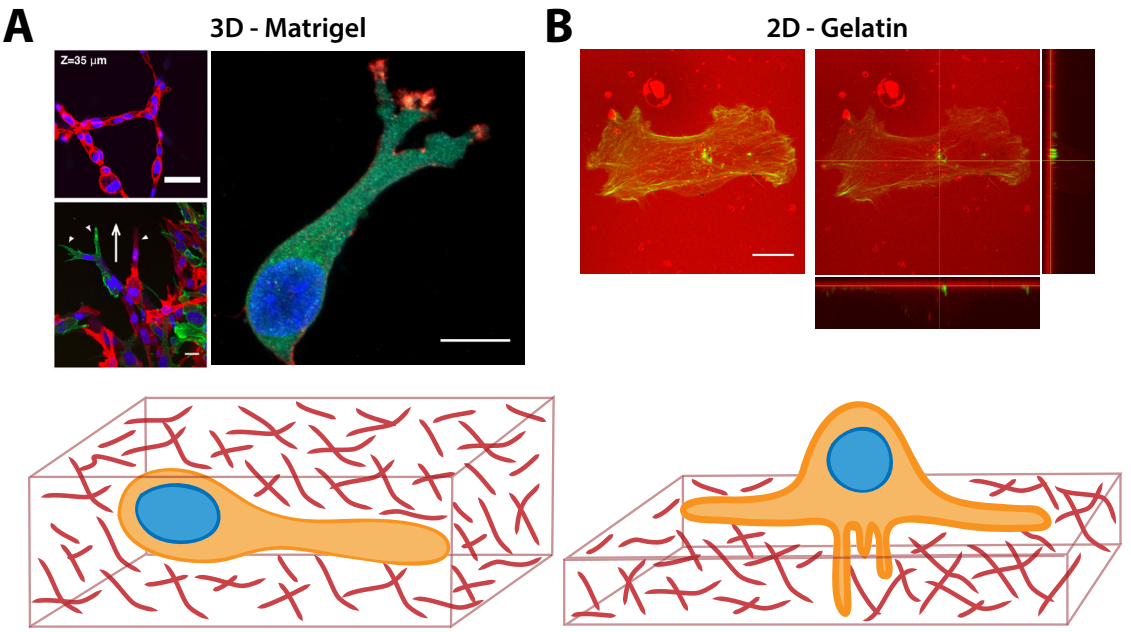

Figure D1: Cell plasticity in 3D and 2D environments

In the recent years, several studies have highlighted the close relationship between FA and invadopodia. Not all cancer cells develop invadopodia to degrade and migrate into the matrix; some cell types instead form FA with proteolytic activity (Wang and McNiven, 2012). FA and invadopodia share several factors and regulatory pathways. On the one hand, major components of FA such as vinculin, paxillin or β1-integrin also localise at invadopodia (Block et al., 2008; Branch et al., 2012). On the other hand, FAK modulates Src-dependent invadopodium formation and localisation (Chan et al., 2009) and regulates ECM degradation at FA (Wang and McNiven, 2012). FA are proposed to act as references for later podosome formation (McNiven, 2013; Oikawa et al., 2008), as scaffolding and regulatory proteins are recruited that will constitute part of the newly formed invadopodia. Based on the increased localisation of pTyr397-FAK at central FA in WIP-deficient cells (where invadopodia usually form in MDA-MB-231 cells), we propose that WIP participates in the regulation of FA turnover or stability and maturation into invadopodia. In the absence of WIP, FA would be stabilised, prolonging their duration, but initiation of invadopodia would be impaired.

Some authors propose the existence of a "hybrid" structure that would form instead of FA and/or invadopodia at the leading edge of invading cells (McNiven, 2013). The fact that WIP regulates invasion in different types of protrusions, such as invadopodia (2D) and pseudopods formed in Matrigel (3D) (Figs. R17 and R24), suggests that their origin is related, lending strength to the "hybrid" hypothesis. Based on the similarity of the effects of WIP depletion on invasiveness in 2D and 3D matrices, we focused on the mechanisms that regulate invadopodium dynamics, as this structure has been widely analysed and constitutes a robust model of study. Although the best known WIP functions are dependent on its interaction with N-WASP, WIP also binds several proteins such as cortactin or Nck that contribute to initial or later steps of invadopodium development (Anton et al., 1998; Clark et al., 2007; Kinley et al., 2003; Oikawa et al., 2008; Oser et al., 2010; Oser et al., 2009; Yamaguchi et al., 2005). We found that the cortactin-binding domain of WIP, but not its Nck-binding domain, is necessary to promote invadopodium formation in WIP-overexpressing MDA-MB-231 cells (Fig. R38). The migratory behaviour of Nck-depleted cells is remarkably similar to that of cells lacking WIP –as Nck-depleted cells show a decrease in migratory abilities due to alterations in persistence of movement (Chaki et al., 2013), suggesting that the two events are related. Moreover, Src-dependent phosphorylation of Tyr421 or Tyr466 residues of cortactin is necessary for Nck recruitment and initiation of invadopodium development (Oser et al., 2010). Although WIP interacts with both of these proteins, WIP binding to Nck appears dispensable for promoting invadopodia (Fig. R38). We thus speculate that WIP is a necessary platform for Nck recruitment by cortactin, either by direct binding to cortactin, which would facilitate cortactin-Nck interaction, or through N-WASP interaction (Fig. D2).

Whilst in the absence of WIP, FAK and Src appear fully active compared to control cells, we observed that for invadopodium formation, Src inhibition by PP2 mimicked the absence of WIP (Fig. R31). The defects observed in WIP-deficient cells were overcome by Src overexpression (Fig. R32), in contrast to WIRE-deficient cells, which showed lower phosphorylation of Tyr416-pSrc than controls (Fig. R28). These data imply that WIP is acting upstream Src, but further analyses will be needed to determine the way WIP regulates this process. We propose that Nck is involved in WIP-mediated inasion, since cells lacking WIP and Nck behave similarly (Chaki et al., 2013), and Src inhibition by PP2

delocalised Nck to the cell periphery as in WIP-deficient cells (Fig. R29). In addition to its role in invadopodium formation through cortactin activation (Oser et al., 2010), Nck associates to p21-activated kinase (PAK) and PIX, acting as a scaffold to recruit paxillin to FA (Hashimoto et al., 2001; Turner et al., 1999). How Nck constitutes an essential piece in the invadopodium machinery is still unclear but, as observed for cortactin, Tks5 is necessary for Nck recruitment to invadopodia (Stylli et al., 2009). Tks5 is likewise needed to engage cortactin at podosomes (Crimaldi et al., 2009). Together with these studies, our data from WIP mutant experiments suggest that invadopodium dynamics is regulated by a multi-protein complex formed by cortactin, Nck, Tks5 and WIP. We conjecture that Src overexpression in WIP-deficient cells provides an additional pool of active kinase that triggers cortactin, promoting Nck recruitment to central areas of the cell, which allows FA disassembly and invadopodium initiation.

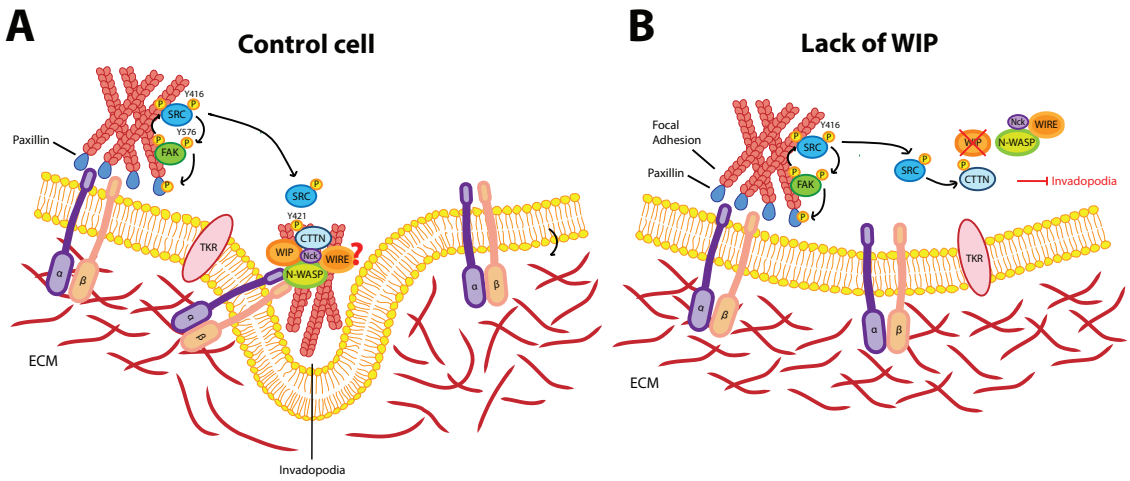

Figure D2: Model of the mechanisms that drive WIP-dependent invadopodium formation. In MDA-MB-231 control cells, active Src phosphorylates cortactin, allowing Nck recruitment, necessary to dissociate FA and initiate invadopodium formation. A complex formed by cortactin, WIP and N-WASP facilitates initiation and assembly of invadopodia by promoting actin polymerisation. In the absence of WIP, FA disassembly is impaired, as is recruitment of invadopodial components.

6.2.2 Absence of WICH/WIRE alters maturation of invasive protrusions

The effects of WIRE depletion were particularly evident in Matrigel experiments, in which the morphology of these cells differed completely (shorter protrusions, rounded cell shape) from controls and cells lacking WIP (Figs. R16 and R21). A similar phenotype is found when N-WASP is knocked down in MDA-MB-231 cells (Gligorijevic et al., 2012; Yu

et al., 2012), and is associated with a defect in MT1-MMP traffic towards the membrane, which impairs matrix degradation (Yu et al., 2012). Inhibition of MMP activity in an inverse invasion assay decreased invasion of control and WIP-deficient cells, but we detected no further inhibition in WIRE-deficient cells (Fig. R16). This implies that MMP activity is already compromised in these cells. Indeed, analysis of MT1-MMP distribution in cells lacking WICH/WIRE showed more protein at the cell periphery, which could derive from a defect in MT1-MMP recycling from the membrane to endocytic compartments (Fig. R37). Reduction of WICH/WIRE or wiskostatin inactivation of N-WASP induced an increase in the size and number of vesicles surrounded by F-actin and cortactin dots (Fig. R37). Further analysis is needed to identify the origin of these vesicles, which will help to determine the direction of the altered trafficking.

Results in cells invading gelatin support these findings. In this system, although we observed invadopodium formation in cells lacking WIRE, these structures were immature, as degradation was significantly reduced (Fig. R25). Similarities between the effects of WICH/WIRE and N-WASP deficiency, as well as the results of wiskostatin treatment, indicate that WICH/WIRE-N-WASP interaction is critical for WICH/WIRE function in cancer cells (Fig. R36). Nonetheless, reconstitution of WIRE-deficient cells with mutant WIP lacking the N-WASP-binding domain was successful (Fig. R39), whereas overexpression of mutant WIP lacking the Nck-binding domain did not lead to cell recovery of invasive ability (Fig. R39). As Nck levels are reduced in the absence of WICH/WIRE (Fig. R29), Nck might have an important role in WICH/WIRE-mediated invasion. Whether WICH/WIRE regulates N-WASP function directly or through Nck binding in this system is still not known. Diverse roles have been attributed to WICH/WIRE, which depends in some cases on N-WASP interaction (Aspenstrom, 2004; Kato and Takenawa, 2005; Kovacs et al., 2011) and in others is independent, and acts through its actin-binding domain (Aspenstrom, 2004; Misra et al., 2010b). WICH/WIRE is involved in PDGF receptor endocytosis (Aspenstrom, 2004), but little is known of its overall role in endocytosis and/or recycling. By regulating N-WASP-dependent endocytosis, WICH/WIRE could be involved in MT1-MMP recycling, which would cause immature invadopodia (Fig. D3).

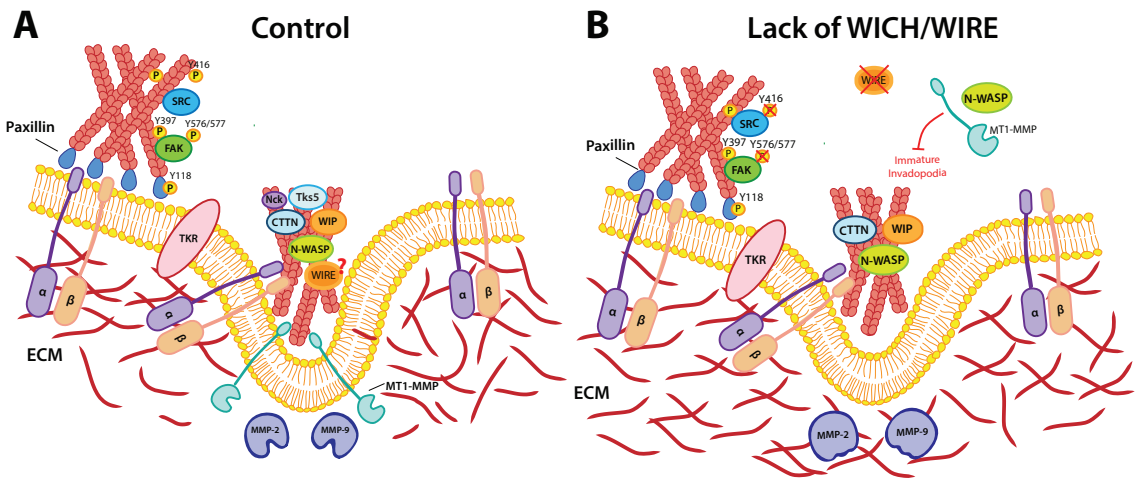

Figure D3: Model of the mechanisms that drive WICH/WIRE-dependent degradation. In MDA-MB-231 control cells, N-WASP mediates MT1-MMP transport to the membrane through binding to F-actin, which gives rise to a mature invadopodium that degrades the ECM. In the absence of WICH/WIRE, N-WASP activity is altered, affecting MT1-MMP traffic to the invadopodia, which results in immature invadopodia unable to degrade the ECM.

6.3 WIP AND WICH/WIRE EXPRESSION IS PRECISELY REGULATED

WIP and WICH/WIRE are co-expressed in some cell types such as THP-1 monocytes (where WICH/WIRE can bypass WIP deficiency by binding N-WASP and thus contribute to chemotaxis (Tsuboi, 2006)) and MEF (as seen in vaccinia-induced actin polymerisation studies (Donnelly et al., 2013)). Here we demonstrate that WIP and WICH/WIRE are co-expressed in diverse BCC lines and modulate invasion of MDA-MB-231 cells in distinct ways. In this model, neither endogenous nor exogenous expression of WICH/WIRE was sufficient to rescue the lack of WIP. In contrast, WIP overexpression rescues the defect derived from WICH/WIRE loss, whereas endogenous WIP does not compensate WICH/WIRE function. This indicates that WIP plays an exclusive, substantial role, and suggests complementary functions for the two proteins in these cells. Our results show that expression of both proteins is accurately regulated since 1) WIP overexpression reduces WICH/WIRE expression (Fig. R34), 2) WIRE depletion induces WIP overexpression (Fig. R15), and 3) exogenous WIP expression rescues invadopodium function in WIRE-deficient cells (Fig. R35).

Our data indicate that WIP can adopt the cell functions of WICH/WIRE, since an increase in WIP levels recovers the ability to degrade matrix in cells that lack WICH/WIRE.

The fact that WIP overexpression significantly reduces WICH/WIRE levels supports this hypothesis. Conversely, the failure of WICH/WIRE to overcome the lack of WIP suggests that the domains shared by these proteins are insufficient to induce invadopodium formation; this supports the idea of a multiple complex that regulates invadopodium initiation and assembly. WICH/WIRE depletion promoted a significant increase in WIP expression. These data not only indicate that WIP can assume WICH/WIRE functions, but it also explains why a larger percentage of WICH/WIRE-deficient cells tend to form invadopodia compared to controls (Fig. R25).

The results presented here indicate that Nck contributes to WIP and WICH/WIRE functions during invasion. WIP-Nck interaction is important for actin polymerisation (Ditlev et al., 2012; Donnelly et al., 2013), and N-WASP activity increases when WIP and Nck are present (Tehrani et al., 2007). Whether Nck is recruited to invadopodia via direct interaction with WIP or as part of a multistep/multiprotein complex remains to be elucidated, but it appears to be critical for invadopodium-mediated invasion. Ditlev and collaborators recently proposed that N-WASP-Arp2/3 complex-mediated actin polymerisation follows a 4:2:1 Nck/N-WASP/Arp2/3 complex stoichiometry, in which two Nck molecules □one that binds to WIP and the other to N-WASP□ interact in parallel with Arp2 and Arp3 subunits (Ditlev et al., 2012). This interesting new concept allows us to hypothesise that an imbalance in the proportion of Nck that binds WIP, WICH/WIRE and N-WASP could lead to distinct effects on actin polymerisation and invadopodium function (Fig. D4). In MDA-MB-231 cells, in which N-WASP binds both WIP and WICH/WIRE, invadopodia are functional (Fig. R33), whereas in WIP-lacking cells, this 4:2:1 ratio could be displaced, allowing more Nck molecules free to bind the N-WASP/WICH/WIRE complex. WIP-ΔNBD expression in WIRE-deficient cells was insufficient to rescue degradation, indicating that Nck binding to this complex is essential for mature invadopodium development. Nonetheless, WIP-ΔNBD expression in control cells promoted invadopodium-mediated degradation; this shows that Nck binding to WIP is not necessary for induction of invadopodia, but its absence promotes their fully degradative capacity. In contrast, in the absence of WICH/WIRE, equilibrium would be displaced to the WIP/N-WASP complex (added to WIP overexpression induced after WICH/WIRE depletion), which would promote Nck binding to WIP/N-WASP as well as development of invadopodia (which are not necessarily active).

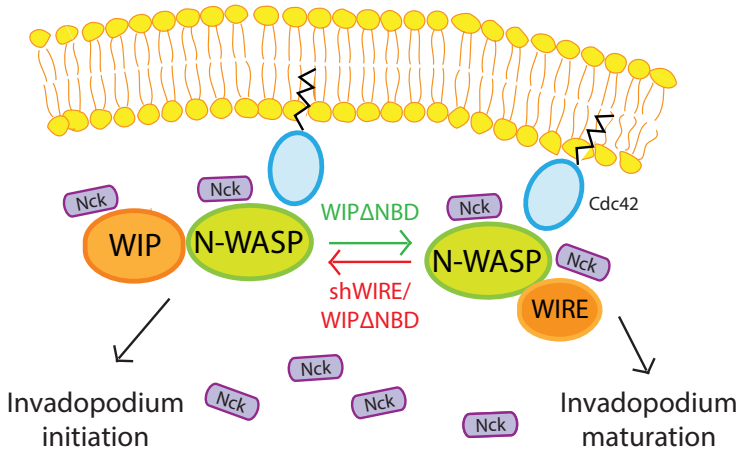

Figure D4: Summary of N-WASP-WIP-Nck and N-WASP-WICH/WIRE-Nck dynamic interactions. Overexpression of the WIP-ΔNBD mutant in MDA-MB-231 cells does not affect invadopodium formation, but increases matrix degradation by active invadopodia, presumably by allowing free Nck binding to the N-WASP/WICH/WIRE complex. Conversely, when WIRE is reduced and endogenous WIP and WIP-ΔNBD are present, WIP does not rescue the ability of invadopodia to degrade, as Nck might not bind N-WASP/WICH/WIRE.

6.4 WIP CONSTITUTES A KEY ELEMENT OF THE BCC MESENCHYMAL PHENOTYPE

WIP is overexpressed significantly in all basal B cells compared to luminal cells. This correlates with two other cytoskeletal components claimed to be invasive in breast cancer, cortactin and fascin. Whereas data for cortactin are inconsistent (Cai et al., 2010; Dedes et al., 2010; Sheen-Chen et al., 2011), several studies show that fascin expression is strongly related to breast tumour invasiveness and EMT (Rezaul et al., 2010; Rodriguez-Pinilla et al., 2006; Sarrio et al., 2008). Although statistical analysis supports the association between elevated WIP or fascin expression and the basal B phenotype, we only found significant differences in WIP expression in each basal B cell line tested, not only between groups, but also in correlation with their invasive behaviour *in vitro*. This finding at the protein level confirms previous studies (Charafe-Jauffret et al., 2006) and suggests that WIP might be a diagnostic marker whose expression correlates with poor prognosis in various cancer types and co-expresses with genes involved in proliferation and apoptosis (Staub et al., 2009). The connection between WIP expression and the mesenchymal phenotype is also seen in prostate cancer cells, where EMT induction leads to overexpression of WIP and other genes linked to cell adhesion and integrin

signalling, promoting cell motility (Gu et al., 2007).

Our analyses indicate that expression of neither N-WASP nor WICH/WIRE correlates with invasive behaviour. Some studies report N-WASP overexpression at certain stages of the metastatic process in breast and other cancer types (Jin et al., 2013; Yu et al., 2012), but others propose it as a tumour suppressor in breast cancer (Martin et al., 2008); categorisation of this protein thus continues to be debated. These discrepancies might be due to the nature of *in vitro* analysis, although in similar conditions, we observed differences for other proteins. It is important to recall that expression of any of these proteins can differ at distinct cell stages. Further analysis is thus needed in human tissue samples and at different metastatic stages to validate the *in vitro* analyses.

Our data indicate that WIP is necessary to maintain a mesenchymal phenotype in MDA-MB-231 and Hs578T cells, as its reduction promotes loss of the mesenchymal marker vimentin and induces expression of characteristics of an epithelial phenotype (E-cadherin and β-catenin). During tumour progression, cell plasticity is essential to facilitate metastasis; for individual or collective invasion, epithelial cells must lose their interconnecting adherent junctions as well as their adhesion to the ECM. Once cells have reached a new tissue, they must likewise establish and regain cell-cell interactions. This transition shares common regulatory pathways that involve Rac, Src, FAK integrins and Wnt signalling pathways (Janmey et al., 2013; Savagner, 2001). These signals are activated by external factors from the ECM such as collagen, EGF or TGFβ (Savagner et al., 1994), or by mechanical forces that regulate cell behaviour (Janmey et al., 2013). Adherent junctions and the actin cytoskeleton are essential to convey these signals, frequently by inducing changes in gene expression through the myocardin-related transcription factor (MAL/MRTF) or YAP (Yes-associated protein)/TAZ (transcriptional co-activator with PDZ-binding motif) pathways, adjusting cell response to changes in ECM stiffness or composition (Halder et al., 2012; McGee et al., 2011). Our findings on the WIP contribution to regulation of cell adhesion, proliferation and mesenchymal behaviour suggest that WIP is a candidate as a regulator of mechanotransduction in cancer cells. We also determined that nuclear WIP is expressed and distributed differently in MDA-MB-231 cells, depending on the matrix in which these cells are cultured (Fig. R11); this

suggests that WIP is involved in signal transduction to the nucleus. WIP was nonetheless insufficient to induce invasiveness and mesenchymal-like characteristics in luminal cells, and thus probably acts with other proteins to promote these changes.

The results presented here demonstrate the importance of WIP in cell plasticity and mechanosensing, identifying new subjects of study for WIP and related proteins. Its implication in diverse processes related to cancer progression encourages us to further characterise the way WIP acts at each stage of the disease. Knowing its functions and regulation throughout cancer development might allow its use as a therapeutic target.

Conclusions

7. CONCLUSIONS

1. The actin-regulating protein WIP is expressed more abundantly in invasive basal B-like breast cancer cells than in non-invasive luminal-like breast cancer cells, whereas the closely related protein WICH/WIRE is expressed independently of the molecular phenotype and invasive behaviour of breast cancer cells.

2. The WIP protein is localised at the distal tip of invasive protrusions and invadopodia of MDA-MB-231 breast cancer cells, where F-actin and cortactin are also found.

3. Endogenous expression of WIP and WICH/WIRE proteins in MDA-MB-231 cells is necessary for their efficient invasion of diverse biological and artificial matrices.

4. Cellular expression of WIP and WICH/WIRE is interdependent, and is regulated by changes in response to altered expression of the other.

5. WIP and WICH/WIRE proteins contribute to MDA-MB-231 cell invasion via different mechanisms; WIP reduces the ability to form invadopodia and WICH/WIRE is necessary for maturation.

6. Silencing of WIP protein in MDA-MB-231 cells reduces persistence of protrusions and alters the distribution of proteins involved in adhesion and invasion, including active FAK, paxillin and Nck.

7. Silencing of WICH/WIRE protein in MDA-MB-231 cells reduces the activity of the kinase Src and the expression of the adaptor protein Nck. The lack of WICH/WIRE in these cells modifies their morphology in Matrigel and reduces their capacity to invade the matrix.

8. Exogenous expression of WIP protein in MDA-MB-231 cells overcomes the ability to form mature invadopodia in the absence of WICH/WIRE, suggesting that WIP replaces the cellular role of WICH/WIRE during cancer cell invasion.

9. Endogenous expression of WIP protein is necessary to maintain a mesenchymal phenotype in basal B breast cancer cells, but its exogenous expression in epithelial-like luminal breast cancer cells is not sufficient to induce mesenchymal characteristics.

CONCLUSIONES

1. La proteína reguladora de actina WIP se expresa más abundantemente en células invasivas de carcinoma mamario basal B que en células no invasivas de tipo luminal, mientras que la proteína relacionada WICH/WIRE se expresa de forma independiente del fenotipo molecular y del comportamiento invasivo de células de cáncer de mama.

2. La proteína WIP ha sido localizada mediante inmunofluorescencia en el extremo de protrusiones invasivas e invadopodia de céúlas de cáncer de mama MDA-MB-231, donde se también se encuentran F-actina y cortactina.

3. La expresión endógena de WIP y WICH/WIRE en MDA-MB-231 es necesaria para la invasión eficiente de estas células en diversas matrices de origen biológico o artificiales.

4. La expresión de WIP y WICH/WIRE es interdependiente, siendo regulada por cambios en respuesta a modificaciones en la expresión de cada una de ellas.

5. Las proteínas WIP y WICH/WIRE contribuyen a la invasión por parte de células MDA-MB-231 mediante distintos mecanismos: WIP reduce la habilidad para formar invadopodia mientras que WICH/WIRE es necesario para su maduración.

6. El silenciamiento de la expression de WIP en MDA-MB-231 disminuye la persistencia de las protrusiones celulares y altera la distribución de las proteínas implicadas en la adhesión celular y la invasión: FAK activa, paxilina y Nck.

7. El silenciamiento de la expresión de WICH/WIRE en MDA-MB-231 reduce la actividad de la quinasa Src y los niveles de expresión de la proteína adaptadora Nck. La ausencia de WICH/WIRE en estas células modifica su morfología en Matrigel y disminuye su capacidad para invadir la matrix.

8. La expresión exógena de WIP rescata la capacidad para formar invadopodia maduros en ausencia de WICH/WIRE en MDA-MB-231, sugiriendo que WIP puede desempeñar las funciones de WICH/WIRE durante la invasión tumoral.

9. La expresión endógena de WIP es necesaria para conservar un fenotipo mesenquimal en células de carcinoma mamario de tipo basal B, pero su sobreexpresión en células de tipo luminal, con características epiteliales, no es suficiente para inducir un fenotipo mesenquimal en estas células.

Abbreviations

8. ABBREVIATIONS LIST

a.a. : amino acids
ADP: Adenosine diphosphate
Arp2/3: Actin-related proteins 2 and 3
ATP: Adenosine triphosphate
BCC: Breast cancer cell
BM: Basement membrane
CIA: Circular invasion assay
CTCF: Corrected total cell fluorescence
CR16: corticosteroids and regional expression 16
DMEM: Dulbecco's modified Eagle's medium
EMT: Epithelial to mesenchymal transition
ER: Estrogen receptor
FA: Focal adhesions
FAK: Focal adhesion kinase
HER2: Human epidermal receptor 2
IF: Immunofluorescence
IP: Immunoprecipitation
LB: Luria broth
MET: Mesenchymal to epithelial transition
MMP: Metalloproteinase
Nck: non-catalytic region of tyrosine kinase adaptor protein
N-WASP: Neural-WASP
PFA: Paraformaldehyde
PEI: Polyethylenimine
PIP_2: Phosphatidylinositol 4,5-bisphosphate
PR: Progesteron receptor
RPMI: Roswell Park Memorial Institute
RT: Room temperature
SDS-PAGE: sodium dodecyl sulphate polyacrylamide gel electrophoresis
SD: Standard deviation
SEM: Standard error of the mean
SH3: Src-homology 3
Src: Rous Sarcoma virus homologue family protein
WB: Western blot
2D: two-dimensional
3D: three-dimensional

WAS: Wiskott-Aldrich syndrome
WASP: Wiskott-Aldrich syndrome protein
WICH/WIRE: WIP-CR16 homologous/WIP-related
WIP: WASP-interacting protein
WT: wild type

References

9. REFERENCES

Alberts, B. 2008. Molecular biology of the cell. Garland Science, New York.

Angelucci, C., G. Maulucci, G. Lama, G. Proietti, A. Colabianchi, M. Papi, A. Maiorana, M. De Spirito, A. Micera, O.B. Balzamino, A. Di Leone, R. Masetti, and G. Sica. 2012. Epithelial-stromal interactions in human breast cancer: effects on adhesion, plasma membrane fluidity and migration speed and directness. *PloS one*. 7:e50804.

Anton, I.M., M.A. de la Fuente, T.N. Sims, S. Freeman, N. Ramesh, J.H. Hartwig, M.L. Dustin, and R.S. Geha. 2002. WIP deficiency reveals a differential role for WIP and the actin cytoskeleton in T and B cell activation. *Immunity*. 16:193-204.

Anton, I.M., G.E. Jones, F. Wandosell, R. Geha, and N. Ramesh. 2007. WASP-interacting protein (WIP): working in polymerisation and much more. *Trends in cell biology*. 17:555-562.

Anton, I.M., W. Lu, B.J. Mayer, N. Ramesh, and R.S. Geha. 1998. The Wiskott-Aldrich syndrome protein-interacting protein (WIP) binds to the adaptor protein Nck. *The Journal of biological chemistry*. 273:20992-20995.

Artym, V.V., Y. Zhang, F. Seillier-Moiseiwitsch, K.M. Yamada, and S.C. Mueller. 2006. Dynamic interactions of cortactin and membrane type 1 matrix metalloproteinase at invadopodia: defining the stages of invadopodia formation and function. *Cancer research*. 66:3034-3043.

Aspenstrom, P. 2002. The WASP-binding protein WIRE has a role in the regulation of the actin filament system downstream of the platelet-derived growth factor receptor. *Experimental cell research*. 279:21-33.

Aspenstrom, P. 2004. The mammalian verprolin homologue WIRE participates in receptor-mediated endocytosis and regulation of the actin filament system by distinct mechanisms. *Experimental cell research*. 298:485-498.

Ayala, I., M. Baldassarre, G. Giacchetti, G. Caldieri, S. Tete, A. Luini, and R. Buccione. 2008. Multiple regulatory inputs converge on cortactin to control invadopodia biogenesis and extracellular matrix degradation. *J Cell Sci*. 121:369-378.

Banon-Rodriguez, I., J. Monypenny, C. Ragazzini, A. Franco, Y. Calle, G.E. Jones, and I.M. Anton. 2011. The cortactin-binding domain of WIP is essential for podosome formation and extracellular matrix degradation by murine dendritic cells. *Eur J Cell Biol*. 90:213-223.

Banon-Rodriguez, I., J. Saez de Guinoa, A. Bernardini, C. Ragazzini, E. Fernandez, Y.R. Carrasco, G.E. Jones, F. Wandosell, and I.M. Anton. 2013. WIP regulates persistence of cell migration and ruffle formation in both mesenchymal and amoeboid modes of motility. *PloS one*. 8:e70364.

Beckmann, M.W., D. Niederacher, H.G. Schnurch, B.A. Gusterson, and H.G. Bender. 1997. Multistep carcinogenesis of breast cancer and tumour heterogeneity. *J Mol Med (Berl)*. 75:429-439.

Bissell, M.J., and D. Radisky. 2001. Putting tumours in context. *Nature reviews. Cancer*. 1:46-54.

Blick, T., E. Widodo, H. Hugo, M. Waltham, M.E. Lenburg, R.M. Neve, and E.W. Thompson. 2008. Epithelial mesenchymal transition traits in human breast cancer cell lines. *Clinical & experimental metastasis*. 25:629-642.

Block, M.R., C. Badowski, A. Millon-Fremillon, D. Bouvard, A.P. Bouin, E. Faurobert, D. Gerber-Scokaert, E. Planus, and C. Albiges-Rizo. 2008. Podosome-type adhesions and focal adhesions, so alike yet so different. *Eur J Cell Biol*. 87:491-506.

Bowden, E.T., P.J. Coopman, and S.C. Mueller. 2001. Invadopodia: unique methods for measurement of extracellular matrix degradation in vitro. *Methods in cell biology*. 63:613-627.

Branch, K.M., D. Hoshino, and A.M. Weaver. 2012. Adhesion rings surround invadopodia and promote maturation. *Biology open*. 1:711-722.

Brennan, K., G. Offiah, E.A. McSherry, and A.M. Hopkins. 2010. Tight junctions: a barrier to the initiation and progression of breast cancer? *Journal of biomedicine & biotechnology*. 2010:460607.

Bryce, N.S., E.S. Clark, J.L. Leysath, J.D. Currie, D.J. Webb, and A.M. Weaver. 2005. Cortactin promotes cell motility by enhancing lamellipodial persistence. *Current biology : CB*. 15:1276-1285.

Buday, L., L. Wunderlich, and P. Tamas. 2002. The Nck family of adapter proteins: regulators of actin cytoskeleton. *Cellular signalling*. 14:723-731.

Burger, K.L., B.S. Learman, A.K. Boucherle, S.J. Sirintrapun, S. Isom, B. Diaz, S.A. Courtneidge, and D.F. Seals. 2014. Src-dependent Tks5 phosphorylation regulates invadopodia-associated invasion in prostate cancer cells. *The Prostate*. 74:134-148.

Cai, J.H., R. Zhao, J.W. Zhu, X.L. Jin, F.J. Wan, K. Liu, X.P. Ji, Y.B. Zhu, and Z.G. Zhu. 2010. Expression of cortactin correlates with a poor prognosis in patients with stages II-III colorectal adenocarcinoma. *Journal of gastrointestinal surgery : official journal of the Society for Surgery of the Alimentary Tract*. 14:1248-1257.

Calle, Y., I.M. Anton, A.J. Thrasher, and G.E. Jones. 2008. WASP and WIP regulate podosomes in migrating leukocytes. *Journal of microscopy*. 231:494-505.

Calvo, F., N. Ege, A. Grande-Garcia, S. Hooper, R.P. Jenkins, S.I. Chaudhry, K. Harrington, P. Williamson, E. Moeendarbary, G. Charras, and E. Sahai. 2013. Mechanotransduction and YAP-dependent matrix remodelling is required for the generation and maintenance of cancer-associated fibroblasts. *Nature cell biology*. 15:637-646.

Campellone, K.G., and M.D. Welch. 2010. A nucleator arms race: cellular control of actin assembly. *Nature reviews. Molecular cell biology*. 11:237-251.

Cavallaro, U., and G. Christofori. 2004. Cell adhesion and signalling by cadherins and Ig-CAMs in cancer. *Nature reviews. Cancer*. 4:118-132.

Chabadel, A., I. Banon-Rodriguez, D. Cluet, B.B. Rudkin, B. Wehrle-Haller, E. Genot, P. Jurdic, I.M. Anton, and F. Saltel. 2007. CD44 and beta3 integrin organize two functionally distinct actin-based domains in osteoclasts. *Molecular biology of the cell*.

18:4899-4910.

Chaki, S.P., R. Barhoumi, M.E. Berginski, H. Sreenivasappa, A. Trache, S.M. Gomez, and G.M. Rivera. 2013. Nck enables directional cell migration through the coordination of polarized membrane protrusion with adhesion dynamics. *J Cell Sci*. 126:1637-1649.

Chan, K.T., C.L. Cortesio, and A. Huttenlocher. 2009. FAK alters invadopodia and focal adhesion composition and dynamics to regulate breast cancer invasion. *The Journal of cell biology*. 185:357-370.

Charafe-Jauffret, E., C. Ginestier, F. Monville, P. Finetti, J. Adelaide, N. Cervera, S. Fekairi, L. Xerri, J. Jacquemier, D. Birnbaum, and F. Bertucci. 2006. Gene expression profiling of breast cell lines identifies potential new basal markers. *Oncogene*. 25:2273-2284.

Charras, G., and E. Paluch. 2008. Blebs lead the way: how to migrate without lamellipodia. *Nature reviews. Molecular cell biology*. 9:730-736.

Chou, H.C., I.M. Anton, M.R. Holt, C. Curcio, S. Lanzardo, A. Worth, S. Burns, A.J. Thrasher, G.E. Jones, and Y. Calle. 2006. WIP regulates the stability and localization of WASP to podosomes in migrating dendritic cells. *Current biology : CB*. 16:2337-2344.

Clark, E.S., B. Brown, A.S. Whigham, A. Kochaishvili, W.G. Yarbrough, and A.M. Weaver. 2009. Aggressiveness of HNSCC tumors depends on expression levels of cortactin, a gene in the 11q13 amplicon. *Oncogene*. 28:431-444.

Clark, E.S., A.S. Whigham, W.G. Yarbrough, and A.M. Weaver. 2007. Cortactin is an essential regulator of matrix metalloproteinase secretion and extracellular matrix degradation in invadopodia. *Cancer research*. 67:4227-4235.

Condeelis, J., and J.E. Segall. 2003. Intravital imaging of cell movement in tumours. *Nature reviews. Cancer*. 3:921-930.

Crimaldi, L., S.A. Courtneidge, and M. Gimona. 2009. Tks5 recruits AFAP-110, p190RhoGAP, and cortactin for podosome formation. *Experimental cell research*. 315:2581-2592.

de la Fuente, M.A., Y. Sasahara, M. Calamito, I.M. Anton, A. Elkhal, M.D. Gallego, K. Suresh, K. Siminovitch, H.D. Ochs, K.C. Anderson, F.S. Rosen, R.S. Geha, and N. Ramesh. 2007. WIP is a chaperone for Wiskott-Aldrich syndrome protein (WASP). *Proceedings of the National Academy of Sciences of the United States of America*. 104:926-931.

Dedes, K.J., M.A. Lopez-Garcia, F.C. Geyer, M.B. Lambros, K. Savage, R. Vatcheva, P. Wilkerson, D. Wetterskog, M. Lacroix-Triki, R. Natrajan, and J.S. Reis-Filho. 2010. Cortactin gene amplification and expression in breast cancer: a chromogenic in situ hybridisation and immunohistochemical study. *Breast cancer research and treatment*. 124:653-666.

Destaing, O., E. Planus, D. Bouvard, C. Oddou, C. Badowski, V. Bossy, A. Raducanu, B. Fourcade, C. Albiges-Rizo, and M.R. Block. 2010. beta1A integrin is a master regulator of invadosome organization and function. *Molecular biology of the cell*. 21:4108-4119.

Ditlev, J.A., P.J. Michalski, G. Huber, G.M. Rivera, W.A. Mohler, L.M. Loew, and B.J. Mayer. 2012. Stoichiometry of Nck-dependent actin polymerization in living cells. *The Journal of cell biology*. 197:643-658.

Dominguez, R., and K.C. Holmes. 2011. Actin structure and function. *Annual review of biophysics*. 40:169-186.

Donnelly, S.K., I. Weisswange, M. Zettl, and M. Way. 2013. WIP provides an essential link between Nck and N-WASP during Arp2/3-dependent actin polymerization. *Current biology : CB*. 23:999-1006.

Eden, S., R. Rohatgi, A.V. Podtelejnikov, M. Mann, and M.W. Kirschner. 2002. Mechanism of regulation of WAVE1-induced actin nucleation by Rac1 and Nck. *Nature*. 418:790-793.

Etienne-Manneville, S., and A. Hall. 2002. Rho GTPases in cell biology. *Nature*. 420:6.

Fidler, I.J. 2003. The pathogenesis of cancer metastasis: the 'seed and soil' hypothesis revisited. *Nature reviews. Cancer*. 3:453-458.

Franci, C., M. Takkunen, N. Dave, F. Alameda, S. Gomez, R. Rodriguez, M. Escriva, B. Montserrat-Sentis, T. Baro, M. Garrido, F. Bonilla, I. Virtanen, and A. Garcia de Herreros. 2006. Expression of Snail protein in tumor-stroma interface. *Oncogene*. 25:5134-5144.

Franco, A., S. Knafo, I. Banon-Rodriguez, P. Merino-Serrais, I. Fernaud-Espinosa, M. Nieto, J.J. Garrido, J.A. Esteban, F. Wandosell, and I.M. Anton. 2012. WIP Is a Negative Regulator of Neuronal Maturation and Synaptic Activity. *Cereb Cortex*. 22:1191-1202.

Frank, R., and H. Overwin. 1996. SPOT synthesis. Epitope analysis with arrays of synthetic peptides prepared on cellulose membranes. *Methods in molecular biology*. 66:149-169.

Friedl, P., and K. Wolf. 2003. Tumour-cell invasion and migration: diversity and escape mechanisms. *Nature reviews. Cancer*. 3:362-374.

Friedl, P., and K. Wolf. 2008. Tube travel: the role of proteases in individual and collective cancer cell invasion. *Cancer research*. 68:7247-7249.

Friedl, P., and K. Wolf. 2009. Proteolytic interstitial cell migration: a five-step process. *Cancer metastasis reviews*. 28:129-135.

Galichon, P., S. Finianos, and A. Hertig. 2013. EMT-MET in renal disease: should we curb our enthusiasm? *Cancer letters*. 341:24-29.

Gallego, M.D., M.A. de la Fuente, I.M. Anton, S. Snapper, R. Fuhlbrigge, and R.S. Geha. 2006. WIP and WASP play complementary roles in T cell homing and chemotaxis to SDF-1alpha. *International immunology*. 18:221-232.

Garcia, E., G.E. Jones, L.M. Machesky, and I.M. Anton. 2012. WIP: WASP-interacting proteins at invadopodia and podosomes. *Eur J Cell Biol*. 91:869-877.

Geysen, H.M., R.H. Meloen, and S.J. Barteling. 1984. Use of peptide synthesis to probe viral antigens for epitopes to a resolution of a single amino acid. *Proceedings of the National Academy of Sciences of the United States of America*. 81:3998-4002.

Giampieri, S., C. Manning, S. Hooper, L. Jones, C.S. Hill, and E. Sahai. 2009. Localized and reversible TGFbeta signalling switches breast cancer cells from cohesive to single cell motility. *Nature cell biology*. 11:1287-1296.

Gimona, M., R. Buccione, S.A. Courtneidge, and S. Linder. 2008. Assembly and biological role of podosomes and invadopodia. *Current opinion in cell biology*. 20:235-241.

Gligorijevic, B., J. Wyckoff, H. Yamaguchi, Y. Wang, E.T. Roussos, and J. Condeelis. 2012. N-WASP-mediated invadopodium formation is involved in intravasation and lung metastasis of mammary tumors. *J Cell Sci*. 125:724-734.

Goley, E.D., and M.D. Welch. 2006. The ARP2/3 complex: an actin nucleator comes of age. *Nature reviews. Molecular cell biology*. 7:713-726.

Gritsenko, P.G., O. Ilina, and P. Friedl. 2012. Interstitial guidance of cancer invasion. *The Journal of pathology*. 226:185-199.

Gu, X., L.F. Zerbini, H.H. Otu, M. Bhasin, Q. Yang, M.G. Joseph, F. Grall, T. Onatunde, R.G. Correa, and T.A. Libermann. 2007. Reduced PDEF expression increases invasion and expression of mesenchymal genes in prostate cancer cells. *Cancer research*. 67:4219-4226.

Guan, J.L. 2010. Integrin signaling through FAK in the regulation of mammary stem cells and breast cancer. *IUBMB life*. 62:268-276.

Gupta, G.P., and J. Massague. 2006. Cancer metastasis: building a framework. *Cell*. 127:679-695.

Hakkinen, K.M., J.S. Harunaga, A.D. Doyle, and K.M. Yamada. 2011. Direct comparisons of the morphology, migration, cell adhesions, and actin cytoskeleton of fibroblasts in four different three-dimensional extracellular matrices. *Tissue engineering. Part A*. 17:713-724.

Halder, G., S. Dupont, and S. Piccolo. 2012. Transduction of mechanical and cytoskeletal cues by YAP and TAZ. *Nature reviews. Molecular cell biology*. 13:591-600.

Harunaga, J.S., and K.M. Yamada. 2011. Cell-matrix adhesions in 3D. *Matrix biology : journal of the International Society for Matrix Biology*. 30:363-368.

Hashimoto, S., A. Tsubouchi, Y. Mazaki, and H. Sabe. 2001. Interaction of paxillin with p21-activated Kinase (PAK). Association of paxillin alpha with the kinase-inactive and the Cdc42-activated forms of PAK3. *The Journal of biological chemistry*. 276:6037-6045.

Hennigan, R.F., K.L. Hawker, and B.W. Ozanne. 1994. Fos-transformation activates genes associated with invasion. *Oncogene*. 9:3591-3600.

Higgs, H.N., and T.D. Pollard. 1999. Regulation of actin polymerization by Arp2/3 complex and WASp/Scar proteins. *The Journal of biological chemistry*. 274:32531-32534.

Ho, H.Y., R. Rohatgi, L. Ma, and M.W. Kirschner. 2001. CR16 forms a complex with N-WASP in brain and is a novel member of a conserved proline-rich actin-binding protein family. *Proceedings of the National Academy of Sciences of the United States of America*. 98:11306-11311.

Hotary, K., X.Y. Li, E. Allen, S.L. Stevens, and S.J. Weiss. 2006. A cancer cell metalloprotease triad regulates the basement membrane transmigration program. *Genes & development*. 20:2673-2686.

Ishihara, D., A. Dovas, L. Hernandez, M. Pozzuto, J. Wyckoff, J.E. Segall, J.S. Condeelis, A.R. Bresnick, and D. Cox. 2013. Wiskott-Aldrich syndrome protein regulates leukocyte-dependent breast cancer metastasis. *Cell reports*. 4:429-436.

Janmey, P.A., R.G. Wells, R.K. Assoian, and C.A. McCulloch. 2013. From tissue mechanics to transcription factors. *Differentiation; research in biological diversity*. 86:112-120.

Jayo, A., and M. Parsons. 2012. Imaging of cell adhesion events in 3D matrix environments. *Eur J Cell Biol*. 91:824-833.

Jeschke, U., I. Mylonas, C. Kuhn, N. Shabani, C. Kunert-Keil, C. Schindlbeck, B. Gerber, and K. Friese. 2007. Expression of E-cadherin in human ductal breast cancer carcinoma in situ, invasive carcinomas, their lymph node metastases, their distant metastases, carcinomas with recurrence and in recurrence. *Anticancer research*. 27:1969-1974.

Jin, K.M., M. Lu, F.F. Liu, J. Gu, X.J. Du, and B.C. Xing. 2013. N-WASP is highly expressed in hepatocellular carcinoma and associated with poor prognosis. *Surgery*. 153:518-525.

Kato, M., H. Miki, S. Kurita, T. Endo, H. Nakagawa, S. Miyamoto, and T. Takenawa. 2002. WICH, a novel verprolin homology domain-containing protein that functions cooperatively with N-WASP in actin-microspike formation. *Biochemical and biophysical research communications*. 291:41-47.

Kato, M., and T. Takenawa. 2005. WICH, a member of WASP-interacting protein family, cross-links actin filaments. *Biochemical and biophysical research communications*. 328:1058-1066.

Kenny, P.A., G.Y. Lee, C.A. Myers, R.M. Neve, J.R. Semeiks, P.T. Spellman, K. Lorenz, E.H. Lee, M.H. Barcellos-Hoff, O.W. Petersen, J.W. Gray, and M.J. Bissell. 2007. The morphologies of breast cancer cell lines in three-dimensional assays correlate with their profiles of gene expression. *Molecular oncology*. 1:84-96.

Kim, A.S., L.T. Kakalis, N. Abdul-Manan, G.A. Liu, and M.K. Rosen. 2000. Autoinhibition and activation mechanisms of the Wiskott-Aldrich syndrome protein. *Nature*. 404:151-158.

Kinley, A.W., S.A. Weed, A.M. Weaver, A.V. Karginov, E. Bissonette, J.A. Cooper, and J.T. Parsons. 2003. Cortactin interacts with WIP in regulating Arp2/3 activation and membrane protrusion. *Current biology : CB*. 13:384-393.

Kirkbride, K.C., B.H. Sung, S. Sinha, and A.M. Weaver. 2011. Cortactin: a multifunctional regulator of cellular invasiveness. *Cell adhesion & migration*. 5:187-198.

Koduru, S., M. Massaad, C. Wilbur, L. Kumar, R. Geha, and N. Ramesh. 2007. A novel anti-WIP monoclonal antibody detects an isoform of WIP that lacks the WASP binding domain. *Biochemical and biophysical research communications*. 353:875-881.

Kovacs, E.M., S. Verma, R.G. Ali, A. Ratheesh, N.A. Hamilton, A. Akhmanova, and A.S. Yap. 2011. N-WASP regulates the epithelial junctional actin cytoskeleton through a non-canonical post-nucleation pathway. *Nature cell biology*. 13:934-943.

Krzewski, K., X. Chen, and J.L. Strominger. 2008. WIP is essential for lytic granule polarization and NK cell cytotoxicity. *Proceedings of the National Academy of Sciences of the United States of America*. 105:2568-2573.

Kubow, K.E., and A.R. Horwitz. 2011. Reducing background fluorescence reveals adhesions in 3D matrices. *Nature cell biology*. 13:3-5; author reply 5-7.

Lacroix, M., and G. Leclercq. 2004. Relevance of breast cancer cell lines as models for breast tumours: an update. *Breast cancer research and treatment*. 83:249-289.

Lanzardo, S., C. Curcio, G. Forni, and I.M. Anton. 2007. A role for WASP Interacting Protein, WIP, in fibroblast adhesion, spreading and migration. *The international journal of biochemistry & cell biology*. 39:262-274.

Lanzi, G., D. Moratto, D. Vairo, S. Masneri, O. Delmonte, T. Paganini, S. Parolini, G. Tabellini, C. Mazza, G. Savoldi, D. Montin, S. Martino, P. Tovo, I.M. Pessach, M.J. Massaad, N. Ramesh, F. Porta, A. Plebani, L.D. Notarangelo, R.S. Geha, and S. Giliani. 2012. A novel primary human immunodeficiency due to deficiency in the WASP-interacting protein WIP. *J Exp Med*. 209:29-34.

Le Bras, S., M. Massaad, S. Koduru, L. Kumar, M.K. Oyoshi, J. Hartwig, and R.S. Geha. 2009. WIP is critical for T cell responsiveness to IL-2. *Proceedings of the National Academy of Sciences of the United States of America*. 106:7519-7524.

Legg, J.A., G. Bompard, J. Dawson, H.L. Morris, N. Andrew, L. Cooper, S.A. Johnston, G. Tramountanis, and L.M. Machesky. 2007. N-WASP involvement in dorsal ruffle formation in mouse embryonic fibroblasts. *Molecular biology of the cell*. 18:678-687.

Lemieux, M.G., D. Janzen, R. Hwang, J. Roldan, I. Jarchum, and D.A. Knecht. 2013. Visualization of the actin cytoskeleton: different F-actin-binding probes tell different stories. *Cytoskeleton*.

Li, A., J.C. Dawson, M. Forero-Vargas, H.J. Spence, X. Yu, I. Konig, K. Anderson, and L.M. Machesky. 2010. The actin-bundling protein fascin stabilizes actin in invadopodia and potentiates protrusive invasion. *Current biology : CB*. 20:339-345.

Linder, S. 2009. Invadosomes at a glance. *J Cell Sci*. 122:3009-3013.

Linder, S., C. Wiesner, and M. Himmel. 2011. Degrading devices: invadosomes in proteolytic cell invasion. *Annual review of cell and developmental biology*. 27:185-211.

Lommel, S., S. Benesch, M. Rohde, J. Wehland, and K. Rottner. 2004. Enterohaemorrhagic and enteropathogenic Escherichia coli use different mechanisms for actin pedestal formation that converge on N-WASP. *Cellular microbiology*. 6:243-254.

Lommel, S., S. Benesch, K. Rottner, T. Franz, J. Wehland, and R. Kuhn. 2001. Actin pedestal formation by enteropathogenic Escherichia coli and intracellular motility of Shigella flexneri are abolished in N-WASP-defective cells. *EMBO reports*. 2:850-857.

Machesky, L.M., and R.H. Insall. 1998. Scar1 and the related Wiskott-Aldrich syndrome protein, WASP, regulate the actin cytoskeleton through the Arp2/3 complex. *Current biology : CB*. 8:1347-1356.

Martin, T.A., G. Pereira, G. Watkins, R.E. Mansel, and W.G. Jiang. 2008. N-WASP is a putative tumour suppressor in breast cancer cells, in vitro and in vivo, and is associated with clinical outcome in patients with breast cancer. *Clinical & experimental metastasis*. 25:97-108.

Martinez-Quiles, N., R. Rohatgi, I.M. Anton, M. Medina, S.P. Saville, H. Miki, H. Yamaguchi, T. Takenawa, J.H. Hartwig, R.S. Geha, and N. Ramesh. 2001. WIP regulates N-WASP-mediated actin polymerization and filopodium formation. *Nature cell biology*. 3:484-491.

McGee, K.M., M.K. Vartiainen, P.T. Khaw, R. Treisman, and M. Bailly. 2011. Nuclear transport of the serum response factor coactivator MRTF-A is downregulated at tensional homeostasis. *EMBO reports*. 12:963-970.

McNiven, M.A. 2013. Breaking away: matrix remodeling from the leading edge. *Trends in cell biology*. 23:16-21.

Miki, H., K. Miura, and T. Takenawa. 1996. N-WASP, a novel actin-depolymerizing protein, regulates the cortical cytoskeletal rearrangement in a PIP2-dependent manner downstream of tyrosine kinases. *The EMBO journal*. 15:5326-5335.

Miki, H., T. Sasaki, Y. Takai, and T. Takenawa. 1998. Induction of filopodium formation by a WASP-related actin-depolymerizing protein N-WASP. *Nature*. 391:93-96.

Minn, A.J., Y. Kang, I. Serganova, G.P. Gupta, D.D. Giri, M. Doubrovin, V. Ponomarev, W.L. Gerald, R. Blasberg, and J. Massague. 2005. Distinct organ-specific metastatic potential of individual breast cancer cells and primary tumors. *The Journal of clinical investigation*. 115:44-55.

Misra, A., R. Rajmohan, R.P. Lim, S. Bhattacharyya, and T. Thanabalu. 2010a. The mammalian verprolin, WIRE induces filopodia independent of N-WASP through IRSp53. *Experimental cell research*. 316:2810-2824.

Misra, A., R. Rajmohan, R.P. Lim, S. Bhattacharyya, and T. Thanabalu. 2010b. The mammalian verprolin, WIRE induces filopodia independent of N-WASP through IRSp53. *Experimental cell research*. 316:2810-2824.

Mitra, S.K., D.A. Hanson, and D.D. Schlaepfer. 2005. Focal adhesion kinase: in command and control of cell motility. *Nature reviews. Molecular cell biology*. 6:56-68.

Mitter, D., B.D. Chiaie, H.J. Ludecke, G. Gillessen-Kaesbach, A. Bohring, J. Kohlhase, A. Caliebe, R. Siebert, A. Roepke, M.A. Ramos-Arroyo, B. Nieva, B. Menten, B. Loeys, G. Mortier, and D. Wieczorek. 2010. Genotype-phenotype correlation in eight new patients with a deletion encompassing 2q31.1. *American journal of medical genetics. Part A*. 152A:1213-1224.

Moreau, V., F. Frischknecht, I. Reckmann, R. Vincentelli, G. Rabut, D. Stewart, and M. Way. 2000. A complex of N-WASP and WIP integrates signalling cascades that lead to actin polymerization. *Nature cell biology*. 2:441-448.

Moreau, V., F. Tatin, C. Varon, and E. Genot. 2003. Actin can reorganize into podosomes in aortic endothelial cells, a process controlled by Cdc42 and RhoA. *Molecular and cellular biology*. 23:6809-6822.

Murphy, D.A., and S.A. Courtneidge. 2011. The 'ins' and 'outs' of podosomes and invadopodia: characteristics, formation and function. *Nature reviews. Molecular cell biology*. 12:413-426.

Nakagawa, H., H. Miki, M. Ito, K. Ohashi, T. Takenawa, and S. Miyamoto. 2001. N-WASP, WAVE and Mena play different roles in the organization of actin cytoskeleton in lamellipodia. *J Cell Sci*. 114:1555-1565.

Nakamura, N., C. Rabouille, R. Watson, T. Nilsson, N. Hui, P. Slusarewicz, T.E. Kreis, and G. Warren. 1995. Characterization of a cis-Golgi matrix protein, GM130. *The Journal of cell biology*. 131:1715-1726.

Neve, R.M., K. Chin, J. Fridlyand, J. Yeh, F.L. Baehner, T. Fevr, L. Clark, N. Bayani, J.P. Coppe, F. Tong, T. Speed, P.T. Spellman, S. DeVries, A. Lapuk, N.J. Wang, W.L. Kuo, J.L. Stilwell, D. Pinkel, D.G. Albertson, F.M. Waldman, F. McCormick, R.B. Dickson, M.D. Johnson, M. Lippman, S. Ethier, A. Gazdar, and J.W. Gray. 2006. A collection of breast cancer cell lines for the study of functionally distinct cancer subtypes. *Cancer cell*. 10:515-527.

Nichols, N.R., J.N. Masters, and C.E. Finch. 1990. Changes in gene expression in hippocampus in response to glucocorticoids and stress. *Brain Res Bull*. 24:659-662.

Nurnberg, A., T. Kitzing, and R. Grosse. 2011. Nucleating actin for invasion. *Nature reviews. Cancer*. 11:177-187.

Oikawa, T., T. Itoh, and T. Takenawa. 2008. Sequential signals toward podosome formation in NIH-src cells. *The Journal of cell biology*. 182:157-169.

Oser, M., C.C. Mader, H. Gil-Henn, M. Magalhaes, J.J. Bravo-Cordero, A.J. Koleske, and J. Condeelis. 2010. Specific tyrosine phosphorylation sites on cortactin regulate Nck1-dependent actin polymerization in invadopodia. *J Cell Sci*. 123:3662-3673.

Oser, M., H. Yamaguchi, C.C. Mader, J.J. Bravo-Cordero, M. Arias, X. Chen, V. Desmarais, J. van Rheenen, A.J. Koleske, and J. Condeelis. 2009. Cortactin regulates cofilin and N-WASp activities to control the stages of invadopodium assembly and maturation. *The Journal of cell biology*. 186:571-587.

Perou, C.M., T. Sorlie, M.B. Eisen, M. van de Rijn, S.S. Jeffrey, C.A. Rees, J.R. Pollack, D.T. Ross, H. Johnsen, L.A. Akslen, O. Fluge, A. Pergamenschikov, C. Williams, S.X. Zhu, P.E. Lonning, A.L. Borresen-Dale, P.O. Brown, and D. Botstein. 2000. Molecular portraits of human breast tumours. *Nature*. 406:747-752.

Poincloux, R., O. Collin, F. Lizarraga, M. Romao, M. Debray, M. Piel, and P. Chavrier. 2011. Contractility of the cell rear drives invasion of breast tumor cells in 3D Matrigel. *Proceedings of the National Academy of Sciences of the United States of America*. 108:1943-1948.

Polyak, K., and R.A. Weinberg. 2009. Transitions between epithelial and mesenchymal states: acquisition of malignant and stem cell traits. *Nature reviews. Cancer*. 9:265-273.

Prall, F. 2007. Tumour budding in colorectal carcinoma. *Histopathology*. 50:151-162.

Prehoda, K.E., J.A. Scott, R.D. Mullins, and W.A. Lim. 2000. Integration of multiple signals through cooperative regulation of the N-WASP-Arp2/3 complex. *Science*. 290:801-806.

Ramesh, N., I.M. Anton, J.H. Hartwig, and R.S. Geha. 1997. WIP, a protein associated with wiskott-aldrich syndrome protein, induces actin polymerization and redistribution in lymphoid cells. *Proceedings of the National Academy of Sciences of the United States of America*. 94:14671-14676.

Rezaul, K., J.K. Thumar, D.H. Lundgren, J.K. Eng, K.P. Claffey, L. Wilson, and D.K. Han. 2010. Differential protein expression profiles in estrogen receptor-positive and -negative breast cancer tissues using label-free quantitative proteomics. *Genes & cancer*. 1:251-271.

Riedl, J., A.H. Crevenna, K. Kessenbrock, J.H. Yu, D. Neukirchen, M. Bista, F. Bradke, D. Jenne, T.A. Holak, Z. Werb, M. Sixt, and R. Wedlich-Soldner. 2008. Lifeact: a versatile marker to visualize F-actin. *Nature methods*. 5:605-607.

Robinson, B.D., G.L. Sica, Y.F. Liu, T.E. Rohan, F.B. Gertler, J.S. Condeelis, and J.G. Jones. 2009. Tumor microenvironment of metastasis in human breast carcinoma: a potential prognostic marker linked to hematogenous dissemination. *Clinical cancer research : an official journal of the American Association for Cancer Research*. 15:2433-2441.

Rodriguez-Pinilla, S.M., D. Sarrio, E. Honrado, D. Hardisson, F. Calero, J. Benitez, and J. Palacios. 2006. Prognostic significance of basal-like phenotype and fascin expression in node-negative invasive breast carcinomas. *Clinical cancer research : an official journal of the American Association for Cancer Research*. 12:1533-1539.

Rohatgi, R., L. Ma, H. Miki, M. Lopez, T. Kirchhausen, T. Takenawa, and M.W. Kirschner. 1999. The interaction between N-WASP and the Arp2/3 complex links Cdc42-dependent signals to actin assembly. *Cell*. 97:221-231.

Rottner, K., J. Hanisch, and K.G. Campellone. 2010. WASH, WHAMM and JMY: regulation of Arp2/3 complex and beyond. *Trends in cell biology*. 20:650-661.

Ruusala, A., T. Pawson, C.H. Heldin, and P. Aspenstrom. 2008. Nck adapters are involved in the formation of dorsal ruffles, cell migration, and Rho signaling downstream of the platelet-derived growth factor beta receptor. *The Journal of biological chemistry*. 283:30034-30044.

Sabeh, F., I. Ota, K. Holmbeck, H. Birkedal-Hansen, P. Soloway, M. Balbin, C. Lopez-Otin, S. Shapiro, M. Inada, S. Krane, E. Allen, D. Chung, and S.J. Weiss. 2004. Tumor cell traffic through the extracellular matrix is controlled by the membrane-anchored collagenase MT1-MMP. *The Journal of cell biology*. 167:769-781.

Sarrio, D., S.M. Rodriguez-Pinilla, D. Hardisson, A. Cano, G. Moreno-Bueno, and J. Palacios. 2008. Epithelial-mesenchymal transition in breast cancer relates to the basal-like phenotype. *Cancer research*. 68:989-997.

Sasahara, Y., R. Rachid, M.J. Byrne, M.A. de la Fuente, R.T. Abraham, N. Ramesh, and R.S. Geha. 2002. Mechanism of recruitment of WASP to the immunological synapse and of its activation following TCR ligation. *Molecular cell*. 10:1269-1281.

Satelli, A., and S. Li. 2011. Vimentin in cancer and its potential as a molecular target for cancer therapy. *Cellular and molecular life sciences : CMLS*. 68:3033-3046.

Savagner, P. 2001. Leaving the neighborhood: molecular mechanisms involved during epithelial-mesenchymal transition. *BioEssays : news and reviews in molecular, cellular and developmental biology*. 23:912-923.

Savagner, P., B. Boyer, A.M. Valles, J. Jouanneau, and J.P. Thiery. 1994. Modulations of the epithelial phenotype during embryogenesis and cancer progression. *Cancer treatment and research*. 71:229-249.

Scales, T.M., and M. Parsons. 2011. Spatial and temporal regulation of integrin signalling during cell migration. *Current opinion in cell biology*. 23:562-568.

Schlaepfer, D.D., S.K. Mitra, and D. Ilic. 2004. Control of motile and invasive cell phenotypes by focal adhesion kinase. *Biochimica et biophysica acta*. 1692:77-102.

Schuuring, E., E. Verhoeven, W.J. Mooi, and R.J. Michalides. 1992. Identification and cloning of two overexpressed genes, U21B31/PRAD1 and EMS1, within the amplified chromosome 11q13 region in human carcinomas. *Oncogene*. 7:355-361.

Sheen-Chen, S.M., C.Y. Huang, Y.Y. Liu, C.C. Huang, and R.P. Tang. 2011. Cortactin in breast cancer: analysis with tissue microarray. *Anticancer research*. 31:293-297.

Smith, S.C., and D. Theodorescu. 2009. Learning therapeutic lessons from metastasis suppressor proteins. *Nature reviews. Cancer*. 9:253-264.

Staub, E., J. Groene, M. Heinze, D. Mennerich, S. Roepcke, I. Klaman, B. Hinzmann, E. Castanos-Velez, C. Pilarsky, B. Mann, T. Brummendorf, B. Weber, H.J. Buhr, and A. Rosenthal. 2009. An expression module of WIPF1-coexpressed genes identifies patients with favorable prognosis in three tumor types. *J Mol Med (Berl)*. 87:633-644.

Stylli, S.S., T.T. Stacey, A.M. Verhagen, S.S. Xu, I. Pass, S.A. Courtneidge, and P. Lock. 2009. Nck adaptor proteins link Tks5 to invadopodia actin regulation and ECM degradation. *J Cell Sci*. 122:2727-2740.

Suetsugu, S., and T. Takenawa. 2003. Translocation of N-WASP by nuclear localization and export signals into the nucleus modulates expression of HSP90. *The Journal of biological chemistry*. 278:42515-42523.

Tehrani, S., N. Tomasevic, S. Weed, R. Sakowicz, and J.A. Cooper. 2007. Src phosphorylation of cortactin enhances actin assembly. *Proceedings of the National Academy of Sciences of the United States of America*. 104:11933-11938.

Thanabalu, T., R. Rajmohan, L. Meng, G. Ren, P.R. Vajjhala, and A.L. Munn. 2007. Verprolin function in endocytosis and actin organization. Roles of the Las17p (yeast WASP)-binding domain and a novel C-terminal actin-binding domain. *The FEBS journal*. 274:4103-4125.

Thiery, J.P. 2002. Epithelial-mesenchymal transitions in tumour progression. *Nature reviews. Cancer*. 2:442-454.

Thiery, J.P., and J.P. Sleeman. 2006. Complex networks orchestrate epithelial-mesenchymal transitions. *Nature reviews. Molecular cell biology*. 7:131-142.

Timpson, P., E.J. McGhee, and K.I. Anderson. 2011a. Imaging molecular dynamics in vivo--from cell biology to animal models. *J Cell Sci*. 124:2877-2890.

Timpson, P., E.J. McGhee, J.P. Morton, A. von Kriegsheim, J.P. Schwarz, S.A. Karim, B. Doyle, J.A. Quinn, N.O. Carragher, M. Edward, M.F. Olson, M.C. Frame, V.G. Brunton, O.J. Sansom, and K.I. Anderson. 2011b. Spatial regulation of RhoA activity during pancreatic cancer cell invasion driven by mutant p53. *Cancer research*. 71:747-757.

Tsuboi, S. 2006. A complex of Wiskott-Aldrich syndrome protein with mammalian verprolins plays an important role in monocyte chemotaxis. *Journal of immunology*. 176:6576-6585.

Tsuboi, S., and J. Meerloo. 2007. Wiskott-Aldrich syndrome protein is a key regulator of the phagocytic cup formation in macrophages. *The Journal of biological chemistry*. 282:34194-34203.

Turner, C.E., M.C. Brown, J.A. Perrotta, M.C. Riedy, S.N. Nikolopoulos, A.R. McDonald, S. Bagrodia, S. Thomas, and P.S. Leventhal. 1999. Paxillin LD4 motif binds PAK and PIX through a novel 95-kD ankyrin repeat, ARF-GAP protein: A role in cytoskeletal remodeling. *The Journal of cell biology*. 145:851-863.

van Rossum, A.G., W.H. Moolenaar, and E. Schuuring. 2006. Cortactin affects cell migration by regulating intercellular adhesion and cell spreading. *Experimental cell research*. 312:1658-1670.

Viklund, I.M., P. Aspenstrom, V. Meas-Yedid, B. Zhang, J. Kopec, D. Agren, G. Schneider, M. D'Amato, J.C. Olivo-Marin, P. Sansonetti, G.T. Van Nhieu, and S. Pettersson. 2009. WAFL, a new protein involved in regulation of early endocytic transport at the intersection of actin and microtubule dynamics. *Experimental cell research*. 315:1040-1052.

Wang, Y., and M.A. McNiven. 2012. Invasive matrix degradation at focal adhesions occurs via protease recruitment by a FAK-p130Cas complex. *The Journal of cell biology*. 196:375-385.

Wanger, M., T. Keiser, J.M. Neuhaus, and A. Wegner. 1985. The actin treadmill. *Canadian journal of biochemistry and cell biology = Revue canadienne de biochimie et biologie cellulaire*. 63:414-421.

Weber, C.E., N.Y. Li, P.Y. Wai, and P.C. Kuo. 2012. Epithelial-mesenchymal transition, TGF-beta, and osteopontin in wound healing and tissue remodeling after injury. *Journal of burn care & research : official publication of the American Burn Association*. 33:311-318.

Winder, S.J., and K.R. Ayscough. 2005. Actin-binding proteins. *J Cell Sci*. 118:651-654.

Witz, C.A., I.A. Montoya-Rodriguez, S. Cho, V.E. Centonze, L.F. Bonewald, and R.S. Schenken. 2001. Composition of the extracellular matrix of the peritoneum. *Journal of the Society for Gynecologic Investigation*. 8:299-304.

Wolf, K., and P. Friedl. 2011. Extracellular matrix determinants of proteolytic and non-proteolytic cell migration. *Trends in cell biology*. 21:736-744.

Wyckoff, J.B., Y. Wang, E.Y. Lin, J.F. Li, S. Goswami, E.R. Stanley, J.E. Segall, J.W. Pollard, and J. Condeelis. 2007. Direct visualization of macrophage-assisted tumor cell intravasation in mammary tumors. *Cancer research*. 67:2649-2656.

Yamaguchi, H., M. Lorenz, S. Kempiak, C. Sarmiento, S. Coniglio, M. Symons, J. Segall, R. Eddy, H. Miki, T. Takenawa, and J. Condeelis. 2005. Molecular mechanisms of invadopodium formation: the role of the N-WASP-Arp2/3 complex pathway and cofilin. *The Journal of cell biology*. 168:441-452.

Yamashita, N., E. Tokunaga, H. Kitao, Y. Hisamatsu, K. Taketani, S. Akiyoshi, S. Okada, S. Aishima, M. Morita, and Y. Maehara. 2013. Vimentin as a poor prognostic factor for triple-negative breast cancer. *Journal of cancer research and clinical oncology*. 139:739-746.

Yarar, D., C.M. Waterman-Storer, and S.L. Schmid. 2007. SNX9 couples actin assembly to phosphoinositide signals and is required for membrane remodeling during endocytosis. *Developmental cell*. 13:43-56.

Yoder, B.J., E.J. Wilkinson, and N.A. Massoll. 2007. Molecular and morphologic distinctions between infiltrating ductal and lobular carcinoma of the breast. *The breast journal*. 13:172-179.

Yu, X., and L.M. Machesky. 2012. Cells assemble invadopodia-like structures and invade into matrigel in a matrix metalloprotease dependent manner in the circular invasion assay. *PloS one*. 7:e30605.

Yu, X., T. Zech, L. McDonald, E.G. Gonzalez, A. Li, I. Macpherson, J.P. Schwarz, H. Spence, K. Futo, P. Timpson, C. Nixon, Y. Ma, I.M. Anton, B. Visegrady, R.H. Insall, K. Oien, K. Blyth, J.C. Norman, and L.M. Machesky. 2012. N-WASP coordinates the delivery and F-actin-mediated capture of MT1-MMP at invasive pseudopods. *The Journal of cell biology*. 199:527-544.

Zufferey, R., D. Nagy, R.J. Mandel, L. Naldini, and D. Trono. 1997. Multiply attenuated lentiviral vector achieves efficient gene delivery in vivo. *Nature biotechnology*. 15:871-875.

Appendices

European Journal of Cell Biology 91 (2012) 869–877

Contents lists available at SciVerse ScienceDirect

European Journal of Cell Biology

journal homepage: www.elsevier.com/locate/ejcb

WIP: WASP-interacting proteins at invadopodia and podosomes

Esther García[a,*], Gareth E. Jones[b], Laura M. Machesky[c], Inés M. Antón[a,**]

[a] Centro Nacional de Biotecnología (CNB-CSIC), 28049 Madrid, Spain
[b] The Randall Division of Cell & Molecular Biophysics, King's College London, London SE1 1UL, UK
[c] The Beatson Institute for Cancer Research, Switchback, Rd., Bearsden, Glasgow, G61 1BD, UK

ARTICLE INFO

Article history:
Received 11 May 2012
Received in revised form 12 June 2012
Accepted 14 June 2012

Keywords:
WASP-interacting protein (WIP)
Invasion
Migration
Podosome
Invadopodia
Extracellular matrix (ECM)

ABSTRACT

Regulated cell invasion resulting from migratory and matrix-degrading events is an essential step in physiological processes such as the inflammatory response and tissue repair. Cell invasion is also thought to be a critical parameter in pathological conditions such as cancer metastasis. The migration of normal and cancer cells is largely driven by the actin cytoskeleton, which controls cell shape, adhesion and contractility. Podosomes and invadopodia are actin-rich protrusions that drive invasion in normal and cancer cells. These structures protrude from the basal region of the cell facing the extracellular matrix, where they adhere to and degrade the matrix, thus facilitating invasive migration. WASP (Wiskott–Aldrich syndrome protein) and WIP (WASP-interacting protein) localise to the actin rich core of podosomes and play a critical role in their formation. More recently, studies performed on microarray data sets from cancer patients of several tumour categories show a strong correlation between reduced WIP expression and improved prognosis. In this article, we identify endogenous WIP at the distal tips of cancer cell invasive protrusions and we summarise recent advances in the study of the roles of WIP- and WASP-protein families during migration and invasion of normal and cancer cells related to podosome and invadopodium generation.

Introduction

Cell invasion through interstitial tissue is dependent on several specific characteristics of the migrating cell. For example, in response to a chemotactic signal the cell senses the gradient and alters its pseudopod dynamics and, in cases where the surrounding extracellular matrix (ECM) is dense, the cell must degrade the matrix in order to move forward. Cell contractility is also necessary, with the actomyosin cytoskeleton driving changes in cell shape as well as generating the power to retract the cell rear thus promoting net cell movement (Friedl and Wolf, 2009). Cells develop different protrusions during these invasive events depending on the nature of the surrounding matrix, including filopodia, lamellipodia and blebs (Fackler and Grosse, 2008; Mattila and Lappalainen, 2008; Ridley, 2011). When cells confront physical barriers to migration, they often develop specialised structures for adhesion and degradation, known as podosomes and invadopodia (Linder et al., 2011; Murphy and Courtneidge, 2011).

Several substantial reviews have recently appeared on the structure and biology of podosomes and invadopodia (Linder et al., 2011; Murphy and Courtneidge, 2011) so they will only briefly be summarised here. The major constituents within the core of podosomes and invadopodia are filamentous actin (f-actin) and a host of actin polymerisation regulators. Surrounding the core, adhesion and scaffolding proteins, matrix degrading enzymes, membrane remodelling proteins and kinases are present (Gimona et al., 2008; Linder et al., 2011). Actin polymerisation driven by interaction between the Arp2/3 (actin-related proteins 2 and 3) complex and the nucleation promoting factors (NPFs) WASP (Wiskott–Aldrich syndrome protein) and N-WASP (neural WASP) is essential for podosome and invadopodium formation (Calle et al., 2004; Yamaguchi et al., 2005). Within cells, (N-)WASP is associated with a second protein, WIP (WASP-interacting protein), that is bound to the N-terminal domain of (N-)WASP (Martinez-Quiles et al., 2001; Moreau et al., 2000) (Fig. 1). Given the close association of these two proteins, it seems reasonable to surmise that WIP, which regulates (N-)WASP location, stability and function (Anton et al., 2007), may also play a significant role in the formation and proper function of podosomes and invadopodia. Endogenous WIP is located at podosome cores along with WASP (Chou et al., 2006; Tsuboi, 2007) and there is growing evidence that WIP plays

* Corresponding author at: Centro Nacional de Biotecnología (CNB-CSIC), Darwin 3, 28049 Madrid, Spain. Tel.: +34 915854552; fax: +34 915854506.
** Corresponding author at: Centro Nacional de Biotecnología (CNB-CSIC), Darwin 3, 28049 Madrid, Spain. Tel.: +34 915855312; fax: +34 915854506.
E-mail addresses: eggonzalez@cnb.csic.es (E. García), ianton@cnb.csic.es (I.M. Antón).

0171-9335/$ – see front matter © 2012 Elsevier GmbH. All rights reserved.
http://dx.doi.org/10.1016/j.ejcb.2012.06.002

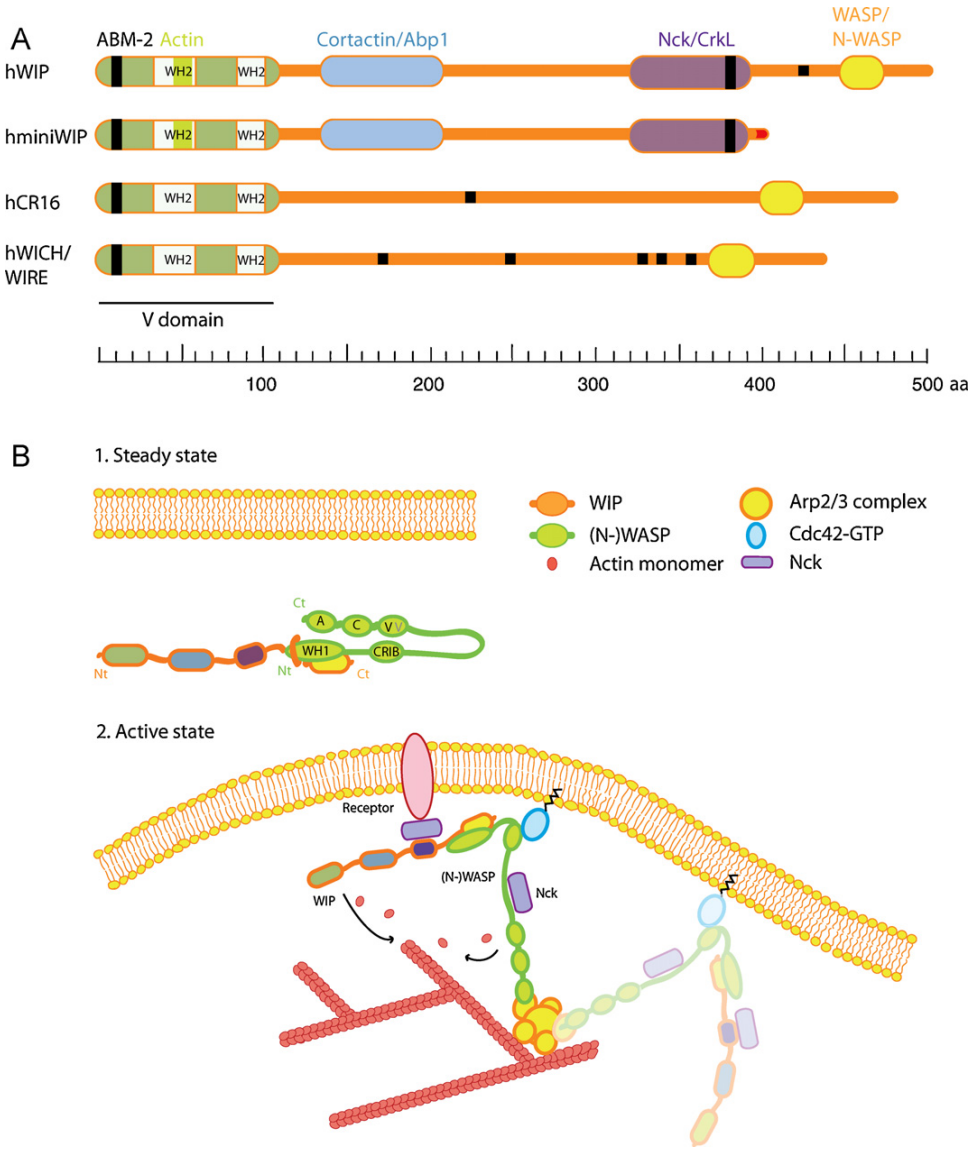

Fig. 1. Schematic of human WIP family proteins and model for the mechanism of activation of the WIP/(N-)WASP complex. (A) The WIP family includes WIP, CR16 and WICH/WIRE. All members share a similar structure composed of a verprolin homology domain (V domain) that includes two WASP homology 2 (WH2) domains for actin binding. The V domain is followed by multiple proline-rich motifs, shown in WIP to bind cortactin and actin- binding protein (Abp-1) or the adaptors Nck or CrkL, and a (N-)WASP binding site. Mini-WIP is a WIP isoform that lacks the (N-)WASP binding site. WIP-family proteins contain between two and six actin-based motility 2 domains (ABM-2) for profilin binding. (B) In resting cells WIP and (N-)WASP form a cytoplasmic complex. WIP wraps around the WH1 (WASP homology 1) domain of (N-)WASP favouring the inactive conformation. Following cell stimulation, WIP binding to adaptor molecules (CrkL or Nck as depicted) recruits the complex to the membrane. The combination of WIP and (N-)WASP phosphorylation together with Nck and Cdc42-GTP binding to (N-)WASP releases intramolecular interactions and expose the VCA (verprolin-cofilin-acidic region) domain. Once (N-)WASP is activated, the VCA domain interacts with actin monomers and activates the Arp2/3 complex leading to actin filament formation. A recent model proposes a 4:2:1 stoichiometry for Nck/N-WASP/Arp2/3 (Ditlev et al., 2012). Nt: N terminal; Ct: carboxyl terminal.

an essential role in proper podosome organisation and function (Banon-Rodriguez et al., 2011; Tsuboi, 2006).

In the last two decades, significant advances in our knowledge of the structure and development of invasive protrusions have been made, but there is still much debate about the structural differences between podosomes and invadopodia and the role of WIP in their function (Sung and Weaver, 2011). As both structures are associated with proteolytic-dependent 3-dimensional (3D) migration and they contain many of the same proteins (Gimona et al., 2008; Linder et al., 2011) some authors maintain that they are essentially the same structure. Variations are proposed to arise merely from the variability inherent in diverse studies utilising diverse cell types, substrata or techniques. Another camp of investigators considers that these structures are indeed different in composition, formation and regulation. We maintain that morphologically, invadopodia and podosomes can be distinguished. In general, the width and length of invadopodia are much greater than those of podosomes, and invadopodia protrude much further into an underlying matrix. Invadopodia are also more stable structures and have a lifetime of hours, while podosomes generally last for minutes (Chou et al., 2006; Li et al., 2010; Linder et al., 2011). Although there is no hard and fast rule for protein specific markers of podosomes *vs* invadopodia, vinculin forms distinct rings around actin in podosomes that morphologically

distinguishes them from invadopodia (Gimona et al., 2008), while Nck1 specifically localises to invadopodia (Oser et al., 2011). Here, we use the term podosome to describe degradative actin structures found in immune-related cells -monocytes, macrophages, dendritic cells (DCs) and osteoclasts-, TNF-stimulated endothelial cells, smooth muscle cells and transformed fibroblasts, saving the term invadopodia for those structures formed by cancer cells.

In contrast, there is full agreement on the biological importance of podosomes and invadopodia *in vivo* (Gligorijevic et al., 2012; Linder et al., 1999). While invadopodia have been exclusively linked to tumour metastasis, the role of podosomes seems to be more diverse. Although the main role for podosomes was initially thought to be related to adhesion and migration, these structures may also degrade ECM or act as mechanosensors (Linder et al., 2011; Saltel et al., 2011). These functions in the cell confer to podosomes a biological role in the proper function of the immune system (Calle et al., 2004), in bone remodelling during development, growth and bone repair in osteoclasts (Gimona et al., 2008) or remodelling of the basement membrane from arterial vessels by endothelial cells (Rottiers et al., 2009). Consequently, some human diseases can be related to the absence or impaired function of these structures. Mutations in WASP underline the immune deficiency Wiskott–Aldrich Syndrome (WAS), characterised by thrombocytopenia, eczema, and recurrent infections (Derry et al., 1994). In addition to the proliferation defects observed in lymphocytes from WAS patients, these also show abnormalities in their morphology, maturation and migration (Ramesh et al., 1999; Snapper et al., 2005; Snapper and Rosen, 1999). As macrophages and DCs from WAS patients are unable to form podosomes (Burns et al., 2001; Linder et al., 1999) this might explain the defects in immune cell trafficking in WAS patients (Thrasher et al., 1998).

The biological function of invadopodia is intimately related to tumour dissemination. Metastasis is a multistep process in which cancer cells detach from the primary tumour, invade through the surrounding ECM, intravasate into the blood or lymphatic vessels, extravasate at a distant tissue and proliferate as a secondary tumour (Fidler, 2003; Meyer and Hart, 1998). This process is responsible for 90% of cancer mortality and involves several signal cascades, some of which drive actin cytoskeleton reorganisation to modify cell–cell and cell–substratum adhesions, increasing their motility linked to their newly acquired ability to degrade the ECM. The unique presence of invadopodia in cancer cells suggests a promising role for these protrusions in tumour metastasis *in vivo*. Furthermore, in the last few years, several invadopodia proteins are also markers of poor prognosis in cancer and are associated with a metastatic phenotype in several cancer types (Cai et al., 2010; Machesky and Li, 2010).

In the present article, we review recent results that sustain the roles of WASP-interacting proteins in podosome and invadopodium dynamics and we also provide original data describing for the first time the localisation of endogenous WIP at the tips of invasive protrusions of cancer cells invading into a 3D matrix.

WASP-interacting proteins

Regulated actin filament assembly and disassembly is essential for cell locomotion, phagocytosis and endocytosis, proliferation and cell growth (Dominguez and Holmes, 2011). Severing of preformed filaments or the addition or removal of actin monomers to initiate, elongate or shorten pre-existing structures regulate this process. WASP family members are key regulators of this process due to a direct interaction between the Arp2/3 complex and activated (N-)WASP or related proteins (Machesky and Insall, 1998) (Fig. 1). WASP and its close homologue N-WASP are activated and/or localised by direct binding of GTP-loaded Cdc42 (Rohatgi et al., 1999), whilst the three members of the SCAR-WAVE (suppressor of cAMP receptor/WASP-family verprolin homology protein) subgroup are indirectly activated and/or localised by GTP-loaded Rac (Eden et al., 2002; Etienne-Manneville and Hall, 2002). Besides (N-)WASP and SCAR-WAVE, other members of this family (WASH, WHAMM and JMY) as well as cortactin act as NPFs to activate Arp2/3-dependent actin nucleation (Campellone and Welch, 2010; Rottner et al., 2010).

The mammalian WIP family of (N-)WASP-interacting proteins consists of three known members: CR16 (corticosteroids and regional expression 16), WICH/WIRE (*WI*P-*C*R16 *h*omologous/*WI*P-*re*lated) and WIP itself (Fig. 1A). All of them have been reported to bind actin at their N-terminal verprolin (V) homology domain and the N-WASP WH1/EVH1 (WASP Homology 1 and Ena/VASP Homology 1) domain at their C-terminal region (Aspenstrom, 2002; Ho et al., 2001; Kato et al., 2002; Sasahara et al., 2002).

CR16

CR16 was first described as a glucocorticoid-regulated brain protein (Nichols et al., 1990). Its sequence – 483 amino acids (a.a.) long – is similar to that one described for WIP (25% identity) (Anton et al., 2007). Not much is known about the functions of this protein that is mainly expressed in brain and testis. Surprisingly, no effect in central nervous system has been reported for CR16 deficiency, but knock out mice show male-specific sterility due to abnormal spermatogenesis at Sertoli cells (Suetsugu et al., 2007).

WICH/WIRE

Human WICH/WIRE protein, which name is due to its simultaneous discovery by two different groups (Aspenstrom, 2002; Kato et al., 2002), is 440 a.a.-long and shares 30% similarity with WIP (Anton et al., 2007). In porcine aortic endothelial cells (PAE) WICH/WIRE mediates actin cytoskeleton reorganisation -promoting formation of stress fibres, filopodia and ruffle-like protrusions- in a WASP-independent manner (Aspenstrom, 2004). Moreover, induction of filopodia in mouse embryonic fibrobasts by WICH/WIRE is mediated by the Insulin Receptor Substrate p53 (IRSp53) and dependent on Cdc42 activation but independent of N-WASP interaction (Misra et al., 2010). In contrast, WIP is able to induce filopodia formation in NIH 3T3 fibroblasts, but in this case N-WASP appears to be essential for this process (Martinez-Quiles et al., 2001). It is clear that cells use multiple pathways to induce assembly of filopodia and these are likely to depend on the cell types and the experimental conditions, so it is hard to make direct conclusions from these experiments.

Through interaction with N-WASP, WICH/WIRE can drive cross-linking of actin filaments (Kato and Takenawa, 2005) and participate in the endocytosis of the platelet-derived growth factor receptor beta (PDGFRβ) in transfected PAE cells (Aspenstrom, 2004). A novel role for WICH/WIRE-N-WASP complex has been reported recently in Caco-2 epithelial cells: WICH/WIRE is recruited by N-WASP to the zonula adherens junctions whose integrity is compromised in the absence of any of these proteins. Moreover, WICH/WIRE forms a complex with N-WASP and E-cadherin, showing a direct link between cadherin junctions and cytoskeleton regulation (Kovacs et al., 2011).

WIP

Human WIP is a proline-rich protein 503 a.a.-long that is ubiquitously expressed, although higher levels are detected in haematopoietic cells (de la Fuente et al., 2007; Ramesh et al., 1997). Two isoforms of WIP have been described to date: Prlp2 and mini-WIP (Koduru et al., 2007). Prlp2 expression originates from the

alternative splicing of one of the last exons of the WIPF1 gene, but it seems to be an uncommon event and not much is known about the functions that this isoform may play in the cell (Anton et al., 2007). Similarly, mini-WIP results from a truncated transcription of the WIPF1 gene that gives rise to a 403 a.a.-long protein which lacks the C-terminal WASP-binding domain (WBD) (Fig. 1A). Mini-WIP is mainly expressed in peripheral blood cells (Koduru et al., 2007) and in some cancer cells (our unpublished data).

WIP controls actin cytoskeleton dynamics by its direct interaction with actin (Ramesh et al., 1997) and *via* several other cytoskeleton regulatory proteins such as cortactin (or the blood cell variant HS-1), Nck, CrkL and profilin (Anton et al., 2007). But the best-characterized role for this protein in regulating the reorganisation of the actin cytoskeleton is linked to its ability to interact with WASP and N-WASP (Fig. 1B). WIP not only regulates WASP activity but also promotes WASP stability, protecting WASP from degradation by calpain and proteasome in immune system cells (Chou et al., 2006; de la Fuente et al., 2007). Accordingly, WIP and (N-)WASP exist as a complex: indeed, more than 80% of both proteins co-precipitate from cell lysates (de la Fuente et al., 2007; Sasahara et al., 2002). WASP and N-WASP remain in an auto-inhibited conformation (Kim et al., 2000; Miki et al., 1998) and phosphorylation of WIP facilitates WASP binding to Arp2/3 and promotes the initiation of a new branched filament (Higgs and Pollard, 1999; Sasahara et al., 2002). Additionally, WIP is involved in (N-)WASP recruitment to specific subcellular locations (Ditlev et al., 2012; Chou et al., 2006; Sasahara et al., 2002) and can also regulate N-WASP activation by Cdc42 *in vitro*, by promoting its inactive conformation (Martinez-Quiles et al., 2001). In *Drosophila*, a novel mechanism that regulates the interaction of WASP and Solitary (WIP homologue in flies) during formation of podosome-like structures for myoblast fusion has been recently described (Jin et al., 2011). Blown fuse competes with WASP for Solitary/WIP binding, promoting WIP exchange and increased dynamics of WASP-mediated actin polymerisation. The subsequent formation of densely packed and highly branched actin filaments generates adequate mechanical force to permit membrane protrusion.

WIP has been reported to play diverse roles in many different cell types. According to the high levels observed in lymphoid cells, WIP is critical for immune cell function, as its absence affects proliferation, proper activation and migration of T cells (Anton et al., 2002; Gallego et al., 2006; Le Bras et al., 2009). Moreover, it is also implicated in immune synapsis formation in T cells and correct polarisation and transport of lytic granules to the synapses in NK cells (Anton et al., 2002; Krzewski et al., 2008). In addition, recruitment of the WASP/WIP complex to the plasma membrane is important for phagocytic cup formation in macrophages (Tsuboi and Meerloo, 2007).

Interestingly, a recent study has demonstrated a novel role for WIP in neuritogenesis. WIP-null neurons generate a more branched neurite/dendrite morphology than control cells *in vitro* and *in vivo* (Franco et al., 2012). Wiskostatin treatment suggests that the change in neuronal shape may be caused by constitutive activation of N-WASP in the absence of WIP. WIP is additionally essential for endocytosis and actin reorganisation in yeast (Thanabalu et al., 2007) and plays a critical role during pathogen infection as it is implicated in actin tail generation by the vaccinia virus and some bacteria (Lommel et al., 2004; Moreau et al., 2000).

Recent evidence supports the biological importance of WIP in development and disease. Similar to WAS patients, reduced WASP levels – as a result of the diminished WIP levels – have been reported in a novel immune-deficiency due to a mutation in WIPF1 gene (Lanzi et al., 2012). On the other hand, eight patients with micro-deletions in 2q31.1, where the smallest overlapping region correlates with WIPF1 gene, showed symptoms of developmental delay, growth retardation or microcephaly in at least half of the cases (Mitter et al., 2010). How these non-immune symptoms might be caused by a defect in WIP expression as well as their potential link to WIP function at neuron development, are topics that deserve further investigation.

Role of actin-related proteins in invasion/ECM degradation

Studies of what role might be played by WIP family proteins in the mechanism of cell invasion are at an early stage. Little is known about the expression of CR16 and WICH/WIRE in cancer cells, and variable expression patterns for WICH/WIRE have been reported in several cell types (Aspenstrom, 2002; Kato and Takenawa, 2005). In addition, there is no strong evidence for either of these proteins localising to invasive protrusions.

Although the evidence for specific subcellular localisation of other WIP family members is weak, it is well known that endogenous WIP localises in podosomes of DCs (Chou et al., 2006). Overexpressed exogenous WIP also localises to endothelial cell podosomes (Moreau et al., 2003), osteoclast podosomes (Chabadel et al., 2007) and in the invadopodia of WIP-GFP expressing MTLn3 cells (Yamaguchi et al., 2005). In this report we further describe that endogenous WIP is located in the invadopodia of MDA-MB-231 cells plated onto thin gelatin matrices (2D) (Fig. 2A), and also in the invadopodia-like protrusions these cells develop when plated within Matrigel and induced to migrate in a Circular Invasion Assay (Yu and Machesky, 2012) (Fig. 2B). This method represents a robust and amenable tool to study cell invasion in a mimic 3D system (Yu and Machesky, 2012). In this context, invadopodia are defined as actin filament-rich structures containing cortactin and showing matrix degradative capacity.

Some essential invadopodia and podosome proteins can directly interact with WIP and other members of the WIP family, including (N-)WASP, cortactin and Tks5 (Kinley et al., 2003; Oikawa et al., 2008; Ramesh et al., 1997). WIP directly associates with WASP and this complex is recruited to newly formed podosomes (Chou et al., 2006). Consequently, in the absence of WIP, podosome formation is severely compromised (Banon-Rodriguez et al., 2011; Chabadel et al., 2007; Tsuboi, 2007). WIP is essential for WASP stability and localisation at podosomes in osteoclasts and DCs, but interestingly, WIP itself is not sufficient to induce podosome formation, as WASP-null DCs expressing normal levels of WIP are unable to develop podosomes (Chou et al., 2006). On the other hand, overexpression of WASP in WIP-null cells also fails to recover podosome development in DCs. Furthermore, blocking the WASP-binding domain within WIP also inhibits the formation of podosomes in a myeloid cell line (Tsuboi, 2007). Taken together these data suggest that both proteins act as a functional unit to regulate podosome formation and function.

WASP is exclusively expressed in haematopoietic cells whilst N-WASP is ubiquitously expressed. Similar to the role of WASP in podosome formation, N-WASP participates in invadopodia generation. N-WASP silencing in MTLn3 cells leads to a decrease in invadopodium formation, while silencing other members of Scar/WAVE family like WAVE1 or WAVE2 does not have such effects. In addition, over-expression of the WBD of WIP is effective in reducing the number of invadopodia formed by these cells (Yamaguchi et al., 2005) suggesting that the WIP/N-WASP complex is required for invadopodium generation. A role for N-WASP in invadopodia-mediated invasion has also been recently confirmed *in vivo*: cells from mammary tumours developed in mice after inoculation of N-WASP depleted MTLn3 cells show a decreased ability to form proteolytic protrusions, invade and intravasate, leading to a reduced number of circulating tumour cells and lung metastases (Gligorijevic et al., 2012). The decrease in invasive migration was similar to that obtained when using an MMP inhibitor, indicating

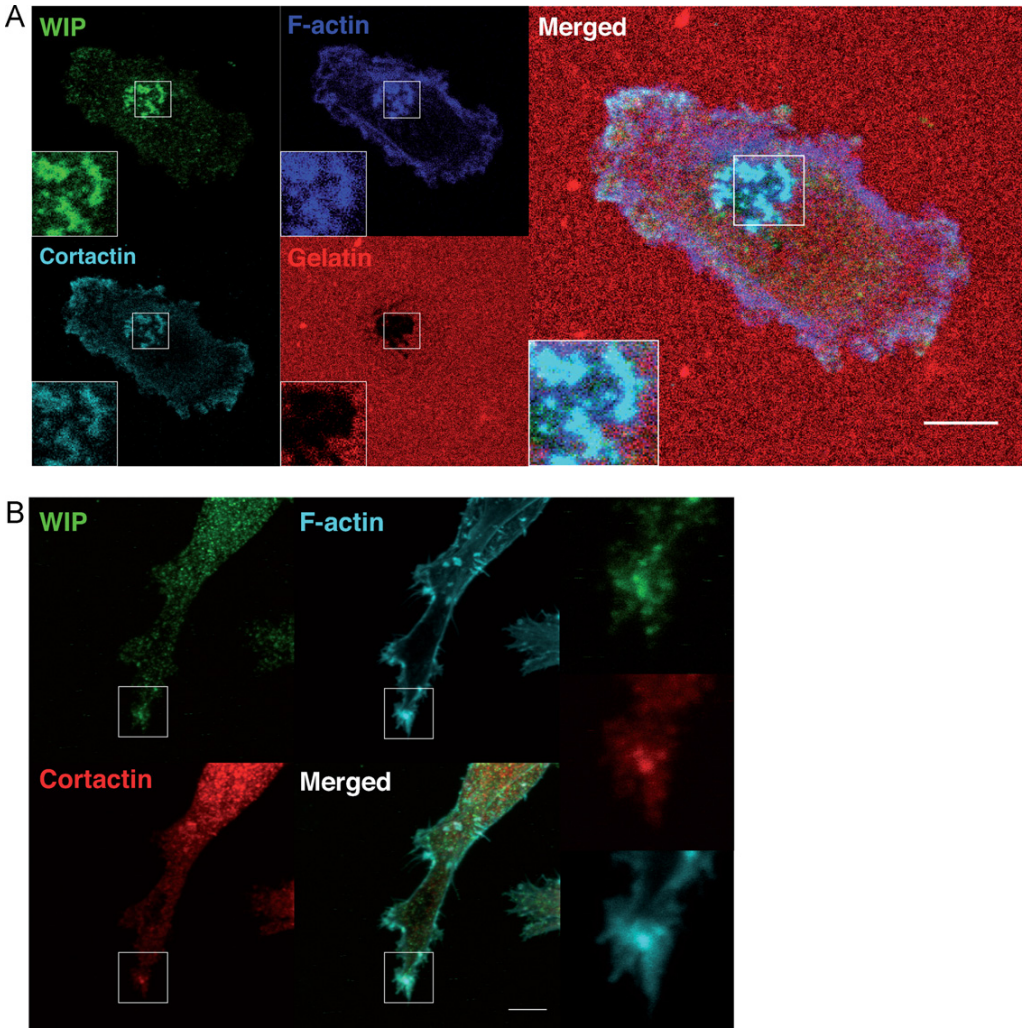

Fig. 2. Endogenous WIP localises at invasive protrusions developed in 2D and 3D matrices. Immunofluorescence of MDA MB 231 plated on: (A) Rhodamine-gelatin coated glass coverslips. The cells were incubated on labelled gelatin (red) for 6 h and after fixation with 4% paraformaldehyde, were stained for WIP (anti-WIP H-224 Santa Cruz; green) and invadopodial markers: f-actin (phalloidin, blue) and cortactin (clone 4F11, cyan). The degraded matrix appears as dark areas in the gelatin. Magnifications of the boxed area show the distribution of WIP, f-actin, cortactin and gelatin separately and merged. (B) Circular Invasion Assay (CIA). The cells were plated on 35 mm micro-dishes using biocompatible silicon inserts (both from Ibidi) to generate a cell-free space. After 24 h incubation and removal of the insert, 250 μl of 4.5 mg/ml BD Matrigel™ was overlaid above the cell monolayer, leaving it to polymerise for 2 h at 37 °C. After growth medium addition to stimulate cell motility, the cells were allowed to invade the polymerised Matrigel for 24 h, fixed with 4% paraformaldehyde and stained for f-actin (blue), cortactin (red) and WIP (green). Magnifications of the boxed area show the distribution of WIP, f-actin and cortactin separately. All scale bars 5 μm. Images represent original data, not published previously.

that N-WASP-dependent migration might directly relate to MMP activity. Interestingly, WAVE1 silenced MTLn3 cells have comparable ability to form invadopodia-like spots to control cells, but these protrusions are not functional as they are unable to degrade the ECM (Yamaguchi et al., 2005). The potential interaction of WICH/WIRE and WAVE could support a specific function in the full functional maturation *i.e.* degradative capacity of invadopodia.

Src activity is essential for podosomes and invadopodium development in normal and transformed cells (Destaing et al., 2008; Kelley et al., 2010). Several Src substrates are phosphorylated in podosomes and invadopodia with the best-known examples including cortactin (Ayala et al., 2008) and Tks5 (Seals et al., 2005). Both Src and cortactin are crucial for assembly and proper function of podosomes and invadopodia (Artym et al., 2006; Burger et al., 2011; Seals et al., 2005; Webb et al., 2006).

Cortactin is a widely expressed protein that interacts with Arp2/3 complex, f-actin and, through its C-terminal SH3 domain, with multiple proline-rich proteins (Kirkbride et al., 2011). Cortactin plays a dual role in invasive protrusions: on the one hand, cortactin acts as a scaffolding protein recruiting Arp2/3, N-WASP and cofilin to invadopodia (Oser et al., 2009; Tehrani et al., 2007). On the other hand, phosphorylated cortactin is essential for ECM degradation in invadopodia since it is reported to have a role in recruiting MMPs to the invadopodial protrusion (Clark et al., 2007). Cortactin interacts with WIP through its SH3 domain (Kinley et al., 2003) and this interaction seems to be essential for proper podosome formation and ECM degradation. WIP-null DCs expressing a WIP mutant lacking the cortactin-binding domain (WIPΔCBD) are able to form cytoskeletal structures that appear podosome-like upon superficial observation, but close examination demonstrates that these structures are somewhat disorganised (Banon-Rodriguez et al., 2011). Interestingly, given the reported role of cortactin as an essential recruiter of WIP-WASP and Arp2/3 complex, the f-actin core of cortactin-depleted cells appears to be nearly

normal but the vinculin ring is impaired. Critically, these structures are not functional, as they cannot perform localised ECM degradation. These data suggest that whilst cortactin may not in fact be essential for the correct localisation of WIP/WASP and Arp2/3, it is essential for restricted MMP delivery and subsequent activity of MMPs at podosomes. WIP may thus mediate recruitment of cortactin-binding vesicles loaded with MMPs to podosomes suggesting that this interaction is also necessary for proper functioning of podosomes during cell invasion into the ECM (Banon-Rodriguez et al., 2011). Nevertheless, additional analyses will be required in order to: (a) investigate whether WIP-null cells expressing the WIPΔCBD construct are able to recruit cortactin to podosomes by an alternative mechanism (see also Tks5 below) and (b) determine whether WIP or other members of WIP family could be mediating MMP recruitment to invasive protrusions through N-WASP interaction.

Also localised at invasive protrusions, Tks5 acts as an adaptor protein crucial for podosome and invadopodium-mediated invasion (Crimaldi et al., 2009; Seals et al., 2005; Thompson et al., 2008; Burger et al., 2011). Although there still is some debate about how Tks5 contributes to formation of podosomes and invadopodia, it clearly is important in assembly and/or maturation. Notably, Tks5 silencing in Src-transformed fibroblasts, smooth muscle cells or human cancer cell lines, leads to an altered formation of podosomes and invadopodia, disturbing cell invasion (Crimaldi et al., 2009; Seals et al., 2005). However, decrease of Tks5 in THP-1 macrophages impairs matrix degradation whilst podosomes are still formed (Burger et al., 2011). The distinctions between these observations can be caused by the different cells used in these studies, the remaining Tks5 levels and/or specificity for Src-dependent signalling (Burger et al., 2011). Furthermore, redundant signals may be compensating the absence of Tks5 after long-term culture: as a result of Tks4 reduction in mouse embryo fibroblasts, Tks5 overexpression occurs leading to recovered ability to form podosomes (Buschman et al., 2009). These findings, added to the fact that Tks5 is also able to bind WIP (Oikawa et al., 2008), suggest that together with cortactin these proteins may cooperate for invadopodium formation. Consequently, interactions between cortactin, Tks5 and WIP need further investigation in order to elucidate how each of these proteins contributes to the development of these protrusions and their maturation into fully functional matrix-degrading entities.

Despite their morphological differences, podosomes/invadopodia and FA (focal adhesions) are related organelles that share many structural and regulatory components as well as functional capabilities. In cancer cells or transformed fibroblasts, both cell constituents, dot-shaped podosomes/invadopodia and stretch-like FA, show degradative capability (Wang and McNiven, 2012). These similarities raise the possibility that a sequential mechanism could contribute to their formation under certain cellular or environmental conditions. In fact, a single study suggests that prior to podosome formation, Tks5 localises to pre-existing FA where N-WASP is recruited driving podosome formation (Oikawa et al., 2008). The intimate relationship between FA and invasive protrusions is also supported by studies performed on Focal Adhesion Kinase (FAK). FAK depletion in cancer cell lines increases formation of non-degradative invadopodia and more stable FA on the cell periphery (Chan et al., 2009). FAK reduction results in relocation of active Src from more stable FA to invadopodia, stimulating phosphorylation of cortactin and Tks5 at developing invadopodia (Chan et al., 2009; Wang and McNiven, 2012). Furthermore, some cancer cell lines develop degrading FA, which requires MT1-MMP activity and is regulated by FAK in a Src-dependent manner (Wang and McNiven, 2012). Therefore, the described role for FAK in breast cancer progression (McLean et al., 2005) – besides being a critical mediator of the integrin signalling cascade which modulates cell proliferation and apoptosis – could be mediated by regulating the switch from FA to invadopodia during invasive migration.

Podosomes can work as mechanosensors whose formation and structural integrity depend on both soluble factors present in serum, and integrin ligands (Monypenny et al., 2011): DC plated on the integrin ligand fibronectin in the absence of serum mainly form focal contacts (FA precursors) and fail to form fully assembled podosomes. When the serum-free culture medium is supplemented with chemotactic factors, DCs show podosomes similarly to DCs cultured with 10% serum in a WASP/WIP-dependent manner (Monypenny et al., 2011). WIP depletion from murine fibroblasts results in enlarged FA that leads to enhanced substratum adhesion and alters migration in these cells (Lanzardo et al., 2007). Moreover, WIP-null DCs that consequently lack podosomes show a higher frequency of focal contacts/FA than wild type cells (Chou et al., 2006). It therefore appears that WIP expression is closely related to FA dynamics. However, how WIP deficiency affects FA formation and turnover remains unclear and the speculative hypothesis that FA could act as precursors or hallmarks to podosome/invadopodium development needs a great deal of further study. Most of the present knowledge on FA generation results from analyses performed on cells cultured in 2D systems, and significant efforts are being made to develop or improve imaging techniques aimed to visualise the formation and dynamics of FA in a 3D environment (Kubow and Horwitz, 2011) (see Geraldo et al. and Parsons and Jayo in this issue).

In summary, Tks5, (N-)WASP and cortactin seem to play a substantial role not only in early development of invasive protrusions, but also in their functionality. Interestingly, WIP interactions with each of these proteins have been reported over the last few years and efforts are now being made to determine the sequence of events and signals that drive formation of these protrusions. In this context it is tantalising to pinpoint WIP as a player in the interrelationship between podosomes/invadopodia and FA. It would also be interesting to look at whether podosomes/invadopodia affect the stability or turnover of FA, as these structures seem to have some common components with sometimes antagonistic roles in cells (Chan et al., 2009).

WIP-mediated cancer cell invasion

Several actin-associated proteins are up- or down-regulated in metastatic cell lines and tumours. Some have been proposed as cancer prognostic markers such as for cortactin (Cai et al., 2010; Di Modugno et al., 2006) and fascin (Machesky and Li, 2010). New evidence suggests a potential role for WIP in cancer cell invasion and metastasis: analyses performed on the expression of WIPF1 in colorectal cancer, breast cancer, and gliomas show a strong correlation between low WIP expression and improved prognosis in these patients (Staub et al., 2009). Moreover, WIPF1 co-expresses with a group of genes associated with proliferation and apoptosis events; these genes include the oncogenes c-myc, ESR1 and p53 (Staub et al., 2009). Similarly, a positive correlation between WIP mRNA levels and invasiveness of luminal and basal-like breast cancer cell lines has been reported (Charafe-Jauffret et al., 2006). WIP expression has been also associated with a mesenchymal phenotype after epithelial–mesenchymal transition (EMT) of prostate cancer cells by silencing the PDEF (epithelium specific Ets transcription factor). PDEF knockdown results in increased prostate cell migration and invasion. Moreover, PDEF regulates genes involved in cell adhesion, integrin signalling, and vascular endothelial growth factor signalling. Accordingly to this regulation, the decrease in PDEF is related to an increase of WIP levels (Gu et al., 2007).

Taken together, the implication of WIP in invadopodium formation added to its prognostic value and the correlation between WIP levels and mesenchymal invasive phenotype, support the plausible role of this protein in cancer cell invasion and hence its potential role in metastasis. These findings have stimulated a further investigation of the role of WIP during physiological and pathological invasion and migration. Combined efforts in our laboratories aim to identify the mechanisms controlling WIP expression, distribution and recruitment, interactions and downstream signals underlying its function.

Concluding remarks and future perspectives

WIP is a key component of podosomes and invadopodia of invasive cells. At the functional level WIP contributes to podosome/invadopodium formation at least at three complementary levels: (a) initiating actin filament formation through the (N-)WASP-Arp2/3 pathway; (b) modulating MMP distribution and degradative capability; and (c) participating in the reorganisation of integrin-mediated adhesions in response to changes in the environmental cues. This cooperative effort is essential in cancer development, where WIP may play a key role to allow the response of cancer cells to the tumour environment (*e.g.* increased secretion of soluble factors such as transforming growth factor beta 1, insulin growth factor or vascular endothelial growth factor) leading to invadopodia formation, tissue invasion and metastasis. To this end, it would be worth testing whether co-overexpression of WIP and N-WASP is sufficient to induce spontaneous formation of invadopodia in non-invasive cancer cell lines.

We hope that our collaborative approaches will unravel WIP as a novel point of diagnostic value or of therapeutic intervention for the treatment of metastasis, since the modulation of WIP activity to inhibit invadopodia formation could block cancer spreading. The therapeutical potential of the regulation of WIP functions could extend to treatment for inflammatory diseases and neurological alterations.

For the future, a great deal of further work is required to answer many open questions, including the nature and regulation of the WIP/(N-)WASP complex and how WASP and N-WASP might behave differently in this complex. Most of cytoplasmic WIP and (N-)WASP exist as a complex (de la Fuente et al., 2007; Sasahara et al., 2002). However very little information on the mechanism of formation of the complex is currently available. Is it concomitantly occurring with the translation of both proteins? Are there any post-translational modifications involved in the process? Is specific protein location a requirement to form the complex? After assembly, the activity of the WIP/WASP complex might be modified by WIP phosphorylation at serine residues following TCR (T cell receptor) engagement (Sasahara et al., 2002). However, WIP/WASP dissociation is not required for downstream signalling (Dong et al., 2007). This raises another question: is disengagement of the WIP/(N-)WASP complex required for further activation in other signalling cascades? If so, is phosphorylation or other protein modifications of either WIP or N-WASP controlling it? And finally, how are other members of the complex, such as Cdc42, involved? WIP can be a negative regulator of Cdc42-induced activation of (N-)WASP to trigger Arp2/3 complex-mediated actin polymerisation *in vitro*, which was shown using pyrene–actin polymerisation assays and recombinant proteins (Martinez-Quiles et al., 2001). In this assay, the effect of WIP is almost absent in the presence of PIP2, but it is unclear what the effect of PIP2 in the plasma membrane at endogenous levels might have. Additionally, it is not clear if the role of WICH/WIRE is distinct from WIP, as many cell types appear to express both proteins.

With all these antecedents, our present and future work mainly focuses on the description of the role of WIP in invasive cells, and it is intimately linked to the understanding of the dynamics of engagement/disengagement of the WIP/(N-)WASP complex during podosome and invadopodium formation. Future experiments should lead to the description of the detailed mechanisms contributing to fine-tune the WIP/(N)-WASP complex assembly and disassembly.

Acknowledgements

We thank Dr. Y. Calle (London, UK) for insightful suggestions and critical reading of the manuscript. This work was supported by grants from Spanish Ministry of Science and Innovation (BFU2010-21374/BMC) and CIBERNED (Instituto de Salud Carlos III) to IMA. EGG held a contract from the CAM. Work in the laboratory of GEJ is supported by the MRC (G1100041) and an EU FP7 award (237946, T3Net).

References

Anton, I.M., de la Fuente, M.A., Sims, T.N., Freeman, S., Ramesh, N., Hartwig, J.H., Dustin, M.L., Geha, R.S., 2002. WIP deficiency reveals a differential role for WIP and the actin cytoskeleton in T and B cell activation. Immunity 16, 193–204.

Anton, I.M., Jones, G.E., Wandosell, F., Geha, R., Ramesh, N., 2007. WASP-interacting protein (WIP): working in polymerisation and much more. Trends Cell Biol. 17, 555–562.

Artym, V.V., Zhang, Y., Seillier-Moiseiwitsch, F., Yamada, K.M., Mueller, S.C., 2006. Dynamic interactions of cortactin and membrane type 1 matrix metalloproteinase at invadopodia: defining the stages of invadopodia formation and function. Cancer Res. 66, 3034–3043.

Aspenstrom, P., 2002. The WASP-binding protein WIRE has a role in the regulation of the actin filament system downstream of the platelet-derived growth factor receptor. Exp. Cell Res. 279, 21–33.

Aspenstrom, P., 2004. The mammalian verprolin homologue WIRE participates in receptor-mediated endocytosis and regulation of the actin filament system by distinct mechanisms. Exp. Cell Res. 298, 485–498.

Ayala, I., Baldassarre, M., Giacchetti, G., Caldieri, G., Tete, S., Luini, A., Buccione, R., 2008. Multiple regulatory inputs converge on cortactin to control invadopodia biogenesis and extracellular matrix degradation. J. Cell Sci. 121, 369–378.

Banon-Rodriguez, I., Monypenny, J., Ragazzini, C., Franco, A., Calle, Y., Jones, G.E., Anton, I.M., 2011. The cortactin-binding domain of WIP is essential for podosome formation and extracellular matrix degradation by murine dendritic cells. Eur. J. Cell Biol. 90, 213–223.

Burger, K.L., Davis, A.L., Isom, S., Mishra, N., Seals, D.F., 2011. The podosome marker protein Tks5 regulates macrophage invasive behavior. Cytoskeleton (Hoboken) 68, 694–711.

Burns, S., Thrasher, A.J., Blundell, M.P., Machesky, L., Jones, G.E., 2001. Configuration of human dendritic cell cytoskeleton by Rho GTPases, the WAS protein, and differentiation. Blood 98, 1142–1149.

Buschman, M.D., Bromann, P.A., Cejudo-Martin, P., Wen, F., Pass, I., Courtneidge, S.A., 2009. The novel adaptor protein Tks4 (SH3PXD2B) is required for functional podosome formation. Mol. Biol. Cell 20, 1302–1311.

Cai, J.H., Zhao, R., Zhu, J.W., Jin, X.L., Wan, F.J., Liu, K., Ji, X.P., Zhu, Y.B., Zhu, Z.G., 2010. Expression of cortactin correlates with a poor prognosis in patients with stages II-III colorectal adenocarcinoma. J. Gastrointest. Surg. 14, 1248–1257.

Calle, Y., Chou, H.C., Thrasher, A.J., Jones, G.E., 2004. Wiskott–Aldrich syndrome protein and the cytoskeletal dynamics of dendritic cells. J. Pathol. 204, 460–469.

Campellone, K.G., Welch, M.D., 2010. A nucleator arms race: cellular control of actin assembly. Nature reviews. Mol. Cell Biol. 11, 237–251.

Chabadel, A., Banon-Rodriguez, I., Cluet, D., Rudkin, B.B., Wehrle-Haller, B., Genot, E., Jurdic, P., Anton, I.M., Saltel, F., 2007. CD44 and beta3 integrin organize two functionally distinct actin-based domains in osteoclasts. Mol. Biol. Cell 18, 4899–4910.

Chan, K.T., Cortesio, C.L., Huttenlocher, A., 2009. FAK alters invadopodia and focal adhesion composition and dynamics to regulate breast cancer invasion. J. Cell Biol. 185, 357–370.

Charafe-Jauffret, E., Ginestier, C., Monville, F., Finetti, P., Adelaide, J., Cervera, N., Fekairi, S., Xerri, L., Jacquemier, J., Birnbaum, D., Bertucci, F., 2006. Gene expression profiling of breast cell lines identifies potential new basal markers. Oncogene 25, 2273–2284.

Chou, H.C., Anton, I.M., Holt, M.R., Curcio, C., Lanzardo, S., Worth, A., Burns, S., Thrasher, A.J., Jones, G.E., Calle, Y., 2006. WIP regulates the stability and localization of WASP to podosomes in migrating dendritic cells. Curr. Biol. 16, 2337–2344.

Clark, E.S., Whigham, A.S., Yarbrough, W.G., Weaver, A.M., 2007. Cortactin is an essential regulator of matrix metalloproteinase secretion and extracellular matrix degradation in invadopodia. Cancer Res. 67, 4227–4235.

Crimaldi, L., Courtneidge, S.A., Gimona, M., 2009. Tks5 recruits AFAP-110, p190RhoGAP, and cortactin for podosome formation. Exp. Cell Res. 315, 2581–2592.
de la Fuente, M.A., Sasahara, Y., Calamito, M., Anton, I.M., Elkhal, A., Gallego, M.D., Suresh, K., Siminovitch, K., Ochs, H.D., Anderson, K.C., Rosen, F.S., Geha, R.S., Ramesh, N., 2007. WIP is a chaperone for Wiskott–Aldrich syndrome protein (WASP). Proc. Natl. Acad. Sci. U.S.A. 104, 926–931.
Derry, J.M., Ochs, H.D., Francke, U., 1994. Isolation of a novel gene mutated in Wiskott–Aldrich syndrome. Cell 79, following 922.
Destaing, O., Sanjay, A., Itzstein, C., Horne, W.C., Toomre, D., De Camilli, P., Baron, R., 2008. The tyrosine kinase activity of c-Src regulates actin dynamics and organization of podosomes in osteoclasts. Mol. Biol. Cell 19, 394–404.
Di Modugno, F., Mottolese, M., Di Benedetto, A., Conidi, A., Novelli, F., Perracchio, L., Venturo, I., Botti, C., Jager, E., Santoni, A., Natali, P.G., Nistico, P., 2006. The cytoskeleton regulatory protein hMena (ENAH) is overexpressed in human benign breast lesions with high risk of transformation and human epidermal growth factor receptor-2-positive/hormonal receptor-negative tumors. Clin. Cancer Res. 12, 1470–1478.
Ditlev, J.A., Michalski, P.J., Huber, G., Rivera, G.M., Mohler, W.A., Loew, L.M., Mayer, B.J., 2012. Stoichiometry of Nck-dependent actin polymerization in living cells. J. Cell Biol. 197, 643–658.
Dominguez, R., Holmes, K.C., 2011. Actin structure and function. Annu. Rev. Biophys. 40, 169–186.
Dong, X., Patino-Lopez, G., Candotti, F., Shaw, S., 2007. Structure–function analysis of the WIP role in T cell receptor-stimulated NFAT activation: evidence that WIP-WASP dissociation is not required and that the WIP NH2 terminus is inhibitory. J. Biol. Chem. 282, 30303–30310.
Eden, S., Rohatgi, R., Podtelejnikov, A.V., Mann, M., Kirschner, M.W., 2002. Mechanism of regulation of WAVE1-induced actin nucleation by Rac1 and Nck. Nature 418, 790–793.
Etienne-Manneville, S., Hall, A., 2002. Rho GTPases in cell biology. Nature 420, 6.
Fackler, O.T., Grosse, R., 2008. Cell motility through plasma membrane blebbing. J Cell Biol. 181, 879–884.
Fidler, I.J., 2003. The pathogenesis of cancer metastasis: the 'seed and soil' hypothesis revisited. Nature reviews. Cancer 3, 453–458.
Franco, A., Knafo, S., Banon-Rodriguez, I., Merino-Serrais, P., Fernaud-Espinosa, I., Nieto, M., Garrido, J.J., Esteban, J.A., Wandosell, F., Anton, I.M., 2012. WIP is a negative regulator of neuronal maturation and synaptic activity. Cereb. Cortex 22, 1191–1202.
Friedl, P., Wolf, K., 2009. Proteolytic interstitial cell migration: a five-step process. Cancer Metastasis Rev. 28, 129–135.
Gallego, M.D., de la Fuente, M.A., Anton, I.M., Snapper, S., Fuhlbrigge, R., Geha, R.S., 2006. WIP and WASP play complementary roles in T cell homing and chemotaxis to SDF-1alpha. Int. Immunol. 18, 221–232.
Gimona, M., Buccione, R., Courtneidge, S.A., Linder, S., 2008. Assembly and biological role of podosomes and invadopodia. Curr. Opin. Cell Biol. 20, 235–241.
Gligorijevic, B., Wyckoff, J., Yamaguchi, H., Wang, Y., Roussos, E.T., Condeelis, J., 2012. N-WASP-mediated invadopodium formation is involved in intravasation and lung metastasis of mammary tumors. J. Cell Sci. 125, 724–734.
Gu, X., Zerbini, L.F., Otu, H.H., Bhasin, M., Yang, Q., Joseph, M.G., Grall, F., Onatunde, T., Correa, R.G., Libermann, T.A., 2007. Reduced PDEF expression increases invasion and expression of mesenchymal genes in prostate cancer cells. Cancer Res. 67, 4219–4226.
Higgs, H.N., Pollard, T.D., 1999. Regulation of actin polymerization by Arp2/3 complex and WASp/Scar proteins. J Biol. Chem. 274, 32531–32534.
Ho, H.Y., Rohatgi, R., Ma, L., Kirschner, M.W., 2001. CR16 forms a complex with N-WASP in brain and is a novel member of a conserved proline-rich actin-binding protein family. Proc. Natl. Acad. Sci. U.S.A. 98, 11306–11311.
Jin, P., Duan, R., Luo, F., Zhang, G., Hong, S.N., Chen, E.H., 2011. Competition between Blown fuse and WASP for WIP binding regulates the dynamics of WASP-dependent actin polymerization in vivo. Dev. Cell 20, 623–638.
Kato, M., Miki, H., Kurita, S., Endo, T., Nakagawa, H., Miyamoto, S., Takenawa, T., 2002. WICH, a novel verprolin homology domain-containing protein that functions cooperatively with N-WASP in actin-microspike formation. Biochem. Biophys. Res. Commun. 291, 41–47.
Kato, M., Takenawa, T., 2005. WICH, a member of WASP-interacting protein family, cross-links actin filaments. Biochem. Biophys. Res. Commun. 328, 1058–1066.
Kelley, L.C., Ammer, A.G., Hayes, K.E., Martin, K.H., Machida, K., Jia, L., Mayer, B.J., Weed, S.A., 2010. Oncogenic Src requires a wild-type counterpart to regulate invadopodia maturation. J. Cell Sci. 123, 3923–3932.
Kim, A.S., Kakalis, L.T., Abdul-Manan, N., Liu, G.A., Rosen, M.K., 2000. Autoinhibition and activation mechanisms of the Wiskott–Aldrich syndrome protein. Nature 404, 151–158.
Kinley, A.W., Weed, S.A., Weaver, A.M., Karginov, A.V., Bissonette, E., Cooper, J.A., Parsons, J.T., 2003. Cortactin interacts with WIP in regulating Arp2/3 activation and membrane protrusion. Curr. Biol. 13, 384–393.
Kirkbride, K.C., Sung, B.H., Sinha, S., Weaver, A.M., 2011. Cortactin: a multifunctional regulator of cellular invasiveness. Cell Adhes. Migr. 5, 187–198.
Koduru, S., Massaad, M., Wilbur, C., Kumar, L., Geha, R., Ramesh, N., 2007. A novel anti-WIP monoclonal antibody detects an isoform of WIP that lacks the WASP binding domain. Biochem. Biophys. Res. Commun. 353, 875–881.
Kovacs, E.M., Verma, S., Ali, R.G., Ratheesh, A., Hamilton, N.A., Akhmanova, A., Yap, A.S., 2011. N-WASP regulates the epithelial junctional actin cytoskeleton through a non-canonical post-nucleation pathway. Nat. Cell Biol. 13, 934–943.
Krzewski, K., Chen, X., Strominger, J.L., 2008. WIP is essential for lytic granule polarization and NK cell cytotoxicity. Proc. Natl. Acad. Sci. U.S.A. 105, 2568–2573.
Kubow, K.E., Horwitz, A.R., 2011. Reducing background fluorescence reveals adhesions in 3D matrices. Nat. Cell Biol. 13, 3–5, author reply 5–7.
Lanzardo, S., Curcio, C., Forni, G., Anton, I.M., 2007. A role for WASP Interacting Protein, WIP, in fibroblast adhesion, spreading and migration. Int. J. Biochem. Cell Biol. 39, 262–274.
Lanzi, G., Moratto, D., Vairo, D., Masneri, S., Delmonte, O., Paganini, T., Parolini, S., Tabellini, G., Mazza, C., Savoldi, G., Montin, D., Martino, S., Tovo, P., Pessach, I.M., Massaad, M.J., Ramesh, N., Porta, F., Plebani, A., Notarangelo, L.D., Geha, R.S., Giliani, S., 2012. A novel primary human immunodeficiency due to deficiency in the WASP-interacting protein WIP. J. Exp. Med. 209, 29–34.
Le Bras, S., Massaad, M., Koduru, S., Kumar, L., Oyoshi, M.K., Hartwig, J., Geha, R.S., 2009. WIP is critical for T cell responsiveness to IL-2. Proc. Natl. Acad. Sci. U.S.A. 106, 7519–7524.
Li, A., Dawson, J.C., Forero-Vargas, M., Spence, H.J., Yu, X., Konig, I., Anderson, K., Machesky, L.M., 2010. The actin-bundling protein fascin stabilizes actin in invadopodia and potentiates protrusive invasion. Curr. Biol. 20, 339–345.
Linder, S., Nelson, D., Weiss, M., Aepfelbacher, M., 1999. Wiskott–Aldrich syndrome protein regulates podosomes in primary human macrophages. Proc. Natl. Acad. Sci. U.S.A. 96, 9648–9653.
Linder, S., Wiesner, C., Himmel, M., 2011. Degrading devices: invadosomes in proteolytic cell invasion. Annu. Rev. Cell Dev. Biol. 27, 185–211.
Lommel, S., Benesch, S., Rohde, M., Wehland, J., Rottner, K., 2004. Enterohaemorrhagic and enteropathogenic Escherichia coli use different mechanisms for actin pedestal formation that converge on N-WASP. Cell. Microbiol. 6, 243–254.
Machesky, L.M., Insall, R.H., 1998. Scar1 and the related Wiskott–Aldrich syndrome protein, WASP, regulate the actin cytoskeleton through the Arp2/3 complex. Curr. Biol. 8, 1347–1356.
Machesky, L.M., Li, A., 2010. Fascin: invasive filopodia promoting metastasis. Commun. Integr. Biol. 3, 263–270.
Martinez-Quiles, N., Rohatgi, R., Anton, I.M., Medina, M., Saville, S.P., Miki, H., Yamaguchi, H., Takenawa, T., Hartwig, J.H., Geha, R.S., Ramesh, N., 2001. WIP regulates N-WASP-mediated actin polymerization and filopodium formation. Nat. Cell Biol. 3, 484–491.
Mattila, P.K., Lappalainen, P., 2008. Filopodia: molecular architecture and cellular functions. Nature reviews. Mol. Cell Biol. 9, 446–454.
McLean, G.W., Carragher, N.O., Avizienyte, E., Evans, J., Brunton, V.G., Frame, M.C., 2005. The role of focal-adhesion kinase in cancer – a new therapeutic opportunity. Nat. Rev. Cancer 5, 505–515.
Meyer, T., Hart, I.R., 1998. Mechanisms of tumour metastasis. Eur. J. Cancer 34, 214–221.
Miki, H., Sasaki, T., Takai, Y., Takenawa, T., 1998. Induction of filopodium formation by a WASP-related actin-depolymerizing protein N-WASP. Nature 391, 93–96.
Misra, A., Rajmohan, R., Lim, R.P., Bhattacharyya, S., Thanabalu, T., 2010. The mammalian verprolin, WIRE induces filopodia independent of N-WASP through IRSp53. Exp. Cell Res. 316, 2810–2824.
Mitter, D., Chiaie, B.D., Ludecke, H.J., Gillessen-Kaesbach, G., Bohring, A., Kohlhase, J., Caliebe, A., Siebert, R., Roepke, A., Ramos-Arroyo, M.A., Nieva, B., Menten, B., Loeys, B., Mortier, G., Wieczorek, D., 2010. Genotype-phenotype correlation in eight new patients with a deletion encompassing 2q31.1. Am. J. Med. Genet. A 152A, 1213–1224.
Monypenny, J., Chou, H.C., Banon-Rodriguez, I., Thrasher, A.J., Anton, I.M., Jones, G.E., Calle, Y., 2011. Role of WASP in cell polarity and podosome dynamics of myeloid cells. Eur. J. Cell Biol. 90, 198–204.
Moreau, V., Frischknecht, F., Reckmann, I., Vincentelli, R., Rabut, G., Stewart, D., Way, M., 2000. A complex of N-WASP and WIP integrates signalling cascades that lead to actin polymerization. Nat. Cell Biol. 2, 441–448.
Moreau, V., Tatin, F., Varon, C., Genot, E., 2003. Actin can reorganize into podosomes in aortic endothelial cells, a process controlled by Cdc42 and RhoA. Mol. Cell. Biol. 23, 6809–6822.
Murphy, D.A., Courtneidge, S.A., 2011. The 'ins' and 'outs' of podosomes and invadopodia: characteristics, formation and function. Nat. Rev. Mol. Cell Biol. 12, 413–426.
Nichols, N.R., Masters, J.N., Finch, C.E., 1990. Changes in gene expression in hippocampus in response to glucocorticoids and stress. Brain Res. Bull. 24, 659–662.
Oikawa, T., Itoh, T., Takenawa, T., 2008. Sequential signals toward podosome formation in NIH-src cells. J. Cell Biol. 182, 157–169.
Oser, M., Dovas, A., Cox, D., Condeelis, J., 2011. Nck1 and Grb2 localization patterns can distinguish invadopodia from podosomes. Eur. J. Cell Biol. 90, 181–188.
Oser, M., Yamaguchi, H., Mader, C.C., Bravo-Cordero, J.J., Arias, M., Chen, X., Desmarais, V., van Rheenen, J., Koleske, A.J., Condeelis, J., 2009. Cortactin regulates cofilin and N-WASp activities to control the stages of invadopodium assembly and maturation. J. Cell Biol. 186, 571–587.
Ramesh, N., Anton, I.M., Hartwig, J.H., Geha, R.S., 1997. WIP, a protein associated with Wiskott–aldrich syndrome protein, induces actin polymerization and redistribution in lymphoid cells. Proc. Natl. Acad. Sci. U.S.A. 94, 14671–14676.
Ramesh, N., Anton, I.M., Martinez-Quiles, N., Geha, R.S., 1999. Waltzing with WASP. Trends Cell Biol. 9, 15–19.
Ridley, A.J., 2011. Life at the leading edge. Cell 145, 1012–1022.
Rohatgi, R., Ma, L., Miki, H., Lopez, M., Kirchhausen, T., Takenawa, T., Kirschner, M.W., 1999. The interaction between N-WASP and the Arp2/3 complex links Cdc42-dependent signals to actin assembly. Cell 97, 221–231.
Rottiers, P., Saltel, F., Daubon, T., Chaigne-Delalande, B., Tridon, V., Billottet, C., Reuzeau, E., Genot, E., 2009. TGFbeta-induced endothelial podosomes mediate basement membrane collagen degradation in arterial vessels. J. Cell Sci. 122, 4311–4318.

Rottner, K., Hanisch, J., Campellone, K.G., 2010. WASH, WHAMM and JMY: regulation of Arp2/3 complex and beyond. Trends Cell Biol. 20, 650–661.
Saltel, F., Daubon, T., Juin, A., Ganuza, I.E., Veillat, V., Genot, E., 2011. Invadosomes: intriguing structures with promise. Eur. J. Cell Biol. 90, 100–107.
Sasahara, Y., Rachid, R., Byrne, M.J., de la Fuente, M.A., Abraham, R.T., Ramesh, N., Geha, R.S., 2002. Mechanism of recruitment of WASP to the immunological synapse and of its activation following TCR ligation. Mol. Cell 10, 1269–1281.
Seals, D.F., Azucena Jr., E.F., Pass, I., Tesfay, L., Gordon, R., Woodrow, M., Resau, J.H., Courtneidge, S.A., 2005. The adaptor protein Tks5/Fish is required for podosome formation and function, and for the protease-driven invasion of cancer cells. Cancer Cell 7, 155–165.
Snapper, S.B., Meelu, P., Nguyen, D., Stockton, B.M., Bozza, P., Alt, F.W., Rosen, F.S., von Andrian, U.H., Klein, C., 2005. WASP deficiency leads to global defects of directed leukocyte migration in vitro and in vivo. J. Leukoc. Biol. 77, 993–998.
Snapper, S.B., Rosen, F.S., 1999. The Wiskott–Aldrich syndrome protein (WASP): roles in signaling and cytoskeletal organization. Annu. Rev. Immunol. 17, 905–929.
Staub, E., Groene, J., Heinze, M., Mennerich, D., Roepcke, S., Klaman, I., Hinzmann, B., Castanos-Velez, E., Pilarsky, C., Mann, B., Brummendorf, T., Weber, B., Buhr, H.J., Rosenthal, A., 2009. An expression module of WIPF1-coexpressed genes identifies patients with favorable prognosis in three tumor types. J. Mol. Med. 87, 633–644.
Suetsugu, S., Banzai, Y., Kato, M., Fukami, K., Kataoka, Y., Takai, Y., Yoshida, N., Takenawa, T., 2007. Male-specific sterility caused by the loss of CR16. Genes Cells 12, 721–733.
Sung, B.H., Weaver, A., 2011. Cell–cell fusion: a new function for invadosomes. Curr. Biol. 21, R121–R123.
Tehrani, S., Tomasevic, N., Weed, S., Sakowicz, R., Cooper, J.A., 2007. Src phosphorylation of cortactin enhances actin assembly. Proc. Natl. Acad. Sci. U.S.A. 104, 11933–11938.
Thanabalu, T., Rajmohan, R., Meng, L., Ren, G., Vajjhala, P.R., Munn, A.L., 2007. Verprolin function in endocytosis and actin organization. Roles of the Las17p (yeast WASP)-binding domain and a novel C-terminal actin-binding domain. FEBS J. 274, 4103–4125.
Thompson, O., Kleino, I., Crimaldi, L., Gimona, M., Saksela, K., Winder, S.J., 2008. Dystroglycan, Tks5 and Src mediated assembly of podosomes in myoblasts. PLoS One 3, e3638.
Thrasher, A.J., Jones, G.E., Kinnon, C., Brickell, P.M., Katz, D.R., 1998. Is Wiskott–Aldrich syndrome a cell trafficking disorder? Immunol. Today 19, 537–539.
Tsuboi, S., 2006. A complex of Wiskott–Aldrich syndrome protein with mammalian verprolins plays an important role in monocyte chemotaxis. J. Immunol. 176, 6576–6585.
Tsuboi, S., 2007. Requirement for a complex of Wiskott–Aldrich syndrome protein (WASP) with WASP interacting protein in podosome formation in macrophages. J. Immunol. 178, 2987–2995.
Tsuboi, S., Meerloo, J., 2007. Wiskott–Aldrich syndrome protein is a key regulator of the phagocytic cup formation in macrophages. J. Biol. Chem. 282, 34194–34203.
Wang, Y., McNiven, M.A., 2012. Invasive matrix degradation at focal adhesions occurs via protease recruitment by a FAK-p130Cas complex. J Cell Biol. 196, 375–385.
Webb, B.A., Eves, R., Mak, A.S., 2006. Cortactin regulates podosome formation: roles of the protein interaction domains. Exp. Cell Res. 312, 760–769.
Yamaguchi, H., Lorenz, M., Kempiak, S., Sarmiento, C., Coniglio, S., Symons, M., Segall, J., Eddy, R., Miki, H., Takenawa, T., Condeelis, J., 2005. Molecular mechanisms of invadopodium formation: the role of the N-WASP-Arp2/3 complex pathway and cofilin. J. Cell Biol. 168, 441–452.
Yu, X., Machesky, L.M., 2012. Cells assemble invadopodia-like structures and invade into matrigel in a matrix metalloprotease dependent manner in the circular invasion assay. PloS One 7, e30605.

Published October 22, 2012

N-WASP coordinates the delivery and F-actin–mediated capture of MT1-MMP at invasive pseudopods

Xinzi Yu,[1] Tobias Zech,[1] Laura McDonald,[1] Esther Garcia Gonzalez,[2] Ang Li,[1] Iain Macpherson,[1] Juliane P. Schwarz,[1] Heather Spence,[1] Kinga Futó,[4] Paul Timpson,[1] Colin Nixon,[1] Yafeng Ma,[1] Ines M. Anton,[2] Balázs Visegrády,[4] Robert H. Insall,[1,3] Karin Oien,[3] Karen Blyth,[1] Jim C. Norman,[1,3] and Laura M. Machesky[1,3]

[1]The Beatson Institute for Cancer Research, Bearsden, Glasgow G61 1BD, Scotland, UK
[2]Centro Nacional de Biotecnologia (CNB-CSIC) Darwin 3, Campus Universidad Autónoma de Madrid Cantoblanco, 28049 Madrid, Spain
[3]College of Medical Veterinary and Life Sciences, University of Glasgow, Glasgow G12 8QQ, Scotland, UK
[4]Department of Biophysics, Medical School, University of Pécs, Pécs H-7624, Hungary

Metastasizing tumor cells use matrix metalloproteases, such as the transmembrane collagenase MT1-MMP, together with actin-based protrusions, to break through extracellular matrix barriers and migrate in dense matrix. Here we show that the actin nucleation–promoting protein N-WASP (Neural Wiskott-Aldrich syndrome protein) is up-regulated in breast cancer, and has a pivotal role in mediating the assembly of elongated pseudopodia that are instrumental in matrix degradation. Although a role for N-WASP in invadopodia was known, we now show how N-WASP regulates invasive protrusion in 3D matrices. In actively invading cells, N-WASP promoted trafficking of MT1-MMP into invasive pseudopodia, primarily from late endosomes, from which it was delivered to the plasma membrane. Upon MT1-MMP's arrival at the plasma membrane in pseudopodia, N-WASP stabilized MT1-MMP via direct tethering of its cytoplasmic tail to F-actin. Thus, N-WASP is crucial for extension of invasive pseudopods into which MT1-MMP traffics and for providing the correct cytoskeletal framework to couple matrix remodeling with protrusive invasion.

Introduction

Actin-driven cell shape alteration and migration as well as enzymatic modification of surrounding ECM are vital for tumor cells to invade and metastasize. Neural Wiskott-Aldrich syndrome protein (N-WASP) is a widely expressed member of the WASP/Scar family, which are major Arp2/3 complex-based actin nucleation–promoting proteins. N-WASP acts as a scaffold to coordinate signals from small GTPases, receptor tyrosine kinases, phospholipids, and SH3-domain–containing proteins to drive actin nucleation. Despite reports that N-WASP can promote filopod assembly (Miki et al., 1998), loss of N-WASP does not affect Cdc42-induced filopod formation in cultured primary fibroblasts, but modestly reduces clathrin-mediated endocytosis (Lommel et al., 2001). N-WASP is implicated in fission of endocytic vesicles and propelling vesicle departure from the plasma membrane (Taunton et al., 2000; Benesch et al., 2002; Merrifield et al., 2002), as well as the actin-driven dorsal ruffling that accompanies macropinocytosis (Legg et al., 2007). N-WASP is also implicated in lamellipodia generation in primary cultured Schwann cells (Jin et al., 2011). Thus, N-WASP–mediated actin nucleation contributes to plasma membrane protrusions and optimal function of both clathrin-dependent and clathrin-independent endocytosis (Yarar et al., 2007).

An emerging body of evidence suggests that N-WASP is linked with cancer progression and invasion. For example, N-WASP is up-regulated in metastatic liver lesions compared with primary colorectal tumors (Yanagawa et al., 2001). Interestingly, N-WASP (but not other WASP/Scar family members)

X. Yu and T. Zech contributed equally to this paper.

Correspondence to Laura M. Machesky: l.machesky@beatson.gla.ac.uk

Abbreviations used in this paper: BM, basement membrane; CIA, circular invasion assay; DCIS, ductal carcinoma in situ; FLIM, fluorescence-lifetime imaging microscopy; IAEDANS, 5-({2-[(iodoacetyl)amino]ethyl}amino)naphthalene-1-sulfonic acid; LE, late endosome; MMP, matrix metalloproteinase; NT, nontargeting; N-WASP, Neural Wiskott-Aldrich syndrome protein; PA, photoactivatable; PMT, photomultiplier tube; TMA, tissue microarray; WT, wild type.

Supplemental Material can be found at:
http://jcb.rupress.org/content/suppl/2012/10/18/jcb.201203025.DC1.html

The Rockefeller University Press $30.00
J. Cell Biol. Vol. 199 No. 3 527–544
www.jcb.org/cgi/doi/10.1083/jcb.201203025

Published October 22, 2012

is concentrated within invadopodia and is required for their formation (Lorenz et al., 2004; Yamaguchi et al., 2005; Oser et al., 2009). Additionally, N-WASP is important for the polarized formation of punctate structures, termed invadopodia precursors, in the leading edges of chemotaxing cells on 2D rigid glass substrates (Desmarais et al., 2009). The efficient function of invadopodia requires coordination of multiple machineries, including N-WASP–Arp2/3–mediated actin polymerization, cross-linking (fascin), maturation (cortactin), and accumulation of proteases such as matrix metalloproteinases (MMPs; Yamaguchi et al., 2005; Artym et al., 2006; Clark et al., 2007). However, the function of N-WASP in cancer cell migration and invasion has not yet been investigated in 3D ECM, nor has the effect of N-WASP depletion on trafficking of matrix degrading enzymes been investigated.

MMPs are multifunctional zinc-dependent endopeptidases involved in both signaling and matrix remodeling. Of this family, the membrane-anchored MT1-MMP is implicated both in the breaching of basement membranes (BMs) and in cell invasion through interstitial type-I collagen tissues (Sabeh et al., 2004; Hotary et al., 2006). MT1-MMP expression is correlated with the malignancy of multiple tumor types including lung, gastric, colon, breast, cervical carcinomas, gliomas, and melanomas (Seiki et al., 2003). Sabeh et al. (2004) have demonstrated that MT1-MMP serves as the dominant protease of both tumor cells and fibroblasts to degrade type-I collagen. Cells lacking MT1-MMP display no defects in 2D proliferation or migration across collagen-coated surfaces, but their capacity to invade is severely impaired (Sabeh et al., 2004). Cell surface MT1-MMP activity can be modulated by various routes, such as endocytosis (Jiang et al., 2001), recycling, autocatalytic processing, and posttranslational regulation (Ludwig et al., 2008; Poincloux et al., 2009). MT1-MMP accumulates at invadopodia and is important for focal degradation of ECM at these sites (Nakahara et al., 1997; Linder, 2007; Caldieri et al., 2009). Delivery and docking of MT1-MMP–containing vesicles at invadopodia requires membrane fusion machinery such as the vSNARE, VAMP7, and exocyst complex members as well as Rab8 (Bravo-Cordero et al., 2007; Steffen et al., 2008; Poincloux et al., 2009). Rab8 promotes polarized transport of newly synthesized membrane proteins in fibroblasts, and thus may control trafficking of newly synthesized MT1-MMP from the Golgi complex to the plasma membrane (Peränen et al., 1996). Here, we demonstrate that N-WASP–mediated actin polymerization drives invasive pseudopods, into which MT1-MMP is delivered, and we provide a novel F-actin–mediated mechanism for directed receptor targeting and stabilization of the invasive degrading machinery of cancer cells.

Results

N-WASP expression is increased in invasive breast cancer

To investigate the role of N-WASP in breast cancer invasion, we first assessed N-WASP expression in human breast cancer tissues. Normal breast, ductal carcinoma in situ (DCIS), and invasive ductal carcinoma were analyzed using immunohistochemistry to stain for N-WASP. N-WASP appeared weak, but showed specific cytoplasmic staining of epithelial cells in normal tissue and DCIS lesions. Knockdown cells prepared for histological analysis showed negative to weak staining in comparison with nontargeting (NT) control MDA-MB-231 (unpublished data). In contrast, N-WASP expression was up-regulated in invasive breast cancer samples (Fig. 1 A). To quantify N-WASP expression in human breast cancers, a tissue microarray (TMA; Biomax Z7020004) of 75 cores including normal/hyperplasia and tumor samples was stained and scored for N-WASP using the weighted histo-score method (see Materials and methods; Kirkegaard et al., 2006). N-WASP expression in invasive breast cancer was significantly higher than in normal or DCIS tissues ($P < 0.05$; Fig. 1 B). Furthermore, in normal mouse mammary glands, N-WASP consistently showed weak to moderate expression throughout various stages of mammary ductal homeostasis (Fig. 1 C), whereas mammary tumors from the MMTV-PyMT ($n = 9$) and MMTV-erbB2 (activated HER2, $n = 5$) mouse models (Muller et al., 1988; Fluck and Schaffhausen, 2009) consistently showed a dramatic increase in N-WASP expression (Fig. 1 D).

N-WASP drives cell elongation and the extension of long pseudopodia in 3D matrices

Most studies of N-WASP depletion have not revealed a role for N-WASP in peripheral lamellipodia extension or motility in 2D on rigid substrates (Snapper et al., 2001; Bryce et al., 2005; Kowalski et al., 2005; Misra et al., 2007; Sarmiento et al., 2008; Desmarais et al., 2009), although N-WASP has been implicated in filopodia (Hüfner et al., 2002; Bu et al., 2009) and lamellipodia formation in Schwann cells (Jin et al., 2011) and circular dorsal ruffles (Legg et al., 2007). We found that MDA-MB-231 invasive breast cancer cells depleted of N-WASP with two individual oligos by ∼90% using siRNA (Fig. S1 A) showed normal shape and motility parameters on a rigid 2D surface (Fig. S1, C and D). Protein levels of Scar/WAVE1, Scar/WAVE2, and WASH do not detectably change upon N-WASP depletion (Fig. S1 B). This suggests that in MDA-MB-231 cells, like most other cells studied to date, N-WASP does not have a detectable nonredundant role in motility on a 2D surface.

However, in 3D microenvironments, depletion of N-WASP dramatically affected the ability of MDA-MB-231 cells to invade in a 3D invasion assay where the cells crawled first through a filter (0 µM in Fig. 2 A) and then into a thick plug of Matrigel toward a gradient of serum with 25 nM of EGF (Hennigan et al., 1994). There was no difference between the N-WASP–depleted and NT cells in the number of cells that were able to migrate through the filter, which indicates that noninvasive migration was not impaired by N-WASP depletion. However, N-WASP–depleted cells showed greatly impaired invasive activity in Matrigel plugs, with invading cells reduced to around 10% (siN-WASP #1) and 30% (siN-WASP #2) compared with control (Fig. 2 A). To understand why cells depleted of N-WASP failed to invade, we first examined their morphology. In the inverted invasion assay, normal MDA-MB-231 cells elongated and formed elaborate long trains of cells connecting each other end-to-end and projecting into the Matrigel (Fig. 2 B and Video 1). N-WASP knockdown cells, in contrast, crossed over to the other side of the filter and then piled up as rounded cell aggregates that did not elongate or invade (Fig. 2 B and Video 2).

Published October 22, 2012

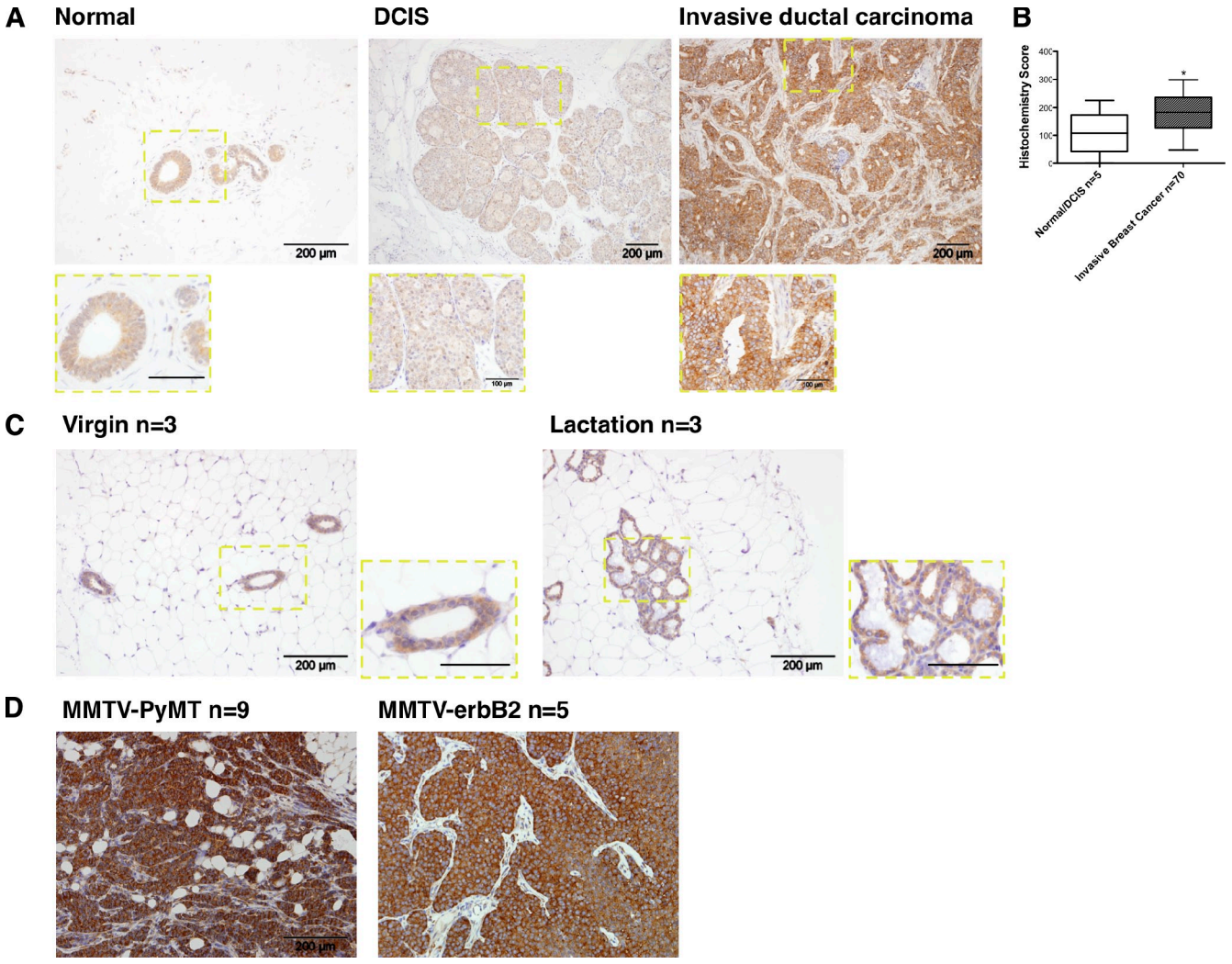

Figure 1. **N-WASP expression increases in both human and mouse invasive breast cancers.** (A) Immunohistochemical staining of N-WASP in human breast cancer tissues. Left and middle panels show expression of N-WASP in human normal tissue and DCIS. The right panel shows the expression level of N-WASP in human invasive ductal carcinoma. The insets show enlarged images of N-WASP staining in different tissues. (B) Bar graphs indicate histochemistry scores of normal/DCIS and invasive breast cancer cores from a 75-core human breast cancer TMA. All error bars indicate means ± SD; *, $P < 0.05$ by *t* test. (C) Immunohistochemical staining of N-WASP in mouse virgin and lactating mammary glands. Samples from three mice were stained and imaged. The insets show enlarged images of N-WASP staining in mouse virgin and lactating mammary glands. (D) Immunohistochemical staining of N-WASP in primary tumors from MMTV-PyMT ($n = 9$) and MMTV-erbB2 ($n = 5$) mouse models. Bars: (main panels) 200 µm; (insets) 100 µm.

N-WASP–depleted cells were also impaired in invasion in a modified version of the circular invasion assay (CIA; Kam et al., 2008), which enabled resolution of subcellular structures by both live cell time-lapse and fixed cell immunofluorescence (Fig. 3 A; Yu and Machesky, 2012). This assay is based on a wound-healing assay that is overlaid with Matrigel, and the cells invade into an empty space, rather than toward a specific attractant. Movement in the CIA was dependent on ECM remodeling, as knockdown of MT1-MMP, or inhibition with a broad MMP inhibitor, GM6001, reduced migration speed by 30–50% (Yu and Machesky, 2012). Similar to cells depleted for MT1-MMP, N-WASP–depleted cells (using two separate oligos siN-WASP #1 and siN-WASP #2) did not migrate far from the start point of the CIA (marked by black lines) and showed a 40% reduction of cell speed and persistence as analyzed with the ImageJ Chemotaxis Plugin (Fig. 3 A and Video 3).

In CIA, instead of extending elongated cylinder-like pseudopods, N-WASP–depleted cells displayed a threefold reduction in cell length/width ratio and small spiky protrusions (Fig. 3 B). However, dilution of the Matrigel with PBS (2.5 mg/ml Matrigel or 1.25 mg/ml Matrigel rather than the usual 5 mg/ml Matrigel) restored both migration velocity and directionality (Fig. 3 B and Video 4), which indicates that the Matrigel is providing a physical barrier to movement. In addition, the morphology of the knockdown cells in diluted Matrigel resembled the controls (longer pseudopodia and elongated shape; Fig. 3 B). Thus, we conclude that depletion of N-WASP in a 3D environment suppresses long pseudopod formation and invasion.

N-WASP is important for path generation during invasion in 3D matrix

During invasion, some cells become path-generating "leaders," which degrade matrices to lay down microtunnels for following

Published October 22, 2012

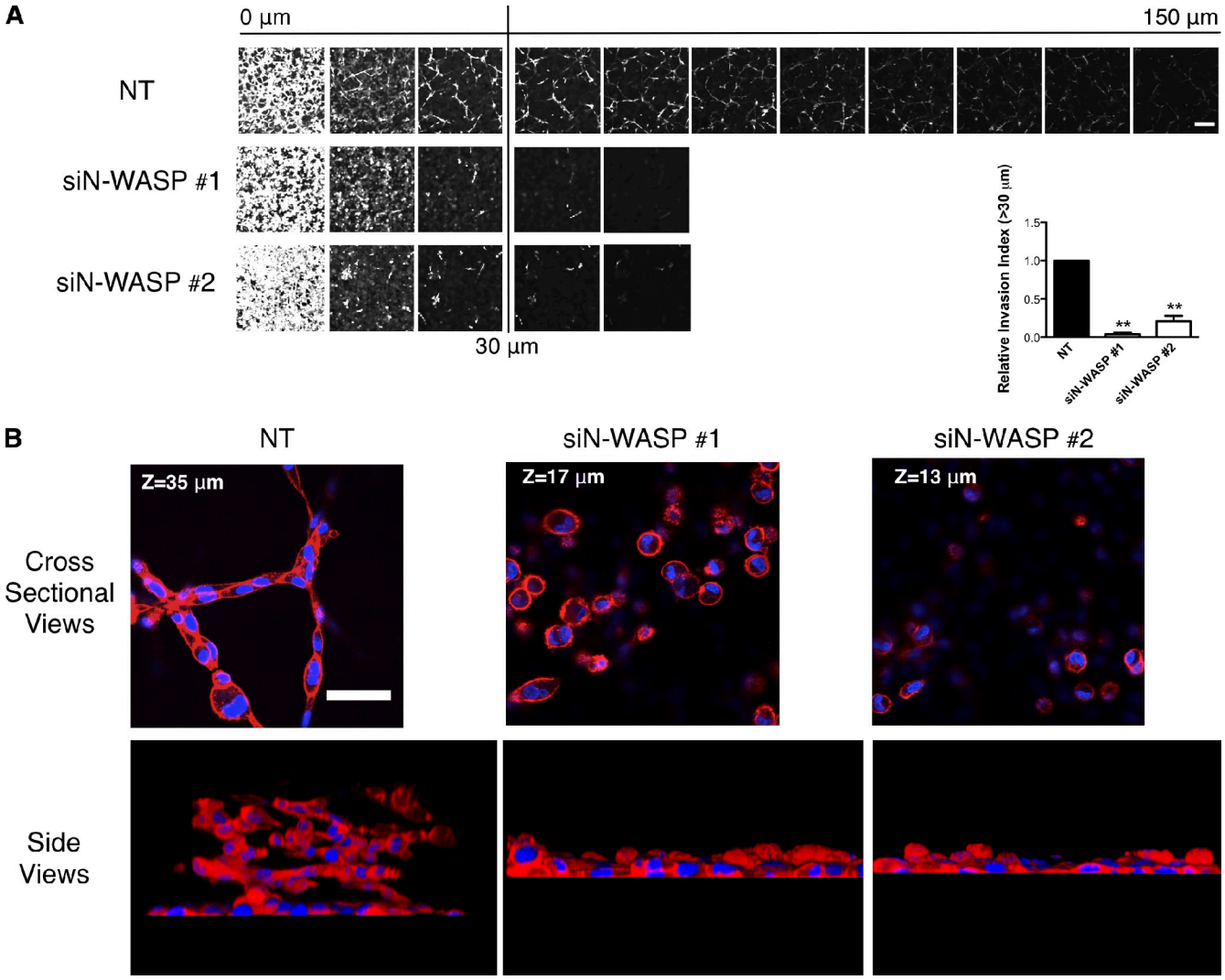

Figure 2. **N-WASP mediates leading cell collective invasion into 3D matrices.** (A) Cells that migrated into Matrigel plugs in an inverted invasion assay were stained with CalceinAM and visualized by confocal microscopy. Serial optical sections were captured at 15-µm intervals and presented as a sequence in which the individual optical sections are placed alongside one another, with increasing depth from left to right as indicated. The assays were quantified by measuring the fluorescence intensity of cells penetrating 30 µm and greater. 0 µm indicates cells that crawled through the filter but did not enter the gel. The invasion capacity was expressed as a percentage of the total fluorescence intensity of all cells within the plug, as shown in the bar graph. At least three independent experiments were performed. All error bars indicate means ± SD; **, $P < 0.01$ by a *t* test. Bar, 100 µm. (B) Matrigel plugs containing cells from inverted invasion assays were fixed and stained with phalloidin (actin, red) and DAPI (DNA, blue). Strands of invading cells are shown in cross section and side views. Bar, 50 µm.

cells (Fisher et al., 2009; Scott et al., 2010). If the function of N-WASP was to be limiting for matrix remodeling, but not for movement or chemotaxis in 3D matrix, nor for joining together with other cells in an invasion stream, we would expect that addition of normal cells together with N-WASP–depleted cells might rescue the invasion defect caused by N-WASP depletion. Indeed, in both the CIA (Fig. 4 A) and the inverted invasion assay (Fig. 4 C), addition of normal (GFP-expressing, NT siRNA–transfected) green cells to red N-WASP knockdown (RFP-expressing, siN-WASP–transfected) cells significantly rescued the invasion defect of the N-WASP knockdown cells (Fig. 4, A and C). In a mixed population of GFP- and RFP-expressing NT cells, the green and red cells showed a roughly 50:50 ratio as leading or following cells, as the white arrowheads indicate in Fig. 4 (A, left, and B). However, in ∼90% of invasion strands, GFP-expressing NT cells are the path-generating "leader" cells when mixed with RFP-siN-WASP cells (Fig. 4 A, right, white arrowheads; and Fig. 4 B). N-WASP–depleted (red) cells rarely assumed the position as a leader in the invasion front, and they were less elongated than the NT cells (Fig. 4, A and C). Consistently, in the inverted invasion assay, RFP-expressing siN-WASP cells displayed impaired invasion, but invaded nearly normally when mixed with GFP-NT cells (Fig. 4 C). Therefore, we conclude that N-WASP–depleted cells are unlikely to have a defect in movement in 3D matrix, but they are impaired in the formation of elongated pseudopodia and path generation.

N-WASP knockdown cells are defective in matrix degradation by MT1-MMP

To directly address the possibility that N-WASP–depleted cells were defective in matrix remodeling, we explored their ability to remodel uncrosslinked collagen (Sabeh et al., 2004; Wolf

Published October 22, 2012

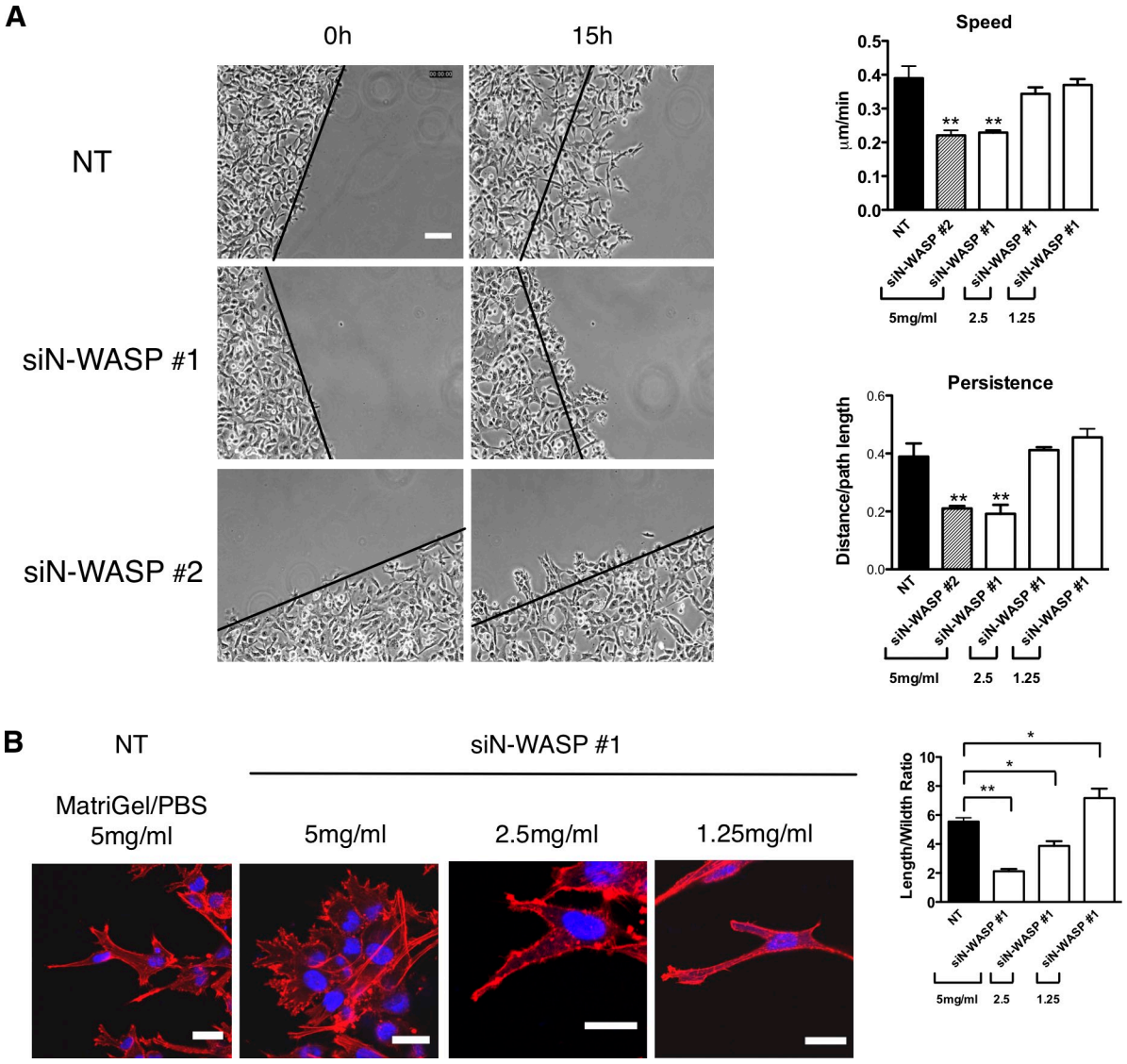

Figure 3. **N-WASP is required for extension of elongated matrix degrading pseudopods and propulsion through dense matrix.** (A) MDA-MB-231 cells treated with siRNA NT and N-WASP invading under Matrigel (photos show 5 mg/ml Matrigel, bar graphs show concentrations as indicated) in a CIA. Black lines indicate the start of the cell front at t = 0 h. Cell migration speed and persistence in CIA are shown in the bar graph. Persistence is obtained by using the Euclidean distance divided by the total distance between the start and end points of cell movement. At least three independent experiments were performed and quantified. Error bars indicate means ± SD; **, P < 0.01 by *t* test. Bar, 100 μm. (B) Cells invading in CIA were fixed and stained with phalloidin (actin, red) and DAPI (DNA, blue) for confocal imaging. The length of actin pseudopods and the ratio of cell length/width in CIA are shown in the bar graph. Error bars indicate means ± SD; **, P < 0.01; *, P < 0.05 by *t* test. At least 30 cells were analyzed in three independent experiments. Bars, 20 μm.

et al., 2007) and native cross-linked BMs (Hotary et al., 2006). When NT control cells were plated onto thin uncrosslinked collagen matrix, they rapidly degraded large areas of matrix underneath the cell (Fig. 5 A; Sabeh et al., 2004). However, knockdown of MT1-MMP or N-WASP nearly completely prevented this remodeling (Fig. 5 A; Sabeh et al., 2004). In a more quantifiable assay, where the cells were embedded in a collagen matrix containing DQ collagen (Wolf et al., 2007), the amount of degradation of DQ collagen was reduced by 40–50% upon inhibition or knockdown of MT1-MMP or N-WASP (Fig. 5 B). We next analyzed the ability of cells to degrade native peritoneal BM as described previously (Hotary et al., 2006). This isolated BM appears as two layers of continuous and organized sheets of type IV collagen- and laminin-rich ECM flanked by a layer of stroma. MDA-MB-231 cells transfected with a NT siRNA were able to degrade BM collagen IV efficiently within the 3-d culture period. However, N-WASP–depleted cells left the BM collagen IV relatively unscathed (Fig. 5 C). Quantification of the remaining collagen IV staining intensity shows a 50% reduction of matrix remodeling by siN-WASP cells compared with control (Fig. 5 D). Likewise, siRNA depletion of MT1-MMP or addition of 5 μM GM6001 significantly blocked the ability of MDA-MB-231 cells to degrade and remodel the BM collagen IV as described previously (Fig. 5, C and D; Kowalski et al., 2005; Chun et al., 2006). Collectively, these data provide clear and direct evidence that N-WASP has a role in matrix degradation and contributes to the breakdown of physiological BMs such as would be encountered in a tumor environment.

Published October 22, 2012

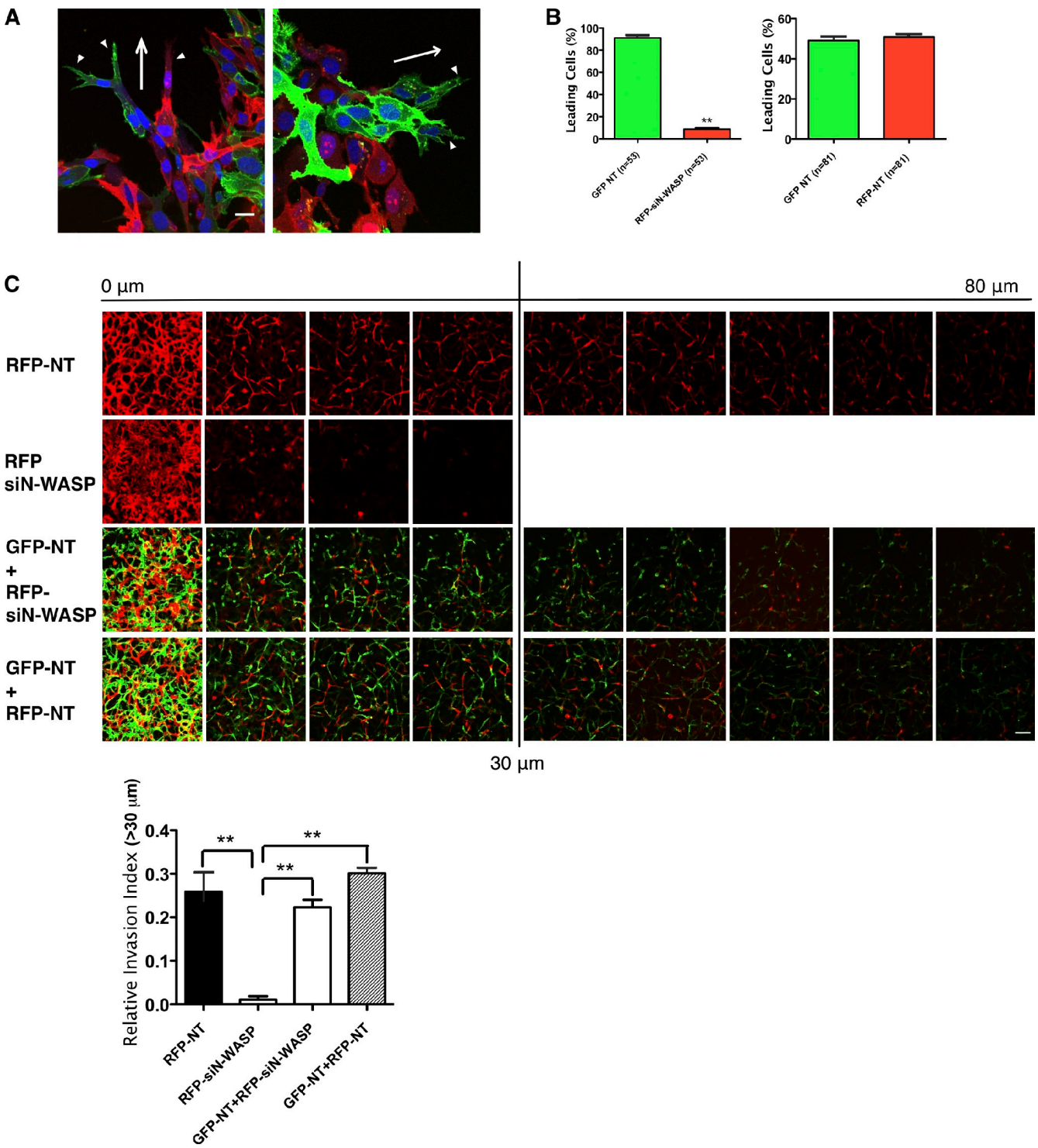

Figure 4. **N-WASP is required for path generation during invasion.** (A) Equal numbers of RFP-expressing cells transfected with either NT or N-WASP siRNA (red) were mixed with GFP-labeled cells treated with NT siRNA (green) in CIA. Cells were fixed and stained for DNA (blue) to show path-generating and following cells in the invading strands. Arrowheads indicate leading cells of invasive cell strands. Arrows indicate the direction to the wound edge. At least three independent experiments were performed and quantified. Bar, 10 µm. (B) Bar graphs indicate the percentage of leading and total cells of GFP- and RFP-positive cells. Error bars indicate means ± SD; **, $P < 0.01$ by *t* test. (C) A similar setup was used as in A, except that NT or N-WASP siRNA RFP-expressing cells alone were seeded for inverted invasion assay. Serial optical sections were captured at 10-µm intervals and presented as a sequence in which the individual optical sections are placed alongside one another with increasing depth from left to right as indicated. Images at 0 µm indicate cells that came though the filter but did not enter the gel. Invasion capacity was expressed as a percentage of the total fluorescence intensity of all cells invading beyond 30 µm within the plug as shown in the bar graph. At least three independent experiments were performed and quantified. Bar, 100 µm.

Published October 22, 2012

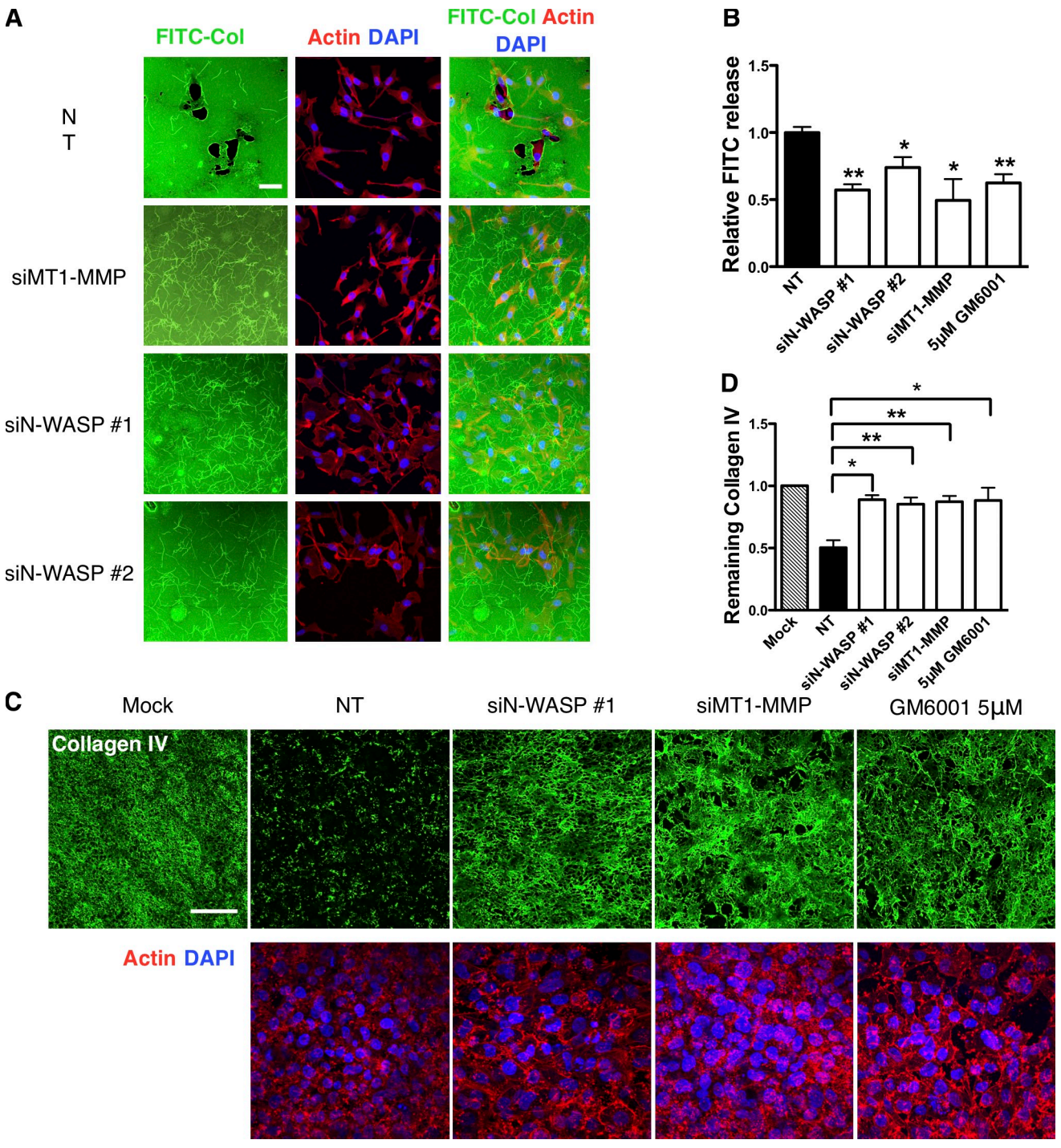

Figure 5. **N-WASP is crucial for pericellular collagenolysis in vitro and on native BMs.** (A) Immunofluorescence images of cells on FITC-conjugated type-I collagen film (green). Cells were labeled for filamentous actin (red, phalloidin) and DNA (blue, DAPI). Bar, 50 µm. (B) Quantification of FITC fluorescence release after incubating cells with DQ collagen matrix from three independent experiments. (C) MDA-MB-231 cells were cultured atop of mouse peritoneal BM for 3 d and then fixed and stained for collagen IV (green), actin (phalloidin, red), and DNA (DAPI, blue). The cells remodel and degrade BM, and the remaining collagen IV is shown by antibody staining (green). Bar, 100 µm. (D) The total fluorescence intensity of remaining collagen IV is represented in the bar graph. At least three independent experiments were performed and quantified. Error bars indicate means ± SD; **, $P < 0.01$; *, $P < 0.05$ by *t* test.

N-WASP drives invasive pseudopods into which MT1-MMP traffics from Rab7-positive late endosomes (LEs)

Because loss of N-WASP inhibited MT1-MMP dependent matrix degradation, we hypothesized that actin-rich regions of invasive pseudopods might be sites of MT1-MMP trafficking (Frittoli et al., 2011). To first address whether N-WASP played a direct role in MT1-MMP protein levels, internalization, or recycling, we measured total and surface levels of MT1-MMP, rates of internalization, and recycling, and found no effect of N-WASP depletion (Fig. S2, A–C). We next hypothesized that N-WASP likely has a more indirect role in trafficking and may

Published October 22, 2012

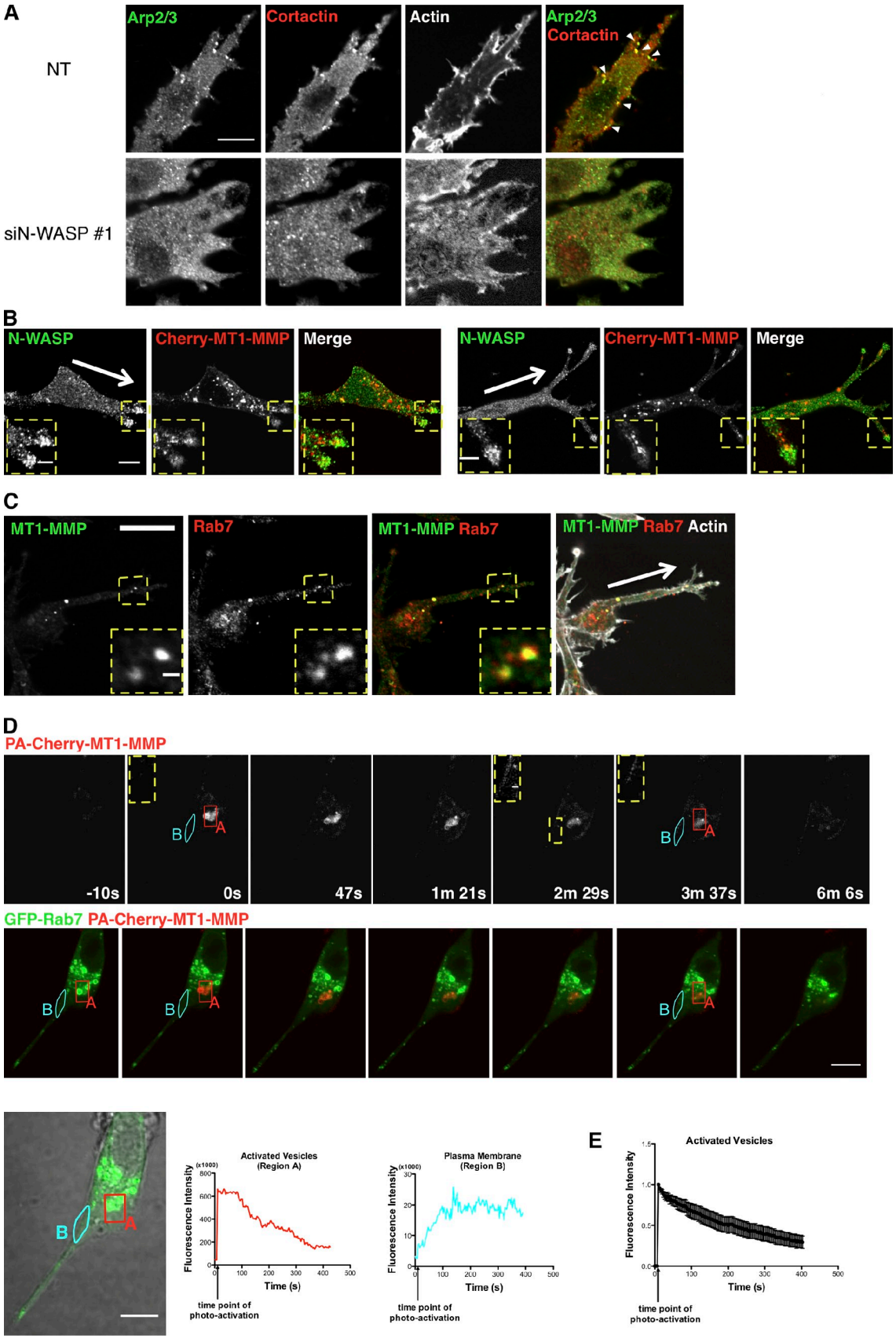

Figure 6. **MT1-MMP traffics from a late endosomal compartment to the plasma membrane and associates with N-WASP.** (A) NT and N-WASP knockdown cells invading in CIA were fixed and stained with anti-Arp2/3 and cortactin to reveal actin-rich puncta (arrowheads) in NT cells (top). (B) Immunofluorescence images of invading cells expressing mCherry-MT1-MMP (red) and staining for endogenous N-WASP (green) in CIA, with arrows pointing toward the wound edge. Bar, 10 µm. Enlarged images show details (boxed regions) of the invasive pseudopods containing MT1-MMP vesicles and N-WASP puncta.

Published October 22, 2012

promote MT1-MMP to preferentially traffic into invasive pseudopodia, and to be stabilized at sites of invasive matrix remodeling. The leading pseudopods of invading NT cells displayed numerous N-WASP–dependent puncta rich in cortactin, actin, N-WASP, and Arp2/3 complex, and also showed degradation of nearby surrounding matrix (Fig. 6 A; Yu and Machesky, 2012). Notably, these puncta, which contacted the Matrigel, also contained vinculin (82%, n = 17 cells) and focal adhesion kinase (74%, n = 12 cells; Fig. S3). But as previously reported (Yu and Machesky, 2012), cells also displayed some puncta at the glass bottom surface that lacked N-WASP but were rich in vinculin and FAK, which we assume were focal adhesion structures (Fig. S3). MT1-MMP also partially colocalized with N-WASP in the matrix contacting cytoskeletal puncta (Yu and Machesky, 2012), and we frequently observed vesicles containing MT1-MMP directly trafficking into invasive pseudopods in CIA. These vesicles often localized adjacent to the puncta rich in N-WASP or overlapped with the N-WASP–rich invadopodia-like structures (Fig. 6 B). Thus, we conclude that the majority of N-WASP– and Arp2/3 complex–rich puncta that we observed in invasive pseudopodia in the CIA also contained FAK and vinculin, and were most likely hybrid invadopodia/focal adhesion structures formed by a coalescence of these structures, which are more distinct in 2D (Wang and McNiven, 2012).

Additionally, a significant portion of MT1-MMP could be found in intracellular vesicles. Co-labeling with endocytic markers revealed that the majority of this vesicular MT1-MMP was in a Rab7- and CD151-positive LE compartment, which is in agreement with previous studies showing localization of MT1-MMP to a VAMP7-positive compartment (Fig. 6 C and Fig. S4 A; Steffen et al., 2008). We also saw partial colocalization with Rab8, in agreement with previous studies (unpublished data; Bravo-Cordero et al., 2007). Using live-cell video microscopy, we found that MT1-MMP cotrafficked bi-directionally in invasive pseudopods together with Rab7 and CD151, but not the early endosome marker Rab4 (Fig. S4 A and Video 5). The trafficking into invasive pseudopods was affected by loss of N-WASP, as >70% of NT cells contained five or more MT1-MMP vesicles within the pseudopods (n = 23; Fig. S4 B), whereas N-WASP–depleted cells (>90%) had fewer MT1-MMP vesicles within these structures (n = 41; Fig. S4 B). Because only a few studies have shown trafficking back to the plasma membrane from the LE compartment (Zech et al., 2011; Dozynkiewicz et al., 2012), we tested whether the LE vesicles that were rich in MT1-MMP were capable of delivering MT1-MMP to the plasma membrane, or were rather only involved in its degradation. We constructed a photoactivatable mCherry-tagged MT1-MMP (PA-mCherry-MT1-MMP) to follow MT1-MMP dynamics in live cells during the invasion process. We used GFP-Rab7 as a marker for the LE compartment, and when we photoactivated Rab7-positive vesicles, we initially observed a flash of PA-mCherry-MT1-MMP on this compartment, which subsequently redistributed to the nearby plasma membrane (Fig. 6 D and Video 6). We measured the time course over which photoactivated PA-mCherry-MT1-MMP fluorescence was lost from Rab7 vesicles, and found that this corresponded to the subsequent increase of fluorescence on the nearby plasma membrane (Fig. 6 D, graphs). The fluorescence intensity of the activated vesicles was recorded in multiple cells (n = 10) and plotted in Fig. 6 E, where we can see clearly that the PA-mCherry-MT1-MMP exits quickly from the Rab7 compartments upon activation. Thus, a proportion of the MT1-MMP in the Rab7-positive LE vesicles that we observe in invading cells is in transit to the plasma membrane from this compartment. We were not able to measure traffic specifically into the tips of invasive pseudopodia (rather than generally to the nearby plasma membrane) because the signal from PA-mCherry-MT1-MMP was not bright enough.

A link formed between MT1-MMP and actin contributes to delivery and stabilization of MT1-MMP at the plasma membrane of invasive pseudopods

To determine whether N-WASP contributed to entrapment of MT1-MMP at pseudopod tips, we investigated the dynamic behavior of MT1-MMP within invasive structures. We hypothesized that the cytoplasmic tail of MT1-MMP might connect to the actin cytoskeleton and thus be tethered in actin networks generated by N-WASP in invasive pseudopodia. We performed photobleaching experiments to test whether MT1-MMP at the plasma membrane in invasive pseudopodia had reduced mobility compared with MT1-MMP in other regions of the cell surface (e.g., at the plasma membrane adjacent to the nucleus). Photobleaching of mCherry-MT1-MMP in invading pseudopod tips in matrix of control NT-transfected cells revealed a very low, 5%, mobile fraction, indicating that nearly 95% of the enzyme doesn't exchange with the neighboring plasma membrane and isn't replaced by vesicular trafficking within the time frame of our experiment (1 min; Fig. 7, A and B). Indeed, the photoactivation experiments in Fig. 6 indicate that the delivery of PA-mCherry-MT1-MMP to the plasma membrane occurs over a period of several minutes, not seconds. In contrast, 22 ± 4% of mCherry-MT1-MMP on the cell body

(C) Endogenous MT1-MMP vesicles colocalize with endogenous Rab7. Arrows point toward the wound edge. Bar, 20 µm. Inset images show the LE/LY vesicles containing both MT1-MMP and Rab7 (enlarged views of the boxed regions). (D) MDA-MB-231 cells expressing PA mCherry-MT1-MMP (red) and GFP-Rab7 (green) were plated in CIA and imaged by confocal microscopy. Photo-activation was achieved with a 405-nm laser aimed at a small area (region A) containing GFP-Rab7–positive vesicles (also MT1-MMP), marked by the red box. Images were then captured at 3.2 s per frame over a period of >6 min (Video 6). Single-section confocal images of activated mCherry-MT1-MMP and images of merged mCherry-MT1-MMP and GFP-Rab7 at certain time points were presented. The insets are enlarged images showing increased signals of photoactivated mCherry-MT1-MMP on the plasma membrane area near the activated vesicles. The enlarged area is indicated with the yellow dotted line at time point "2 m 29 s." The same areas are shown in time points "0 s" and "3 m 37 s." The integrated fluorescence intensity of activated region A (red) and a area of plasma membrane (region B) near the activated vesicles (light blue) was quantified for each frame of Video 6, and the values are plotted against elapsed time. (E) Quantification of fluorescence intensity of activated mCherry-MT1-MMP vesicles in multiple experiments indicated the exit rate of photoactivated mCherry-MT1-MMP from the Rab7-positive compartment (n = 10). Error bars indicate means ± SEM. Bars: (A) 20 µm; (B) 5 µm; (C) 1 µm; (D) 10 µm; (B–D, insets) 1 µm.

Published October 22, 2012

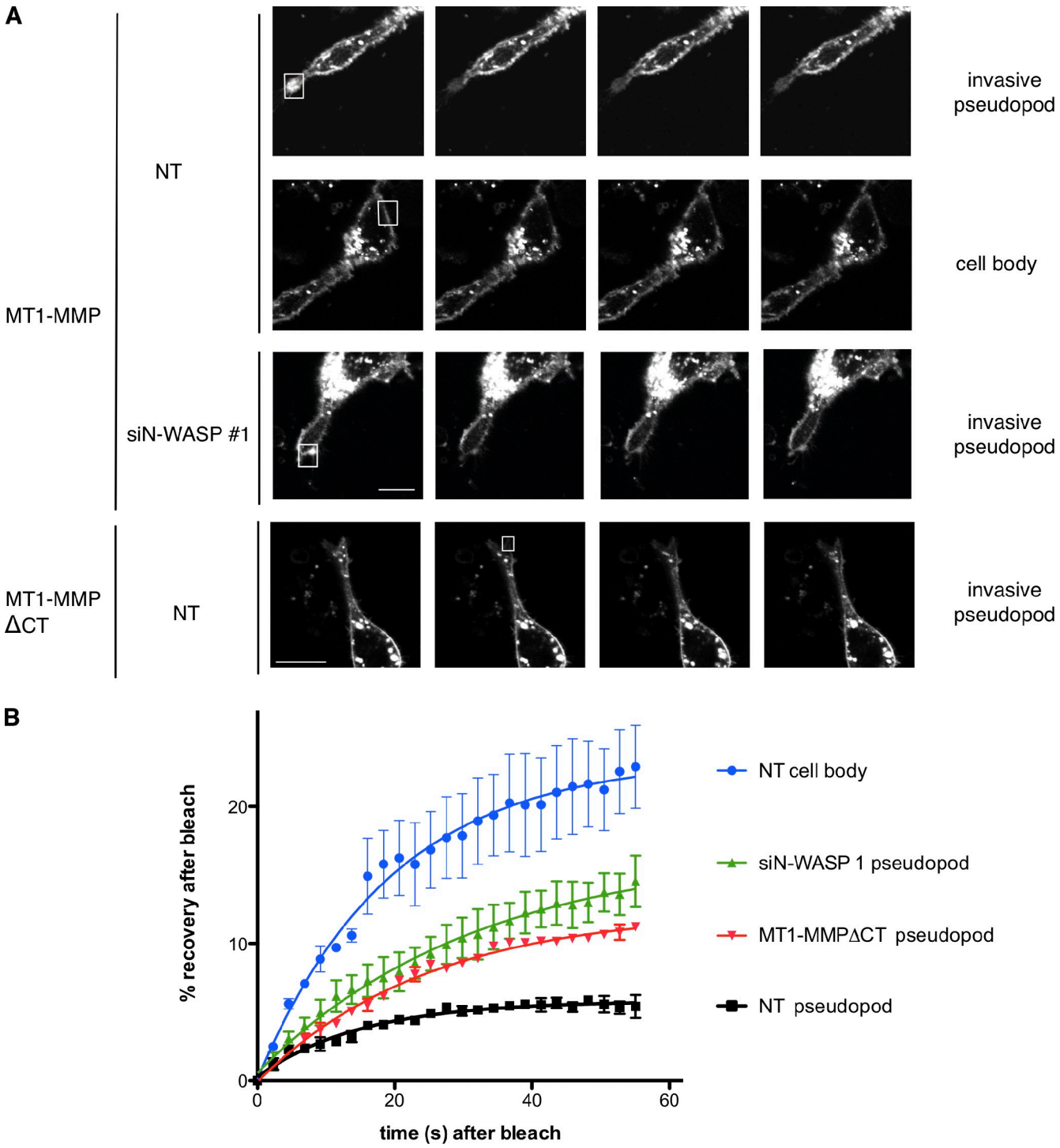

Figure 7. **MT1-MMP is tethered to invasive pseudopods in an N-WASP–dependent manner.** (A) MDA-MB-231 were transfected with mCherry-MT1-MMP or mCherry-MT1-MMPΔCT, as indicated, as well as GFP-actin, and subjected to CIA. Selected actin-rich areas in invasive pseudopods or areas of the cell body (boxes shown in A and quantified in B) of NT or N-WASP–depleted cells as indicated were photobleached using a 405-nm laser, and recovery of mCherry-MT1-MMP fluorescence was recorded for 58 s. (B) Quantification of fluorescence recovery was of at least 30 cells in three independent experiments. Error bars indicate means ± SEM. Bar, 10 µm.

plasma membrane is mobile and recovers quickly ($t_{1/2}$ = ~15 s) after bleaching (Fig. 7, A and B). Depletion of N-WASP, which causes loss of actin-rich hotspots and blunting of pseudopods, led to an increase of the mobile MT1-MMP fraction in pseudopods to 15 ± 3% compared with NT-transfected cells (Fig.7, A and B). Thus we conclude that N-WASP is important for stabilizing MT1-MMP in invasive pseudopods, possibly via assembly of dense actin meshworks in these structures. These invasive pseudopods not only need to generate mechanical force to push and pull against the matrix, but also direct and sustain MT1-MMP–based degradation. To demonstrate such an inside-out mechanism of MT1-MMP capture, we analyzed

Published October 22, 2012

the mobile fraction of MT1-MMP-ΔCT (MT1-MMP without its cytoplasmic domain), which is ineffective at rescuing (Uekita et al., 2001). We found that MT1-MMP-ΔCT has an increased mobile fraction of ∼12% compared with around 5% for full-length mCherry-MT1-MMP in invasive pseudopods of NT cells (Fig. 7, A and B). To further explore the role of actin networks in stabilization of MT1-MMP in invasive pseudopodia, we treated cells either with siRNA against Arp2 to block Arp2/3 complex–mediated actin assembly or with 2 µM Latrunculin A to partially depolymerize filamentous actin (Fig. S5, C and D). In both cases, mCherry-MT1-MMP became more mobile in the plasma membrane of remaining pseudopodia in Matrigel. The observation that GFP-actin exchanged much faster in LatA-treated cells (Fig. S5 E) verified that the LatA mobilized the actin network as expected. Thus, branched actin networks formed by Arp2/3 complex and filamentous actin stabilize MT1-MMP in pseudopods.

Because it has been recently highlighted that some receptors can be sorted on membranes putatively via links with actin filament networks (Puthenveedu et al., 2010), we hypothesized that MT1-MMP might directly interact with F-actin, and we tested whether binding to F-actin could determine MT1-MMP mobility on the plasma membrane. We first performed biochemical experiments to see if F-actin could deplete soluble peptides corresponding to the MT1-MMP tail from the supernatants in a centrifugation experiment. MT1-MMP wild-type (WT) cytoplasmic tail or peptides of cytoplasmic tail where the LLY motif, previously found to be important for MT1-MMP to confer invasiveness (Uekita et al., 2001), was exchanged to AAA (labeled as LLY/A in the figures) were incubated with F-actin purified from rabbit muscle. Actin filaments readily depleted MT1-MMP cytoplasmic tail peptides but not mutant LLY/A peptides from the supernatants (Fig. 8, A–D). We further explored the specificity of the interaction of the MT1-MMP tail peptide with actin filaments using a fluorescence anisotropy experiment (see Materials and methods), where fluorescently labeled short actin filaments were incubated with soluble peptides corresponding to either WT or mutant LLY/A MT1-MMP tail or a scrambled peptide of the MT1-MMP tail that preserves the overall positive charge of the WT peptide (Fig. 8 E). Fluorescence anisotropy also revealed specific binding to the WT with a K_d = 43 ± 6.5 µM, but not the mutant peptides, which suggests that the LLY motif was important for the interaction between MT1-MMP and actin filaments.

To further investigate whether the interaction between F-actin and MT1-MMP could also be observed in living cells, we transfected MDA-MB-231 cells with MT1-MMP-GFP and Lifeact-TagRFP to measure fluorescence-lifetime imaging microscopy (FLIM) in invasive pseudopods. Cells transfected only with the MT1-MMP-GFP donor showed an average fluorescence lifetime of 2.4 ns at the tips of invasive pseudopods. In contrast, cells containing both the MT1-MMP-GFP donor and Lifeact-TagRFP as an acceptor showed a significant shift of 150 ps in the fluorescence lifetime of MT1-MMP-GFP to 2.25 ns (Fig. 8 F), thus confirming that the cytoplasmic tail of MT1-MMP has the ability to interact with actin in invasive pseudopods. Mutation of the LLY motif to AAA also abolished the FLIM signal (Fig. 8 F) and increased the motility of the protease in invasive pseudopods in the FRAP experiment (Fig. S5, F and G), thus demonstrating that this interaction is dependent on this motif in cells (Fig. 8 F). We also further investigated the ability of MT1-MMP with the LLY/AAA mutation to drive invadopodia assembly (Fig. 8 G). Although WT MT1-MMP could rescue cells depleted of MT1-MMP by siRNA, the LLY/A mutant MT1-MMP was unable to rescue. Likewise, LLY/A mutant MT1-MMP was unable to rescue the reduction of invasion observed in the circular Matrigel invasion assay (Fig. S5, A and B; Yu and Machesky, 2012).

To investigate whether F-actin binding of MT1-MMP in invasive pseudopods is necessary and sufficient for a cell to increase invasion, we replaced the cytoplasmic tail of MT1-MMP with the actin-binding domain of ezrin (aa 552-585; MT1-MMP$^{EZ\text{-}ABD}$) and compared the invasion and invadopodia formation with cells transfected with either MT1-MMP or MT1-MMP ΔCT. The mCherry-MT1-MMP$^{EZ\text{-}ABD}$ construct shows similar distribution to WT MT1-MMP, with a slightly increased intracellular pool (Fig. 8 G). We also compared the mobility of WT mCherry-MT1-MMP and mCherry-MT1-MMP$^{EZ\text{-}ABD}$ in invasive pseudopods using FRAP and did not find any significant difference in the mobility of these proteins (Fig. S5 G). For invadopodia degradation assays, we first depleted endogenous MT1-MMP using siRNA against the 5′ untranslated region in MDA-MB-231 cells and then transfected WT and mutant MT1-MMP into them. Consistently, full-length MT1-MMP dramatically increased MDA-MB-231 cell degradation on a thin layer of gelatin (Fig. 8 G), which agrees with previous work (Nakahara et al., 1997). The actin-binding domain mutant of MT1-MMP (mCherry-MT1-MMP$^{EZ\text{-}ABD}$) was able to promote matrix degradation in a similar fashion (Fig. 8 G). In contrast, MT1-MMP-ΔCT– and MT1-MMP-LLY/A–expressing cells barely show any gelatin degradation (Fig. 8 G). Collectively, these observations indicate that the capacity of the cytoplasmic tail to recruit MT1-MMP to the subplasmalemmal actin cytoskeleton facilitates the concentration of MT1-MMP at actin-enriched sites to confer effective matrix degradation during invasion.

Discussion

N-WASP had been previously described as a component of invadopodia and their precursor structures, but the molecular mechanism of how N-WASP drives invasion hasn't been studied in 3D (Lorenz et al., 2004; Yamaguchi et al., 2005). N-WASP has recently been implicated in breast cancer metastasis in a mouse model (Gligorijevic et al., 2012). Here we provide a direct mechanism by which N-WASP drives invasive migration via the generation of elongated pseudopods that allow cells to remodel matrix and generate force to crawl through it. Although N-WASP and its hematopoietic homologue WASP have been implicated in chemotaxis on a 2D surface (Isaac et al., 2010), we did not find any evidence of significantly reduced noninvasive migration of N-WASP–depleted cells through filters in 3D (Fig. 2). Furthermore, when we diluted Matrigel in the CIA (Fig. 3), this restored the migration speed of

Published October 22, 2012

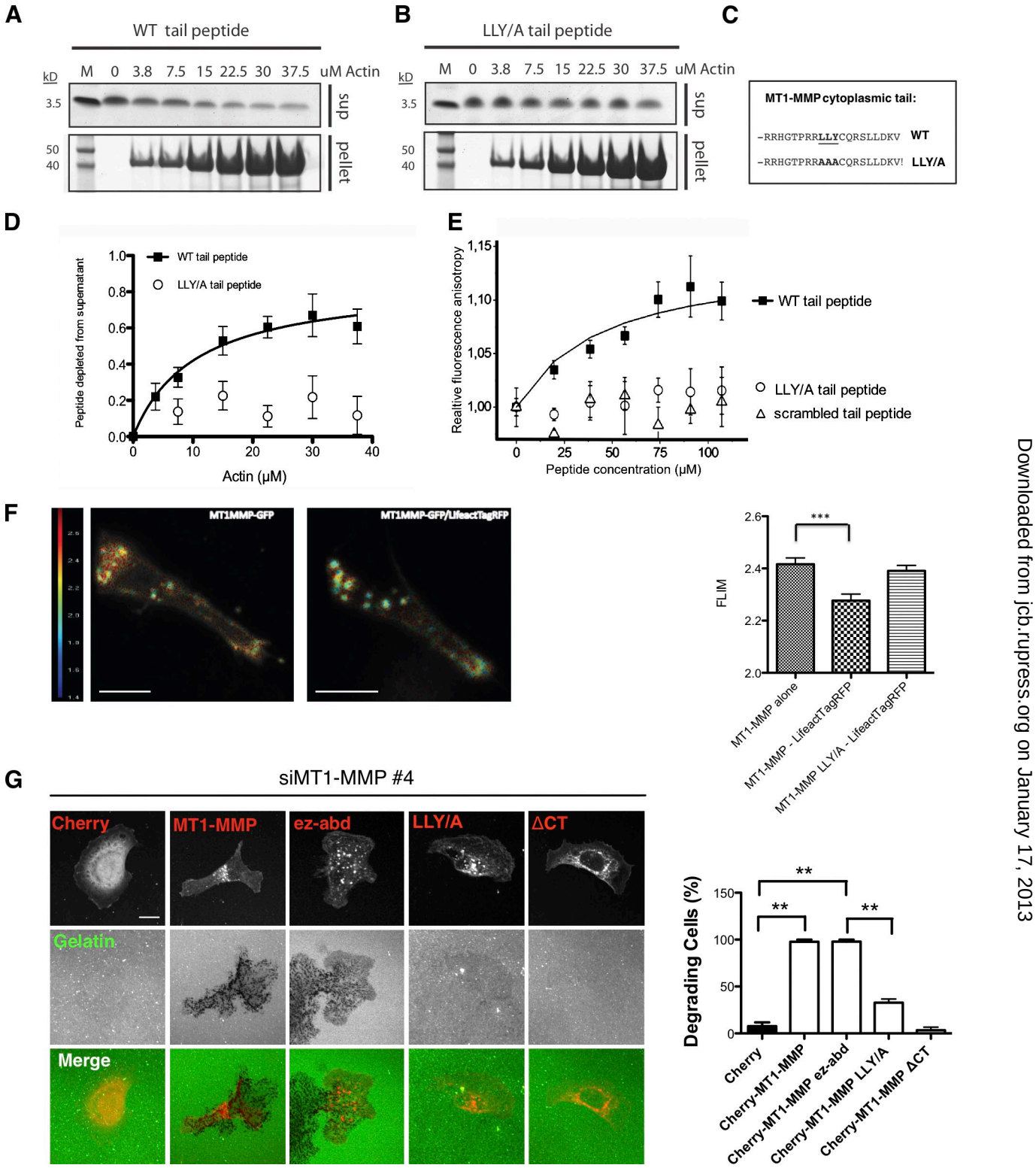

Figure 8. **MT1-MMP actin binding is both necessary and sufficient to induce matrix degradation.** (A–C) 25 μM final concentration of WT (A and C) cytoplasmic MT1-MMP tail peptide or LLY/AAA (B and C) cytoplasmic MT1-MMP tail peptide were tested for their ability to bind to increasing amounts of F-actin in an in vitro binding assay. Actin was allowed to polymerize for 1 h. After centrifugation, 10% of total F-actin pellets (p) and supernatants (s) were run on a 4–12% NuPAGE gel using MES running buffer. (D) Quantification of Coomassie gel densitometry of peptide bands. $n = 5$. (E) Relative steady-state fluorescence anisotropy was measured between IAEDANS-labeled filamentous actin (2 μM) and increasing concentration of MT1 peptide constructs: MT1_tail (closed squares), MT1tail_L1Y/A (open circles), and MT1tail_scrambled (open triangles). The binding curve was fitted with the equation given in the Materials and methods section ("Steady-state fluorescence anisotropy experiments"), and the K_d value was calculated (see Results). (F) MDA-MB-231 cells were transfected with MT1-MMP-GFP alone or together with Lifeact-TagRFP and invaded in Matrigel in CIA. Cells were imaged using a spinning disc FLIM system. Fluorescence lifetime was measured in the pseudopod area and quantified from 30 cells in $n = 3$. Bar, 10 μm. (G) Immunofluorescence images of mCherry, mCherry-MT1-MMP, mCherry-MT1-MMPΔCT, and mCherry-MT1-MMP$^{EZ\text{-}ABD}$ expressing MDA-MB-231 MT-MMP knockdown cells (red) on

Published October 22, 2012

N-WASP–depleted cells to normal, which indicates that migration through Matrigel was not likely hindered by a loss of the ability of N-WASP–depleted cells to generate a gradient of the growth factor components found in Matrigel. Finally, when we mixed N-WASP–depleted cells 50:50 with normal NT controls, this rescued invasion into thick gels, and N-WASP–depleted cells rarely participated as "leader cells" in the invasion chains (Fig. 4). Thus, we conclude that N-WASP contributes to the formation of elongated protrusions rich in actin cytoskeletal components (F-actin, cortactin, and Arp2/3 complex), and that these protrusions are required to overcome the physical barrier to cell translocation provided by ECM.

The main morphological defects of N-WASP–depleted cells migrating in 3D included blunted pseudopods, loss of actin-rich punctae, and reduced numbers of MT1-MMP vesicles in leading pseudopodia. MT1-MMP has previously been implicated as a Rab8 vesicle cargo (Bravo-Cordero et al., 2007). Although we saw overlap of MT1-MMP with the Rab8 compartment, the overwhelming majority of MT1-MMP vesicular structures that we saw were Rab7 positive. This agrees with a previous study also showing colocalization of MT1-MMP with a VAMP7-positive compartment (Steffen et al., 2008). Although it may seem surprising that MT1-MMP largely recycles from a Rab7-positive LE, it is becoming increasingly apparent that invasive cancer cells recycle several receptors, including integrins, from this compartment. We recently demonstrated that α5β1 integrin traffics to the plasma membrane from a Rab7- and WASH-positive compartment to promote invasion (Zech et al., 2011), that Rab25 and CLIC3 promote the recycling of α5β1 integrin from the late endosomal/lysosomal compartment, and that this has implications for pancreatic cancer metastasis and poor prognosis (Dozynkiewicz et al., 2012). It is thus emerging that trafficking from the LE compartment of both integrins and MT1-MMP is an important driver of invasive migration. Taking advantage of a PA-mCherry-MT1-MMP probe, we have shown that MT1-MMP traffics to the nearby plasma membrane from Rab7 containing LE/LY. Ideally, we would have liked to focus here on delivery to specific actin puncta in pseudopods, but the PA-mCherry-MT1-MMP probe was not bright enough to visualize specific delivery to pseudopod tips. Thus it remains for the future to determine how N-WASP affects polarized vesicle delivery into invasive pseudopods and whether these vesicles dock specifically at actin hotspots or whether the MT1-MMP is later captured at these sites.

N-WASP–depleted cells degraded quantitatively less collagen or native peritoneal BM than control cells in multiple assays (Fig. 5). Surprisingly though, N-WASP depletion did not affect the overall expression of MT1-MMP, its surface expression level, proteolytic processing, or the rate of internalization or recycling. Rather, depletion of N-WASP led to loss of prominent clustered actin-rich hotspots in invasive pseudopodia during 3D invasion and to increased mobility of the major collagenase MT1-MMP in the plasma membrane. Although MT1-MMP is generally localized in internal vesicles and on the plasma membrane, we could clearly see enrichment of MT1-MMP in actin hotspots (Fig. 6 B), and we observed trafficking of small mCherry-MT1-MMP vesicles into invasive pseudopods (Fig. S4). We were surprised by how relatively immobile MT1-MMP was in the plasma membrane of invading pseudopods, with only 5% exchanging within 1 min of photobleaching. But previous studies have already highlighted that receptor mobility in a 3D environment can be significantly different from what is observed in a 2D tissue culture models (Serrels et al., 2009). Depletion of N-WASP or loss of the MT1-MMP cytoplasmic tail increased the mobility of the receptor two- to threefold and caused a concomitant reduction of invasive migration and matrix remodeling capacity. We did not observe a direct interaction between N-WASP and MT1-MMP by coimmunoprecipitation (unpublished data), but rather we found that the cytoplasmic tail of MT1-MMP contained a filamentous actin-binding sequence that regulated MT1-MMP mobility in pseudopodia. Loss of this sequence ablated actin interaction and invasive matrix remodeling while increasing MT1-MMP mobility in the invasive pseudopod. Restoration using an actin-binding motif from ezrin rescued the stabilization of MT1-MMP and degradative capacity of cells.

Recently, a mechanism for recruitment of MT1-MMP to a new form of degradative focal adhesions has been proposed that is dependent on a p130Cas–FAK complex through interaction with the MT1-MMP cytoplasmic tail (Wang and McNiven, 2012). However, in this study, disruption of the MT1–MMP–p130Cas–FAK complex function solely impaired MT1-MMP–mediated degradation at focal adhesions, but not invadopodia, which suggests that a different machinery might be responsible for targeting MT1-MMP to invadopodia-like structures, at least in 2D. In contrast, other laboratories have reported p130Cas and FAK, as well as vinculin and paxillin, at invadopodia sites (Alexander et al., 2008; Branch et al., 2012), and shown that p130Cas and FAK are mechanosensitive proteins involved in invadopodia maturation and responsiveness to myosin-II activity. FAK has also been identified as a negative regulator of invadopodia in MTLn3 breast cancer cells (Chan et al., 2009), where focal adhesions and invadopodia may compete for the same tyrosine phosphorylated proteins. In our CIA, where cells contacted both Matrigel and a glass substratum, we observed that the majority of small puncta contacting matrix in invasive pseudopods also contained FAK and vinculin (Fig. S3). This suggests that in our 3D experimental conditions, hybrid structures form, which have elements of both focal adhesions and invadopodia. Clearly, various cell types have different requirements for vinculin, FAK, and p130Cas and invadopodia for invasion and invadopodia assembly. Evidence indicates that hybrid focal adhesion/invadopodia structures involving these molecules can drive invasive behavior in 3D and that sometimes seemingly contradicting results (Alexander et al., 2008; Chan et al., 2009; Wang and McNiven, 2012) about the role of focal adhesion molecules in invasion probably reflect the complexity of the system and the

Alexa Fluor 488–conjugated gelatin (green). The percentage of cells showing matrix degradation was quantified after 3 h incubation. At least 30 cells of each expressing construct were imaged for quantification from three independent experiments. Bar, 10 µm.

Published October 22, 2012

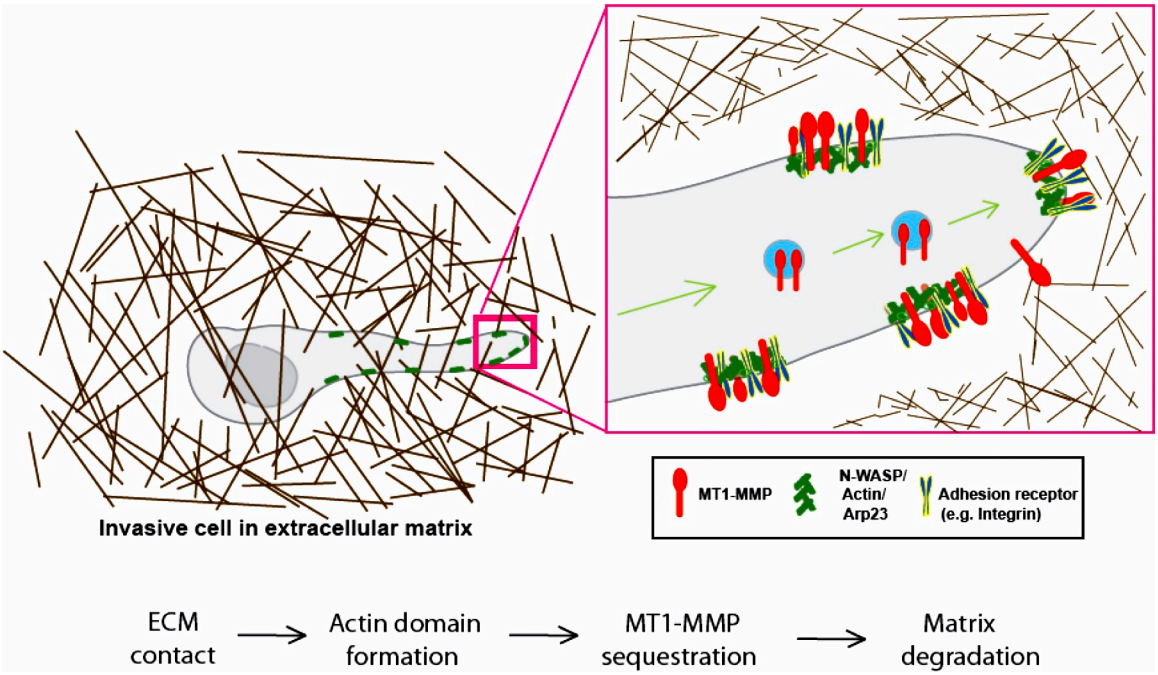

Figure 9. **Model of how N-WASP, MT1-MMP, and F-actin coordinate to function during cell invasion in 3D matrices.** N-WASP localizes to and concentrates at the front of invading pseudopods, where it polymerizes F-actin (green) to form actin-rich hotspots that also contain cortactin and Arp2/3 complex. MT1-MMP (red) was delivered via LE/lysosomal trafficking to the plasma membrane, where it is captured and anchored by F-actin. MT1-MMP becomes enriched at degradation sites by interacting with actin patches.

large number of factors that impact on whether a cell can migrate efficiently or degrade matrix.

The short cytoplasmic tail of MT1-MMP (20 aa) has previously been shown to directly interact with the µ2 subunit of the clathrin adaptor complex AP2 via a dileucine motif LL^{572}. However, interfering with internalization of MT1-MMP using aptamer peptides did not inhibit invasive migration (Wickramasinghe et al., 2010). Our data strongly suggest that N-WASP does not significantly regulate the overall levels or endocytic trafficking of MT1-MMP (Fig. S2) but rather controls the spatial organization and proper positioning of MT1-MMP with respect to active actin-based protrusions. We provide evidence that coupling to the actin cytoskeleton makes MT1-MMP more effective at degrading matrix at contact sites, and this is supported by previous observations of invadopodia-like structures forming specifically at places where invading cells encounter barriers to migration (Wolf et al., 2007; Wolf and Friedl, 2009). This is also supported by Hoshino et al. (2012), who used FRAP experiments and observed slower mobility of MT1-MMP at invadopodia than at other regions of the plasma membrane. We propose a model whereby N-WASP generates actin networks in invasive pseudopodia, where MT1-MMP is handed over from cargo vesicles (Fig. 9) to actin-rich regions of pseudopodia generated by N-WASP. Once MT1-MMP is resident in invading pseudopodia, it is then specifically stabilized by actin networks to make degradation more effective for coupling with invasion (Fig. 9).

Materials and methods

Cell culture and transfection

All reagents used for cell culture were purchased from Invitrogen unless otherwise indicated. MDA-MB-231 breast adenocarcinoma cells were obtained from the American Type Culture Collection and grown in complete DME supplemented with 10% FBS and 2 mM L-glutamine. Cells were grown in a humidified incubator with 5% CO_2 at 37°C. DNA plasmids and siRNA were transfected using the Amaxa "Nucleofector" system (Solution V, Program X-013; Lonza), according to the manufacturer's instructions.

Antibodies and reagents

We diluted antibodies 1:1,000 for Western blotting and 1:200 for immunofluorescence. Antibodies were obtained from the following sources: Altas (Sigma-Aldrich), rabbit polyclonal anti–N-WASP (HPA005750); Millipore, mouse monoclonal anti-cortactin (4F11), rabbit polyclonal anti-p34-Arc (ARPC2), and mouse monoclonal anti-MT1-MMP (MAB3328); BD, rabbit polyclonal anti-Rab7; Ambion, monoclonal mouse anti-GAPDH; Santa Cruz Biotechnology, Inc., polyclonal rabbit anti-EGFR; Invitrogen, rhodamine phalloidin, anti–mouse IgG, anti–rabbit IgG Alexa Fluor antibody, and DQ collagen; Jackson ImmunoResearch Laboratories, HRP–conjugated secondary antibodies; GenScript, >90% purity biotinylated MT1-MMP cytoplasmic tail peptides. The human issue microarray was obtained from Biomax (catalog no. Z7020004).

Immunoblotting

Cells processed for Western blotting were lysed in RIPA buffer (50 mM Tris-HCl, 150 mM NaCl, 1% NP-40, and 0.25% sodium deoxycholate) with protease inhibitor cocktail (Thermo Fisher Scientific). After SDS-PAGE and transfer to polyvinylidene fluoride membranes (GE Healthcare), ECL chemiluminescence detection kits (Thermo Fisher Scientific) were used to detect proteins of interest according to the manufacturer's instructions and with appropriate HRP-conjugated secondary antibody (1:10,000 dilution). Western blot images were recorded and processed using GeneSnap software and Bio-imaging system (Syngene). Western blots are representative of at least three repeats showing typical levels of knockdown. Quantification of Western blots was done using ImageJ to outline the bands on the blots and measure the pixel density.

Constructs and siRNAs

The plasmid containing mCherry-MT1-MMP was a gift from P. Chavrier (Institute Curie, Paris, France). GFP-Rab4 was a gift from G. Gould (University of Glasgow, Scotland, UK). GFP-Rab7 and GFP-CD151 were obtained from Addgene and GFP-LAMP1 was obtained from Origene. GFP-Lifeact and RFP-Lifeact were gifts from R. Wedlich-Soldner (AG Cellular Dynamics

Published October 22, 2012

and Cell Patterning, Max Planck Institute of Biochemistry, Martinsried, Germany; Riedl et al., 2008). The PA-mCherry vector was a gift from V. Verkhusha (Department of Anatomy and Structural Biology and Gruss-Lipper Biophotonics Center, Albert Einstein College of Medicine, New York, NY; Subach et al., 2009). mCherry was replaced with PA-mCherry in the previously described mCherry-MT1-MMP construct (Steffen et al., 2008). Primers to generate the MT1-MMPΔCT and ezrin actin-binding domain fusion constructs from MT1-MMP are 5′-CTTGCAGTCTTCTTCTTC-3′ and 5′-CTTGCAGTCTTCTTCATCCACAACGAGAAC-3′, respectively. N-WASP siRNA oligo #1 was from QIAGEN, the target sequence is 5′-CAGATACGACAGGGTATCCAA-3′; N-WASP siRNA oligo #2 was obtained from Thermo Fisher Scientific, the target sequence is 5′-TAGAGAGGGTGCTCAGCTAAA-3′. N-WASP shRNA was from Open Biosystems clone ID V2HS_244163. NT control siRNA and ON-TARGETplus SMARTpool siRNA targeting MT1-MMP were purchased from Thermo Fisher Scientific. Oligos targeting the noncoding sequence of MT1-MMP were obtained from QIAGEN, and the target sequences are MT1-MMP siRNA oligo #1, 5′-GACAGCGGTCTAGGAATTCAA-3′; and MT1-MMP siRNA oligo #4, 5′-CACAAGGACTTTGCCTCTGAA-3′.

Histochemistry staining and scoring of TMA

The weighted histoscore is calculated using the following formula: (0 × percentage of negative staining) + (1 × percentage of weak staining) + (2 × percentage of moderate staining) + (3 × percentage of strong staining). This gives a value between 0 and 300. This value represents the staining intensity of each core of TMA (Kirkegaard et al., 2006).

Confocal live cell imaging

MDA-MB-231 cells transfected with mCherry-MT1-MMP together with GFP-Lifeact, GFP-Rab7, GFP-CD151, GFP-LAMP1, or GFP-Rab4 were set up for CIA supplied with DME (supplemented with 10% FBS and 1% glutamine). Cells were imaged with an inverted confocal microscope (Fluoview FV1000; Olympus) equipped with a uPlan-SApochromat 60×/1.35 NA oil objective lens in an atmosphere of 5% CO_2 at 37°C. The images were collected with a photomultiplier tube (PMT) in place, using the acquisition software FV10-ASW1.7. The images were captured every 10 s for 30, 50, or 90 frames in multiple experiments. FRAP analysis of cells in CIA was performed using the same microscope with pixel resolution 512 × 512 and 2% power of 488 nm and 561 nm laser power. Effective photobleaching of mCherry was achieved using 70% of 405 nm laser power, 10 µs/pixel dwell time, and a 300-ms bleach time. Images were captured every 2 s for 30 frames.

Invasion assays

Inverted invasion assays were performed as described previously (Hennigan et al., 1994). In brief, Matrigel (BD) was diluted with PBS to 5 mg/ml and polymerized in transwell inserts (Corning) at 37°C for at least 1 h. Inserts were then inverted, and 5×10^4 cells were seeded directly onto the outside surface of the filter. For experiments with GFP- and RFP-expressing cells, RFP-labeled cells were depleted with N-WASP using siRNA oligos. 2.5×10^4 cells of each fluorescent cells were thoroughly mixed and applied to the filter. Serum-free medium was finally added to transwell inserts, and medium supplemented with 10% FBS and 25 ng/ml EGF was added atop the Matrigel. Invading cells were stained with Calcein-AM (Invitrogen) for 1 h at 72–96 h after seeding. Cells failing to cross the filter were removed with tissue, and confocal microscopy was used to visualize cells that crossed through the filter. Serial optical sections were captured at 10- or 15-µm intervals using an inverted confocal microscope (Fluoview FV1000) fitted with a uPlan-SApochromat 60×/1.35 NA oil objective lens. The confocal microscope was equipped with PMT, and the acquisition software was FV10-ASW1.7. The obtained images were analyzed and reconstructed with Volocity software. We measured the fluorescence intensity for each section using the ImageJ plugin Area Calculator. For experiments with GFP- and RFP-expressing cells, the fluorescence intensity of GFP and RFP channels were quantified and added up for each section to obtain the fluorescence intensity. Finally, the relative index of invasion was calculated as the fluorescence intensity of cells that had invaded beyond 30 µm versus the total fluorescence intensity of all cells captured in the sections imaged. At least three independent experiments were performed using duplicate samples. For immunofluorescence imaging, samples were fixed in 4% formaldehyde for 30 min, followed by washing and permeabilization with 0.1% Triton X-100 for 30 min. Samples were then washed and stained with rhodamine phalloidin and DAPI overnight at 4°C and subsequently washed three times with PBS.

Fluorescence resonance energy transfer detection by FLIM analysis

MD-MB-231 cells were prepared for CIA as mentioned but incubated in 20 mM Hepes-containing medium. Fluorescence resonance energy transfer was detected with a LIFA System (Lambert Instruments) on an inverted microscope (Eclipse TE 2000-U; Nikon) equipped with a Yokogawa CSU 22 confocal scanner unit and a modulated 60-mW 488-nm laser (Deepstar; Omicron) as a light source, which, in combination with the modulated intensifier from the LIFA system, allows measurement of fluorescence lifetimes using frequency domain. Lifetime images were acquired using the standard 488-nm filter set integrated in the spinning disk scan head. Standard halogen illumination in combination with filter blocks for GFP (470/40×, T495LP, 525/50M) or RFP (560/40×, 585LP, 632/60M) were used to check the samples for expression of the probes. Erythrosine was used as reference standard with a known lifetime of 0.086 ns. Donor (D) lifetime, τ, was analyzed using the FLIM software (version 1.2.1; Lambert Instruments).

Time-lapse microscopy with modified CIA

For the CIA method, "wounds" were created by placing a silicon self-stick cellular stopper (Thermo Fisher Scientific) in the center of a 35-mm glass bottom dish (Ibidi) before seeding 6×10^5 MDA-MB-231 cells. After 16 h, 5 mg/ml of Matrigel diluted in PBS was overlaid onto the "wounded" cell monolayer to create a matrix barrier against the cellular surface and allowed to polymerize for 2 h before adding growth medium on the top of the set Matrigel. The wounded monolayer, with overlaid Matrigel and DME (Invitrogen), supplemented with 10% FBS and 1% glutamine, was then imaged with a time-lapse microscope (TE 2000; Nikon) with a Plan-Fluor 10× objective lens (Nikon). The cells were incubated in a humidified atmosphere of 5% CO_2 at 37°C for 24 h or longer for real-time imaging with a charge-coupled device camera (CoolSnap HQ2; Photometrics) equipped with an PFS (Perfect Focus System) device before fixation and immunofluorescence. The imaged cells were tracked using ImageJ plugin Manual Tracking, and the tracking results were analyzed using the ImageJ plugin Chemotaxis Tool to calculate cell speed and persistence. Persistence was calculated as the ratio between the Euclidean distance and the total distance traveled, with a value of 1 equal to a cell traveling in a straight line. This quantification was done in least three independent experiments for each assay.

Type-I collagen film degradation assay

A collagen film assay was performed as described in a previous study, with modifications (Sabeh et al., 2004). In brief, 200 µl FITC conjugated type I collagen (Sigma-Aldrich) was distributed evenly on glass-bottom microwell dishes (14-mm microwell; MatTek) and allowed to dry for 2–3 h to form a uniform collagen film. 5×10^4 MDA-MB-231 cells were seeded to the collagen film and incubated for 48 h. Cells then were fixed and labeled with rhodamine phalloidin and DAPI (Molecular Probes). Images were captured with a confocal microscope (Fluoview FV1000) fitted with a uPlan-SApochromat 60×/1.35 NA oil objective lens. The confocal microscope was equipped with a PMT to capture images, and the acquisition software was FV10-ASW1.7.

Quantitative 3D collagen degradation assay

A 3D collagen degradation assay was performed as described previously, with modifications (Wolf and Friedl, 2009). In brief, CHL-1 cells treated with NT, N-WASP, MT1-MMP siRNA, or 5 µM GM6001 MMP inhibitor were embedded into collagen I lattices (BD) containing DQ-FITC–labeled type I collagen monomers (2%; Molecular Probes). After 40 h of culture, solid-phase collagen including cells was pelleted, and the supernatant containing released FITC-collagen fragments was analyzed spectrofluorimetrically (QuantaMasterTM 40 spectrofluorometer; Photon Technology International). The degradation of fibrillar collagen for each sample was calculated as fluorescence released from DQ-FITC–labeled type I collagen monomers subtracted by background fluorescence, which was calculated by pelleting nondigested cell-free collagen lattices. Quantification of degradation was done in at least three independent experiments in duplicate for each assay.

Quantification of cell length/width ratio

To measure cell length/width ratio (Fig. 3 B), at least 30 confocal images of cells stained with rhodamine phalloidin and DAPI were captured. To obtain the length of cells, we drew a line from rear point of the main cell body passing the center of nucleus to the tip of the longest pseudopod, which was defined as the cell length. For the cell width, we drew a line passing the center of the nucleus that crosses the widest point of cell main body. The ratio of length/width reflects cell morphology in CIA. This quantification was done in at least three independent experiments for each assay.

Invadopodia gelatin degradation assay

Invadopodia gelatin degradation assays were performed as described previously (Artym et al., 2006). In brief, coverslips were acid-washed and coated with 50 µg/ml poly-L-lysine for 15 min, washed with PBS, and cross-linked with 0.5% glutaraldehyde for 15 min. The coverslips were then inverted

Published October 22, 2012

on an 80-µl drop of 1 mg/ml Alexa Fluor 488–conjugated gelatin (Invitrogen) for 10 min. After washing with PBS, the coverslips were then quenched with 5 mg/ml sodium borohydride for 3 min followed by another washing with PBS. Finally coverslips were sterilized with 70% ethanol for 5 min and incubated in complete growth medium for 1 h before use. To assess the ability of cells to form invadopodia, cells were cultured on cross-linked fluorescent conjugated matrix for 3 h. The percentage of cells showing degradation was quantified and shown in a bar graph.

BM degradation and transmigration assay

Peritoneal BM was prepared as previously described (Witz et al., 2001; Hotary et al., 2006). In brief, the peritoneal BM was isolated by stripping the overlying mesothelial cells from C57BL/6 mouse mesentery using 1 N ammonium hydroxide and mounting the isolated mesentery on 6.5-mm diameter Transwells (BD). After washing with PBS, 5×10^4 MDA-MB-231 cells were seeded on the top of the BMs in DME supplemented with 10% FBS. 1 ml of medium was placed in the lower chambers. After 3 d of culture, the samples were fixed in 4% formaldehyde and stained for collagen IV on both sides. BM and cells were visualized with an inverted confocal microscope fitted with a uPlan-SApochromat 60×/1.35 NA oil objective lens (Fluoview FV1000; Olympus). The confocal microscope was equipped with a PMT to capture images, and the acquisition software was FV10-ASW1.7. To quantify remaining collagen IV staining, z-stack images of 10 BM areas were collected from the top of the BM to the bottom. The extended focus projection images of z stacks were used to analyze the total staining of collagen IV. Quantification was done in at least three independent experiments in duplicate for each assay.

Cell surface biotinylation and MT1-MMP trafficking assays

Cell surface proteins were biotinylated by incubating the cells with 0.5 mg/ml sulfo-NHS-SS-biotin (Pierce) as described previously (Le et al., 1999). Cleared cell lysate containing 400 µg of total protein from each sample was incubated with NeutrAvidin Agarose Resin (Thermo Fischer Scientific) to pull down biotinylated proteins. The samples were then analyzed by immunoblotting for MT1-MMP or EGFR. Three independent experiments have been performed on three occasions.

MT1-MMP internalization and recycling assays were performed as described previously for integrins (Roberts et al., 2001), with the following modifications: monoclonal mouse anti–MT1-MMP (MAB3328) was used to coat the ELISA plates at 5 µg/ml at 4C° overnight. MDA-MB-231 cells were not serum-starved; receptor internalization conditions for recycling were 30 min at 37°C; 10 µg/ml collagen was added to the cells during the internalization and recycling periods. In brief, cells were cooled on ice with ice-cold PBS and labeled with 0.2 mg/ml NHS-SS-biotin (Pierce) for 30 min on a rocker at 4°C. Labeled cells were washed two times with cold PBS on ice and transferred to 37°C medium in the presence (for internalization experiments only) or absence of 0.6 µM primaquine for the indicated times. Medium was aspirated and the cells were rapidly cooled down on ice with the addition of ice-cold PBS. Remaining cell surface biotin was removed with 20 mM MesNa in 50 mM Tris, pH 8.6, and 100 mM NaCl for 15 min on a rocker at 4°C. The reaction was quenched with 20 mM iodoacetamide for 10 min, and, subsequently, cells were lysed and centrifuged, and 50 µl of postnuclear supernatant was plated on the prepared antibody-coated 96-well plated and incubated overnight at 4°C.

F-actin sedimentation assay

Rabbit muscle actin was purified as described previously (Spudich and Watt, 1971; Machesky and Hall, 1997). In brief, muscle acetone powder was extracted in 20 ml G buffer (2 mM Tris, pH 8, 0.2 mM ATP, 0.5 mM DTT, and 0.2 mM $CaCl_2$) per gram of acetone powder on ice for 30 min. This was sedimented for 30 min at 30,000 *g* at 2°C, and the extraction step followed by centrifugation was repeated. The combined supernatants were made up to 50 mM KCl and 2 mM $MgCl_2$, and the solution was stirred at room temperature for 30 min and then on ice for 30 min. Finally, the solution was brought up to 0.8 M KCl and stirred for a further 30 min on ice before sedimentation at 100,000 *g* for 2 h at 4°C. The pellets were resuspended in G buffer with Dounce homogenization and dialyzed for 2 d into G buffer, then sedimented for 2 h at 100,000 *g* to pellet the oligomers. The top two thirds of the supernatant was removed and used as G-actin. MT1-MMP cytoplasmic tail peptides were solubilized in G buffer at 2 µg/µl. Cytoplasmic tail peptides (final concentration, 25 µm) in G buffer were mixed with the indicated concentrations of G-actin, brought to a final concentration of 0.1 KCl to allow F-actin polymerization, and incubated for 1 h at room temperature. Suspensions were pelleted for 1 h at 100,000 *g* 4°C in a Beckman table-top ultracentrifuge. Pellets and supernatants were brought to a volume of 100 µl with NuPAGE samples buffer, and 10 µl were run on a 4–12% NuPAGE gel.

Steady-state fluorescence anisotropy experiments

The steady-state fluorescence anisotropy measurements were performed with a Jobin Yvon (HORIBA) spectrofluorometer equipped with a thermostable cuvette holder. The experiments were performed at pH 8.0 in a buffer containing 2 mM Tris/HCl, 0.2 mM ATP, 0.005% NaN_3, 0.5 mM 2-mercaptoethanol, 100 mM KCl, and 2 mM $CaCl_2$ (buffer F). The excitation wavelength for 5-({2-[(iodoacetyl)amino]ethyl}amino)naphthalene-1-sulfonic acid (IAEDANS) was 350 nm, and the fluorescence anisotropy of the IAEDANS was recorded at 490 nm. The optical slits were set to 5 nm in both the excitation and emission side. Actin was labeled with IAEDANS fluorescent probes on Cys374 (Visegrády et al., 2004). The labeling ratio (the probe concentration vs. actin concentration) for IAEDANS was 0.9.

We have used a quadratic equation to fit the binding data and calculate the K_d: $[PL]/[P] = (([P] + [L] + K_d) - (([P] + [L] + K_d)^2 - 4 \times [P] \times [L])^{0.5})/2 \times [L]$, where [PL] is the concentration of the peptide bound to actin, [L] is the total concentration of the peptide, which is varied, [P] is the total concentration of actin, and [PL]/[P] is the fraction of ligand bound to receptor.

Online supplemental material

Fig. S1 shows that depletion of N-WASP does not affect cell migration on a 2D rigid surface, and also shows representative knockdowns of N-WASP and normal migration parameters when cells are on a rigid 2D surface. Fig. S2 shows that depletion of N-WASP has no effects on MT1-MMP levels, endocytosis, or recycling rates. Also shown are Western blots of MT1-MMP levels and the results of endocytosis and recycling assays using biotinylated surface labeling of MT1-MMP. Fig. S3 shows that the focal adhesion proteins vinculin and FAK partially colocalize with invadopodia-like structures in CIA. The figure also shows cells migrating in the CIA and morphology of focal adhesions and invadopodia-like structures. Fig. S4 shows that MT1-MMP colocalizes to LE/LY but not EE compartments. The figure also shows still images from movies of MT1-MMP colocalizing with late endocytic but not early endocytic compartments, and shows preferential localization of MT1-MMP–containing vesicles to the leading half of cells migrating in CIA. Fig. S5 shows MT1-MMP cytoplasmic tail mutant expression and the effect on cell invasion in CIA and mobility in FRAP. The figure also shows a Western blot of expression levels of MT1-MMP and mutants in cells depleted of endogenous MT1-MMP but rescued with mutants. Also shown is the lack of rescue of invasion in CIA when MT1-MMP knockdown is replaced with LLY/AAA mutant and various control FRAP experiments of MT1-MMP in pseudopodia of cells invading in CIA. Video 1 shows 3D reconstruction of MDA-MB-231 cells invading into Matrigel in 3D invasion assay, corresponding to Fig. 2 B. Video 2 shows a 3D reconstruction of N-WASP knockdown MDA-MB-231 cells invading into Matrigel in a 3D invasion assay corresponding to Fig. 2 B. Video 3 shows migration of cells invading in CIA with control and N-WASP knockdown, corresponding to stills in Fig. 3 A. Video 4 shows invasive migration of cells in CIA in various concentrations of Matrigel, corresponding to Fig. 3 B. Video 5 shows colocalization of mCherry-MT1-MMP with GFP-Rab7 corresponding to stills shown in Fig. S4 A. Video 6 shows photoactivated MT1-MMP trafficking from a Rab7-positive LE to the plasma-membrane, corresponding to still images in Fig. 6 D. Video 7 shows mCherry-MT1-MMP vesicles trafficking into invading pseudopods in NT cells while invading in CIA, but not in N-WASP knockdown cells, and corresponds to stills shown in Fig. S4 B. Online supplemental material is available at http://www.jcb.org/cgi/content/full/jcb.201203025/DC1.

We thank Drs. Stephen Weiss (University of Michigan) and Gareth Jones (King's College London) for helpful advice and for comments on our manuscript. We thank Prof. Barry Gusterson (Glasgow University) for helpful advice and for help with the breast cancer TMA scoring.

We thank Kurt Anderson, Margaret O'Prey, and Tom Gilbey of the Beatson Advanced Imaging Resource imaging facility for help with imaging. L.M. Machesky, J.C. Norman, and R.H. Insall thank Cancer Research UK for core funding. L.M. Machesky and X. Yu were also funded by the Medical Research Council UK on a Research Senior Fellowship G117/569 to L.M. Machesky, and X. Yu is currently funded by Association for International Cancer Research grant 11-0119 to L.M. Machesky.

Submitted: 7 March 2012
Accepted: 28 September 2012

Published October 22, 2012

References

Alexander, N.R., K.M. Branch, A. Parekh, E.S. Clark, I.C. Iwueke, S.A. Guelcher, and A.M. Weaver. 2008. Extracellular matrix rigidity promotes invadopodia activity. *Curr. Biol.* 18:1295–1299. http://dx.doi.org/10.1016/j.cub.2008.07.090

Artym, V.V., Y. Zhang, F. Seillier-Moiseiwitsch, K.M. Yamada, and S.C. Mueller. 2006. Dynamic interactions of cortactin and membrane type 1 matrix metalloproteinase at invadopodia: defining the stages of invadopodia formation and function. *Cancer Res.* 66:3034–3043. http://dx.doi.org/10.1158/0008-5472.CAN-05-2177

Benesch, S., S. Lommel, A. Steffen, T.E. Stradal, N. Scaplehorn, M. Way, J. Wehland, and K. Rottner. 2002. Phosphatidylinositol 4,5-biphosphate (PIP2)-induced vesicle movement depends on N-WASP and involves Nck, WIP, and Grb2. *J. Biol. Chem.* 277:37771–37776. http://dx.doi.org/10.1074/jbc.M204145200

Branch, K.M., D. Hoshino, and A.M. Weaver. 2012. Adhesion rings surround invadopodia and promote maturation. *Biology Open*. 1:711–722. http://dx.doi.org/10.1242/bio.20121867

Bravo-Cordero, J.J., R. Marrero-Diaz, D. Megías, L. Genís, A. García-Grande, M.A. García, A.G. Arroyo, and M.C. Montoya. 2007. MT1-MMP proinvasive activity is regulated by a novel Rab8-dependent exocytic pathway. *EMBO J.* 26:1499–1510. http://dx.doi.org/10.1038/sj.emboj.7601606

Bryce, N.S., E.S. Clark, J.L. Leysath, J.D. Currie, D.J. Webb, and A.M. Weaver. 2005. Cortactin promotes cell motility by enhancing lamellipodial persistence. *Curr. Biol.* 15:1276–1285. http://dx.doi.org/10.1016/j.cub.2005.06.043

Bu, W., A.M. Chou, K.B. Lim, T. Sudhaharan, and S. Ahmed. 2009. The Toca-1-N-WASP complex links filopodial formation to endocytosis. *J. Biol. Chem.* 284:11622–11636. http://dx.doi.org/10.1074/jbc.M805940200

Caldieri, G., I. Ayala, F. Attanasio, and R. Buccione. 2009. Cell and molecular biology of invadopodia. *Int Rev Cell Mol Biol*. 275:1–34. http://dx.doi.org/10.1016/S1937-6448(09)75001-4

Chan, K.T., C.L. Cortesio, and A. Huttenlocher. 2009. FAK alters invadopodia and focal adhesion composition and dynamics to regulate breast cancer invasion. *J. Cell Biol.* 185:357–370. http://dx.doi.org/10.1083/jcb.200809110

Chun, T.H., K.B. Hotary, F. Sabeh, A.R. Saltiel, E.D. Allen, and S.J. Weiss. 2006. A pericellular collagenase directs the 3-dimensional development of white adipose tissue. *Cell*. 125:577–591. http://dx.doi.org/10.1016/j.cell.2006.02.050

Clark, E.S., A.S. Whigham, W.G. Yarbrough, and A.M. Weaver. 2007. Cortactin is an essential regulator of matrix metalloproteinase secretion and extracellular matrix degradation in invadopodia. *Cancer Res.* 67:4227–4235. http://dx.doi.org/10.1158/0008-5472.CAN-06-3928

Desmarais, V., H. Yamaguchi, M. Oser, L. Soon, G. Mouneimne, C. Sarmiento, R. Eddy, and J. Condeelis. 2009. N-WASP and cortactin are involved in invadopodium-dependent chemotaxis to EGF in breast tumor cells. *Cell Motil. Cytoskeleton*. 66:303–316. http://dx.doi.org/10.1002/cm.20361

Dozynkiewicz, M.A., N.B. Jamieson, I. Macpherson, J. Grindlay, P.V. van den Berghe, A. von Thun, J.P. Morton, C. Gourley, P. Timpson, C. Nixon, et al. 2012. Rab25 and CLIC3 collaborate to promote integrin recycling from late endosomes/lysosomes and drive cancer progression. *Dev. Cell*. 22:131–145. http://dx.doi.org/10.1016/j.devcel.2011.11.008

Fisher, K.E., A. Sacharidou, A.N. Stratman, A.M. Mayo, S.B. Fisher, R.D. Mahan, M.J. Davis, and G.E. Davis. 2009. MT1-MMP- and Cdc42-dependent signaling co-regulate cell invasion and tunnel formation in 3D collagen matrices. *J. Cell Sci.* 122:4558–4569. http://dx.doi.org/10.1242/jcs.050724

Fluck, M.M., and B.S. Schaffhausen. 2009. Lessons in signaling and tumorigenesis from polyomavirus middle T antigen. *Microbiol. Mol. Biol. Rev.* 73:542–563. http://dx.doi.org/10.1128/MMBR.00009-09

Frittoli, E., A. Palamidessi, A. Disanza, and G. Scita. 2011. Secretory and endo/exocytic trafficking in invadopodia formation: the MT1-MMP paradigm. *Eur. J. Cell Biol.* 90:108–114. http://dx.doi.org/10.1016/j.ejcb.2010.04.007

Gligorijevic, B., J. Wyckoff, H. Yamaguchi, Y. Wang, E.T. Roussos, and J. Condeelis. 2012. N-WASP-mediated invadopodium formation is involved in intravasation and lung metastasis of mammary tumors. *J. Cell Sci.* 125:724–734. http://dx.doi.org/10.1242/jcs.092726

Hennigan, R.F., K.L. Hawker, and B.W. Ozanne. 1994. Fos-transformation activates genes associated with invasion. *Oncogene*. 9:3591–3600.

Hoshino, D., N. Koshikawa, T. Suzuki, V. Quaranta, A.M. Weaver, M. Seiki, and K. Ichikawa. 2012. Establishment and validation of computational model for MT1-MMP dependent ECM degradation and intervention strategies. *PLOS Comput. Biol.* 8:e1002479. http://dx.doi.org/10.1371/journal.pcbi.1002479

Hotary, K., X.Y. Li, E. Allen, S.L. Stevens, and S.J. Weiss. 2006. A cancer cell metalloprotease triad regulates the basement membrane transmigration program. *Genes Dev.* 20:2673–2686. http://dx.doi.org/10.1101/gad.1451806

Hüfner, K., B. Schell, M. Aepfelbacher, and S. Linder. 2002. The acidic regions of WASp and N-WASP can synergize with CDC42Hs and Rac1 to induce filopodia and lamellipodia. *FEBS Lett.* 514:168–174. http://dx.doi.org/10.1016/S0014-5793(02)02358-X

Isaac, B.M., D. Ishihara, L.M. Nusblat, J.C. Gevrey, A. Dovas, J. Condeelis, and D. Cox. 2010. N-WASP has the ability to compensate for the loss of WASP in macrophage podosome formation and chemotaxis. *Exp. Cell Res.* 316:3406–3416. http://dx.doi.org/10.1016/j.yexcr.2010.06.011

Jiang, A., K. Lehti, X. Wang, S.J. Weiss, J. Keski-Oja, and D. Pei. 2001. Regulation of membrane-type matrix metalloproteinase 1 activity by dynamin-mediated endocytosis. *Proc. Natl. Acad. Sci. USA*. 98:13693–13698. http://dx.doi.org/10.1073/pnas.241293698

Jin, F., B. Dong, J. Georgiou, Q. Jiang, J. Zhang, A. Bharioke, F. Qiu, S. Lommel, M.L. Feltri, L. Wrabetz, et al. 2011. N-WASp is required for Schwann cell cytoskeletal dynamics, normal myelin gene expression and peripheral nerve myelination. *Development*. 138:1329–1337. http://dx.doi.org/10.1242/dev.058677

Kam, Y., C. Guess, L. Estrada, B. Weidow, and V. Quaranta. 2008. A novel circular invasion assay mimics in vivo invasive behavior of cancer cell lines and distinguishes single-cell motility in vitro. *BMC Cancer*. 8:198. http://dx.doi.org/10.1186/1471-2407-8-198

Kirkegaard, T., J. Edwards, S. Tovey, L.M. McGlynn, S.N. Krishna, R. Mukherjee, L. Tam, A.F. Munro, B. Dunne, and J.M. Bartlett. 2006. Observer variation in immunohistochemical analysis of protein expression, time for a change? *Histopathology*. 48:787–794. http://dx.doi.org/10.1111/j.1365-2559.2006.02412.x

Kowalski, J.R., C. Egile, S. Gil, S.B. Snapper, R. Li, and S.M. Thomas. 2005. Cortactin regulates cell migration through activation of N-WASP. *J. Cell Sci.* 118:79–87. http://dx.doi.org/10.1242/jcs.01586

Le, T.L., A.S. Yap, and J.L. Stow. 1999. Recycling of E-cadherin: a potential mechanism for regulating cadherin dynamics. *J. Cell Biol.* 146:219–232.

Legg, J.A., G. Bompard, J. Dawson, H.L. Morris, N. Andrew, L. Cooper, S.A. Johnston, G. Tramountanis, and L.M. Machesky. 2007. N-WASP involvement in dorsal ruffle formation in mouse embryonic fibroblasts. *Mol. Biol. Cell*. 18:678–687. http://dx.doi.org/10.1091/mbc.E06-06-0569

Linder, S. 2007. The matrix corroded: podosomes and invadopodia in extracellular matrix degradation. *Trends Cell Biol.* 17:107–117. http://dx.doi.org/10.1016/j.tcb.2007.01.002

Lommel, S., S. Benesch, K. Rottner, T. Franz, J. Wehland, and R. Kühn. 2001. Actin pedestal formation by enteropathogenic *Escherichia coli* and intracellular motility of *Shigella flexneri* are abolished in N-WASP-defective cells. *EMBO Rep.* 2:850–857. http://dx.doi.org/10.1093/embo-reports/kve197

Lorenz, M., H. Yamaguchi, Y. Wang, R.H. Singer, and J. Condeelis. 2004. Imaging sites of N-wasp activity in lamellipodia and invadopodia of carcinoma cells. *Curr. Biol.* 14:697–703. http://dx.doi.org/10.1016/j.cub.2004.04.008

Ludwig, T., S.M. Theissen, M.J. Morton, and M.J. Caplan. 2008. The cytoplasmic tail dileucine motif LL572 determines the glycosylation pattern of membrane-type 1 matrix metalloproteinase. *J. Biol. Chem.* 283:35410–35418. http://dx.doi.org/10.1074/jbc.M801816200

Machesky, L.M., and A. Hall. 1997. Role of actin polymerization and adhesion to extracellular matrix in Rac- and Rho-induced cytoskeletal reorganization. *J. Cell Biol.* 138:913–926. http://dx.doi.org/10.1083/jcb.138.4.913

Merrifield, C.J., M.E. Feldman, L. Wan, and W. Almers. 2002. Imaging actin and dynamin recruitment during invagination of single clathrin-coated pits. *Nat. Cell Biol.* 4:691–698. http://dx.doi.org/10.1038/ncb837

Miki, H., T. Sasaki, Y. Takai, and T. Takenawa. 1998. Induction of filopodium formation by a WASP-related actin-depolymerizing protein N-WASP. *Nature*. 391:93–96. http://dx.doi.org/10.1038/34208

Misra, A., R.P. Lim, Z. Wu, and T. Thanabalu. 2007. N-WASP plays a critical role in fibroblast adhesion and spreading. *Biochem. Biophys. Res. Commun.* 364:908–912. http://dx.doi.org/10.1016/j.bbrc.2007.10.086

Muller, W.J., E. Sinn, P.K. Pattengale, R. Wallace, and P. Leder. 1988. Single-step induction of mammary adenocarcinoma in transgenic mice bearing the activated c-neu oncogene. *Cell*. 54:105–115. http://dx.doi.org/10.1016/0092-8674(88)90184-5

Nakahara, H., L. Howard, E.W. Thompson, H. Sato, M. Seiki, Y. Yeh, and W.T. Chen. 1997. Transmembrane/cytoplasmic domain-mediated membrane type 1-matrix metalloprotease docking to invadopodia is required for cell invasion. *Proc. Natl. Acad. Sci. USA*. 94:7959–7964. http://dx.doi.org/10.1073/pnas.94.15.7959

Oser, M., H. Yamaguchi, C.C. Mader, J.J. Bravo-Cordero, M. Arias, X. Chen, V. Desmarais, J. van Rheenen, A.J. Koleske, and J. Condeelis. 2009. Cortactin regulates cofilin and N-WASp activities to control the stages of invadopodium assembly and maturation. *J. Cell Biol.* 186:571–587. http://dx.doi.org/10.1083/jcb.200812176

Peränen, J., P. Auvinen, H. Virta, R. Wepf, and K. Simons. 1996. Rab8 promotes polarized membrane transport through reorganization of actin and microtubules in fibroblasts. *J. Cell Biol.* 135:153–167. http://dx.doi.org/10.1083/jcb.135.1.153

Poincloux, R., F. Lizárraga, and P. Chavrier. 2009. Matrix invasion by tumour cells: a focus on MT1-MMP trafficking to invadopodia. *J. Cell Sci.* 122:3015–3024. http://dx.doi.org/10.1242/jcs.034561

Puthenveedu, M.A., B. Lauffer, P. Temkin, R. Vistein, P. Carlton, K. Thorn, J. Taunton, O.D. Weiner, R.G. Parton, and M. von Zastrow. 2010. Sequence-dependent sorting of recycling proteins by actin-stabilized endosomal microdomains. *Cell*. 143:761–773. http://dx.doi.org/10.1016/j.cell.2010.10.003

Riedl, J., A.H. Crevenna, K. Kessenbrock, J.H. Yu, D. Neukirchen, M. Bista, F. Bradke, D. Jenne, T.A. Holak, Z. Werb, et al. 2008. Lifeact: a versatile marker to visualize F-actin. *Nat. Methods*. 5:605–607. http://dx.doi.org/10.1038/nmeth.1220

Roberts, M., S. Barry, A. Woods, P. van der Sluijs, and J. Norman. 2001. PDGF-regulated rab4-dependent recycling of alphavbeta3 integrin from early endosomes is necessary for cell adhesion and spreading. *Curr. Biol.* 11:1392–1402. http://dx.doi.org/10.1016/S0960-9822(01)00442-0

Sabeh, F., I. Ota, K. Holmbeck, H. Birkedal-Hansen, P. Soloway, M. Balbin, C. Lopez-Otin, S. Shapiro, M. Inada, S. Krane, et al. 2004. Tumor cell traffic through the extracellular matrix is controlled by the membrane-anchored collagenase MT1-MMP. *J. Cell Biol.* 167:769–781. http://dx.doi.org/10.1083/jcb.200408028

Sarmiento, C., W. Wang, A. Dovas, H. Yamaguchi, M. Sidani, M. El-Sibai, V. Desmarais, H.A. Holman, S. Kitchen, J.M. Backer, et al. 2008. WASP family members and formin proteins coordinate regulation of cell protrusions in carcinoma cells. *J. Cell Biol.* 180:1245–1260. http://dx.doi.org/10.1083/jcb.200708123

Scott, R.W., S. Hooper, D. Crighton, A. Li, I. König, J. Munro, E. Trivier, G. Wickman, P. Morin, D.R. Croft, et al. 2010. LIM kinases are required for invasive path generation by tumor and tumor-associated stromal cells. *J. Cell Biol.* 191:169–185. http://dx.doi.org/10.1083/jcb.201002041

Seiki, M., N. Koshikawa, and I. Yana. 2003. Role of pericellular proteolysis by membrane-type 1 matrix metalloproteinase in cancer invasion and angiogenesis. *Cancer Metastasis Rev.* 22:129–143. http://dx.doi.org/10.1023/A:1023087113214

Serrels, A., P. Timpson, M. Canel, J.P. Schwarz, N.O. Carragher, M.C. Frame, V.G. Brunton, and K.I. Anderson. 2009. Real-time study of E-cadherin and membrane dynamics in living animals: implications for disease modeling and drug development. *Cancer Res.* 69:2714–2719. http://dx.doi.org/10.1158/0008-5472.CAN-08-4308

Snapper, S.B., F. Takeshima, I. Antón, C.H. Liu, S.M. Thomas, D. Nguyen, D. Dudley, H. Fraser, D. Purich, M. Lopez-Ilasaca, et al. 2001. N-WASP deficiency reveals distinct pathways for cell surface projections and microbial actin-based motility. *Nat. Cell Biol.* 3:897–904. http://dx.doi.org/10.1038/ncb1001-897

Spudich, J.A., and S. Watt. 1971. The regulation of rabbit skeletal muscle contraction. I. Biochemical studies of the interaction of the tropomyosin-troponin complex with actin and the proteolytic fragments of myosin. *J. Biol. Chem.* 246:4866–4871.

Steffen, A., G. Le Dez, R. Poincloux, C. Recchi, P. Nassoy, K. Rottner, T. Galli, and P. Chavrier. 2008. MT1-MMP-dependent invasion is regulated by TI-VAMP/VAMP7. *Curr. Biol.* 18:926–931. http://dx.doi.org/10.1016/j.cub.2008.05.044

Subach, F.V., G.H. Patterson, S. Manley, J.M. Gillette, J. Lippincott-Schwartz, and V.V. Verkhusha. 2009. Photoactivatable mCherry for high-resolution two-color fluorescence microscopy. *Nat. Methods*. 6:153–159. http://dx.doi.org/10.1038/nmeth.1298

Taunton, J., B.A. Rowning, M.L. Coughlin, M. Wu, R.T. Moon, T.J. Mitchison, and C.A. Larabell. 2000. Actin-dependent propulsion of endosomes and lysosomes by recruitment of N-WASP. *J. Cell Biol.* 148:519–530. http://dx.doi.org/10.1083/jcb.148.3.519

Uekita, T., Y. Itoh, I. Yana, H. Ohno, and M. Seiki. 2001. Cytoplasmic tail-dependent internalization of membrane-type 1 matrix metalloproteinase is important for its invasion-promoting activity. *J. Cell Biol.* 155:1345–1356. http://dx.doi.org/10.1083/jcb.200108112

Visegrády, B., D. Lorinczy, G. Hild, B. Somogyi, and M. Nyitrai. 2004. The effect of phalloidin and jasplakinolide on the flexibility and thermal stability of actin filaments. *FEBS Lett.* 565:163–166. http://dx.doi.org/10.1016/j.febslet.2004.03.096

Wang, Y., and M.A. McNiven. 2012. Invasive matrix degradation at focal adhesions occurs via protease recruitment by a FAK-p130Cas complex. *J. Cell Biol.* 196:375–385. http://dx.doi.org/10.1083/jcb.201105153

Wickramasinghe, R.D., P. Ko Ferrigno, and C. Roghi. 2010. Peptide aptamers as new tools to modulate clathrin-mediated internalisation—inhibition of MT1-MMP internalisation. *BMC Cell Biol.* 11:58. http://dx.doi.org/10.1186/1471-2121-11-58

Witz, C.A., I.A. Montoya-Rodriguez, S. Cho, V.E. Centonze, L.F. Bonewald, and R.S. Schenken. 2001. Composition of the extracellular matrix of the peritoneum. *J. Soc. Gynecol. Investig.* 8:299–304. http://dx.doi.org/10.1016/S1071-5576(01)00122-8

Wolf, K., and P. Friedl. 2009. Mapping proteolytic cancer cell-extracellular matrix interfaces. *Clin. Exp. Metastasis*. 26:289–298. http://dx.doi.org/10.1007/s10585-008-9190-2

Wolf, K., Y.I. Wu, Y. Liu, J. Geiger, E. Tam, C. Overall, M.S. Stack, and P. Friedl. 2007. Multi-step pericellular proteolysis controls the transition from individual to collective cancer cell invasion. *Nat. Cell Biol.* 9:893–904. http://dx.doi.org/10.1038/ncb1616

Yamaguchi, H., M. Lorenz, S. Kempiak, C. Sarmiento, S. Coniglio, M. Symons, J. Segall, R. Eddy, H. Miki, T. Takenawa, and J. Condeelis. 2005. Molecular mechanisms of invadopodium formation: the role of the N-WASP-Arp2/3 complex pathway and cofilin. *J. Cell Biol.* 168:441–452. http://dx.doi.org/10.1083/jcb.200407076

Yanagawa, R., Y. Furukawa, T. Tsunoda, O. Kitahara, M. Kameyama, K. Murata, O. Ishikawa, and Y. Nakamura. 2001. Genome-wide screening of genes showing altered expression in liver metastases of human colorectal cancers by cDNA microarray. *Neoplasia*. 3:395–401. http://dx.doi.org/10.1038/sj.neo.7900185

Yarar, D., C.M. Waterman-Storer, and S.L. Schmid. 2007. SNX9 couples actin assembly to phosphoinositide signals and is required for membrane remodeling during endocytosis. *Dev. Cell*. 13:43–56. http://dx.doi.org/10.1016/j.devcel.2007.04.014

Yu, X., and L.M. Machesky. 2012. Cells assemble invadopodia-like structures and invade into matrigel in a matrix metalloprotease dependent manner in the circular invasion assay. *PLoS ONE*. 7:e30605. http://dx.doi.org/10.1371/journal.pone.0030605

Zech, T., S.D. Calaminus, P. Caswell, H.J. Spence, M. Carnell, R.H. Insall, J. Norman, and L.M. Machesky. 2011. The Arp2/3 activator WASH regulates α5β1-integrin-mediated invasive migration. *J. Cell Sci.* 124:3753–3759. http://dx.doi.org/10.1242/jcs.080986

Published October 22, 2012

Yu et al., http://www.jcb.org/cgi/content/full/jcb.201203025/DC1

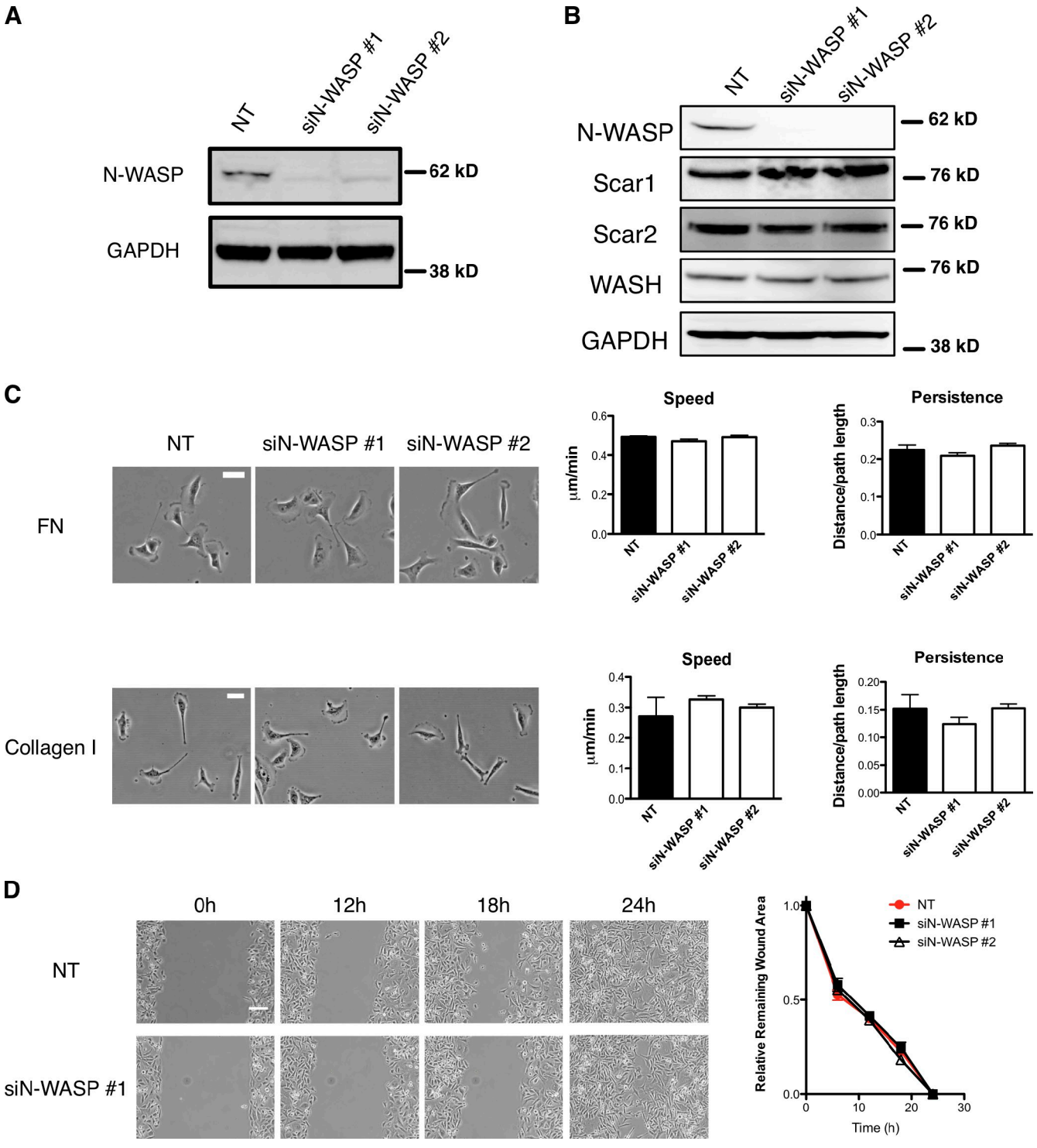

Figure S1. **Depletion of N-WASP does not affect cell migration on a 2D rigid surface.** (A) Western blots of lysates from MDA-MB-231 cells treated with N-WASP siRNA oligo #1 and #2. (B) Western blots show expression levels of other members of the WASP/Scar family in N-WASP–depleted cells. Blots in A and B are representative of at least three repeats. (C) Still images from time-lapse movies of MDA-MB-231 treated with nontargeting control (NT) and two siRNA against N-WASP (siN-WASP #1 and #2) random migration on fibronectin (FN) and collagen I–coated 2D surface. Cell migration speed and persistence were quantified and shown in the bar graphs. All error bars indicate means ± SD. Bars, 20 µm. (D) Still images of time-lapse movies of MDA-MB-231 cells show the wound healing progress at various time points in a scratch wound healing assay. The line graph shows the remaining wound area against time. All error bars indicate means ± SD. Bar, 100 µm. Three independent experiments were performed in C and D.

Published October 22, 2012

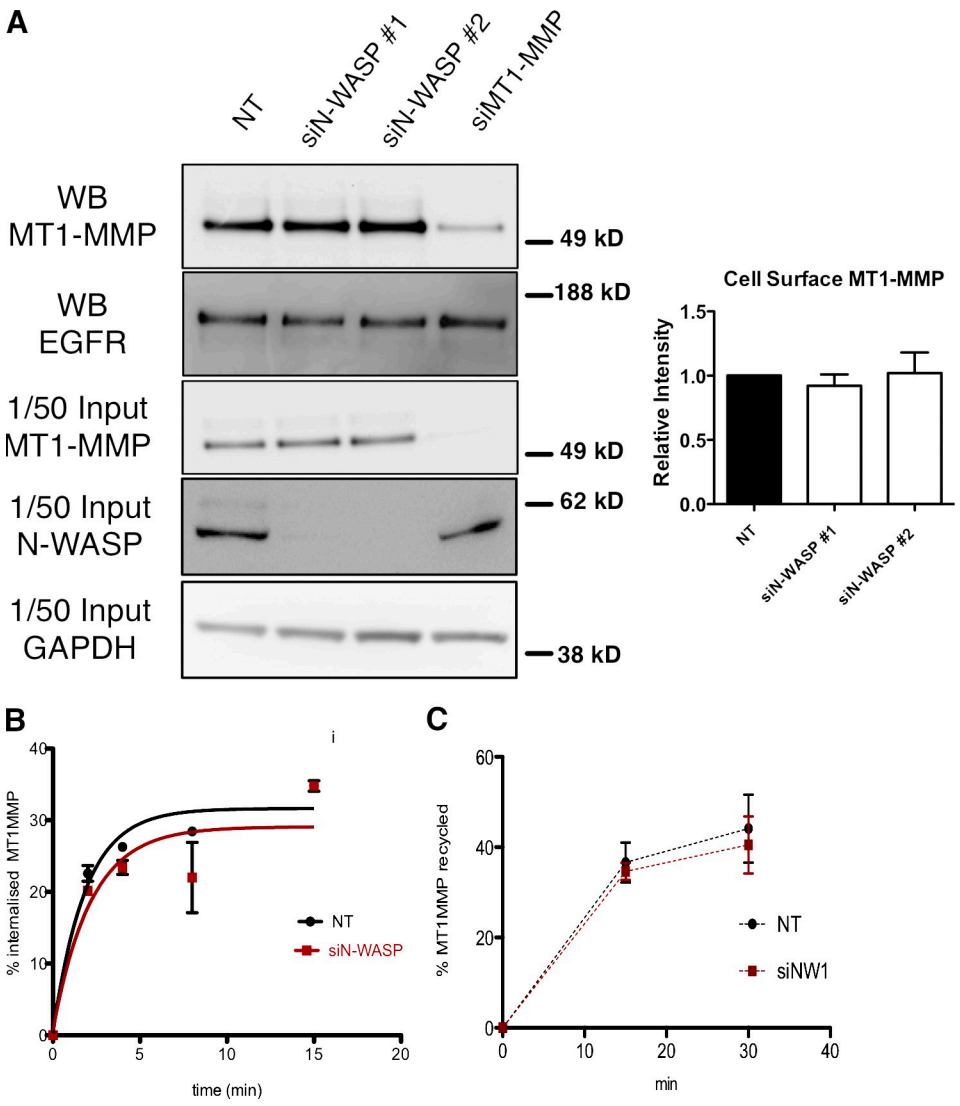

Figure S2. **Depletion of N-WASP has no effects on MT1-MMP levels, endocytosis, or recycling rates.** (A) Cell surface biotinylation assay showing the surface level of MT1-MMP or EGFR (IB = immunoblot). 1/50 input was analyzed to show the depletion of N-WASP and equal loading. *n* = 3 repeats. All error bars indicate means ± SD. (B) MT1-MMP internalization time course graph of NT and siN-WASP–treated MDA-MB-231 cells in the presence of collagen; *n* = 8 repeats in two experiments. (C) MT1-MMP recycling graph of NT and siN-WASP–treated MDA-MB-231 cells in the presence of collagen. *n* = 3 repeats.

Published October 22, 2012

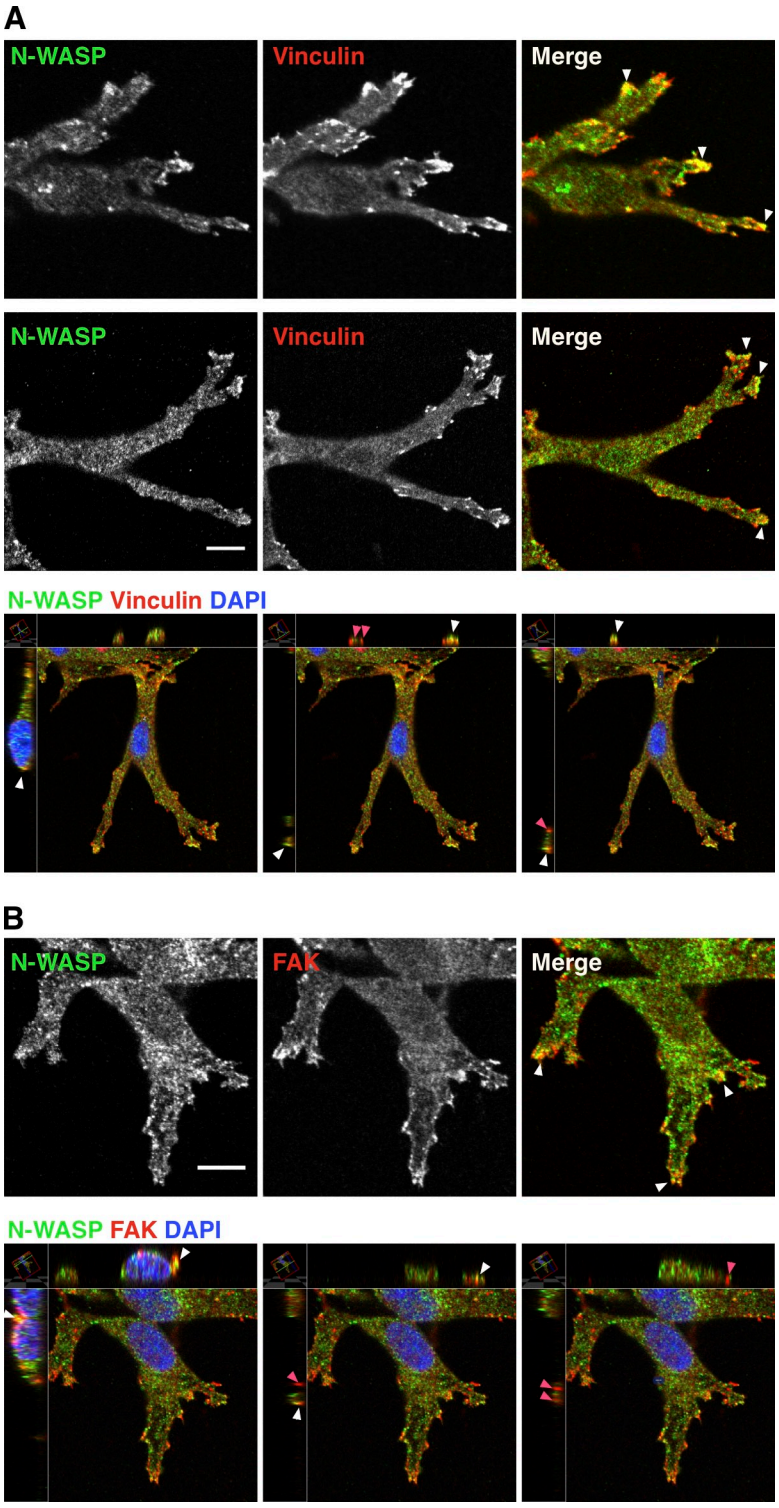

Figure S3. **Focal adhesion proteins vinculin and FAK partially colocalize with invadopodia-like structures in CIA.** (A and B) Immunofluorescence images of cells in CIA stained with N-WASP (green), vinculin (red), FAK (red), and DNA (blue) as indicated. Z-stack confocal images were captured and cell side views are shown to indicate positions of N-WASP–enriched puncta (white arrowheads mark actin and N-WASP hotspots) and vinculin/FAK-enriched puncta near the cell bottom that do not contain N-WASP (pink arrowheads mark focal adhesion–like structures). Bars, 10 µm.

Published October 22, 2012

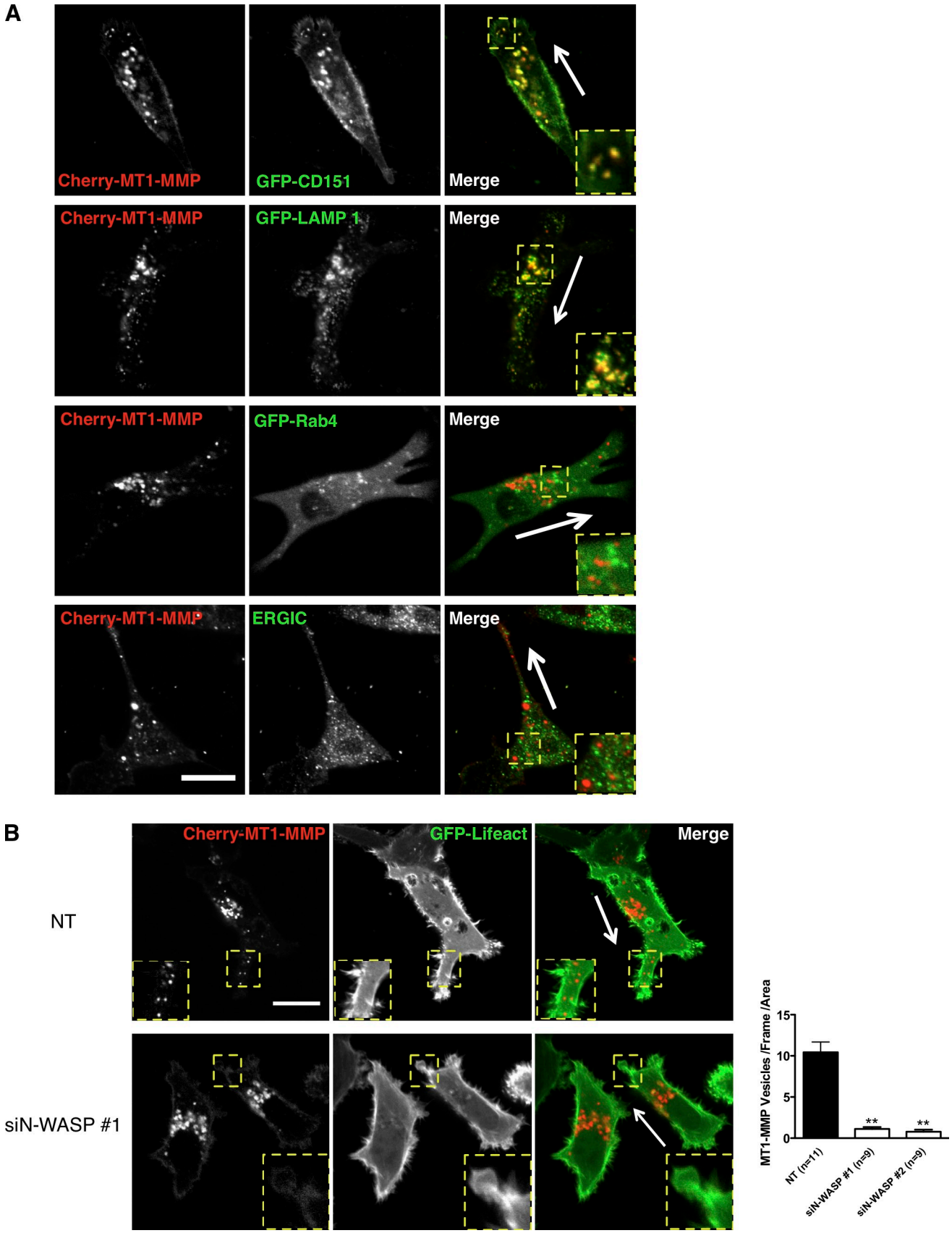

Figure S4. **MT1-MMP colocalizes to LE/LY but not EE compartments.** (A) Still images from live movies indicate mCherry-MT1-MMP colocalizes with late endosomal marker CD151 and lysosomal marker LAMP1 extensively cells in CIA, but there was no colocalization with Rab4 or endoplasmic reticulum–Golgi intermediate compartment (ERGIC). Arrows indicate the direction toward the wound area in CIA. Bar, 10 µm. (B) Still images from Video 7 showing mCherry-MT1-MMP vesicles tethering at the actin-rich invading pseudopods of live cells. The graph shows the number of MT1-MMP–containing vesicles in the leading pseudopod zone per frame (~10-s interval) per unit area (10,000 pixels) in NT and N-WASP knockdown cells. Arrows indicate the direction of the wound area. Insets show enlarged views of the boxed regions. All experiments have been repeated at least three times. All error bars indicate means ± SD; **, $P < 0.01$ by *t* test. Bar, 10 µm.

Published October 22, 2012

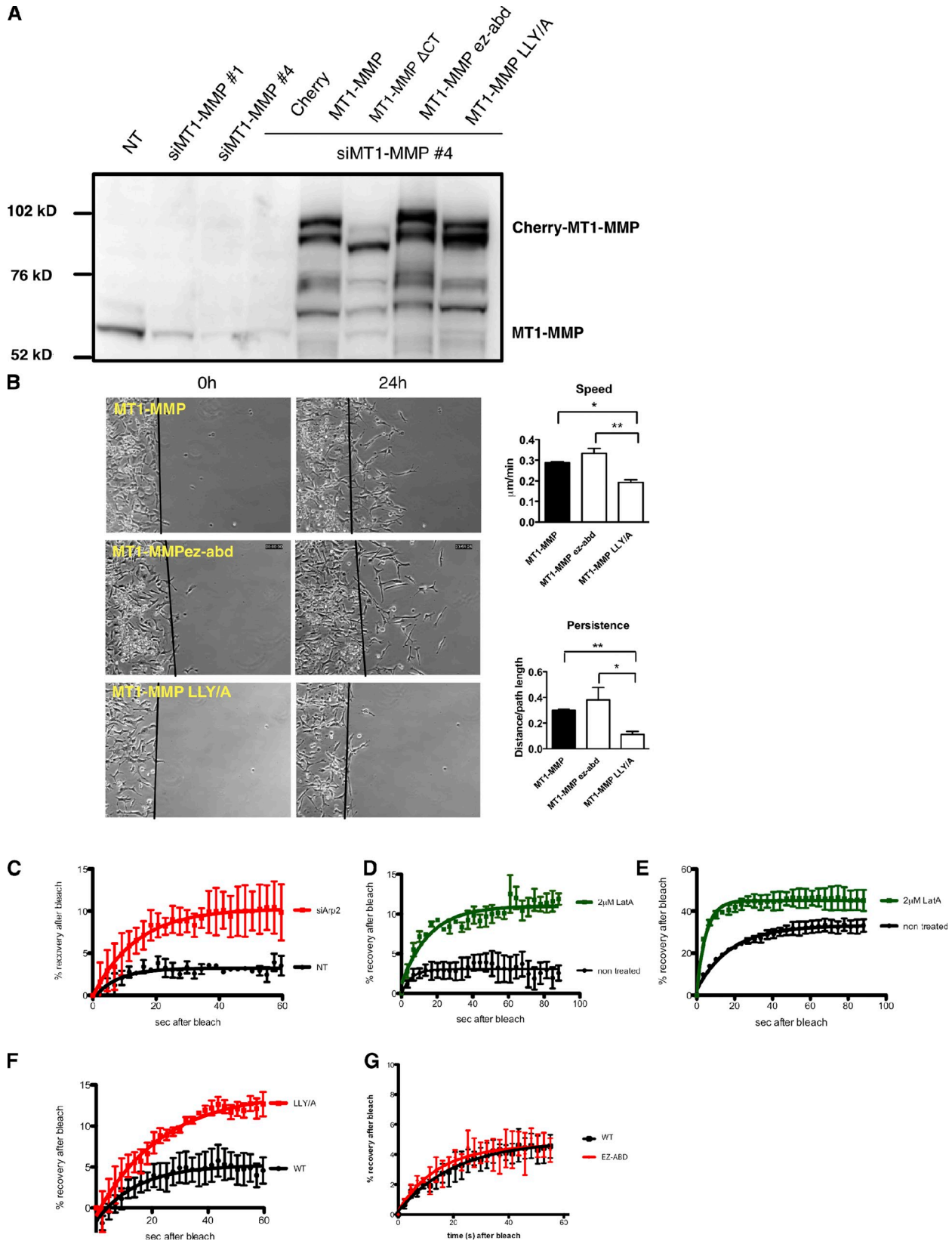

Figure S5. **MT1-MMP cytoplasmic tail mutant expression and the effect on cell invasion in CIA and mobility in FRAP.** (A) Western blot shows representative expression of endogenous MT1-MMP and mCherry-tagged MT1-MMP mutants in Fig. 8 G. (B) Still images of time-lapse movies of MDA-MB-231 cells expressing mCherry-tagged full-length MT1-MMP, MT1-MMP$^{EZ\text{-}ABD}$, and MT1-MMP LLY/AAA mutants during invasion in CIA at various time points. For C–G, MDA-MB-231 invading into a CIA were subjected to FRAP analysis as follows: selected actin-rich areas in invasive pseudopods cells were photobleached using a 405-nm laser, and recovery of fluorescence was recorded. Graphs show quantification of fluorescence recovery of at least 30 cells in three independent experiments. Error bars indicate means ± SEM. (C) FRAP of mCherry-MT1-MMP in NT or siArp2 knockdown in pseudopods of cells invading in CIA, and recovery was recorded over the next 60 s. (D and E) Cells were transfected with mCherry-MT1MMP (D) and GFP-actin (E), and subjected to FRAP analysis in the invasive pseudopod; recovery was recorded for 90 s. For 2 µM LatA treatment, medium was exchanged for LatA-containing medium, and recordings were measured without delay for the next hour. (F) FRAP of mCherry-MT1-MMP compared with a mCherry-MT1-MMP$^{LLY/A}$ mutant in pseudopods of cells migrating in CIA. (G) FRAP of mCherry-MT1-MMP compared with mCherry-MT1-MMP$^{EZ\text{-}ABD}$ in pseudopods in CIA. Selected actin-rich areas in invasive pseudopods were photobleached using a 405-nm laser, and recovery was record according over the next 60s.

Published October 22, 2012

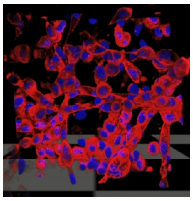

Video 1. **3D construction of MDA-MB-231 cells treated with NT siRNA in an inverted invasion assay.** MDA-MB-231 cells invading into Matrigel plugs were fixed and stained with rhodamine phalloidin (actin, red) and DAPI (DNA, blue). Z-stack confocal images (the depth interval is 1 µm) were taken continuously from the bottom filter into a Matrigel plug using a laser-scanning confocal microscope (Fluoview FV1000; Olympus) with a uPlan-SApochromat 60×/1.35 NA oil objective lens. The image stacks were collected by a PMT and processed by Volocity software to make a 3D reconstruction movie of invading cell strands.

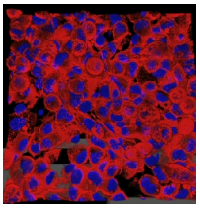

Video 2. **3D construction of MDA-MB-231 cells treated with siRNA N-WASP #1 in an inverted invasion assay.** Similar to Video 1, MDA-MB-231 cells were treated with siRNA N-WASP #1 and applied to the inverted invasion assay. The cells invading into Matrigel plugs were fixed and stained with rhodamine phalloidin (actin, red) and DAPI (DNA, blue). Z-stack confocal images (depth interval is 1 µm) were taken continuously from the bottom filter into the Matrigel plug using a laser-scanning confocal microscope (Fluoview FV1000; Olympus) with a uPlan-SApochromat 60×/1.35 NA oil objective lens. The image stacks were processed by Volocity software to make a 3D reconstruction movie of invading cells.

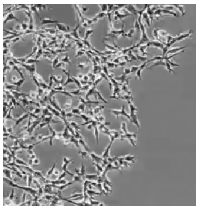

Video 3. **Invasive migration of cells treated with NT and N-WASP siRNA in CIA.** Live time-lapse imaging of MDA-MB-231 cells treated with siRNA NT (A), N-WASP #1 (B), and N-WASP #2 (C) invading under Matrigel CIA. The cells were placed in an incubator in an atmosphere of 5% CO_2 at 37°C. Movies were captured using a microscope (TE 2000; Nikon) equipped with a Plan Fluor 10× objective lens (Nikon) every 3 min for 15 h. The acquisition software was MetaMorph (version 7.7.7). The movies show that cell invasive migration was greatly impaired in N-WASP knockdown cells (B and C) compared with NT cells (A).

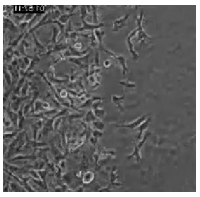

Video 4. **Invading migration of cells in various concentrations of Matrigel in CIA.** Live time-lapse imaging of MDA-MB-231 cells treated with siRNA of NT and N-WASP #1 were overlaid with various concentrations of Matrigel/PBS in CIA: 5 mg/ml (A and B; normal concentration), 2.5 mg/ml (C), and 1.25 mg/ml (D). Movies were captured using a microscope (TE 2000; Nikon) equipped with a 10× objective lens every 3 min (Plan Fluor; Nikon). The acquisition software was MetaMorph (version 7.7.7).

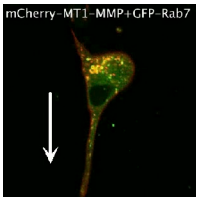

Video 5. **mCherry-MT1-MMP and GFP-Rab7 colocalize and cotraffic to invasive pseudopods.** MDA-MB-231 cells cotransfected with mCherry-MT1-MMP (red) and GFP-Rab7 (green) were overlaid with Matrigel and imaged with a laser-scanning confocal microscope (Fluoview FV1000; Olympus) with a uPlan-SApochromat 60×/1.35 NA oil objective lens every 5 s for 4 min and 15 s. Live time-lapse imaging shows that mCherry-MT1-MMP vesicles traffic to invasive pseudopods together with GFP-Rab7. The arrow indicates the wound direction of CIA.

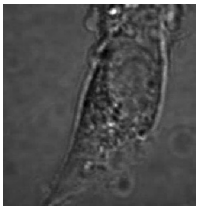

Video 6. **Photoactivated MT1-MMP trafficking from Rab7-positive LE to plasma membrane.** MDA-MB-231 cells cotransfected with PA-mCherry-MT1-MMP (red) and GFP-Rab7 (green) were overlaid with Matrigel and imaged with a laser-scanning confocal microscope (Fluoview FV1000; Olympus) with a uPlan-SApochromat 60×/1.35 NA oil objective lens. A 405-nm laser was used to activate a GFP-Rab7 vesicle containing photoactivated mCherry-MT1-MMP. Live time-lapse imaging shows that the activated mCherry-MT1-MMP gradually accumulates on the plasma membrane after photoactivation of a Rab7 vesicle.

Published October 22, 2012

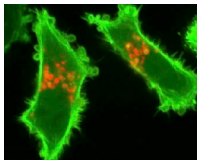

Video 7. **mCherry-MT1-MMP vesicles polarized trafficking to invasive pseudopods.** MDA-MB-231 cells treated with siRNA of NT (left) and N-WASP #1 (right) were cotransfected with mCherry-MT1-MMP (red) and GFP-Lifeact (green). The cells then were overlaid with Matrigel and imaged with a laser-scanning confocal microscope (Fluoview FV1000; Olympus) a uPlan-SApochromat 60×/1.35 NA oil objective lens. The movie shows that mCherry-MT1-MMP vesicles polarized traffic to invading pseudopods in NT cells while invading in CIA, but not in N-WASP knockdown cells. The arrow indicates the wound direction in CIA.